

REPORT ON THE DEVELOPMENT OF
THE MANNED ORBITAL RESEARCH LABORATORY (MORL)
SYSTEM UTILIZATION POTENTIAL

TASK AREA IV
MORL SYSTEM IMPROVEMENT STUDY

FACILITY FORM 602

167 20163
(ACCESSION NUMBER)

325
(PAGES)

CR-66281
(NASA CR OR TMX OR AD NUMBER)

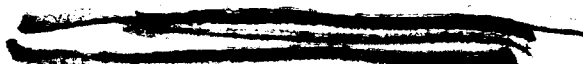
(THRU) 1
(CODE) 3
(CATEGORY)



BOOK 1

SM-48815
DECEMBER 1965

MISSILE & SPACE SYSTEMS DIVISION
DOUGLAS AIRCRAFT COMPANY, INC.
SANTA MONICA/CALIFORNIA



167-48815

REPORT ON THE DEVELOPMENT OF
THE MANNED ORBITAL RESEARCH LABORATORY (MORL)
SYSTEM UTILIZATION POTENTIAL

Task Area IV
MORL System Improvement Study

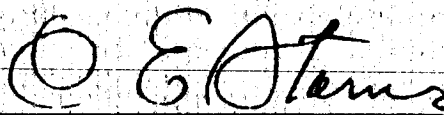
BOOK 1

SM-48815

DECEMBER 1965

PREPARED BY J. L. ALLEN
BRANCH CHIEF
SUBSYSTEMS

APPROVED BY

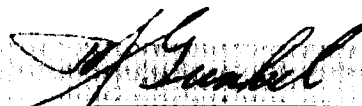


C. E. STARNES
PROGRAM MANAGER

SUBMITTED BY
DOUGLAS AIRCRAFT COMPANY, INC.

PRESENTED TO
NATIONAL AERONAUTICS AND SPACE ADMINISTRATION
LANGLEY RESEARCH CENTER
CONTRACT NO. NAS1-3612

APPROVED BY



R. J. GUNKEL
DIRECTOR, ADVANCED MANNED SPACECRAFT SYSTEMS

DOUGLAS MISSILE & SPACE SYSTEMS DIVISION

The Manned Orbital Research Laboratory (MORL) is a versatile facility for experimental research which provides for:

- **Simultaneous development of space flight technology and man's capability to function effectively under the combined stresses of the space environment for long periods of time.**
- **Intelligent selectivity in the mode of acquisition, collation, and transmission of data for subsequent detailed scientific analyses.**
- **Continual celestial and terrestrial observations.**

Future application potential includes use of the MORL as a basic, independent module, which, in combination with the Saturn Launch Vehicles currently planned for the NASA inventory, is responsive to a broad range of advanced mission requirements.

The laboratory module includes two independently pressurized compartments connected by an airlock. The larger compartment comprises the following functional spaces:

- **A Control Deck from which laboratory operations and a major portion of the experiment program will be conducted.**
- **An Internal Centrifuge in which members of the flight crew will perform re-entry simulation, undergo physical condition testing, and which may be useful for therapy, if required.**
- **The Flight Crew Quarters, which include sleeping, eating, recreation, hygiene, and liquids laboratory facilities.**

The smaller compartment is a Hangar/Test Area which is used for logistics spacecraft maintenance, cargo transfer, experimentation, satellite check-out, and flight crew habitation in a deferred-emergency mode of operation.

The logistics vehicle is composed of the following elements:

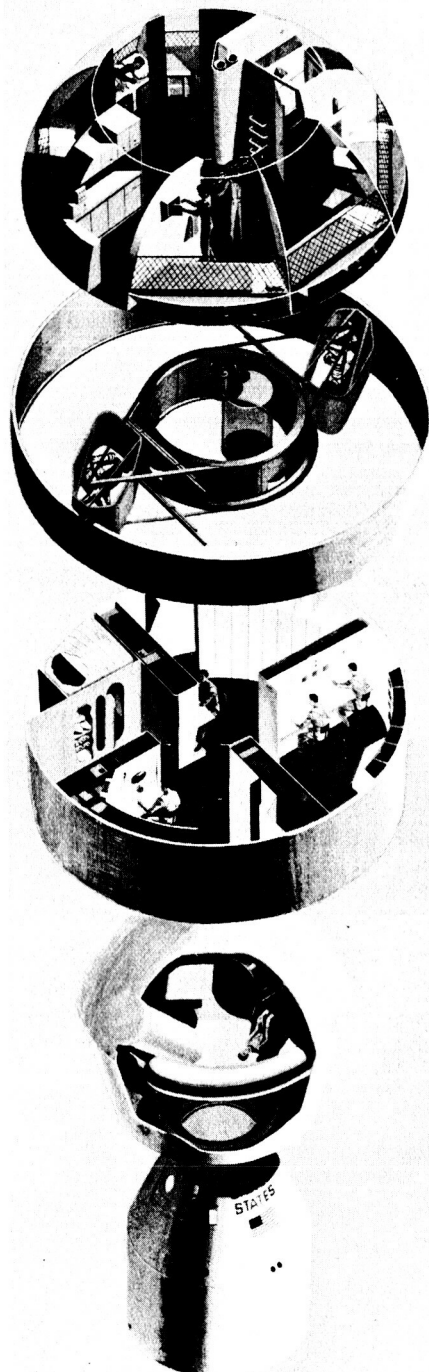
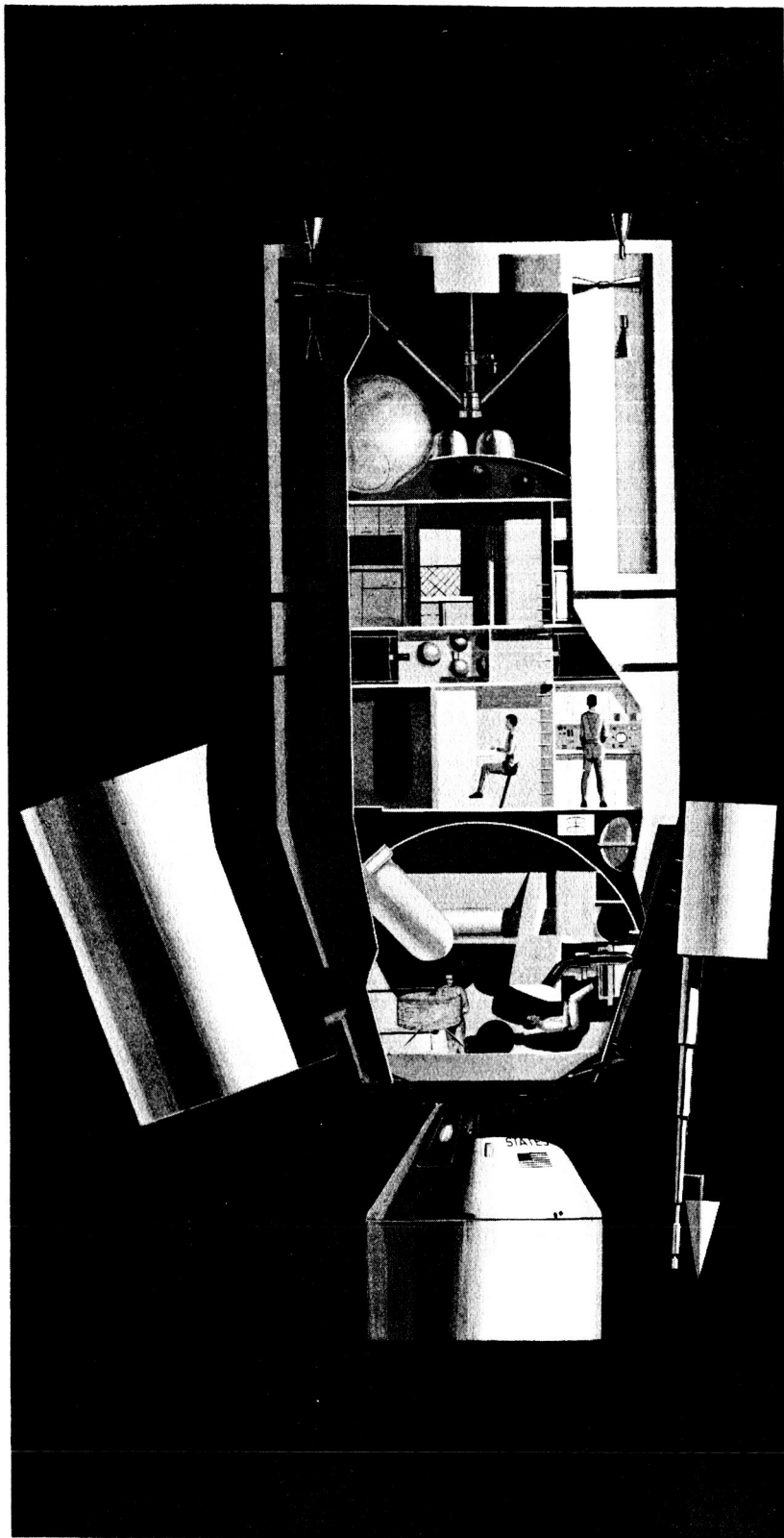
- **A Logistics Spacecraft which generally corresponds to the geometric envelope of the Apollo Command and Service Modules and which includes an Apollo Spacecraft with launch escape system and a service pack for rendezvous and re-entry maneuver propulsion; and a Multi-Mission Module for either cargo, experiments, laboratory facility modifications, or a spacecraft excursion propulsion system.**
- **A Saturn IB Launch Vehicle.**

Integration of this Logistics System with MORL ensures the flexibility and growth potential required for continued utility of the laboratory during a dynamic experiment program.

In addition to the requirements imposed by the experiment program, system design parameters must reflect operational requirements for each phase of the mission to ensure:

- **Functional adequacy of the laboratory.**
- **Maximum utilization of available facilities.**
- **Identification of important parameters for consideration in future planning of operations support.**

For this reason, a concept of operations was developed simultaneously with development of the MORL system.



PRECEDING PAGE BLANK NOT FILMED.

PREFACE

This report is submitted by the Douglas Aircraft Company, Inc., to the National Aeronautics and Space Administration's Langley Research Center. It has been prepared under Contract No. NAS1-3612 and describes the analytical and experimental results of a preliminary assessment of the MORL's utilization potential.

Documentation of study results are contained in two types of reports: A final report consisting of a Technical Summary and a 20-page Summary Report, and five Task Area reports, each relating to one of the five major task assignments. The final report will be completed at the end of the study, while the Task Area reports are generated incrementally after each major task assignment is completed.

The five Task Area reports consist of the following: Task Area I, Analysis of Space Related Objectives; Task Area II, Integrated Mission Development Plan; Task Area III, MORL Concept Responsiveness Analysis; Task Area IV, MORL System Improvement Study; and Task Area V, Program Planning and Economic Analysis.

This document contains 1 of the 5 parts of the Task Area IV report, MORL System Improvement Study. The study evaluates potential improvements to the MORL, necessitated by the limitations identified in Task Area III, and evaluates those improvements stemming from investigations aimed at increasing the effectiveness of the MORL through the addition of new system elements.

The contents and identification of the five parts of this report are as follows: Book 1, Douglas Report SM-48815, presents the summary of the Task Area effort and the results of the configuration, structure, electrical power, logistics system and performance analyses; Book 2, Douglas Report SM-48816, presents the results of the analyses performed on the Environmental Control/Life Support subsystem; Book 3, Douglas Report SM-48817, presents the results of the analyses performed on the Stabilization and Control subsystem; Book 4, Douglas Report SM-48818, presents the results of the analyses performed on the Communications and Telemetry subsystem; Book 5, Douglas Report SM-48819, presents the results of the analyses performed on the Propulsion subsystem.

Requests for further information concerning this report will be welcomed by R.J. Gunkel, Director, Advance Manned Spacecraft Systems, Advance Systems and Technology, Missile & Space Systems Division, Douglas Aircraft Company, Inc.

PRECEDING PAGE BLANK NOT FILMED.

CONTENTS

	LIST OF FIGURES	ix
	LIST OF TABLES	xiii
Section 1.	INTRODUCTION AND SUMMARY	1
	1.1 Mission Analysis Changes	3
	1.2 Changes to Upgrade the Baseline System	8
	1.3 Recommendations for Future Studies	15
Section 2	CONFIGURATION	17
	2.1 Summary	17
	2.2 Description of Baseline Changes-- External	19
	2.3 Description of Baseline Changes-- Internal	75
	2.4 Alternate Configuration Studies	83
Section 3	STRUCTURES	101
	3.1 Introduction	101
	3.2 Summary	102
	3.3 System Description	104
	3.4 Thermal Balance	164
	3.5 Meteoroid Protection	165
	3.6 Study Conclusions and Recommendations	170
Section 4	ELECTRICAL POWER SYSTEM	171
	4.1 Summary	171
	4.2 Load Analysis	174
	4.3 Isotope Brayton Cycle System	176
	4.4 Solar Cell/Battery System	192
	4.5 Comparison of the Isotope Brayton Cycle and Solar Cell/Battery Power Sources for MORL	200
Section 5	LOGISTICS SYSTEM	215
	5.1 Summary	215
	5.2 Introduction	215
	5.3 Missions	216

Section 6	PERFORMANCE OF THE MORL SYSTEM	223
6.1	Payload Requirements	224
6.2	Laboratory Weight	232
6.3	Discretionary Payload	234
Appendix A	AXIAL HANDLING AND STOWAGE SYSTEM (ALTERNATE STUDY)	245
Appendix B	SOLAR CELL PANEL SHADOWING	269
Appendix C	FLOW CHARTS	293
Appendix D	ELECTRICAL LOAD ANALYSIS	297
Appendix E	ISOTOPE COST	307
Appendix F	REFERENCES	311

FIGURES

1-1	Task Area IV Study Plan	2
2-1	General Arrangement of Phase IIb Baseline MORL	20
2-2	PBC Installation within MORL Interstage Area	23
2-3	Two-Arm Radial Stowing System	24
2-4	Radial Stowage of Apollo	25
2-5	Two-Arm Handling System	28
2-6	Radial Stow Port	29
2-7	Multimission Module Adapter Cone	31
2-8	Hangar Latch Panel	34
2-9	Stowing Operation Panel	35
2-10	Hangar Docking Panel	36
2-11	Phase IIb Attitude Reference Installation	41
2-12	Internal Sensor Beam Installation	43
2-13	MORL Experiment Bay	45
2-14	MORL with Experiment Bay in Nose	48
2-15	Alternate Experimental Bay	49
2-16	Sensor Beam in MORL Hangar	53
2-17	Structural Concept--Polar Orbit Radiation Shielding	65
2-18	Synchronous Orbit Shield Thicknesses	67
2-19	Structural Design--Synchronous Orbit Mission	68
2-20	Living Quarters (Nine Crew Bunks)	80
2-21	Living Quarters (12 Men)	82
2-22	General Arrangement of MORL with Annular Interior	84
2-23	MORL Baseline Spin Room	88
2-24	Spin Hall/Centrifuge	90

2-25	Spin Consoles/Centrifuge	91
2-26	MORL Centrifuge Experimental Console Installation	92
2-27	Artificial Gravity Parameters	94
2-28	Dual MORL Artificial Gravity Spin Deployment Version	97
3-1	Structural Concept--Phase IIa MORL Baseline	105
3-2	Structural Concept--Phase IIb MORL Baseline	106
3-3	Alternate Structural Concept--MORL	107
3-4	Corrugated Shear Webs	126
3-5	Beam Shear Web (b/t = 40) Center Section	128
3-6	Radial Stowing Port Design Details	135
3-7	Baseline Structure and Alternate Experimental Bay	150
3-8	Aft-End View of Experimental Bay Door	151
3-9	Side View of Experimental Bay Door	152
3-10	Experimental Bay Door Center Section	153
3-11	Experimental Bay Details	157
4-1	Pu-238 Brayton Cycle System Schematic	177
4-2	Pu-238 Brayton Cycle System	185
4-3	PBC Installation within the MORL Interstage Area	186
4-4	Simplified MORL Solar Cell/Battery System	195
4-5	Time Power Variations (50° Launch Inclination) Single Rectangular Extension Panel	199
4-6	Radiation Optimization	203
4-7	Power System Cost Comparison	207
4-8	Solar Cell Panel Deployment Sequence	208
5-1	Apollo Logistic Vehicle	217
5-2	Polar Orbit Logistics Vehicle	219
5-3	MORL 260-in. Diameter Laboratory, Synchronous Orbit	222
6-1	Long-Term Solar Cycle	225
6-2	Average Density Profiles	226
6-3	MORL Orbital Drag Coefficient as a Function of Angle of Attack	228
6-4	MORL Orbital Pitching Moment Coefficient	228

6-5	SCS Propellant Requirement as a Function of Orbital Altitude for 1972	229
6-6	Optimum Operating Altitude	231
6-7	Synchronous Orbit Altitudes	232
6-8	Typical MORL Ground Trace	233

PRECEDING PAGE BLANK NOT FILMED.

TABLES

1-1	Summary of Baseline System Limitations and Marginal Capabilities	4
1-2	Summary of Design Improvements	9
2-1	Sensor Mounting Activities Task Breakdown	37
2-2	Experiment Bay Utilization (Based on Experiment Plan)	39
2-3	Experiment Bay Control and Display Requirements	57
2-4	MORL Shield Requirements	59
4-1	Power Source Comparison Summary (11 kW System)	172
4-2	Housekeeping Load Analysis Summary -- Normal Operation	175
4-3	Power Source Requirements	176
4-4	PBC Subsystem Functions	178
4-5	Plutonium Brayton Cycle System Design Parameters	181
4-6	PBC System Weight Summary	187
4-7	PBC System Performance at Reduced Power Rating	190
4-8	Baseline and Updated Solar Cell/Battery System Characteristics	193
4-9	Nickel-Cadmium and Silver-Cadmium Battery Characteristics	198
4-10	MORL Launch Weight	202
4-11	Solar Cell System Drag Propellant	205
4-12	Resupply Weight	205
4-13	Solar Cell/Battery Comparison	211
6-1	Laboratory and Subsystem Weights -- Baseline 50° Inclination Mission	235
6-2	Discretionary Payload for Baseline Mission (164 nmi -- 50° Inclination)	242
6-3	Discretionary Payload for Polar Mission (164 nmi -- 90° Inclination)	242
6-4	Discretionary Payload for Synchronous Mission (19,350 nmi -- 28.3° Inclination)	243

Section 1
INTRODUCTION AND SUMMARY

The MORL Phase IIb study was intended as a further development of an improved MORL concept. The objective was to continue the assessment and analysis of space-related objectives and to incorporate the most current subsystem technology. Within this framework, the major emphasis of Task Areas I and II was to further identify the potential returns of Earth-oriented applications and to integrate these goals into the mission development plan. The goal of Task Area III was to determine the extent to which the requirements of the mission development plan could be satisfied. Additionally, any limitations of the current MORL system which might constrain system capability were to be identified for each subsystem.

Improvements and modifications to the baseline system were the major purpose of Task Area IV. These would lead to increased system capability. The changes identified were principally connected with the limitations and marginal capabilities identified in Task Area III. Changes also resulted from the evaluation of the performance growth potential of various subsystems and from the effect of new requirements on the optimized baseline system. Detailed technology requirements and the requisite development program were identified.

The Task Area IV analysis established that the MORL subsystems were highly responsive to the requirements imposed by both the mission development plan and the experiment plan. The laboratory design was found to be sufficiently comprehensive and flexible to accommodate an evolving research program. The study approach of Task Area IV is shown in Figure 1-1. It shows how limitations identified in Task Area III were incorporated in the Task Area IV study for effective resolution.

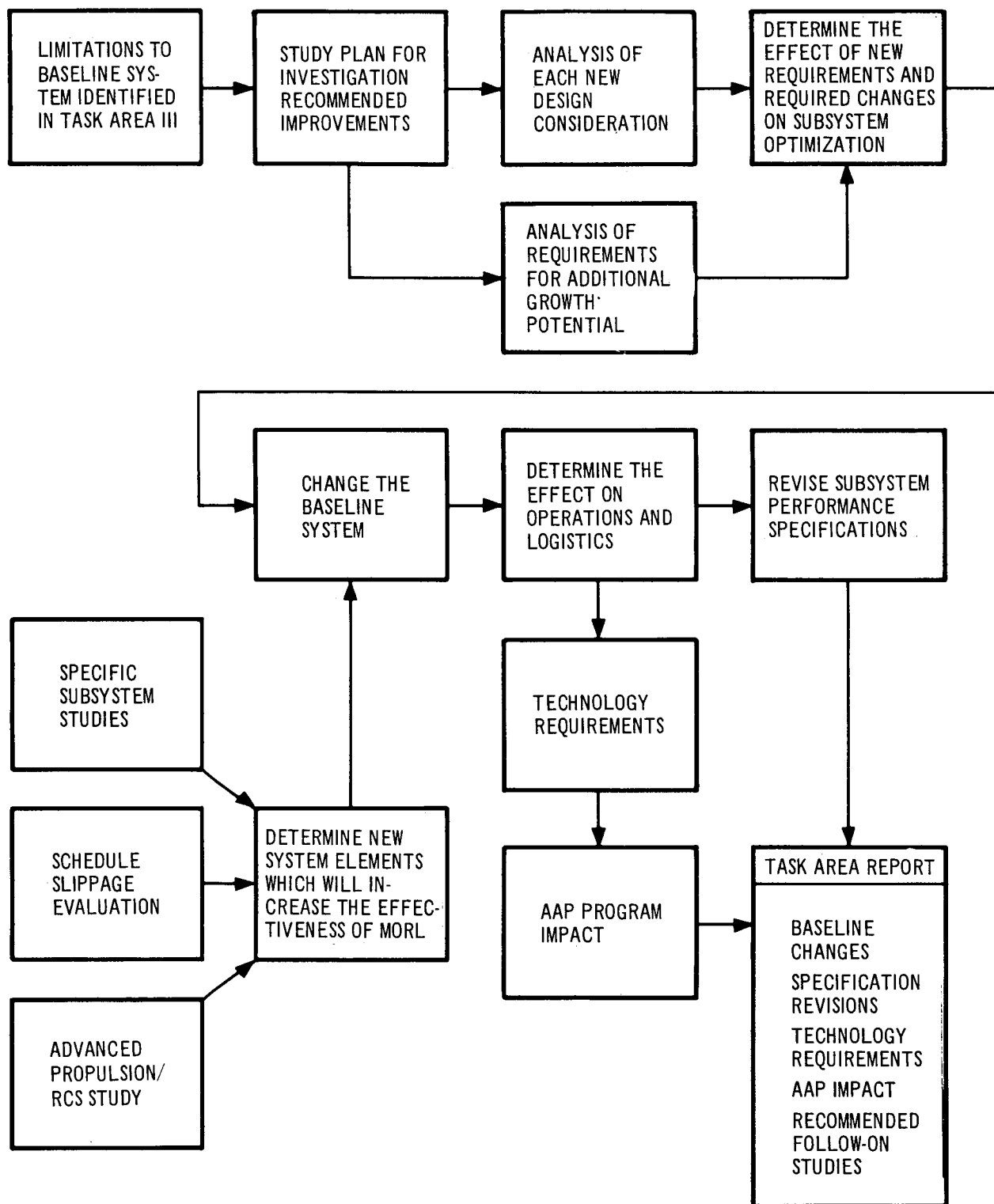


Figure 1-1. Task Area IV Study Plan

This volume describes the baseline changes in the configuration and interior design, and presents results of improvement studies for structures, electrical power, logistics, and vehicle performance. Task Area IV books 2, 3, 4, and 5, describe the Environmental Control/Life Support (EC/LS), Stabilization and Control (SCS), Communications, and Propulsion/Reaction Control (P/RCS) subsystems, respectively.

The baseline system limitation and marginal capabilities stemming from Task Area III are summarized in Table 1-1, which indicates whether the source of the requirement is mission- or experiment-oriented. Table 1-1 also identifies the corresponding mission and the recommended solution, and makes reference to the appropriate Task Area III book from which the data were taken.

1.1 MISSION ANALYSIS CHANGES

The expanded mission analysis revealed that increased radiation shielding provisions are required, particularly for the synchronous mission. The requirements are further complicated by the Starfish artificial electron source and by the solar flares expected in a 1-year period.

The radiation dose to the crew must be reduced to an acceptable level on the 50° mission; an addition of 165 lb of shielding material must be made to the laboratory aft dome to ensure crew safety. This amount of shielding will provide adequate protection for a 1-year period, including two solar flare events, and can be accomplished by increasing the dome thickness by 0.02 in. To provide the same protection on the polar mission, 1,820 lb of shield material are required; this can be provided by increasing the gage of the laboratory bottom, sides, and top dome by 0.07, 0.13, and 0.02 in., respectively. These increases can be easily attained, since the walls and domes are routed from 0.75-in. plate.

The amount of shielding required for the synchronous mission is uncertain; estimates range from 4,400 to 110,000 lb. A structural concept is presented for a 25,000-lb shield, since this is the maximum that can be tolerated when a Saturn V launch vehicle is used.

Table 1-1 (page 1 of 2)
SUMMARY OF BASELINE SYSTEM LIMITATIONS
AND MARGINAL CAPABILITIES

Item	Requirement Source		Limitation of Marginal Capability	Mission Identified with Limitation	Reference Task Area III, Book No.		Recommended Solution from Task Area III	Remarks
	Mission	Experiment						
Radiation protection	X		Limitation	50°	1		Increase provision in base-line design	
Ground contact time and tracking coverage				90°	1		Add provisions for alternate mission	
				Sync	1		Not identified	Launch payload limitation
Launch vehicle	X		Marginal	50°	1 and 2		Add station (Hawaii) to network	
			Limitation	90°	1		Add stations (Hawaii and Guaymas) to network	
Communications	X		Limitation	90° and Sync	1		Use Saturn V launch vehicle	Requires use of a high-gain antenna onboard MORL
EC/LS radiator	X		Marginal	Sync	1		Add unified S-band capability	
Experiment pointing and tracking		X	Limitation	50°	1		Resize (remove 13 tubes)	
							Mount experiment sensors on gimbals	
Gyrocompassing accuracy of 0.5°	X		Marginal	50°	1		Substantiate 0.5° accuracy by analysis and simulation	Applicable to experiments without slewing requirements
Attitude reference accuracy of 0.1° to 0.01°		X	Limitation	50°	1 and 2		Mount sensors on a common rigid base. Perform accuracy analysis. Incorporate in-flight alignment and calibration	Effects of errors associated with sensing, alignment, crew motion, etc., must be considered
							Determine magnitude and type induced by crew motion	Future study required
Ventilation provisions in Hangar/Test area		X	Marginal	50°	1		Add separate air ventilation circuit in Hangar/Test area	
Experiment consoles		X	Marginal	50°	1 and 2		Add console in Hangar/Test area and increase size of console in operations/experimental area	

bay installation). Control of attitude accuracies in excess of this is beyond the capability of the SCS precision stellar-inertial reference and imposes the requirement for experiments to supply their own error-sensing and control.

A significant propellant saving is achieved by a combined operation mode, made possible by sizing the CMG for all normal attitude maneuvers. When the laboratory is in belly-down mode, it utilizes all reaction control system impulse for orbit keeping and is also used for unloading the momentum storage system (control moment gyros).

Tracking, command, and data transmission coverage were found to be limited for the 50° and 90° missions. Increased ground contact time and tracking coverage requirements imposed on the communications and data management system can be met by adding additional tracking stations. For the 50° mission, a station will be required in Hawaii to meet the required 45 min. /day ground contact time. The addition of stations in Hawaii and Guaymas will fulfill the requirements for the 90° inclination orbit. Deletion of the unmanned resupply vehicle simplifies communications and data management by eliminating the requirements for a backup system.

The baseline data management subsystem was found to be limited in meeting the high data rate requirements for data handling, storage, video, and voice resulting from the new mission and experimental requirements. An advance data management concept has been analyzed, and is at the point of preliminary definition.

For the rf unification analysis, the Apollo unified S-band system has been analyzed to determine its adaptability to the baseline MORL signal complex. An adaptation has been deemed feasible, but final decision on a unified rf system for MORL should not be made until further definition of the signal complex.

In the area of data compaction, a survey of data redundancy reduction techniques and related experiments was made. It was concluded that an approximate average gross pulse control modulation (PCM) data reduction ratio of

10:1 could be expected. The necessary data tagging required for ground decommutation, within the context of the baseline PCM channel configuration, results in a net effective reduction ratio for MORL of approximately 2.85:1.

Further analysis of data system requirements is necessary before any recommendation on data compaction can be made.

1.2 CHANGES TO UPGRADE THE BASELINE SYSTEM

A total of 14 baseline changes are summarized in Table 1-2. The changes are either technology time-oriented or design refinements.

The greatest effect on the laboratory involves selection of the Pu-238 Isotope Brayton Cycle (PBC) power system as a replacement for the solar cell/battery power system. This change was the result of an extensive improvement analysis study and it reflects changing technology; the solar panel selection was greatly influenced by an anticipated 1968 to 1969 launch date. Selection of the PBC system provides operational improvements by removing the hazard presented by the solar cells during rendezvous, docking, and extravehicular operations.

In addition, a source of high atmospheric drag was removed which has imposed a significant propellant penalty on the system. The PBC system offers the advantage of serving as a direct source of thermal power to the EC/LS system. Heat transfer for this system is provided from PBC system waste. (A more detailed discussion of the selection of the PBC system is provided in Section 4 of this Volume.)

Deletion of the solar panels resulted in major change to the baseline SCS. Since solar orientation of the laboratory is no longer required, a primary orientation was selected, maintaining one side of the vehicle facing the Earth. This is referred to as the belly-down orientation, and its impact on the SCS system is discussed in Book 3.

Table 1-2 (page 1 of 2)
SUMMARY OF DESIGN IMPROVEMENTS

Phase IIb Design Change	New Baseline Design Feature	Impact on System
Delete solar cell/battery power system	Pu-238 Isotope Brayton Cycle Power (PBC) system	Removes rendezvous/docking docking and EVA hazard Reduces propellant penalty imposed by high atmosphere drag of solar panels Provides waste heat to EC/LS system
Delete solar orientation requirement	Adopt Earth-oriented (belly-down) orientation	Facilitates Earth-oriented measurements Reduces propellant consumption caused by decreased atmospheric drag (improved drag profile)
Replace seven-arm logistics vehicle stowing mechanism	Adopt two-arm stowing mechanism	Reduces complexity of design; increase reliability Reduces launch weight
Provide access to logistics vehicles and multimission modules in pressurized environment	Add six radial stowing parts in Hangar/Test area	Reduces EVA time Provides quick abort capability
Remove domed bulkhead between Hangar/Test area	Redesign floor to serve as compartmenting bulkhead	Provides space required for radial stowage ports Provides space required for experiment bay
Delete all-welded construction used to connect and seal circumferential joints	Redesign to bolted joints with O-rings	Increases flexibility in check-out, assembly, and modification

Table 1-2 (page 2 of 2)

Phase IIb Design Change	New Baseline Design Feature	Impact on System
Increase length of cylindrical portion of outer shell by 38 in.	Relocate EC/LS radiator to forward portion of outer shell cylinder	Provides area required by PBC power system radiator
Replace truss grid honeycomb core conical portion of outer shell	Change core to brake-formed corrugations	Provides required heat transfer between radiator tubes and radiating surface
Delete EC/LS system cryogenic storage and transfer systems	Provide oxygen by electrolysis of water and gaseous nitrogen	Decreases costs and complexity of design; increases reliability
		Allows use of wet foods
Replace separate waste collection, processing, and storage system	Provide combined hardware	Increases operational flexibility and capability (9 men)
Provide for oxygen regeneration mode	Provide carbon dioxide collection capability (retrofit required to close oxygen cycle)	Decreases complexity of design; increases reliability
Change propellant system from IRFNA/MMH to NTO/MMH	Provide increased performance of bipropellant system (I_{sp})	Eliminates oxygen resupply problem when activated
Reduce long-term operating altitude from 200 nmi to 164 nmi and inclination from 28.72° to 50°	Provide maximum attitude control performance for 1972 initial operational period	Reduces propellant consumption and system weight
		Maximize useful MORL payload
		Maximize system logistics capability
		Provide repetitive orbit traces (3-day cycle)

Sections 2 and 3 of this Volume discuss significant baseline changes made in the configuration and structural design areas. Briefly, modifications include the following changes:

1. Redesign of the floor, and removal of the hemispherical bulkhead between hangar and operations area.
2. Reduction of logistics vehicle stowing arms from seven to two.
3. Use of O-ring-sealed bolted flanges to connect and seal the three circumferential joints.
4. Extension of the MORL interstage.
5. Modification of the conic section structure.

The redesign of the floor between the hangar and operations area and removal of the hemispherical bulkhead provides additional usable volume, permits better space utilization, and allows room for radial stowing of logistics vehicles. Radial stowing at six separate ports in the Hangar/Test area allows ready access to the stowed vehicles with all the associated benefits of a flexibly sized laboratory. A significant saving in weight and complexity was accomplished by reducing the vehicle stowing arms; reliability requirements dictated a dual-arm design rather than a single-arm system.

The change to O-ring-sealed bolted flanges to connect and seal the three circumferential joints was based on test data gained during the year. This concept has also been successfully tested at Langley Research Center. It permits flexibility in initial checkout and assembly and subsequent modification greater than provided by the all-welded construction, which required removal of equipment through the airlock hatches.

Although the PBC system removed the shadowing problem from the radiators located in the external walls of the laboratory, the increase in power to 11 kW and the associated increase in heat rejection made it necessary to enlarge the radiator area. The increase from 6 to 11 kW was caused primarily by the increased housekeeping requirements and the expanded experimental program. The housekeeping loads increased from 3.25 to 6.2 kW as a result of increased EC/LS power, increased lighting requirements, and increased logistic requirements. The EC/LS changes account for more than 2.0 kW and the expanded experimental program account for 3.0 kW.

A 15% reserve is allowed for contingencies, resulting in the 11.0-kW requirement at the alternator terminals of the PBC system. To accommodate the additional radiator surface, the MORL interstage was extended 38 in. and the conic section structure was modified to incorporate radiator tubing for an oxygen regeneration mode EC/LS system.

The EC/LS system was redesigned to operate in three different modes other than a single mode (as in Phase IIa). The three modes are (1) basic, (2) nine-man crew, and (3) oxygen regeneration operating modes. The basic mode accommodates a six-man crew and has a completely closed water cycle and an open oxygen cycle, as in the Phase IIa design. However, the current system provides oxygen by the electrolysis of water which is resupplied as required rather than by the resupply of cryogenic oxygen. The nine-man crew mode is capable of functioning for indefinite periods of time without compromising crew safety and with only a slight decrease in operating efficiency and reliability. The current system can also be operated in a closed oxygen cycle mode when appropriate equipments are supplied. This mode has not been available previously.

The atmosphere supply subsystem provides a 147-day supply of oxygen for 6 men. Oxygen stored in the form of water and gaseous oxygen is provided by electrolyzing the water in five electrolysis modules to produce breathing oxygen. Hydrogen will normally be vented overboard. The electrolysis modules may be shut down to conserve electrical power for experiment purposes when required. Three modules have sufficient capacity for a six-man crew and five modules will fulfill needs of a nine-man crew. For a nine-man crew, the water required to satisfy the oxygen needs of the additional three men will be stored in a cargo module and transferred to the MORL tanks as needed.

The waste management system has been redesigned so that waste collection, processing, and storage are combined, eliminating the need for separate hardware for each function. Manual handling of wastes has also been eliminated; crew time in this area is reduced by approximately 15 man-minutes/day.

Incorporation of a larger power system has increased the air heat load on the main laboratory cooling and ventilation circuit, and its capacity has therefore been increased. A separate ventilation circuit was also designed for the Hangar/Test area to accommodate the expected increased usage of this area.

Redesign of the cooling circuit was required to accommodate the change to an 11-kWe PBC system and the oxygen regeneration mode. Size of the EC/LS radiator was increased in order to reject the heat from the additional electrical energy being dissipated. The isotope heating circuit required in Phase IIa was eliminated because waste heat from the BPC system supplies this need.

The change in mission initiation (1972 rather than 1968) has had significant effect on operating altitude. The involved factors are lower-density atmosphere, removal of the solar panels, and altered laboratory primary flight attitude. Long-term orbital characteristics were changed from a 200-nmi altitude and 28.72° inclination to a 164-nmi altitude and a 50° inclination (based on a tradeoff analysis using a 5-year mission with 20 Saturn IB/Apollo logistics appointments). The altitude operating band is 145 to 165 nmi, which represents a tradeoff between logistics spacecraft payload performance and MORL propellant usage. An altitude of 164 nmi at a 50° inclination was chosen, to allow the tracking and communication benefits of a subsynchronous laboratory orbit (repeatable trace three-day cycle).

Investigation of an updated baseline propellant/reaction control system (P/RCS) and an advanced P/RCS resulted in the definition of updated bipropellant, Resistojet, and radioisotope thruster systems which were then integrated with the MORL system. The updated bipropellant system was selected as the MORL Phase IIb baseline P/RCS.

The propellant combination selected for the updated bipropellant system is NTO/MMH. Phase IIa used the IRFNA/MMH combination. This propellant combination results in increased system performance and reduced total system weight. The thruster logic utilized for the updated bipropellant system also allows a system weight saving by reducing the P/RCS total impulse requirement.

Both hydrogen and ammonia propellants are candidates for the advanced Resistojet and radioisotope thrusters. Although the hydrogen system provides a higher specific impulse (and therefore minimum propellant consumption) it requires cryogenic storage, increasing total system weight.

Thrust levels selected for the thruster systems are based on the zero-g baseline orientation. This orientation utilizes the belly-down mode with 4-hour/day excursions for inertial orientations. Thrusters of 100- and 50-lb thrust were selected for the baseline system. A thrust level of 9.8 mlb was selected for the Resistojet thrusters and thrust levels of 16 and 4 mlb were selected for the radioisotope thrusters. Engines of 100-lb thrust were selected to perform all high-thrust mission requirements for both the baseline bipropellant systems and the advanced systems. The orbit injection system for all systems consists of four 100-lb thrust engines, all utilizing the same NTO/MMH bipropellant combination. For the baseline bipropellant system, attitude control is provided by the 50-lb engines. For the advanced systems, roll control is performed by separate 100-lb bipropellant engines. The maximum power demand for the hydrogen Resistojet system is 1.16 kW electrical. This represents approximately 10% of the total PBC capacity.

Because of the logistics and accessibility problems associated with tank transfer a propellant resupply system was found preferable to transferred tanks, although the logistics launch weight is about 75 lb heavier.

Sufficient biowastes (CO_2 , H_2) are available to satisfy the propulsion RCS requirements for the MORL mission. However, the combined MORL system resupply weight can be reduced by 985 lb (for a 90-day period) if a P/RCS utilizing biowaste with a water electrolysis life support system is used. Further detailed tradeoff study is required before a final system can be recommended.

1.3 RECOMMENDATIONS FOR FUTURE STUDIES

The most urgent areas for continued studies are in the Communications/Data Management System, the SCS, and the P/RCS. Areas of particular interest are as follows:

1. Digital or analog transmission tradeoff analysis.
2. Autonomous navigation for MORL.
3. RF unification analysis.
4. Low-thrust P/RCS.
5. Crew Motion Studies--Simulation (in-flight testing) of more realistic models; major impact on CMG torque and momentum sizes.
6. Attitude Reference Studies--Performance analysis to include all error sources (navigation, alignment, and within the experiments).
7. CMG Configuration Selection--Establish values for unassigned laboratory resources (weight, volume, and time), and note effects on CMG.

Section 2 CONFIGURATION

The baseline configuration defined by the system specification (Reference 1) at the close of the MORL Phase IIa study was evaluated to determine its compatibility with the requirements of an expanded experimental program and the 50°, polar, and synchronous orbit missions. In addition, proposed improvements and desirable modifications were evaluated to determine their applicability as baseline revisions; certain of the improvements are clearly beneficial to the laboratory and are adopted as baseline changes. Others, although not adopted by the baseline, are sufficiently valid to be given future considerations.

2.1 SUMMARY

The following text discusses the baseline changes added to the revised system specification, outlines problem areas chargeable to the alternate missions, and identifies alternate concepts and studies which should be pursued in future MORL studies.

2.1.1 Baseline Specification Changes

Analysis of the updated experimental program necessitated the following changes:

1. A sensor mounting beam has been added to the Hangar/Test area to maintain experiment sensor alignment accuracy to within $\pm 0.1^\circ$, by providing close tolerance mounting surfaces and control of structural and thermal stresses.
2. A pressurized experimental bay has been added to the Hangar/Test area to provide a shirt-sleeve environment for the installation, replacement, and service of sensors and experiments; this change significantly reduces requirements for extravehicular activity.
3. An experimental console has been provided in the Hangar/Test area to allow the conduct and the control of experiments located in the Hangar/Test area.

4. An enlarged scientific test console has been provided to assure experimental flexibility and to increase experimental capability.

Analysis of the proposed missions resulted in the requirement for additional radiation shielding. Increase of the material gage of the pressure shell dome of the laboratory by 0.02 in., at a cost of 165 lb, provided adequate shielding for the baseline 50° mission. Shielding for the polar orbit mission can be accomplished with the addition of about 1,800 lb of shielding added as 0.13 in. to the sidewall and 0.072 in. to floor structure. Synchronous orbit shielding cannot be adequately defined without additional knowledge of the radiation environment and protective criteria; however, an exploratory approach is presented to further the understanding of the difficulties encountered.

Studies of proposed laboratory improvements indicated sufficient advantages to justify the following changes:

1. The electrical power generating system has been changed to an Isotope Brayton Cycle system; this resulted in deletion of the solar panels and a 38-in. extension of the laboratory aft interstage.
2. The seven-arm logistics vehicle stowage mechanism has been reduced to a two-arm system, resulting in reduced complexity and weight.
3. The logistics vehicle and experimental modules are stored in six radial ports located in the Hangar/Test area, enabling shirt-sleeve access.
4. A flat common pressure bulkhead has replaced the domed bulkhead between the Hangar/Test area and the operations deck, providing space for the radial stowage ports and increased volume in the experiment bay.

2.1.2 Alternate Candidates for Future Baseline Revisions

The operational advantages of the Isotope Brayton Power system over the solar cell/battery system are clearcut. However, there is a possibility that the isotope fuel blocks will not be available or launch approval will not be obtained for an operational MORL; configuration studies therefore should continue to allot space provisions for a solar cell/battery system.

The need for a dual MORL artificial gravity spin system, to provide a zero-g facility while the laboratory is spinning, requires further evaluation. One concept which has been investigated involves two MORL's spinning about each other; an intermediate section, at the CG of the spinning system has a counterspun multimission module attached. However, need for this added complexity has not been established.

Continued analysis of the MORL configuration is also required. An alternate annular structural arrangement described in Section 2.4 has potentially a more simple interior than the baseline arrangement; the sleeping quarters may also be more readily converted to a radiation-protected biowell, should the laboratory be placed in either the polar or the synchronous orbit. The experiment bay must largely be sized and arranged by continued definition of the experiment program; in addition, there should be further exploration into locating the sensor mounting beam either on the MORL exterior or completely within the experiment bay.

2.2 DESCRIPTION OF BASELINE CHANGES--EXTERNAL

The revised MORL shown in Figure 2-1 has been designed to function in either a zero-g or rotating mode, to meet the following requirements:

1. MORL launch on a Saturn IB for the baseline mission.
2. The nominal crew of six astronauts, with provisions for up to three additional crew members for extended periods, with added logistics.
3. MORL must accommodate a diversified experimental program; adequate volume and subsystem capacity for experiment growth and flexibility must be provided.
4. A shirt-sleeve environment for crew and cargo transfer from the logistics spacecraft to the MORL.
5. Accessibility to allow repair of the vehicle shell, structure, and component parts.
6. All doors must be operable from either side.
7. No propellant lines can pass through the pressure shell; water is the only fluid used for heating and cooling circuits within the pressure shell.
8. No equipment mounted directly to the pressure shell.

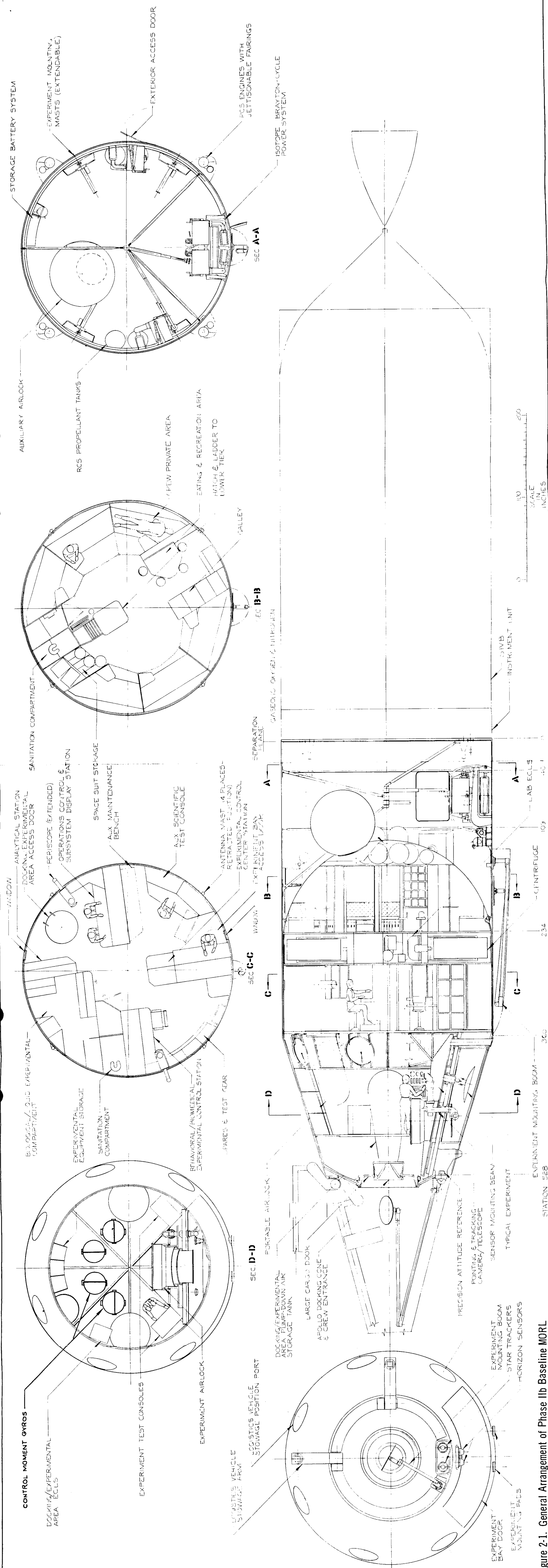


Figure 2-1. General Arrangement of Phase IIb Baseline MORL

9. MORL operations must not be interrupted for normal maintenance and repair of subsystems; adequate redundancy must be available for all critical subsystems.
10. Equipment necessary for minimal operation of the MORL must be operable by a crewman dressed in a pressure suit and biopack, with gloves on and visor closed. This capability must apply either at the time of initial manning or subsequently in the event of atmospheric depressurization.
11. Equipment installations will be designed to satisfy the following requirements:
 - A. All surfaces in contact with the laboratory atmosphere must be above the atmospheric dew point.
 - B. All surface areas which the crew can touch must be below 120°F.
 - C. All external surfaces which may come in contact with pressure suit must be below 200°F.

The Hangar/Test area, located at the forward end of the vehicle, provides for transfer of crew and cargo between the MORL and the logistics spacecraft in a shirt-sleeve environment. The docking port is mounted on the forward section of the outer structure to prevent the docking loads from being transmitted directly to the pressure shell; the six radial stowage ports are also located in the Hangar/Test area, between the flat floor support beams which carry the stowed vehicle loads in the event of artificial-g spinup. Aft of the Hangar/Test area, and separated by a common pressure bulkhead, is the Operational/Experimental area, the primary work station of the vehicle.

2.2.1 Isotope Brayton Power System

This section describes the changes in configuration resulting from the installation of the Isotope Brayton Power system in the MORL vehicle; the comparisons and justifications for making this change are covered in detail in Section 4.

A major consideration in locating the isotope power system was the potential radiation dosage to the crew. Since the radiation dose is inversely proportional to the square of the separation distance between the crew and the power source, the most attractive locations were (1) the Hangar/Test area,

(2) the interstage area, or (3) an extended location on a boom. The latter was rejected because of additional complexity, necessity of extravehicular activities for maintenance and repair, and potential interference with experimentation. The interstage location was selected on the basis of minimum interference with experimental activities in the Hangar/Test area, the requirement for emergency access to space for heat dump, and the convenience of radiator installation on the interstage area. The Isotope Brayton Power system installation in the interstage area is shown in Figure 2-2. The major configurational changes are (1) the extension of the interstage area by 38 in. to provide the necessary radiator area, (2) the deletion of the solar panels and deployment mechanism, and (3) the addition of two heat dump doors for the fuel blocks and one access door for installation of the power units in the area during maintenance periods.

The interstage extension structure used the same construction as the basic shell structure; it consists of the same material gages and radiator assembly; the weight of the extension is approximately 240 lb. Some local stiffening is necessary for the doors and power system attach structure, but these are not sufficient to cause a variation in the basic structures from the baseline; a more detailed description of the structure is noted in Section 3 and in Reference 2.

Deletion of the solar panels and the extension of the interstage result in a volume increase of about 2,300 cu ft, which is satisfactory for the installation requirements of the power generating system and its associated handling equipment. The volume is also available for experiments which require zero g and/or space pressure, although the radiation and temperature environments are higher than the space ambient because of the isotope fuel blocks and the radiators. External installation of equipment and experiments is also simplified by the solar panel deletion; problems associated with shadowing, interference, and RCS impingement on the panels are eliminated.

2.2.2 Two-Arm Logistics Vehicle Handling System

The Phase IIa baseline system provided a handling system with seven separate arms and a rotary ring. During Phase IIb, methods of reducing the

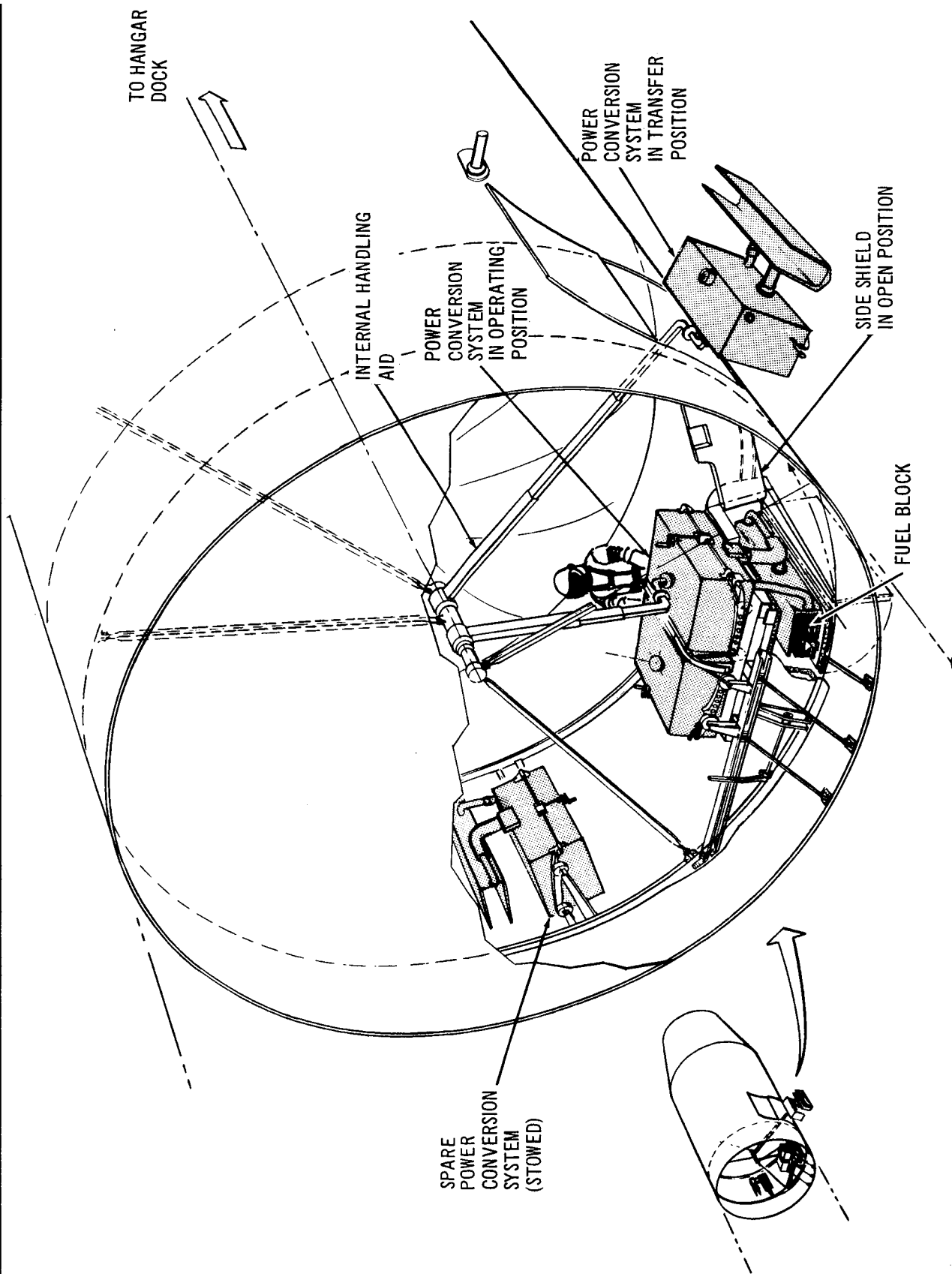


Figure 2-2. Plutonium Brayton Cycle Installation within MORL Interstage Area

complexity of the system were studied, with the goal of better performance, simplicity, and reduction in weight and cost. A two-arm stowage system was designed and incorporated into the baseline configuration, and comparison of the two systems showed the large weight savings offered by the two-arm system. In addition (1) the total number of components used is reduced, (2) the reliability of the stowage system is improved by providing two arms, each capable of servicing each stow position, and (3) the circular track provides potential experimental flexibility.

The baseline configuration of the two-arm handling system is shown in Figures 2-3 and 2-4. The system consists of (1) two arms with movable carriages and attaching latches, (2) a fixed circular track mounted on the front face of the hangar structure, and (3) two powered pivot-post assemblies which move around the circular track. Each of the two arms has a movable carriage which is used for attaching the stowage arm to the vehicle to be

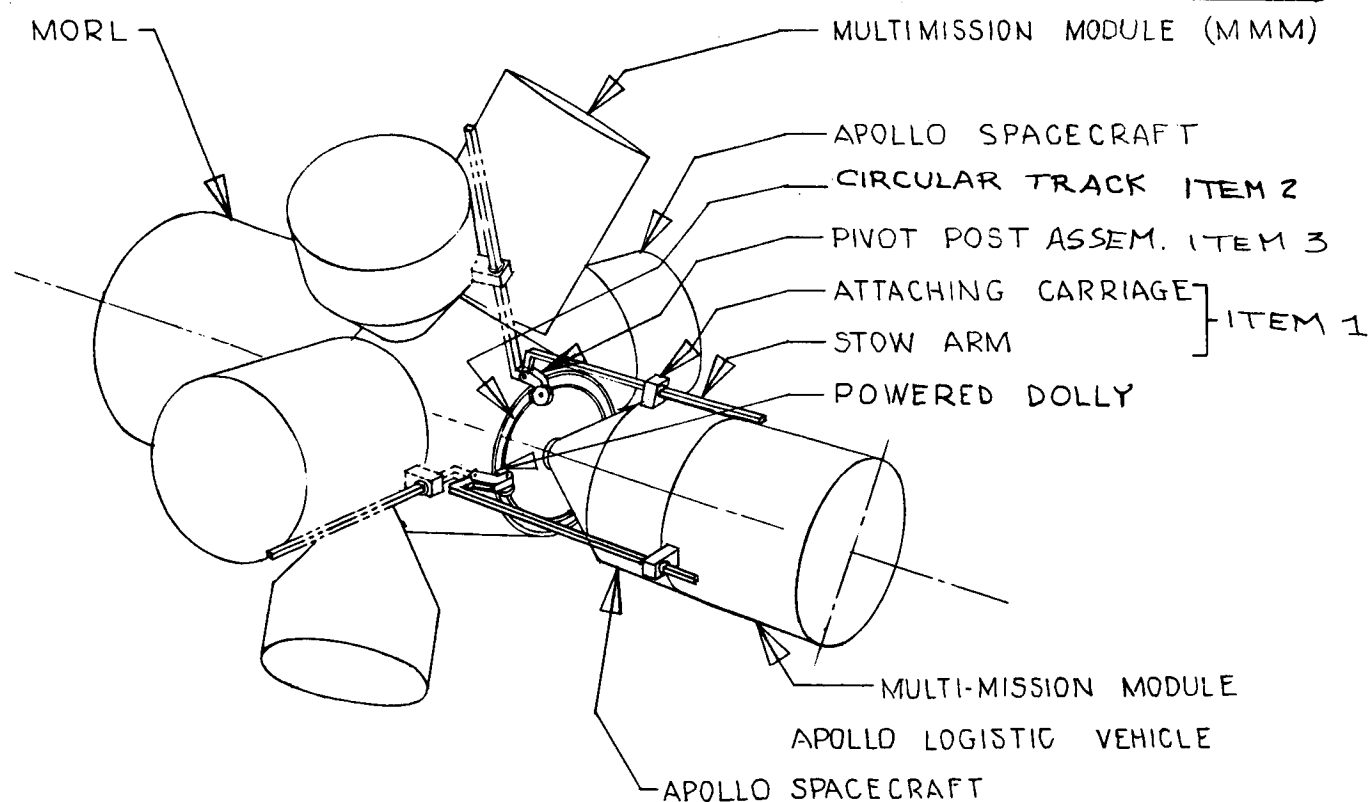


Figure 2-3. Two-Arm Radial Stowing System

Table 1-1 (page 2 of 2)

Item	Requirement Source		Limitation of Marginal Capability	Mission Identified with Limitation	Reference Task Area III, Book No.		Recommended Solution from Task Area III	Remarks
	Mission	Experiment						
Experiment bay		X	Limitation	50°	2		Provide means of mounting equipment sensors inside laboratory	Reduces EVA events required for installation, calibration, maintenance, and removal of external experiment sensors
Communications and data management		X	Limitation	50°	1 and 2		Redesign subsystem to increase capability, capacity, and flexibility	
Tracking and command data coverage		X	Limitation	50°	2		Limit the scope of data coverage required by the experiment. Investigate autonomous navigation for MORL application	

The Phase IIa baseline EC/LS system was found to be larger than necessary for the synchronous orbit. The heat influx from the sun and the Earth in this orbit is lower, so that the required radiator capacity is reduced by approximately 30%. As a result, 13 of the 41 tubes can be deleted. It would be desirable to change the EC/LS radiator for the synchronous mission to prevent the radiator fluid from freezing when the laboratory is in the Earth's shadow; a minor weight reduction is also achieved.

Another significant change to the baseline system was the requirement for an experiment bay in the Hangar/Test area. It contains the vehicle attitude reference system and sensors for a number of experiments; these could not be efficiently accommodated by the baseline design. The design includes a sensor mounting beam, equipment for precise mechanical alignment of sensors, and provisions for pressurization of the compartment to permit installation, replacement, calibration, and maintenance of this equipment in a shirt sleeve environment. Provisions will also be made to allow the direct attachment of larger sensors to an external continuation of the mounting beam contained in the experiment bay.

Further analysis of the basic stabilization and control mode (horizon sensor/gyrocompassing), used for routine belly-down stabilization, substantiated the feasibility of holding attitude to $\pm 0.5^\circ$ in the presence of anticipated disturbances.

A detailed examination of the data bank experiment requirements showed that there is need for extensive use of gimballed mounts to isolate experiment sensors from laboratory motions where the capability of the laboratory stabilization and control system (SCS) is exceeded. Crew motion, which is expected to induce laboratory rates of nominally $0.01^\circ/\text{sec}$, represents an important category of transient disturbance, and influences the need for dynamically isolating experiment sensors. Further study and examination in this area is required.

Precision experimental tolerances require that the experiment sensors and attitude reference instruments (in the 0.1° to 0.01° range) be relocated on a common, rigid mounting base (described above as part of the experiment

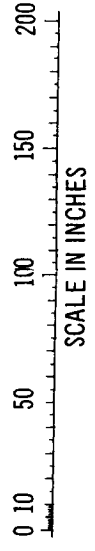
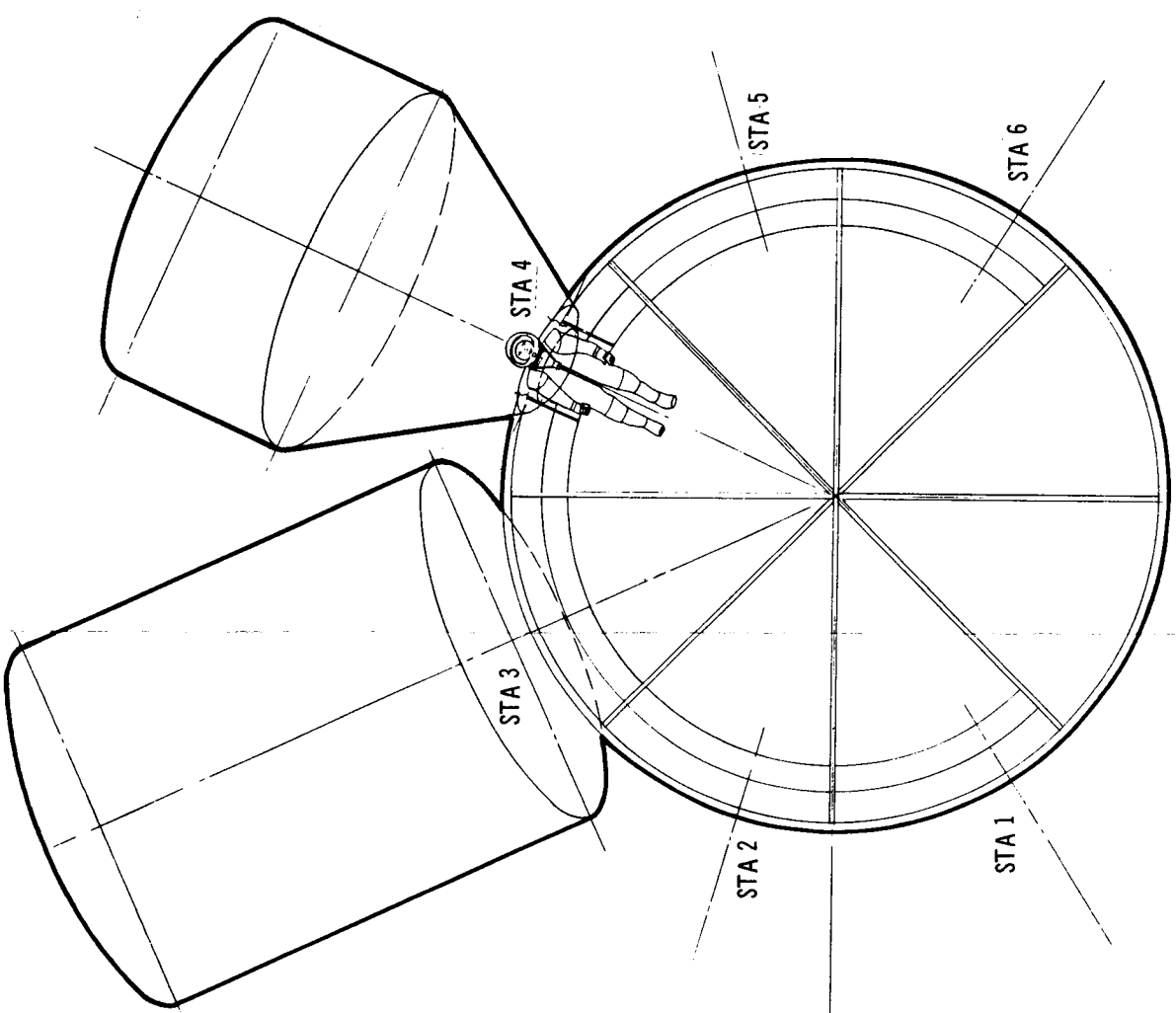
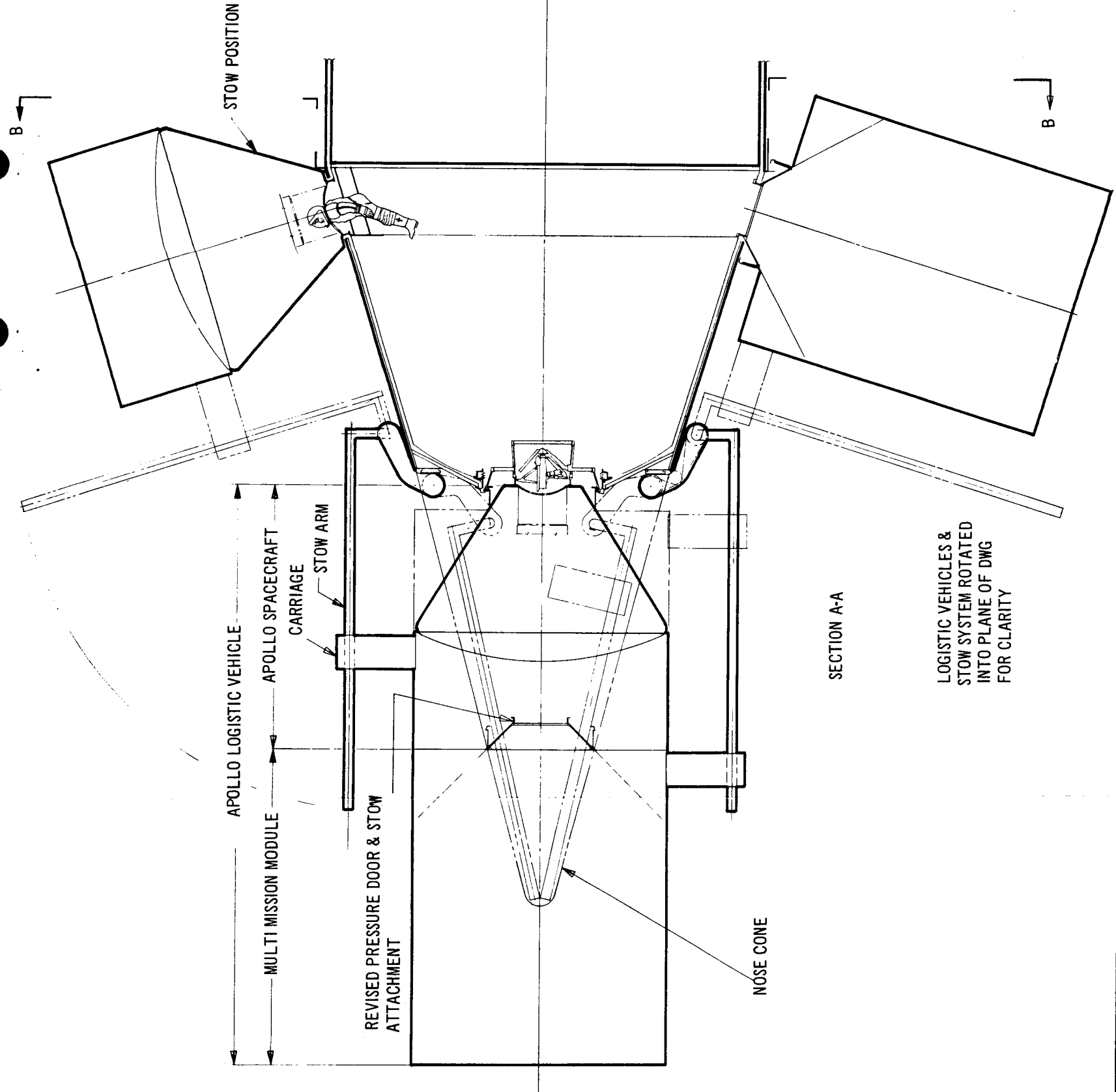
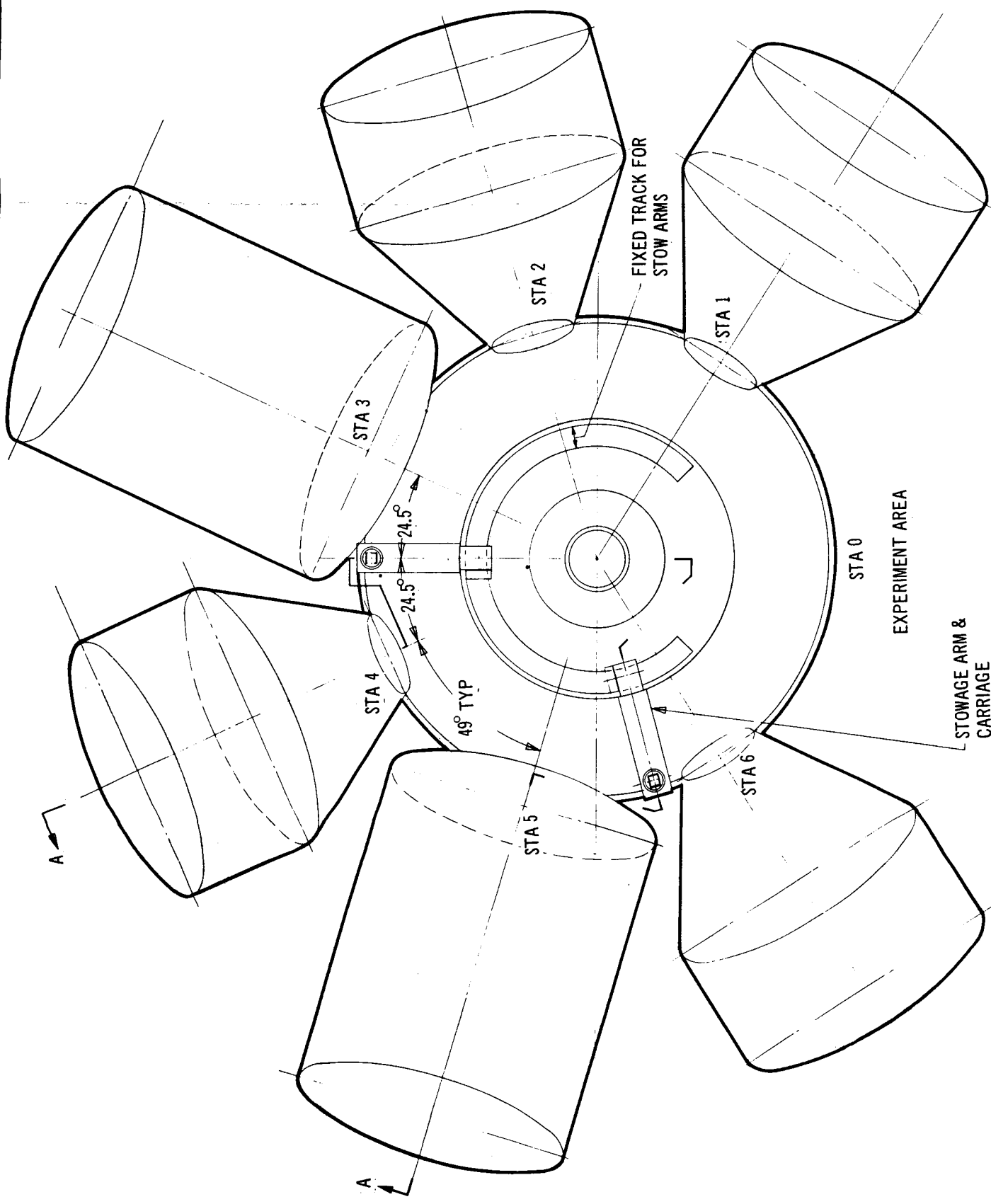


Figure 2-4. Radial Stowage of Apollo

moved. The stowage arms are mounted on pivot posts which enable rotation of the arms in a plane through the MORL longitudinal axis; each pivot post is mounted on a powered dolly which moves along the circular track to locate the arm and carriage into position for attachment to the logistics vehicle. A docked vehicle is stowed by rotating the arm and carriage into the plane of the logistic vehicle attachment point by moving the pivot post along the track; the carriage is then moved along the arm until it mates with the attachment point of the logistic vehicle; the vehicle is separated from MORL and the pivot-post assembly is again moved along the track to place the stowage arm and logistic vehicle into the desired stowage port plane; the arm, carriage, and logistic vehicle are next rotated 180° about the centerline of the arm, and then both arm and vehicle are swung about the pivot post until the longitudinal axis of the logistic vehicle is aligned with the axis of the stowage port; finally, the arm carriage is moved along the arm until the vehicle is mated to the stowage port.

The powered pivot-post assembly consists of the pivot-post mast and a powered dolly on which a motorized drive and hangar is mounted; this supports a shaft and integral double cable pulley. The shaft-mounted pivot post is supported on bearings and is free to rotate about the shaft centerline. At the opposite end, bearings pressed into the pivot-post structure support a shaft to which a double-cable pulley and the stow arm are integrally mounted.

Cables are rigged between the upper and lower pulleys to provide positive drive for the stow arm in both directions. The pivot posts and stow arms are stored within the nose cone in the launch phase. After the nose cone is jettisoned, the drive motor is activated, rotating the stow arm until the arm stop hits the pivot-post position. The torque is transferred from the arm to the pivot post, which then starts to rotate about the lower shaft at the drive position; rotation continues until the pivot-post assembly reaches the operating position; here it is tied to the powered dolly by two lock pins, and the drive motor is turned off. The pivot post and its mounting on the powered dolly, and the stow arm and attaching carriage are similar in concept and design to the corresponding parts shown in Figure A-2 of Appendix A.

The powered dolly assembly is mounted on the fixed circular track, Item 2. It is powered and driven through a gear-reduction drive; rotation is achieved by an open gear driving against a large ring gear, mounted to the circular track. The circular track was discontinued for the lower 90° of the arc, to provide clearance for the star trackers.

The following is a step-by-step description of the stowage arm handling system from docking to stowage of an Apollo spacecraft and a multimission module (MMM), (Figure 2-5).

Step 1 Arm activation

Item 1--Nose cone is jettisoned shortly after first stage burnout.

Item 2--Stow arm and pivot posts are rotated into the operating position and locked. Arm No. 2 is moved to the docking index point, and Arm No. 1 is moved near stowage station No. 1.

Step 2 Apollo logistic vehicle docks to MORL

Crewmen leave Apollo and enter MORL upon successful completion of a logistics vehicle dock (Reference 3). Before the logistic vehicle can be moved from the docking port, the hangar entrance door is closed and sealed. First the probe is removed from the Apollo spacecraft and left in the hangar area, and the Apollo tunnel door is replaced and sealed; the door in the hangar docking structure is then closed and sealed, and the desired stowage position outer meteoroid protection door is opened.

Step 3 Separation of Apollo and MMM

Item 1--Arm No. 2 and attaching carriage is moved to mate with the Apollo spacecraft attaching point, where it is latched.

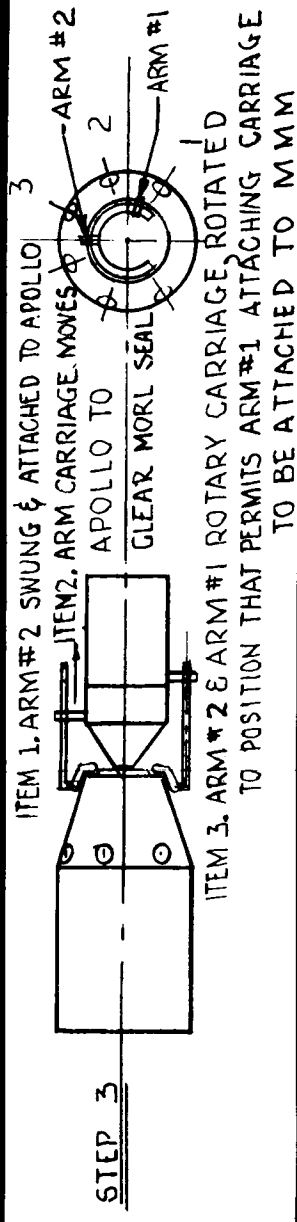
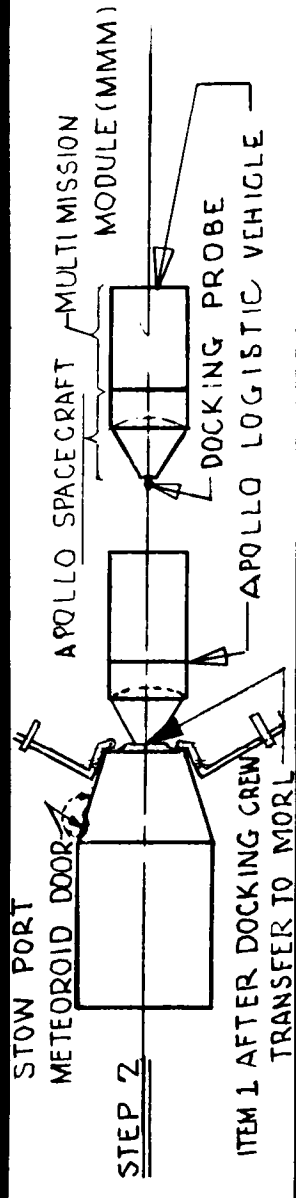
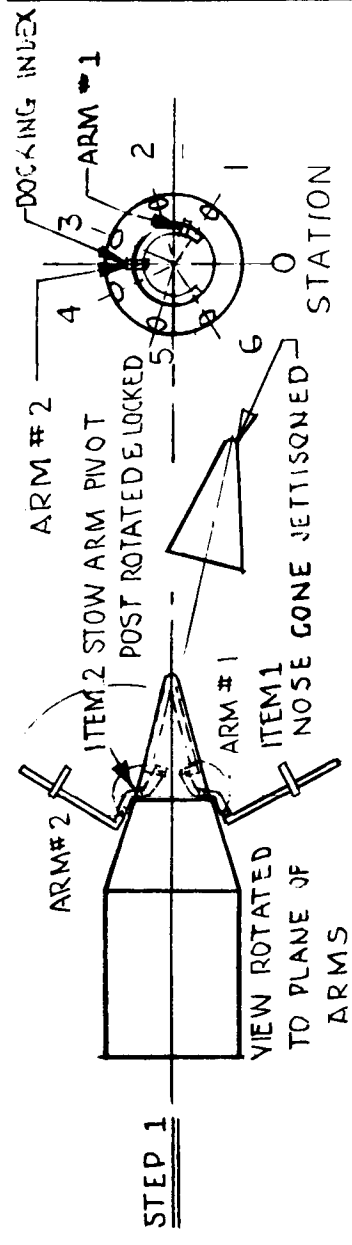
Item 2--MORL latches which hold the logistic vehicle are released; the Arm No. 2 attaching carriage which holds the Apollo is moved parallel to the longitudinal axis to clear the logistics vehicle seals from the docking ring.

Item 3--Arms No. 1 and 2 powered dollies are rotated along the track until Arm No. 1 is in the plane of the MMM attachment fitting. Arm No. 1 is swung to mate its carriage to the MMM, and the attachment is completed.

Step 4 Apollo Stowage in a Radial Stowage Port

Item 1--The joint between the MMM and the spacecraft is separated.

Item 2--Arm No. 1 attaching carriage is moved along the arm until the MMM front seal joint is clear of the rear ring of the spacecraft; Arm No. 1 is then swung to move the MMM clear of Apollo.



- OPERATION STEP 4**
- ITEM 1 JOINT BETWEEN SPACECRAFT & MMM SEPARATED
 - 2. MMM SWUNG TO CLEAR APOLLO—ARM #2 ROTATED TO STATION 4
 - 3. SPACECRAFT ROTATED 180° ABOUT ARM #2
 - 4. ARM #2 SWINGS APOLLO TO STOW PORT CENTERLINE
 - 5. CARRIAGE MOVED TO MATE APOLLO TO STOW POSITION

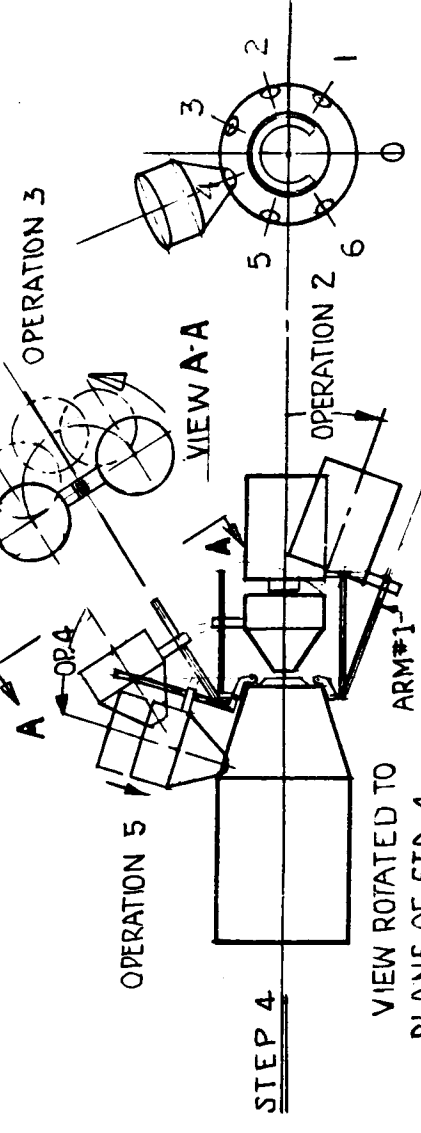
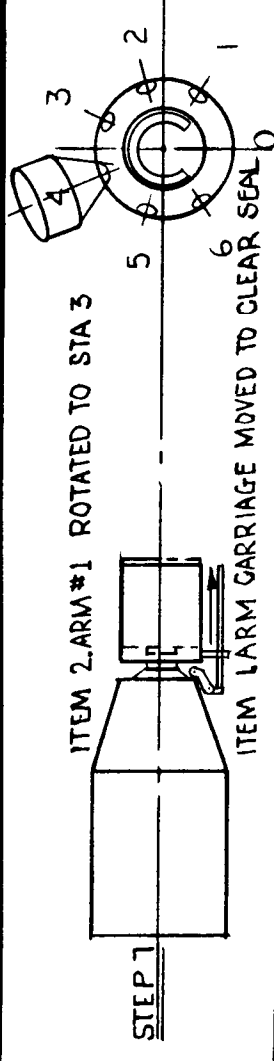
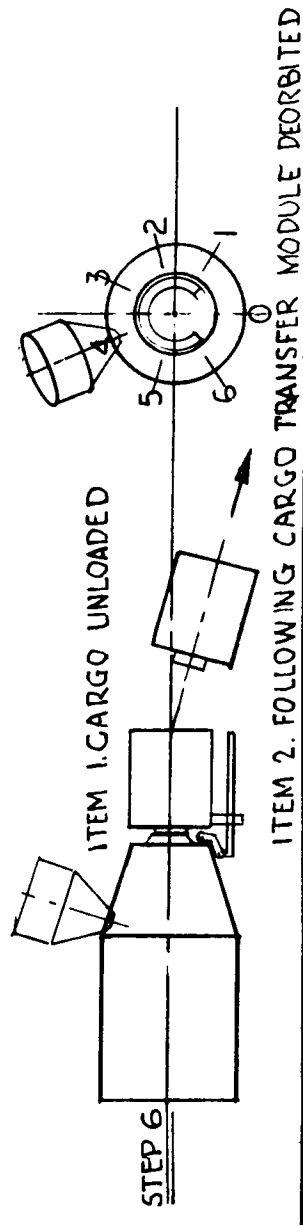
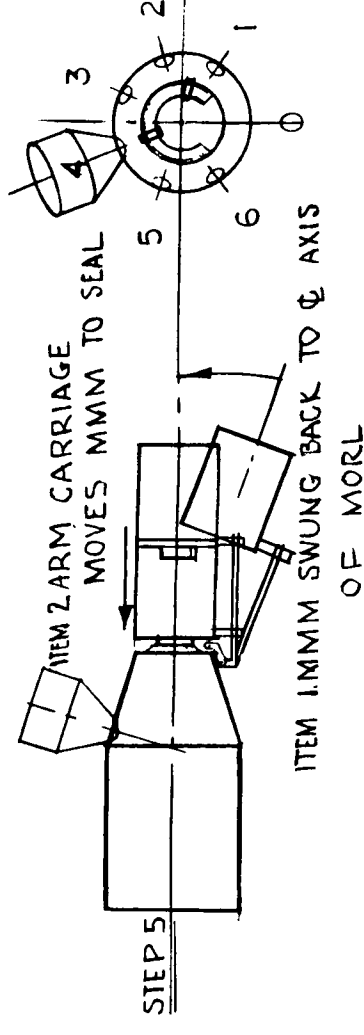
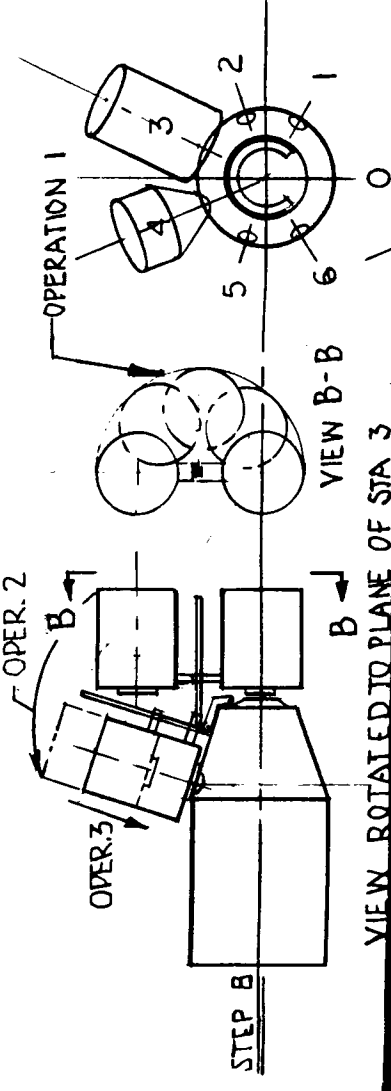


Figure 2-5. Two-Arm Handling System



- OPERATION STEP B**
- ITEM 1. MMM ROTATED 180° ABOUT ARM #1 ϕ
 - 2. ARM #1 SWUNG TO STOW CENTERLINE
 - 3. CARRIAGE RETRACTED TO MATE MMM TO STOW POSITION



Powered Dolly No. 2 is next rotated to place Arm No. 2 and the Apollo into the plane of Stowage Station No. 4 (or another desired stowage port).

Item 3--The arm No. 2 attaching carriage and Apollo are rotated 180° about the centerline of stow Arm No. 2.

Item 4--Arm No. 2 and Apollo are then swung to line the centerline axis of the spacecraft with the centerline of the stowage port.

Item 5--Attaching Carriage No. 2 is moved along the arm towards the stowage port ring until the spacecraft docking ring mates with the stowage port attachment ring.

Item 6--(not shown) The latch ring shown in Figure 2-6 is engaged, the seal is inflated and the spacecraft is stowed.

Item 7--(not shown) After the Apollo tunnel is pressurized by the same procedure as the dock port, the inside hangar door is opened, and the Apollo may be entered from MORL, in a shirt-sleeve atmosphere.

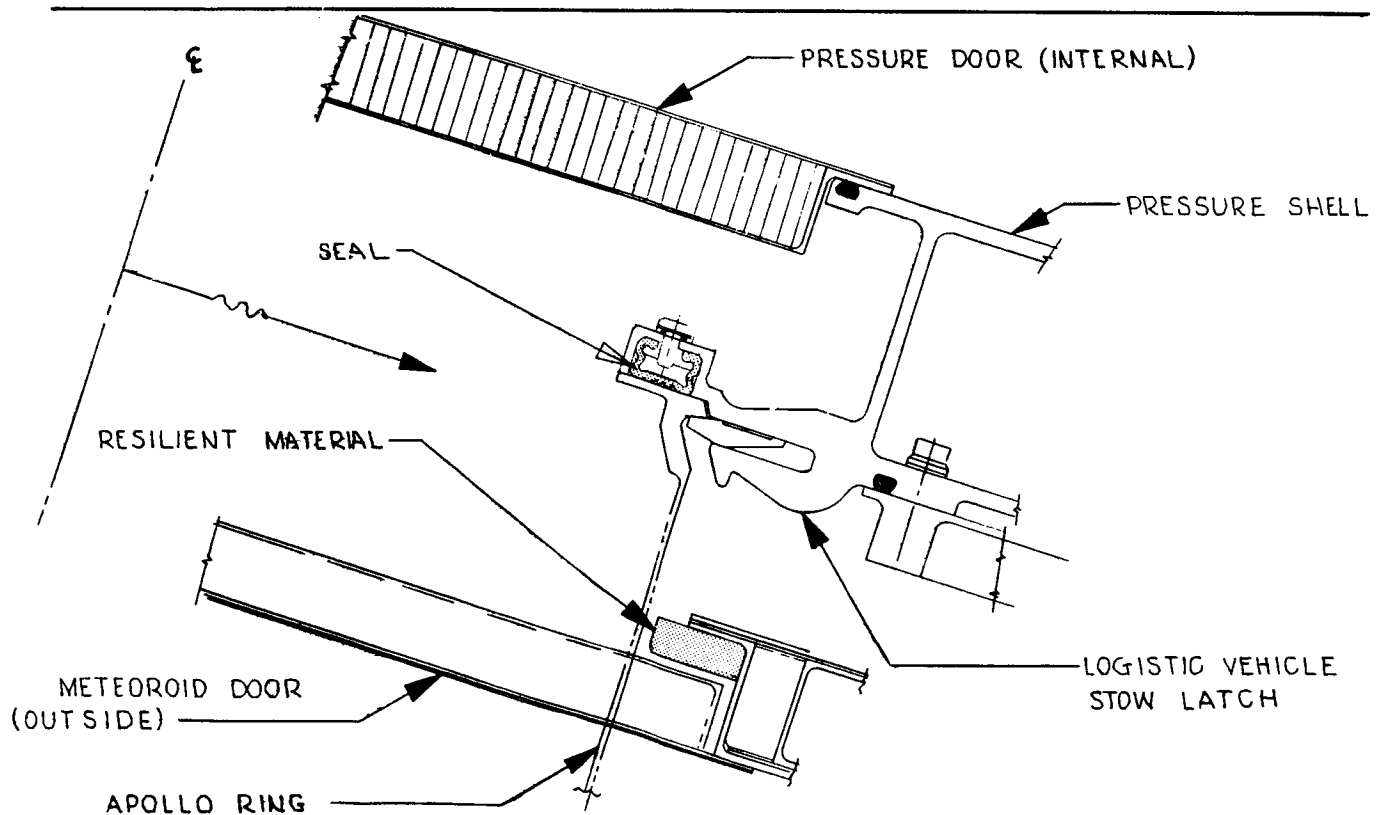


Figure 2-6. Radial Stow Port

Item 8--(not shown) The latches which hold the arm carriage to the Apollo are finally released, and Arm No. 2 is available for other transfer operations.

Step 5 Location of MMM is Dock Port for Cargo Unloading

To unload the large items of cargo designed to go through the large MMM door, the MMM must be placed in nose docking port where the dock port size matches the MMM opening. If all the cargo packages can be unloaded through the smaller, Apollo-size docking ring, the MMM may be placed in the radial stow positions for unloading, but larger items require the large nose port. The following describes the placement of the MMM to the nose dock port for large cargo unloading.

Item 1--Arm No. 1 and attached MMM is swung to return the MMM back to the centerline position of MORL.

Item 2--The Arm No. 1 carriage is retracted until the MMM front seal ring mates to MORL. The MORL expandable lock ring is engaged, which ties the MMM to MORL, and the seal is inflated. The passageway into the cargo module is now pressurized to the MORL atmosphere, and the large door, which is a portion of the docking structure, is opened from inside MORL; it is manually stowed next to the nose pressure dome. Shirt-sleeve entry into the cargo module is now possible from the Hangar/Test area of MORL through the 30-in. opening.

Item 3--(not shown) The bolts which hold the Apollo adapter ring cone are removed, and the adapter cone is moved out of the way; the cargo unloading may now be accomplished, Figure 2-7.

Step 6 Jettison of Used MMM

Item 1--Upon completion of the cargo transfer, the MMM is prepared for jettison (or stowage) by reversing Step 5; the docking structure with the docking cone installed is swung back into the normal position and the large door locked; the pressure in the MMM module passageway is bled to space; the seal and lock ring which holds the module to MORL is released; Arm No. 2 attaching carriage is extended to clear the seal; and the MMM is ready for deorbiting or stowage. The stow arm is released for MMM deorbit, and, at the proper time, the module propulsion system is activated; separation for deorbiting is completed.

Step 7 Release of MMM from Dock Port

Prior to stowage of the MMM, the meteoroid door at the stowage station must be opened.

Item 1--Attach Arm No. 1 to MMM as described in preceding steps. Replace and bolt the Apollo adapter ring cone in the MMM. Replace dock structure door, depressurize MMM passageway, deflate seals, and release lock ring as described in Step 6, Item 1. Arm No. 1 attaching carriage then moves MMM to clear MORL seal and lock ring.

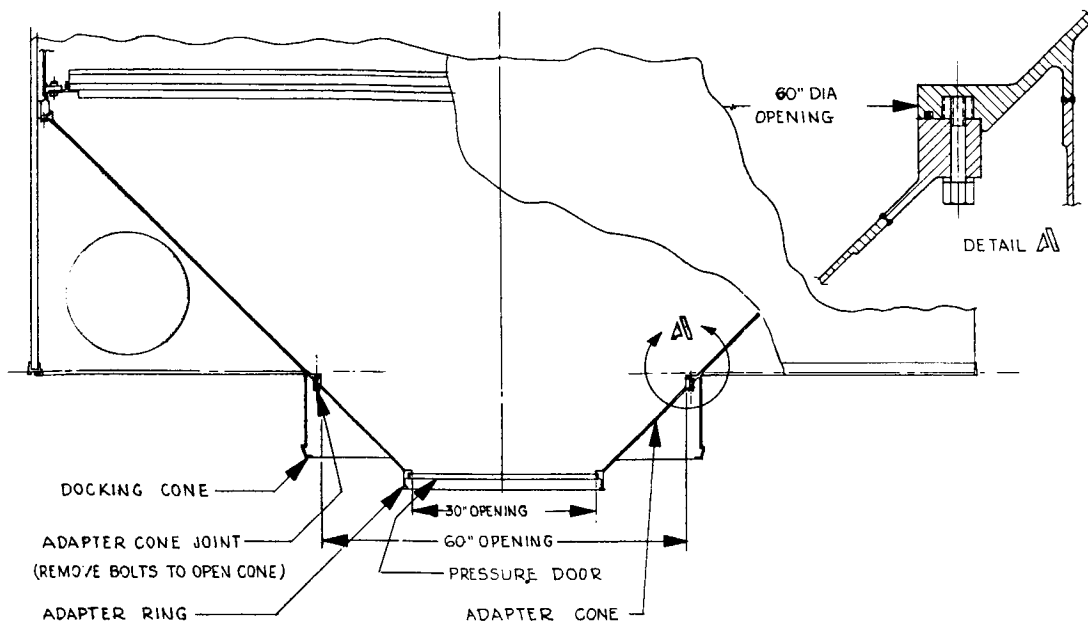


Figure 2-7 Multimission Module Adapter Cone

Item 2 --Arm No. 1 powered dolly is rotated to place Arm No. 1 and MMM into the plane of stowage Station No. 3 (or other desired port).

Step 8 Stowage of MMM in a Stowage Port

Item 1 --Attaching Carriage No. 1 and MMM is rotated 180° about the centerline of stow Arm No. 1.

Item 2 --Arm No. 1 and MMM is then swung until the longitudinal axis of the MMM is lined with the centerline axis of the stowage station.

Item 3 --Attaching Carriage No. 1 is moved along the arm until the MMM front adapter seal is mated to the stow station; the lock ring shown in Figure 2-6 is engaged, the seal is inflated, and the MMM is finally stowed.

Item 4 --(not shown) Entry into the MMM is gained by pressurization of the MMM passageway and articulation of the MMM and MORL stowage port doors, as described in preceding steps.

A dynamic analysis for the two-arm axial stowage system is given in Appendix A. Because the cantilever arm is decreased by moving the arm-supported vehicle towards the pivot port, the moment of inertia about the point of rotation is much smaller for the radial stowage concept than for the axial stowage design. As a result, the impact load will be much smaller than the case illustrated in the dynamic analysis, and the conclusions reached for the axial stowage system can be applied to the radial stowage concept.

2.2.3 Radial Logistics Vehicle Stowage System

The Phase IIa MORL design provided for stowage of seven logistics/experimental modules parallel to the hangar side. During Phase IIb, alternate methods of stowing the logistic vehicles were investigated. The radial stowage concept was selected, based primarily on the ready access to the stowed spacecraft and MMM. This configuration provides greater flexibility in unloading, allows direct access to special experiments, expedites emergency evacuation, saves transfer time for maintenance and check out of the spacecraft, and reduces radiator shadowing effects. Consideration of multiple stowage parts was avoided in early studies because of the possible leakage problems. Recent tests on door seals, performed at Langley Research Center on Douglas-designed parts, indicate that seals can be made which will keep the leakage well below the allowable limits. Earlier design decisions have, therefore, been reconsidered, and the baseline configuration utilizing six stowage ports has been accepted.

The baseline configuration of the radial stowage is shown in Figures 2-3 and 2-4. Six stowage ports of 38-in. diam are placed radially around the hangar shell, spaced 49° apart; this leaves a 90° arc clear along the MORL belly for the experiment bay. To withstand the forces introduced into the MORL structure from the radially stowed vehicles, each port contains a ring, which incorporates the stow latch and mechanism; it is integrated into the pressure shell and tied to the floor beams. An outside door is provided at each port for meteoroid protection; before a vehicle is stored, the outer door is manually opened, and it remains parallel to the hangar shell.

Figure 2-6 shows a cross-section through the stow port. A detailed discussion of the structure is contained in Section 3.3.6.

Because the stow arm attachment point is the same distance from the longitudinal axis for both the Apollo spacecraft and the MMM, the stow port centerlines must be kept in a plane parallel to the stow arm rotary track. To keep the flat bulkhead stiffening beam depth small, the stow port centerlines are as close to the flat bulkhead as possible. All stow ports are identical and built to accept the Apollo docking ring; cargo too large for the Apollo opening must be unloaded from the nose port. Because the MMM docking cone seal ring is much larger than the Apollo ring, it is necessary to add an adapter ring to the MMM that is the same size and shape as the Apollo unit. Figure 2-7 shows the incorporation of the stow ring adapter into the docking cone of the multimission module.

Assessment of the experiment and mission requirements indicated that only six stowage ports are necessary; however, the Apollo command module and the MMM are shaped so that Apollos may be stowed adjacent to each other; however MMM's cannot be so stored. A stowage arrangement using alternate locations for Apollo and MMM's or an unused stowage position between MMM's is required.

Redesign of the logistics vehicle stowing system and the added provision for radial stowage have altered several requirements for controls and displays on the master control panel. The major areas and operations to be monitored from this station are the hangar area, hangar docking operation, MMM, stowing operation, and stow port area. Provisions for continuous monitoring of each operation on a step-by-step basis are included because of the criticality of these tasks.

Provisions for monitoring the hangar area and for control of the MMM fan are shown in Figure 2-8. These changes reflect the requirements stemming from the Apollo vehicle docking procedures. Provisions for monitoring and controlling hangar pressure have been deleted from this portion of the panel, since those procedures were to be used with the unmanned logistics vehicle.

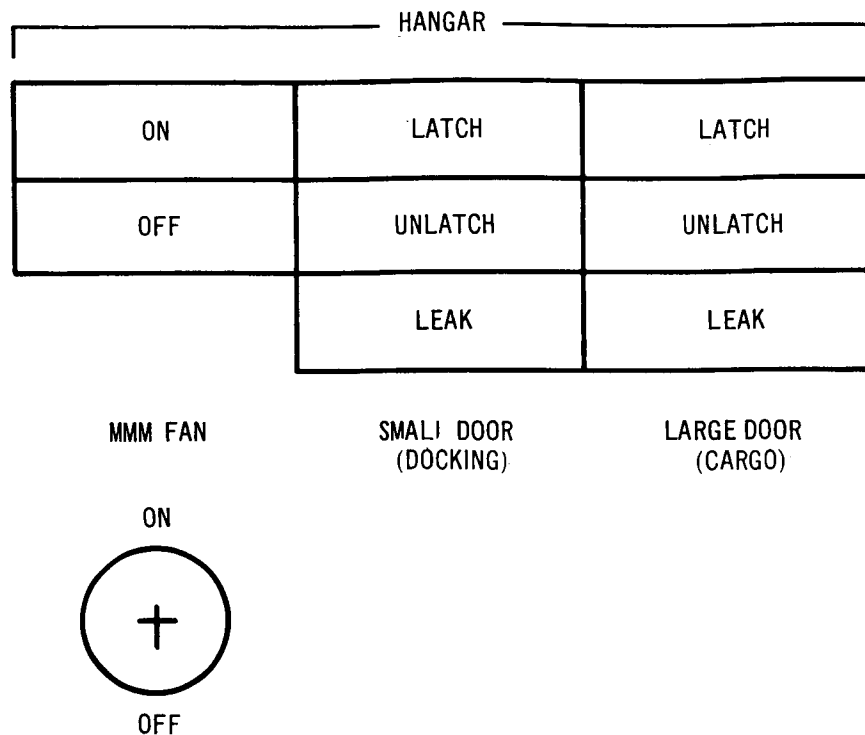


Figure 2-8. Hangar Latch Panel

The hangar docking and stowing portions of the panel were completely revised to reflect use of the Apollo spacecraft, the MMM, and two-arm radial stowing. These areas are shown in Figures 2-9 and 2-10. A television monitor has been added to provide a visual confirmation of the status of all equipment; this capability will be extremely valuable during the final stages of docking and stowing and particularly helpful when stowing units are in close proximity.

Only minor differences between the longitudinal stowage and the radial stowage configurations were found in the stabilization and control system study (Reference Book 3, Douglas Report No. SM 48817). A possible problem was that the modules might interfere with the field of view of the sensors; however, this is a secondary problem, dependent on the combination of vehicles being stowed.

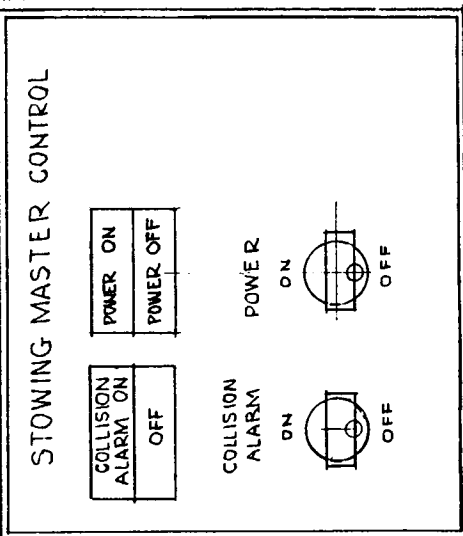
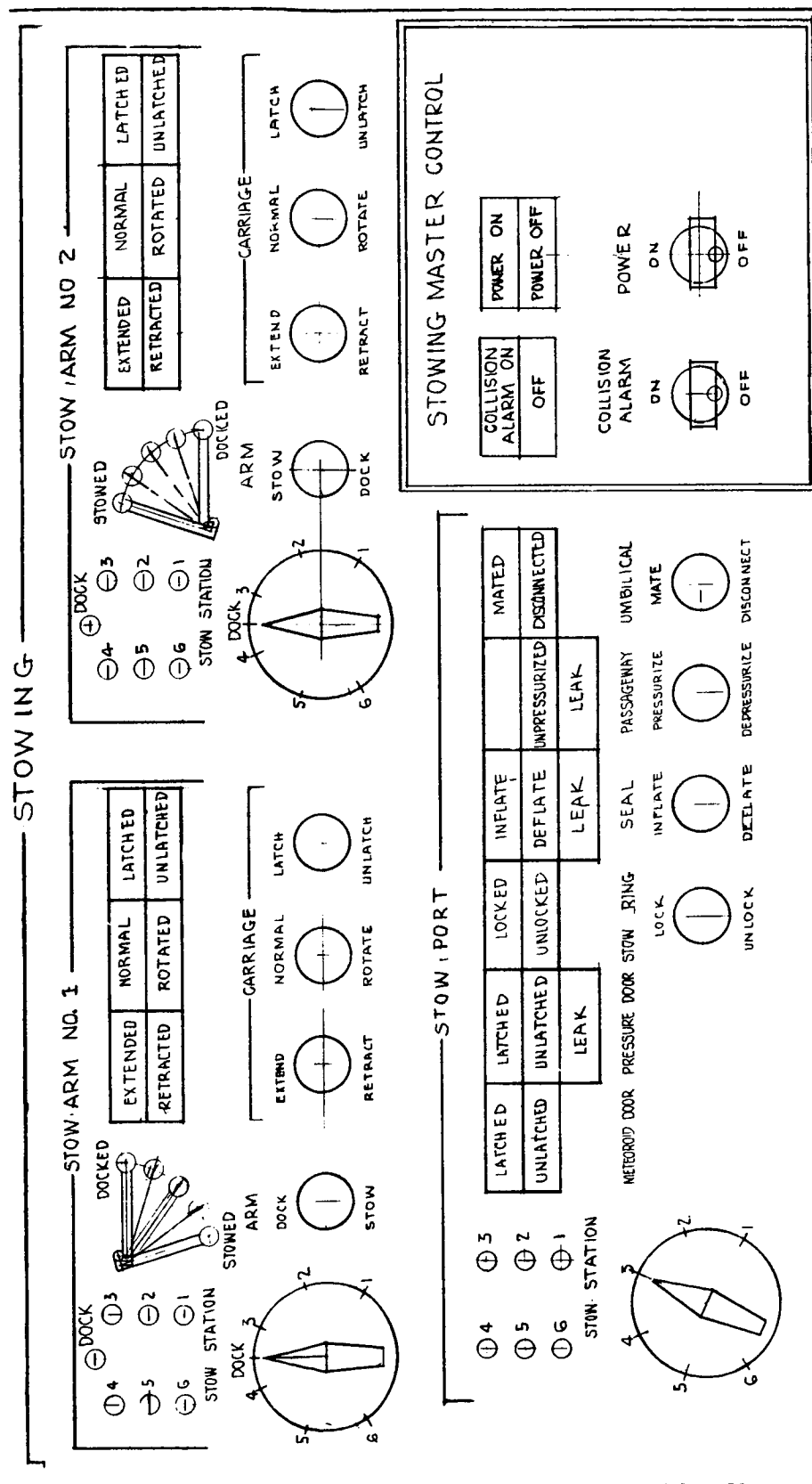


Figure 2-9. Stowing Operation Panel

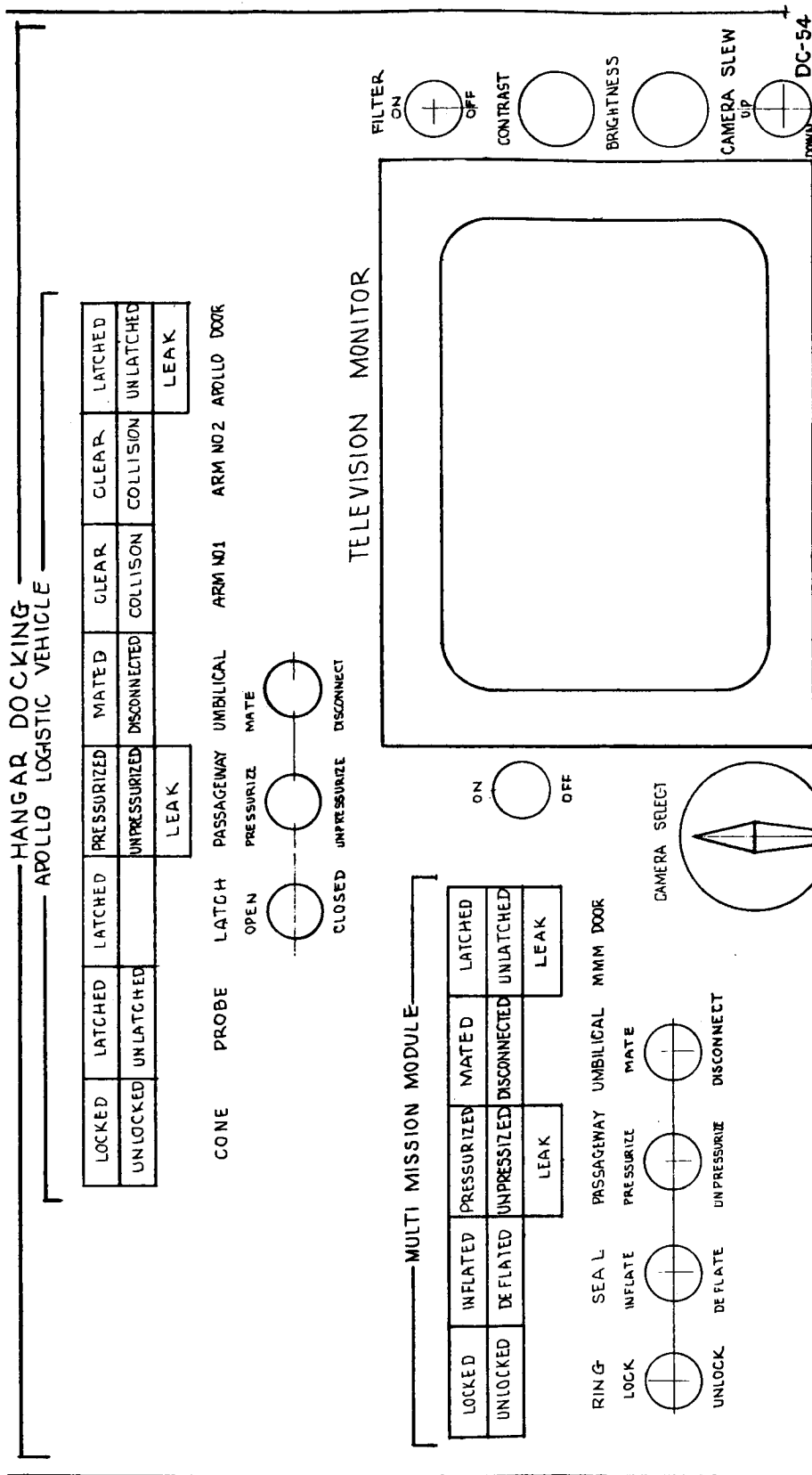


Figure 2-10. Hangar Docking Panel

Effects of the radial storage on the EC/LS system were favorable because of reduced radiator shadowing and radiator installation problems. Increased volumes from the stowed vehicles present no problems and the modules will carry any specialized circulation systems as basic equipment. Leakage from the attached vehicles will be controlled by opening the ports only when necessary.

2.2.4 Experiment Bay

The experiment plan of Task II identified over 20 instruments requiring Earth-pointing sensors. Since each instrument is used for five separate experiments (average), the number of potential assembly and disassembly events approaches 200.

The time-line analysis of the 48-hour study of Task III, noted in Table 2-1, shows that the majority of the 9 man-hours are required by the EVA and not the sensor installation; the time spent may, therefore, be considered lost.

Table 2-1
SENSOR MOUNTING ACTIVITIES TASK BREAKDOWN

Tasks	Men	Minutes	Man-Hours
Obtain experiment equipment	2	30	1.00
Transfer equipment and don suits*	3	15	0.75
Denitrogenate*	3	45	2.25
Exit procedures*	3	50	2.50
Install sensors	2	120	4.00
Monitor EVA*	1	120	2.00
Entry procedures*	3	30	1.50
			<u>14.00</u>

*Tasks caused by extravehicular activities (requires 9.0 man-hours)

Since crew time available for experimentation on MORL during a 3- to 5-year mission is worth from \$40,000 to \$60,000 per man-hour, it seems advisable to find an alternate technique for mounting external sensors to eliminate as much EVA as possible. One approach explored was to build an experiment bay in the Hangar/Test area of the laboratory, allowing sensor assembly in a pressurized environment, followed by exposure to space for experiment performance.

Since some instruments use sensors large enough to make mounting them in an experiment bay impractical, provisions must be made for separate external mounts as well. Table 2-2 lists instruments used in the experiment program; those instruments with sensors probably small enough to fit into an experiment bay, and those with sensors so large they would require external mounts. Table 2-2 also lists the number of separate experiments each instrument is used for. Of 22 instruments, 15 could have sensors mounted in the bay, which involves nearly 60 experiments; this is a potential saving of about 120 assembly and disassembly EVA events, or about 1,080 man-hours.

A major factor to be considered in the design of an experiment bay is that many of the experiments identified in Tasks I and II require precision attitude alignment of instrument sensors to the laboratory inertial reference system in order to achieve the pointing accuracies required. Also, once alignment is secured, it must be maintained by isolating the sensors from disturbances within the laboratory. To maintain this precise alignment on several sensors operating nearly concurrently, a rigid sensor-mounting beam was proposed in Task III. Utilizing this rigid beam (mounted so as to keep the beam in a stress-free state by isolating it from laboratory body-imposed strains) and the optical and mechanical alignment techniques described in Book 3 Douglas Report SM 48817, sensor attitude alignment accuracy of $\pm 0.01^\circ$ can be obtained; this accuracy meets or exceeds the requirements of over 90% of the experiments in the data bank. The sensor-mounting beam must be incorporated in any experiment bay design. The beam should include mounting provisions for precision attitude reference system components (the single-gimbal triad and the two-star trackers), a horizon sensor, and optical alignment equipment, in addition to the experiment equipment.

Table 2-2
EXPERIMENT BAY UTILIZATION
(BASED ON EXPERIMENT PLAN)

Instrument	No. of Experiments
<u>Instruments with Sensors that Could Be Mounted Inside Bay</u>	
Optical driftmeter	5
Optical camera	5
Visible radiometer (wide-band)	4
Visible radiometer (dual-channel)	5
Visible polarimeter	2
Television (high-resolution)	6
Television (dual-channel)	4
Dual star tracker	6
UV spectrometer	5
UV radiometer (dual-channel)	2
IR radiometer	5
IR interferometer	4
IR camera	2
IR spectrometer	2
Multislit/multidetector grating IR/spectrometer	2
Subtotal	59
<u>Instruments with Sensors that Would Be Mounted Outside Bay</u>	
K-band radar profilometer	3
K- or C-band radar	6
S-band polarimeter	7
Microwave radiometer	6
LIDAR (laser detection and ranging)	10
Searchlight and detector	2
Directional spherics receiver	3
Subtotal	37
TOTAL	96

The requirements that originated from Task III dealt mainly with assuring precise sensor attitude alignment. The simplest approach which achieves this requirement is to provide a rigid beam on the outside of the laboratory. However, the number of instruments involved and the resultant EVA events led to consideration of an experiment bay which would allow suitably sized sensors to be mounted, aligned, and maintained on the beam in a pressurized environment.

2.2.4.1 External Sensor-Mounting Beam (No Bay)

A sensor beam is mounted outside the laboratory on the bottom of the Hangar / Test area (the nose), as shown in Figure 2-11. As noted above, the requirement for this beam was generated during the 48-hour study, which specified a rigid base for common mounting of experiment sensors and components of the precision attitude reference system. The experiment plan, as defined in Task III, contained many Earth-centered experiments in the fields of oceanography and meteorology. Since most of the sensors are thus pointed in the same direction, a single mounting structure at one location on the laboratory will suffice. The major advantages of this concept and location are noted below:

1. A rigid, simple structure.
2. Minimum weight penalty.
3. The exterior position of the beam allows more sensors of larger sizes to be mounted than other concepts.
4. The exterior beam position intrudes the least into the Hangar/Test area, and causes the least compromise to use of that interior volume.
5. Access is provided to attitude reference system and horizon sensors from Hangar/Test area.

Major disadvantages of this concept are noted below:

1. Sensor installation, maintenance, and disassembly requires extra-vehicular activity.
2. Optical alignment equipment must be mounted outside; this results in continuous space exposure of optical components and necessitates a long optical path with potential relative motion between internal and external alignment equipment.

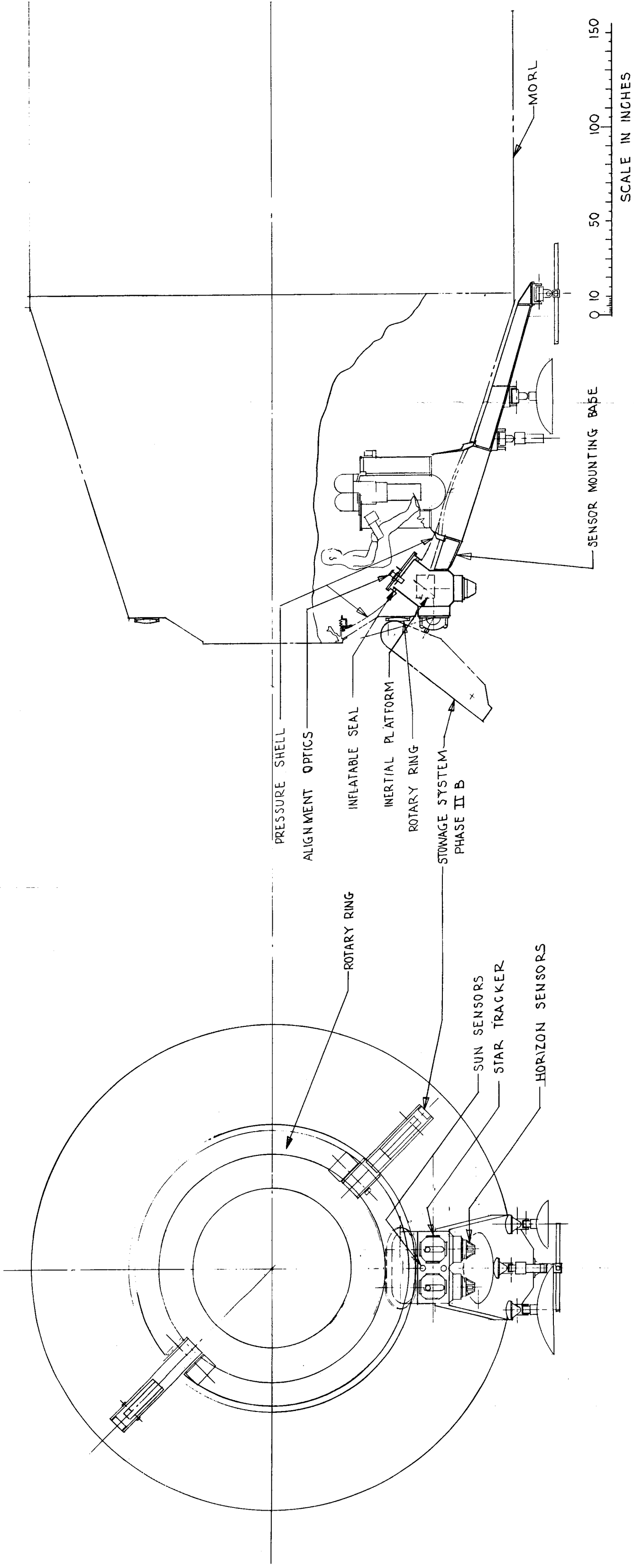


Figure 2-11. Phase IIb Attitude Reference Installation

41-2

41-1

3. Sensors are continuously exposed to the orbital environment.
4. Temperature control may be necessary for the beam, to prevent thermal stress from causing distortions and misalignments.
5. Maintenance of mechanical alignment and checkout of optical alignment between sensors in equipment airlock (for instance, a camera) and the sensor beam may be a problem.
6. The beam requires the largest launch protection fairing of all the concepts.

2.2.4.2 Internal Sensor-Mounting Beam (No Bay)

This concept is merely a variation; in this case, the beam is mounted inside the Hangar/Test area with universal sensor-mounting posts extending through the laboratory pressure shell, Figure 2-12. The main advantages of this approach are as follows:

1. Mounting the beam inside assures a more stress-free environment because minimum thermal stresses are imposed on the beam.
2. The majority of alignment equipment is inside the laboratory, except for optics at the sensor-mounting pads.
3. It may be the lightest of all concepts.
4. The structural concept is simple except for load-balancing flanges and seals, where sensor-mounting posts penetrate the skin.
5. It allows growth to larger sensors, although the total number of sensors that can be mounted would probably be more limited than in the case of the external beam.
6. It allows access to the attitude reference system and horizon sensors from the Hangar/Test area.
7. The concept has minor intrusion into the Hangar/Test area, and it would not seriously compromise future use of that interior volume.

Disadvantages of this concept are as follows:

1. Sensor installation, maintenance, and disassembly require extra-vehicular activity.
2. Sensors are continuously exposed to the orbital environment.
3. Sensor-mounting pads require multiple penetrations of its pressure shell with attendant (minor) structural complexity and increased probability of laboratory atmosphere leakage.

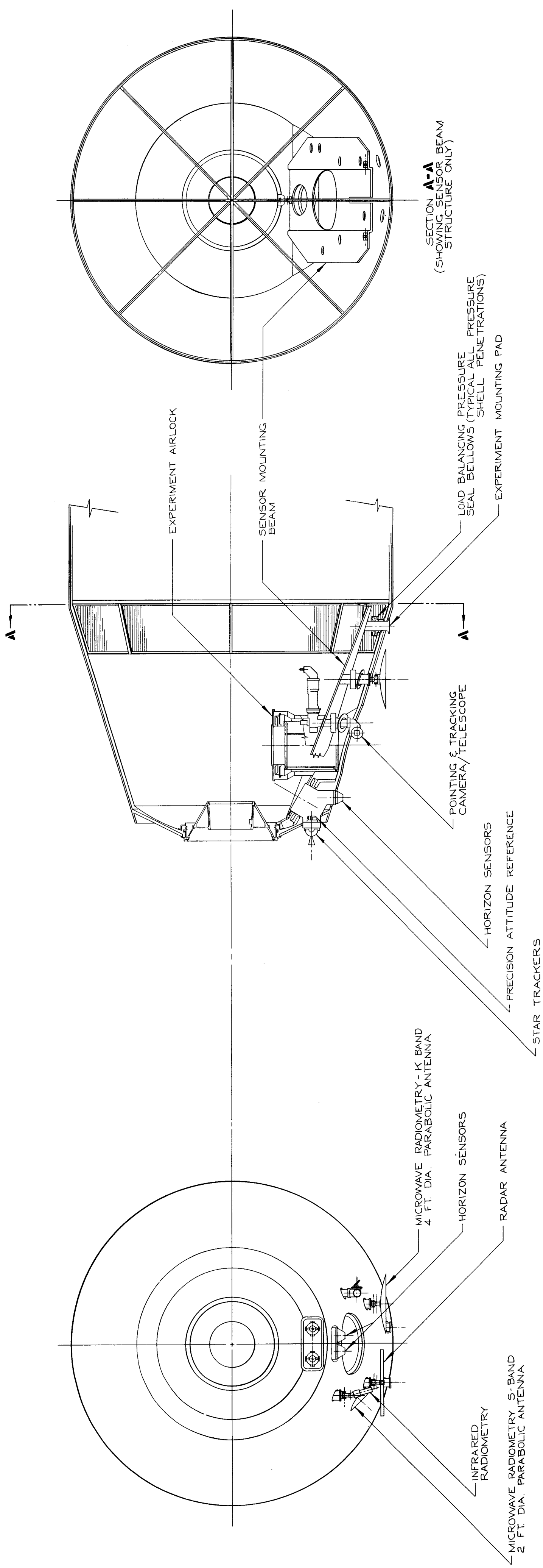


Figure 2-12. Internal Sensor Beam Installation

4. Some optical alignment equipment must be mounted outside the laboratory, which complicates alignment system design and exposes some optical components continuously to the orbital environment.
5. Launch protection fairings are required for sensor-mounting pads.

2.2.4.3 Experiment Bay with Flat Pressure Bulkhead

As shown by Figure 2-13, this concept provides a separately pressurizable section of the Hangar/Test area by partitioning the bay area, with a flat pressure bulkhead or floor. After experiment sensors have been installed in a shirt-sleeve environment, the bay can be evacuated and a pressure door opened to expose the sensors. This door spans 90° of the hangar circumference and extends the full length of the bay. The sensor-mounting beam is located just on top of the pressure floor, inside the environmentally controlled area of the hangar. Sensor units which are to be mounted in the bay are installed on posts integral with the beam and which project through the pressure floor. There are two external sensor-mounting posts which are also integral with the beam but located between the bay aft end bulkhead and the hangar/control deck pressure bulkhead. These posts are for those sensors too large to be mounted inside the bay. An experiment airlock is positioned on the forward end of the beam and penetrates the pressure floor; when the bay door is open, experiments can be placed in the orbital environments from the hangar area. When the bay door is closed, the airlock can be used as a passageway between the hangar area and the bay. Normal access to the bay area is through an entrance hatch in the experimental control center station.

To form the pressure-tight region of the bay, each end is sealed to the MORL by pressure bulkheads. The area between the end bulkheads is sealed from the hangar area by the pressure floor so that it is open to space. Seals need not be provided for the external sensor-mounting posts aft and the attitude reference sensor-mounting well forward. The well located at the front end of the hangar area is provided for the permanent installation of the star trackers and the horizon sensors. The attitude reference sensors are mechanically tied to the mounting beam for precise alignment of experiment sensors. The well is sealed at the pressure floor and is open to the inside hangar area for shirt-sleeve access to the precision attitude reference system components.

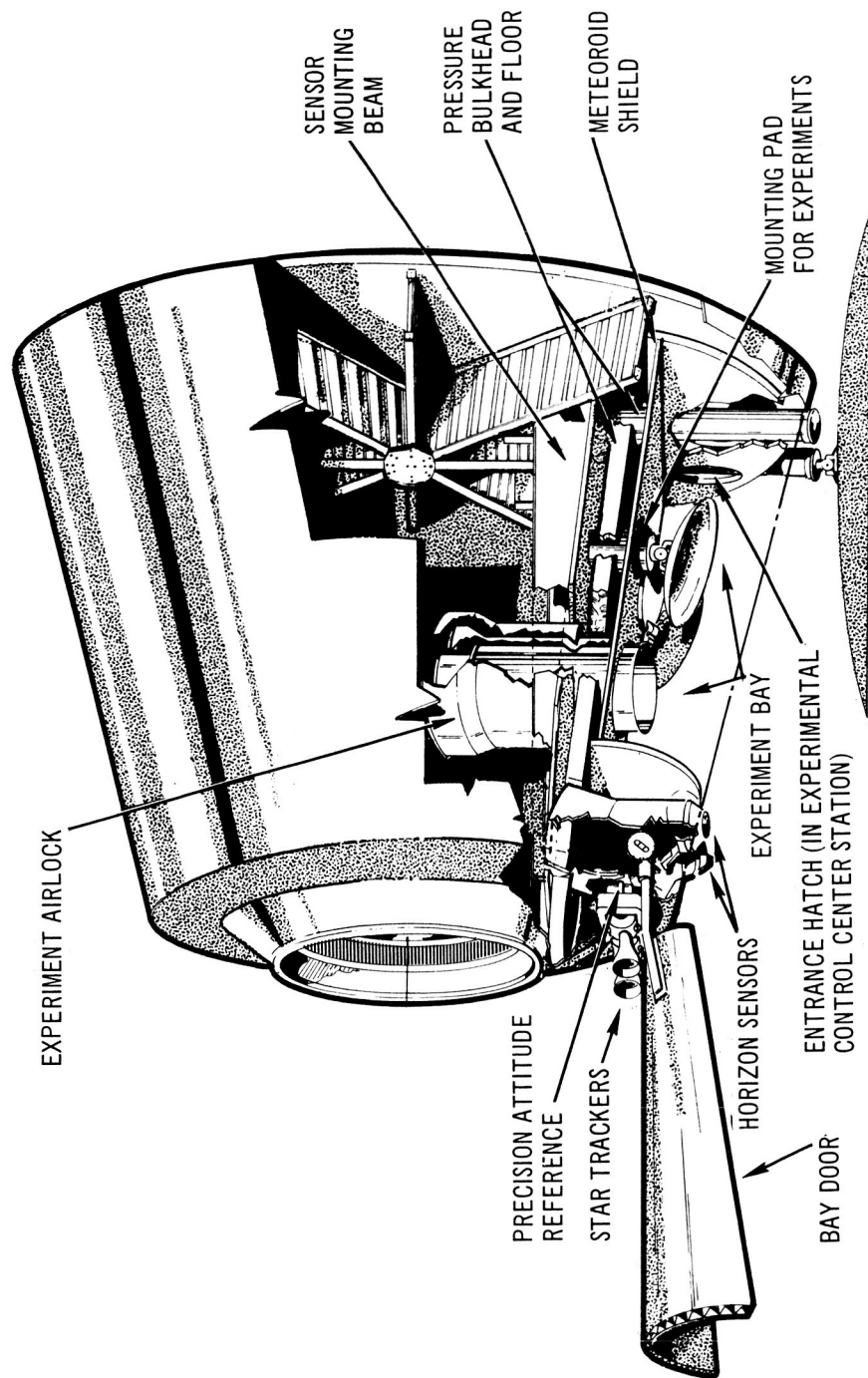


Figure 2-13. MQR-1 – Experiment Bay

The sensor-mounting beam is structurally isolated from all laboratory pressure shell flexures caused by temperature and pressure variations, and it provides the necessary required rigid-machined mounting plates to maintain mechanical alignment between sensors. Since the beam is located inside an environmentally controlled area of the laboratory, movement of the beam as the result of thermal gradient stresses are minimized.

Major advantages of this concept are as follows:

1. Most sensors can be assembled, maintained, and disassembled in a pressurized environment.
2. Sensors mounted in the bay can be optically aligned in a pressurized environment. A majority of alignment components are always in a pressurized environment, since the mounting beam is always inside the laboratory.
3. Thermal gradient warping of the beam is minimized by the interior location.
4. Sensors can be shielded from orbital environment by closing the bay when experiments are not in progress.
5. The design permits shirt-sleeve access from the hangar area to precision attitude reference system and the horizon sensor components.
6. Launch protection fairing requirements are minimized; the bay door provides the main protection, but provisions must be made to shield the horizon sensors, the aft exterior sensor-mounting posts, and their cutouts.

Major disadvantages of this approach are noted below:

1. It is probably the heaviest concept, adding approximately 1,000 lb.
2. Complex structure and mechanism is required, particularly the bay door with its pressure seals and actuating mechanism.
3. Multiple penetrations of the pressure shell are required for sensor-mounting posts, attitude reference sensors, and experiment air-lock, each with pressure compensation flanges and seals.
4. The bay must be pumped down each time the door is opened, which causes some additional complexity in the EC/LS system.
5. Sensor growth in the bay area is limited in size and numbers because of bay space limitations.
6. Extravehicular activity is still required to mount large sensors on the aft exterior posts.

7. Internal access to bay-mounted sensors is limited because of shallow space between the flat pressure floor and the bay door; the entrance hatch is also fairly small (about a 30-in. diam).
8. Equipment or samples in the experiment airlock can only be exposed to space when the bay door is open.
9. The bay concept compromises the flexibility and use of the Hangar/Test area interior volume by segregating a fixed portion for sensor installation.
10. Sensor field of view inside the bay is restricted by the bay walls.
11. The bay door must be at least partially closed during docking activities, probably restricting sensor performance and disrupting the experiment program.
12. Extravehicular activities are necessary to maintain portions of the bay and bay doors (notably the vulnerable seals).

2.2.4.4 Experiment Bay in Nose

This arrangement requires that the MORL be placed in a nose-down attitude during the performance of Earth-centered experiments. The forward end of the Hangar/Test area becomes the experiment bay, as shown in Figure 2-14. This forward area is sealed from the rest of the hangar by a flat pressure bulkhead. A central hatch allows access to the bay when the nose docking port is closed. The sensor-mounting beam is on the inside of the pressure bulkhead in the environmentally controlled region of the hangar. An extension of the beam goes up the side of the nose to the hangar/control deck bulkhead so that the precision attitude reference system star trackers can be mounted near the laboratory's constant-diameter section, permitting a good view of the star fields. Sensor-mounting posts are arranged around the periphery of the central hatches and extend through the pressure bulkhead and the nose structure. The horizon sensors are mounted in a well that extends from the pressure bulkhead through the nose structure, allowing pressurized access to these components. This concept would be most effective if radial docking were acceptable. Experimentation must be suspended during docking operations.

This approach was primarily the result of an investigation of potential reaction control propellant saving that might result from a nose-down attitude. However, it was found that the baseline (belly-down with the laboratory

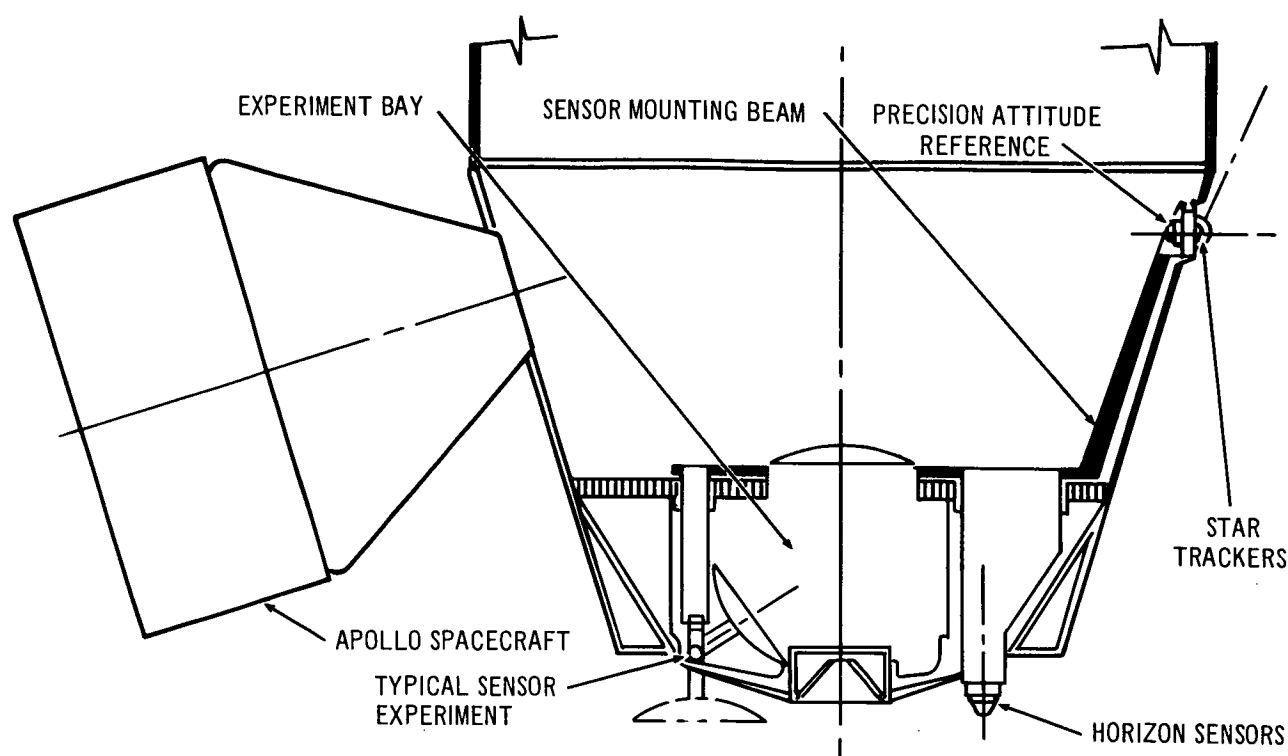


Figure 2-14 MORL with Experiment Bay in Nose

X-axis aligned to the velocity vector) is the most economical; this and the fact that nose docking is the baseline method led to eliminating the experiment bay in the nose from further consideration.

2.2.4.5 Experiment Bay with Conical Pressure Bulkhead (Figure 2-15)

This configuration is essentially similar to the experiment bay with a flat pressure bulkhead. Major differences, as shown in Figure 2-15, are in the shape of the pressure bulkhead and the relative position of the sensor-mounting beam; the bay door is hinged further forward and the locations of the experiment airlock and the horizon sensors are therefore affected. To minimize the structural weight penalty imposed by the bay, a conical bulkhead, of the same shape as the hangar cone, is used instead of the flat pressure bulkhead of Concept 3, presented in Section 2.2.4.3. This conical bulkhead also allows better access room to bay-mounted sensors, and a large entrance hatch (36-in. diam). The beam is positioned as it was in Concept 3. However, now the

pressure bulkhead is above it and the beam is exposed to space when the bay door is opened. Sensors can be mounted directly to the beam and not to posts extended through a pressure bulkhead. Because the beam is exposed to space during experimentation, it must be sufficiently insulated so that no appreciable temperature gradients can be created that could warp the beam.

The whole bay is further forward in position than in Concept 3. The aft end of the bay is 42 in. forward of the main compartment bulkhead and is closed by a flat pressure bulkhead which ties to the forward caps of the compartment bulkhead support beams. The bulkhead support beam which lies in the plane of the centerline of the experimental bay is divided into two beams, 40 in. apart, for a little less than half its length. Those beams are pressure-tight sandwich bulkheads that are bolted to the main compartment bulkhead and the experimental bay end bulkhead. The 42-in.-high by 40-in.-wide rectangular experiment airlock that is formed by this arrangement is closed at its in-board end by a rectangular hatch that hinges back against the main compartment bulkhead. Thus, the experiment airlock can be used even when the bay door is closed; however, there is a problem of limited access to this hatch because of its location between the support beams. A circular hatch, 38 in. in diam, closes off the out-board end of the airlock. Two external mounting posts for large sensors and the horizon sensors are located on either side of the experiment airlock, at the aft end of the bay. The star trackers remain at the forward position, but the horizon sensor has been moved aft because of potential interference with the door and hinge mechanism. Pressurized access to the horizon sensors is available at all times, and is also available to the star tracker when the bay door is closed.

Major advantages of this concept are as follows:

1. Many sensors can be assembled, maintained, and disassembled in a pressurized environment.
2. The conical bulkhead provides an efficient, pressure-tight bay design with resultant small weight penalty.
3. The conical bulkhead allows good access to sensors mounted in the experiment bay, and provides a reasonably large access hatch.
4. Because of the forward position of the bay, the experiment airlock can be located aft of the bay and can be used when the bay door is closed.

5. The mounting beam position outside the conical pressure bulkhead simplifies sensor mounting and eliminates the requirement for load-balancing features on the sensor-mounting posts.
6. The bay-mounted sensors can be optically aligned in a pressurized environment.
7. Sensors can be shielded from orbital environment by closing the bay door when experiments are not in progress.
8. Access is possible to precision attitude reference system star trackers and the horizon sensors in a pressurized environment.
9. Launch protection fairing requirements are minimized; the only shielding required, other than that provided by the door itself, is for the star trackers, horizon sensors, aft external mounting posts, and their cutouts.

Main disadvantages of this configuration are noted below:

1. Complex structure and mechanisms are required for the door, its pressure seals, and actuating mechanism.
2. A significant weight penalty to the laboratory is imposed by the bay, (approximately 600 lb), even though it is lighter than the flat bulkhead presented in Section 2.2.4.3.
3. This concept intrudes the most into the hangar area, possibly compromising the future flexibility of the hangar interior.
4. There are multiple penetrations of the laboratory pressure shell required for the bay door, star trackers, horizon sensors, aft sensor-mounting posts, and experiment airlock.
5. The bay must be pumped down each time its door is opened, which makes for additional complexity in the laboratory EC/LS system.
6. Sensor growth in bay area is limited in size and numbers.
7. Access to the experiment airlock is limited.
8. Field of view of sensors mounted in the experiment airlock may be restricted by radially stowed logistics modules.
9. Extravehicular activity is still required to mount large sensors on aft exterior posts, or to maintain portions of the bay.
10. Sensor field of view inside the bay is restricted by the bay walls; the open bay door also restricts the field of view of the external sensors and the star trackers.
11. The bay door must be at least partially closed during docking activities, which may interrupt the experiment program.
12. The beam is exposed to space, which could result in thermal gradient stresses and warpage.
13. Horizon sensors are separated from precision attitude reference system star trackers.

2.2.4.6 Selected Configuration

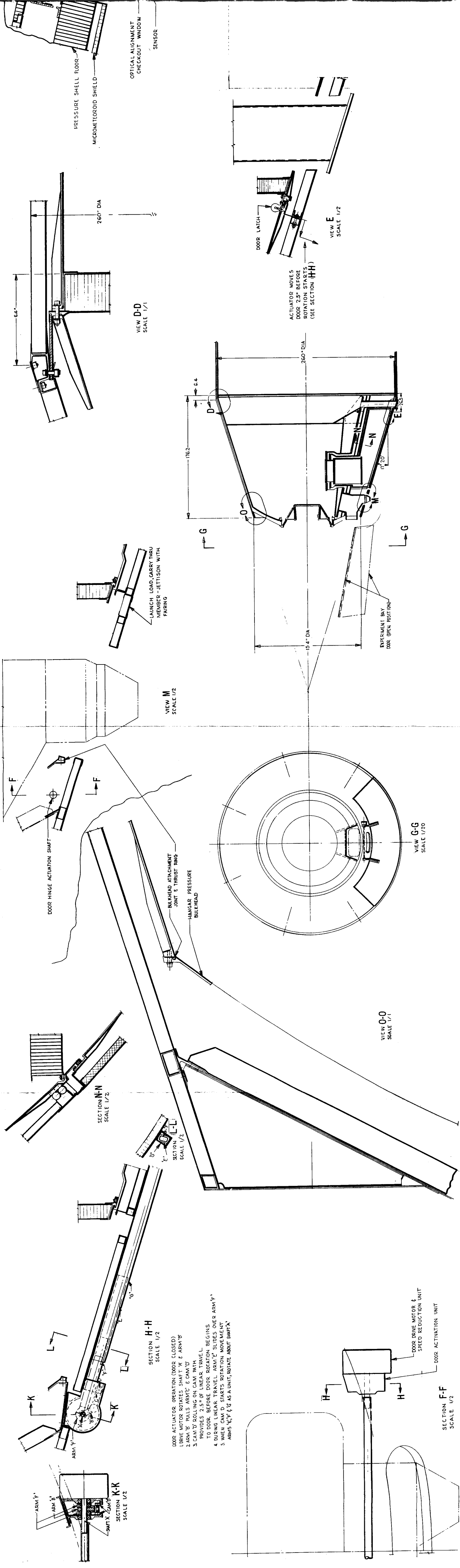
The experiment bay with the flat pressure bulkhead (see Section 2.2.4.3) was chosen as the baseline configuration. It allows internal sensor mounting and intrudes the least into the hangar area.

Relationship of the experiment bay to the MORL hangar area and arrangement of the various components are shown in Figure 2-16. Major components that form the bay are:

1. Pressure bulkhead and floor.
2. Two sets of end bulkheads.
3. Meteoroid shield.
4. Bay door and actuator.
5. Sensor beam.
6. Precision attitude reference and sensor mounting well.
7. Experiment airlock.
8. Experiment mounting pads (interior and exterior).

To add the bay to the hangar area requires that a longitudinal bulkhead be introduced to complete the pressure shell at the bay cutout and provide a tension tie across the hangar shell at the point of discontinuity. To complete the pressure shell, the bulkhead or floor is also attached and sealed to the front pressure dome and to the rear flat bulkhead which form the operation compartment floor.

Each end of the bay is enclosed by a bulkhead, which is sealed to the floor, to help form a pressure-resistant area. The area adjacent to each end bay bulkhead is open to space, to relieve the necessity of providing seals around the sensor-mounting posts (aft) and the sensor-mounting well (forward). Installed within the experiment bay and just under the pressure floor is a meteoroid shield. When the bay is open and exposed, there is the possibility of meteoroids entering and striking the upper surface of the bay area. For belly-down orientation, the path angle of the meteoroid to the vertical axis of MORL cannot exceed the horizon look angle of approximately 74° , or a maximum strike angle to the bay roof of approximately 28° . However, for other orientations of the MORL, the meteoroid strike angle could be as high



53-4

53-3

53-2

53-1

as 90° to the bay roof, and protection against the possibility of meteoroid penetration is provided by this shield.

The bay door and actuating mechanism complete the bay and serves the dual function of providing an aerodynamic cover in the launch phase and a meteoroid shield and pressure seal in the experiment phase. Two straps are used to attach the door to the actuating mechanism and to provide clearance around the horizon-sensor well. A motor and speed-reduction unit is used to open and close the door, in the following sequence:

1. The door is rotated until it has almost reached the closed position.
2. Ledges on the door side move into recesses in the hangar structure.
3. When the door edges contact the MORL structure, the door rotation is stopped.
4. At the end of the rotation cycle, the actuator moves the door parallel to the bay sides, a distance of 2.5 in. This lateral movement slides the door until all projection lips or ledges are under the corresponding ledges of the structure.
5. After the actuator has stopped, the door is mechanically locked to the hangar structure by engaging the lock ring at the aft end.
6. The seal ring around the periphery of the door opening is inflated and the experiment bay is pressurized.

One of the requirements of the experimental program is for an angular alignment tolerance of 0.01° between the precision attitude reference and the installed experiment sensors. To meet this tolerance, a rigid beam is provided, isolated from all structural loads and movements; it provides a rigid tie with machined mounting plates between sensors to maintain mechanical alignment. Stresses and movements introduced by temperature gradients are minimized, since the beam is located in the environmentally controlled hangar. Spherical bearings are mounted on the stiffening beams of the operational compartment floor, and stub shafts from the sensor mounting beam provide a three-point suspension. This isolates the sensor beam from the movements of the MORL structure, which are caused by temperature changes and internal pressure variations.

A mounting well is provided to support the permanent installation of star trackers, precision attitude reference components, and horizon sensors;

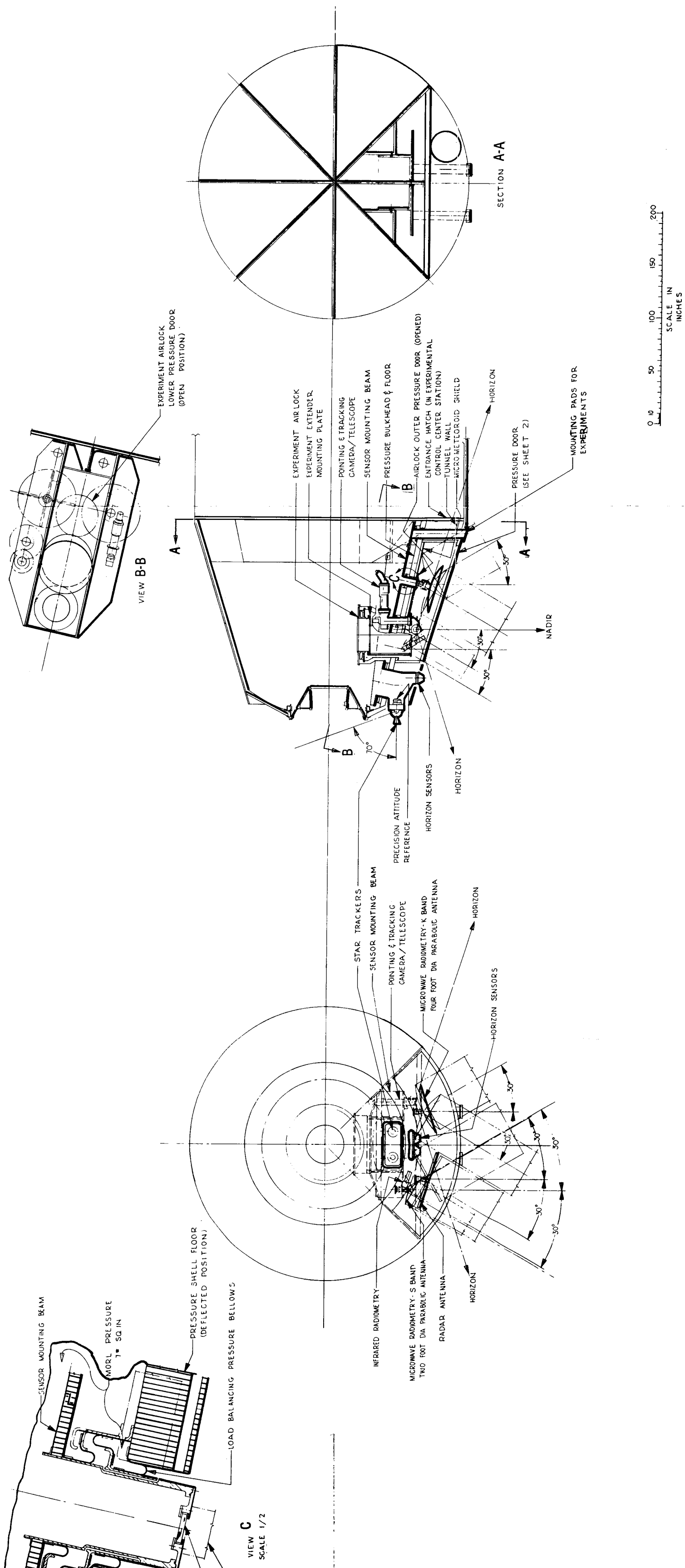


Figure 2-16. Sensor Beam In MORL Hangar

53-0056

2

53-0056

it is located at the front end of the hangar area, and is fastened to the sensor beam. Clearance holes have been provided in the front bulkhead and lower hangar shell for the star trackers and horizon sensors. Because the well is open to the inside hangar area, it allows for the removal and replacement of the precision attitude reference, the horizon sensors, and associated electronic equipment in the shirt-sleeve environment. Part of the optical alignment equipment, used to measure the precise angular alignment between sensors, will be located in this area.

An experiment airlock, similar to the one used in Phase IIa, is incorporated in the bay to introduce experiments to the environment of space without requiring extravehicular activities for the crew. This airlock may be used in conjunction with the experiment bay sensors or for individual experiments; use of the airlock requires that the bay door be opened. The features of construction and operation are similar to those described in Section 2.5 of Reference 3. When the bay is in use, the airlock lower pressure door is opened and stowed next to the meteoroid shield. The airlock may be used as a passageway between the hangar area and the bay when it is not in use.

Before the experiment mounting locations are made final, the projected list of experiments must be integrated into the MORL design, and the type, size, and number of sensors projected for use in the experiment bay must be determined.

Since the mounting pads, experiment airlock, and other units fastened to the sensor beam project through the pressure shell, a flexible seal must be provided between them and the pressure shell. A load-balancing pressure flange and seal is provided for each unit to prevent the introduction of a pressure load on each unit which would be transferred to the sensor-mounting beam. This seal arrangement is described in detail in Section 3.3.

An access door is installed in the sensor-mounting beam for installation and future replacement of pressure seals. Prior to seal removal, the space between the pressure floor cutout and the projecting unit must be sealed to prevent the loss of hangar pressure. An inflatable seal ring is installed below the bellows and around each unit to enable this pressurization. Before

the replacement operation is started, the seal ring is inflated, which seals off the space and allows the seals to be removed and replaced. Clearance of the passageway is provided when the added seal ring is deflated; it does not interfere with the bellows operation or freedom of movement of the sensor shell or posts.

Access to the experiment bay is gained through an entrance hatch located in the floor of the operations deck. A tunnel is installed between the two walls to provide a pressure seal between the floor and the aft bulkhead, since the area is open to space.

The addition of the experiment bay has imposed a number of new control and display requirements. Controls are necessary at the master control panel for remotely actuating components of the experiment bay. Further, it will be necessary to monitor the status of operations involving the experiment bay to ensure against inadvertent loss of Hangar/Test area pressure. The control and display requirements are summarized in Table 2-3.

2.2.5 Radiation Shielding

Radiation shielding requirements in earlier phases of the MORL study program did not appear to be particularly difficult. However, the expanded missions analysis, conducted during the Task III responsiveness analysis (Reference 4) introduced requirements which are more severe, especially in the synchronous orbit case. The requirements are further complicated by the Starfish artificial electron source, and by the number of solar flares that are likely to be encountered in a 1-year period. The shielding requirements for the three missions are summarized in Table 2-4, as determined by the Shield Weight Optimization For Radiobiological Dose (SWORD) computer program output (Reference 4). The shield thicknesses noted are in inches of polyethylene material for six locations.

Table 2-3 (page 1 of 2)
EXPERIMENT BAY CONTROL AND DISPLAY REQUIREMENTS

Area	Type of Control	Type of Display	Function	Remarks
Bay door (exterior)	Actuator		Open/close door	Three-position switch
		Indicator light (3)	Door opening, door closing, or off	
		Dial	Door opening in degrees	Synchro transmitter to synchro receiver
		Indicator light	Door opened or closed	
Door between operations experiment area	Switch		Latch/unlatch lock	
		Indicator light	Lock latched/unlatched	
			Inflate/deflate seal	
		Indicator light (3)	Seal inflated/deflated; seal lock	
Experiment airlock		Indicator light (2)	Door opened/locked	
		Indicator light (2)	Airlock opened/locked	

Table 2-3 (page 2 of 2)

Area	Type of Control	Type of Display	Function	Remarks
Pressure leaks		Indicator light (10)	Location of pressure leak	Areas to be monitored: Precision attitude reference shell Experiment airlock Pointing and tracking camera/telescope Experiment mounting posts (inside bay) Experiment mounting posts Door between bay and operations experiment area

Table 2-4 (page 1 of 2)
MORL SHIELD REQUIREMENTS

Orbit Altitude and Inclination	Case No.	Mission Duration (days)	Artificial Electrons	Solar Cycle	No. of Solar Flares	Total Shield Weight (lb)	Shield (Polyethylene) Thicknesses (in.)*						Absorbed Dose (Rem)					
							Main Shield			Biowell			Mission Total		Flare Total			
							T1	T2	T3	T4	T5	T6	Eyes	Skin	BFO**	Eyes	Skin	BFO**
200 nmi 50 °	1	90	No	Min.	1	No	110	0	0	0.04			97	117	43	55		
	2	180	No	Min.	1	No	110	0	0	0.04			147	176	43	55		
	3	365	No	Min.	1	No	110	0	0	0.04			247	294	43	55		
	4	180	No	Min.	2	No	110	0	0	0.04			193	235	87	109		
	5	365	No	Min.	2	No	165	0	0	0.06			202	216	86	109		
	6	365	No	Min.	2	Yes	165	0	0	0.06	0	0	221	213	103	106		
	7	365	No	Min.	3	No	165	0	0	0.06			249	275	130	163		
	8	365	No	Min.	3	Yes	275	0	0	0.06	0	0.27	226	210	122	107		
	9	90	No	Max.	1	No	55	0	0	0.02			118	269	44	55		
	10	180	No	Max.	1	No	110	0	0	0.04			78	88	43	55		
	11	365	No	Max.	1	No	110	0	0	0.04			108	118	43	55		
	12	365	No	Max.	2	No	110	0	0	0.04			155	177	87	109		
	13	90	Yes	Min.	1	No	386	0	0	0.14			224	258	6	42	53	1
	14	180	Yes	Min.	1	No	826	0	0	0.30			243	300	11	39	52	1
	15	365	Yes	Min.	1	No	1,410	0	0.02	0.48			289	367	23	37	49	1
	16	180	Yes	Min.	2	No	990	0	0	0.35			248	315	14	77	103	2
	17	365	Yes	Min.	2	No	1,650	0	0.07	0.51			284	368	24	68	91	2
	18	365	Yes	Min.	2	Yes	1,490	0	0	0.47	0.12	0.45	284	349	22	60	57	2
	19	365	Yes	Min.	3	No	1,900	0	0.12	0.54			286	370	76	96	128	3
	20	365	Yes	Min.	3	Yes	1,625	0	0	0.49	0.24	0.54	284	354	24	75	77	3

*T1 Common bulkhead between operations deck and Hangar/Test Area
T2 Sidewall area between common bulkhead and dome joint.
T3 Aft hemispherical dome.
T4 Floor segment in operations bay
T5 Sidewall of operations bay
T6 Ceiling segment of operations bay

**BFO--Dose received by the blood-forming organs

59-1

Table 2-4 (page 2 of 2)

Orbit Altitude and Inclination	Case No.	Mission Duration (days)	Artificial Electrons	Solar Cycle	No. of Solar Flares	Biowell	Total Shield Weight (lb)	Shield (Polyethylene) Thicknesses (in.)*						Absorbed Dose (Rem)		
								Main Shield			Biowell			Mission Total		Flare Total
								T1	T2	T3	T4	T5	T6	Eyes	Skin BFO**	Eyes Skin BFO**
200 nmi 90 °	21	90	Yes	Max.	1	No	330	0	0	0.2				228	262	3 42 53 1
	22	180	Yes	Max.	1	No	745	0	0	0.26				243	300	5 38 52 1
	23	365	Yes	Max.	1	No	1,190	0	0	0.42				285	374	9 38 51 1
	24	365	Yes	Max.	2	No	1,375	0	0.02	0.46				286	379	10 73 98 3
	25	90	No	Min.	1	No	1,820	0.19	0.39	0.07				106	111	89 97
	26	180	No	Min.	1	No	1,820	0.21	0.39	0.06				123	125	89 96
	27	180	No	Min.	2	No	1,790	0.21	0.39	0.05				213	222	179 193
	28	180	No	Min.	2	Yes	330	0	0	0.03	0.12	0.53	0.21	218	223	182 191
	29	90	No	Max.	1	No	1,820	0.19	0.39	0.07				98	103	89 97
	30	180	No	Max.	1	No	1,820	0.19	0.39	0.07				106	110	89 97
19,350 nmi 30 °	31	90	Yes	Min.	1	No	2,200	0.18	0.34	0.27				148	170	4 81 95 3
	32	180	Yes	Min.	1	No	2,340	0.15	0.32	0.37				173	203	0.6 81 98 4
	33	180	Yes	Min.	2	No	2,410	0.15	0.32	0.39				245	291	13 160 195 8
	34	180	Yes	Min.	2	Yes	1,420	0	0	0.3	0.61	1.02	0.53	244	290	13 108 122 6
	35	90	Yes	Max.	1	No	2,200	0.18	0.34	0.27				142	163	3 81 95 2
	36	180	Yes	Max.	1	No	2,340	0.15	0.32	0.37				161	190	4 81 98 2
	37	90			1	No	42,000	2.6	3.9	8.9				86	50	7 2
	38	90			1	Yes	41,800	1.4	3.1	9.2	4.0	5.1	0	86	50	4 1
	39	180			1	No	49,500	2.8	4.9	10.1				137	80	4 1
	40	180			1	Yes	48,800	2.2	4.2	10.2	3.8	4.9	0	137	80	4 1
	41	180			2	No	50,300	3.0	5.0	10.1				139	80	8 3
	42	180			2	Yes	49,400	2.3	4.2	10.2	3.8	5.0	0	138	80	7 2

*T1 Common bulkhead between operations deck and Hangar/Test Area
T2 Sidewall area between common bulkhead and dome joint
T3 Aft hemispherical dome
T4 Floor segment in operations bay
T5 Sidewall of operations bay
T6 Ceiling segment of operations bay
**BFO--Dose received by the blood-forming organs

Aluminum may be substituted for polyethylene on an equal weight basis with essentially equal shielding; the shielding is a function of the material atomic number, and polyethylene and aluminum have nearly equal numbers.

Table 2-4 shows that the shield weights range from 110 to 1,900 lb for the 50° orbit mission, depending on which governing parameters are selected, but the weight may increase to a nominal 40,000 lb for the synchronous orbit; the possible range of shield weights indicated is from 4,400 to 110,000 lb. These weights indicate the degree of uncertainty of the environment definition, and preclude strong confidence in present radiation shielding solutions. Solutions are postulated for the 50°-inclination and polar-orbit cases to better determine the configurational problems associated with presently known radiation shielding requirements. These solutions are based on adding shielding material to the periphery of the inhabited areas. Other techniques are possible but were not investigated in this study; however, several of these techniques are listed below:

1. Rearrangement of the laboratory configuration to minimize the operating volume (or inhabited area) and to maximize the inherent protection given by operating equipment and installations. This technique obviously takes advantage of on-board equipment; however, it implies excellent knowledge of the mission and of the necessary equipment to support the mission. It also restricts flexibility.
Use of on-board supplies and materials such as water, propellant, or food to provide shielding. This provides variable shielding, since consumables are used during the mission.
3. Use of personal shielding such as eyeglasses, vests, or smocks which contain high percentages of shield material. The shielding effectiveness as a function of the discomfort of such items has not been evaluated.
4. Investigation of materials and combinations of material to decrease unit weight for the same given shield protection. This evaluation requires definitive knowledge of the actual environment to be encountered; it should be readily simulated in Earth laboratories, once criteria are established.
5. Investigation of methods of installing additional shield materials in an orbital environment.

6. Design and optimization of a biowell to which the crew retreats during high-intensity radiation and normal sleep periods.

Combinations of these and other techniques will probably be necessary; for example, small weight laminar material could be used around the periphery of a vehicle with the interior arranged judiciously to provide equipment protection. Individual shielded clothing could be worn during the waking hours, with a bunk biowell used for sleeping. The dose rate would be higher during the working periods, but decreases during sleep periods so that the time-integrated dose rate is within acceptable limits.

Part of the uncertainty of the present radiation criteria has to do with the artificial electron environment produced from the Starfish high-altitude nuclear bomb tests. General agreement exists that the electrons will eventually disappear, but the rate of dissipation is open to question. One hypothesis, tentatively accepted by Langley Research Center, is that the increased solar activity predicted for the late 1960's and early 1970's will cause the artificial electron field to expand into the Van Allen Belt, where it will be captured, thus leaving the altitudes beneath the belt essentially clear of Starfish electrons. This hypothesis is accepted for this study, and it is assumed the artificial electrons will have been dissipated by the time the MORL is operational.

It is further assumed that shield protection for two solar flare events must be provided, based on the 12 November 1960 solar flare event intensity. The chance of two flare events is based on the Poisson probability distribution corresponding to the observed maximum activity portion of the 11-year solar cycle. (See Reference 4, Task III.) The probability of encountering two events in a 12-month period is approximately 0.27, whereas the probability of three events is about 0.08. Should these events actually be encountered the crew would have to be relieved.

The following sections describe the shielding for each mission, using these assumptions. It is emphasized that only the 50° inclination orbit mission definition is considered as a baseline change.

Shielding requirements are not severe for the 50° inclination baseline mission, using the specified environment, which minimizes artificial electrons. The requirements can be met by adding 165 lb of shielding to the aft dome. This increase requires an additional 20 mils in the material gage, which provides shielding for 365 days of crew exposure and two solar flares, and simultaneously increases the structural pressure safety factor and meteoroid penetration protection. Protection against two solar flares causes a weight penalty of 55 lb over the single solar flare shield weight in this case, and provides for a high probability of mission success. No internal rearrangements are required.

Two solutions were considered for the polar orbit case: use of the baseline structure plus a biowell, for a total weight penalty of 330 lb, or an increase of the shield material at the periphery, without a biowell, for a total weight penalty of 1,820 lb; either method allows 180-day exposure time and provides protection for two solar flares.

In the first case, the baseline structure could be used without change since the increased dome thickness is less than that required for the baseline 50° inclination orbit. The biowell could then be added by placing polyethylene material on the operations bay floor, ceiling, and sidewall, as noted in Table 2-4, Case 28. The polyethylene might be in large panels adhesively attached without disrupting either the arrangement of the equipment or the installations. Total added weight would be only 330 lb, but retreat to the biowell, with the consequent interruption of station activity, is necessary during each solar flare. Depending on the duration of the flare, this could be an annoying restriction, although necessary vehicle functions can be performed from this location.

The second case allows complete flexibility within the laboratory, since the peripheral shielding gives adequate protection against solar flare events. It is the preferred solution at this time because the weight can easily be accommodated by the Saturn V booster.

The shield thickness requirements are noted in Table 2-4, Case 26. The dome thickness is the same as the baseline gage and the dome structure is

used intact. The sidewall and floor shielding require minor structural changes. The sidewall aluminum equivalent of the polyethylene is about 130 mils; it is best added to the pressure shell, as shown in Figure 2-17. The revision could be made without a large tooling change because the sidewall is router-milled of plate stock, and an increase in the sidewall gage requires only a lighter cut. The floor could also be revised without an extensive tooling change, by increasing each face of the sandwich-constructed floor by 36 mils; no manufacturing process changes are necessary for the thickened faces.

All of the shielding requirements noted in Table 2-4 are beyond the ability of the Saturn V booster to lift into synchronous orbit with a MORL vehicle; the shielding weight is limited to about 25,000 lb, to allow integral launch. Because of this considerable weight, the other shielding techniques outlined previously need to be evaluated before a valid shielding design can be recommended. Furthermore, the Task III (Reference 4) analysis shows that the electron field at synchronous altitude may vary by as much as a factor of 10 because of actual environment uncertainty; this results in a shield variation of 4,400 to 110,000 lb. These weights generated an investigation into the problems associated with thick radiation shields.

Heavy shielding may be added to the laboratory at launch time or it may be supplied and attached to the laboratory in orbit. The latter case, however, would expose the crewman for a considerable period of time to the extra-vehicular environment, in which his only protection from radiation is his pressure suit and whatever personal protection he can wear; such exposure is unreasonable. Attachment of shielding internally, where the crewman is more protected, involves access to the entire periphery of the habitable volume and the movement of nearly all equipment installation; this approach is also of marginal validity. Also, the cost of the launch to supply the shielding essentially doubles the initial mission cost. For these reasons, separately supplied shielding installed in orbit was not investigated further.

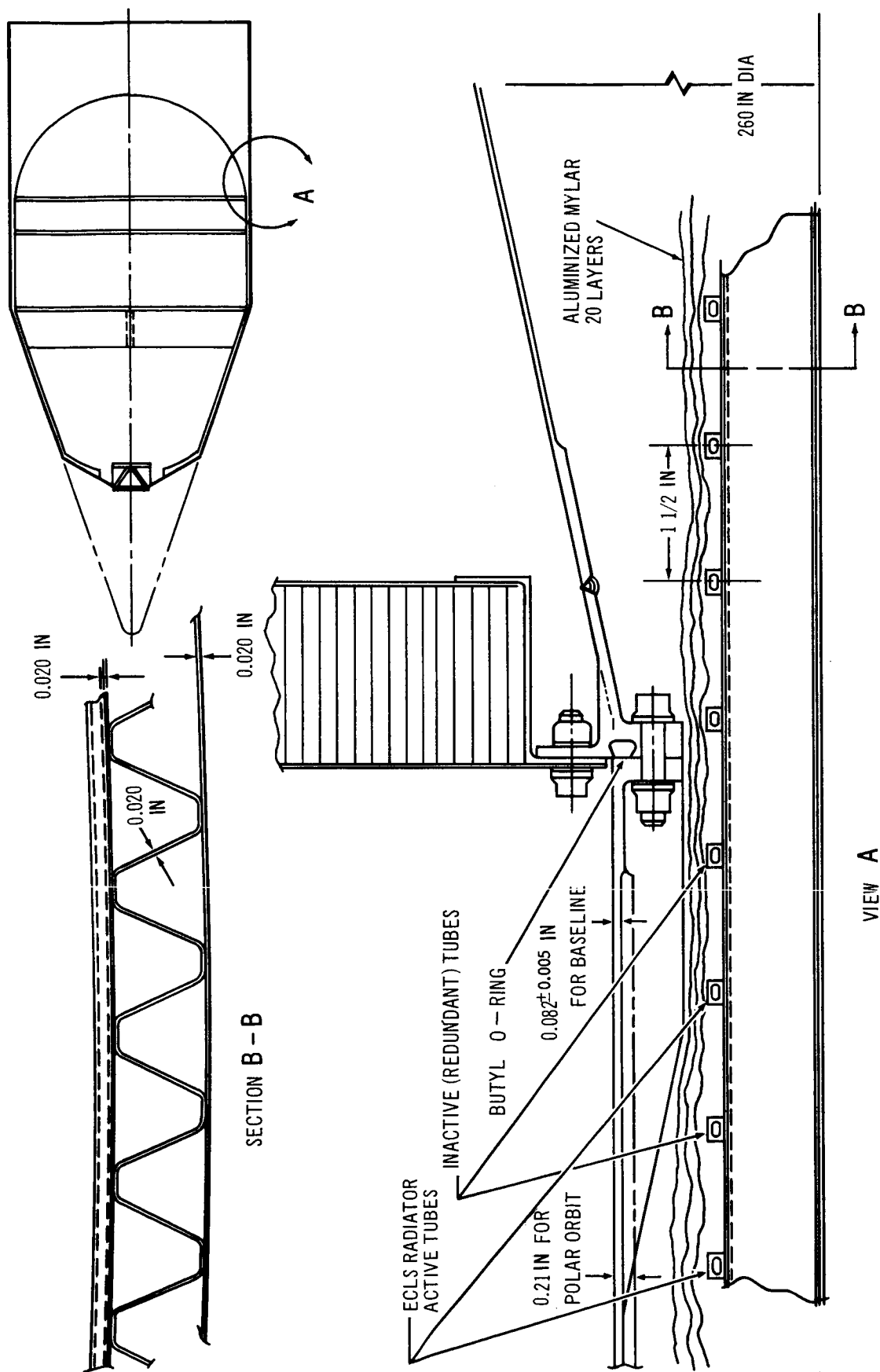


Figure 2-17. Structural Concept - Polar Orbit Radiation Shielding

Figure 2-18 shows how 25,000 lb of peripheral shielding would be utilized. This is the boost limit for a synchronous orbit mission MORL. The required shield thicknesses were derived from Case 37 of Table 2-4, adjusted for a total weight of 25,000 lb.

In the concept shown in Figure 2-19, the baseline load-carrying outer shell is revised to make it a fairing and radiator only, and the shield material is added to the pressure shell, which is converted to the load-carrying member. Meteoroid penetration protection is assured by the thickened basic pressure shell. The radiator structure provides protection during boost for the aluminized Mylar layers used for thermal control. The baseline pressure dome is converted to a plate supported by a tension member, which transmits the dome pressure loads to the beam-supported Hangar/Test area bulkhead. This is necessitated by the impracticality of stretch forming 1.7 in. thick material. The plate is placed 80 in. from the centrifuge, making a second deck that is the same size as the baseline operations deck. The pressure shell and EC/LS radiator assembly are thermally insulated from the load-carrying aft inter-stage area by short length of fiberglass honeycomb section. The aft inter-stage skin is straddle milled from 1/4 in. plate. Corrugated frames which also support the power system radiator tubes, provide the required circumferential stiffening. The internal arrangement of the basic laboratory systems are as shown in the baseline.

Because of study time limitations, no attempt was made to optimize the laboratory, and the lack of shielding in the Hangar/Test area would restrict its use to occasional experimentation setup or transit to and from the logistic vehicles. Operation of the hangar equipment must therefore be from the operations deck, which adds considerable load to that area. In addition, the tension member which runs through the laboratory restricts interior flexibility. The example illustrates that the structural problems associated with heavy shields can be solved, and that weight, cost, and flexibility (rather than structural feasibility) are the paramount problems.

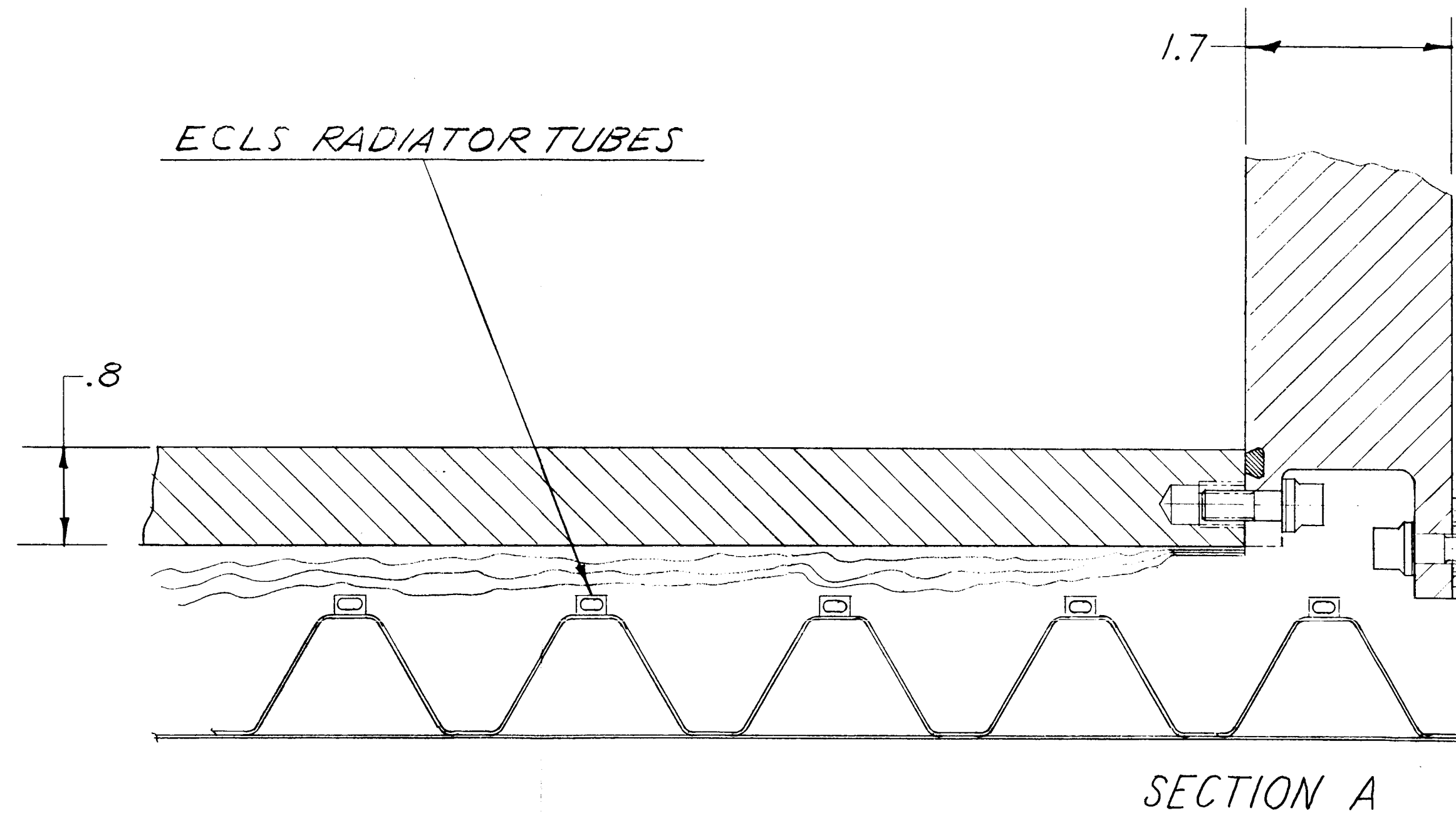
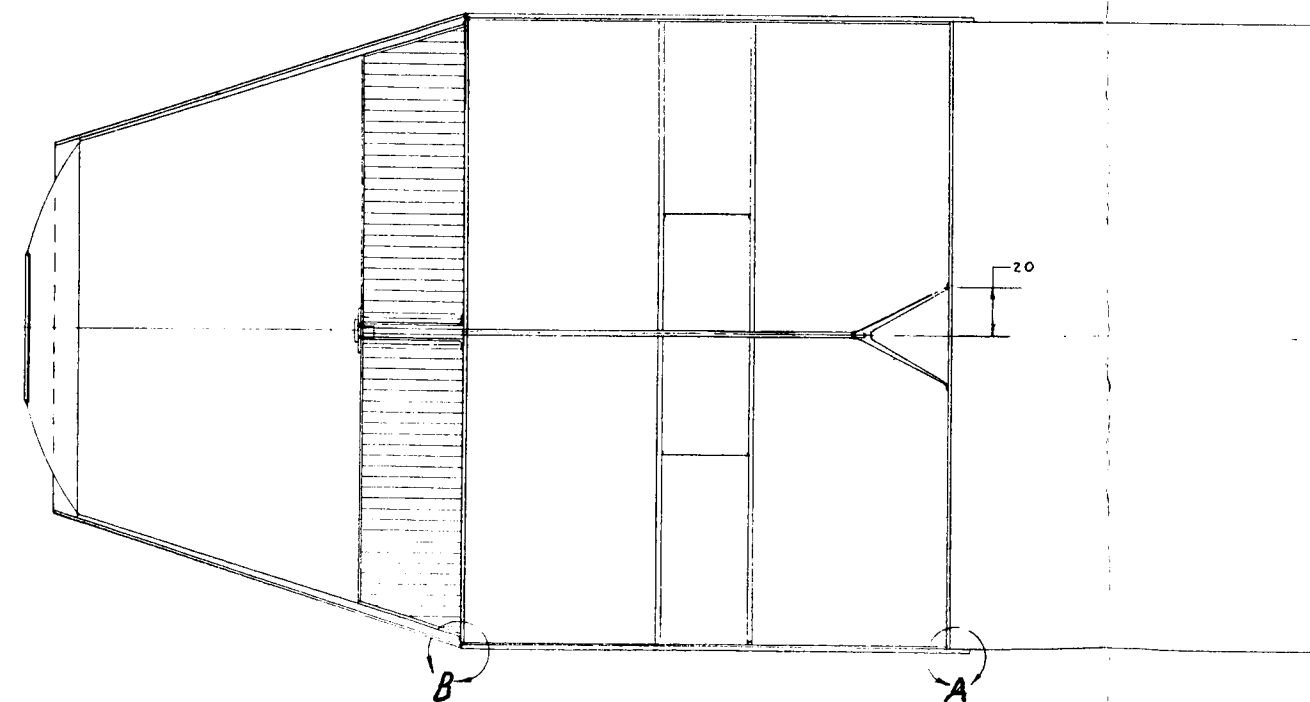
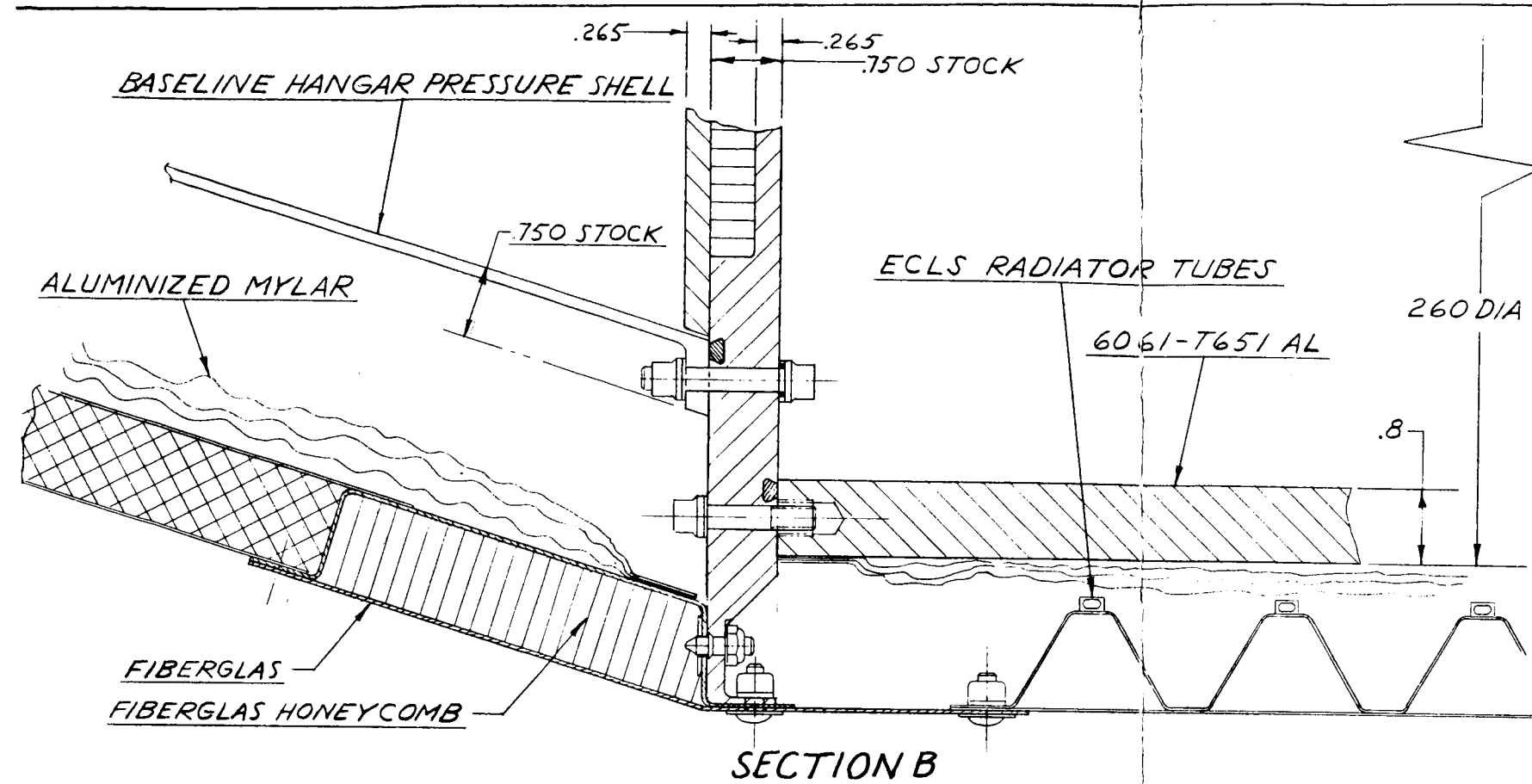
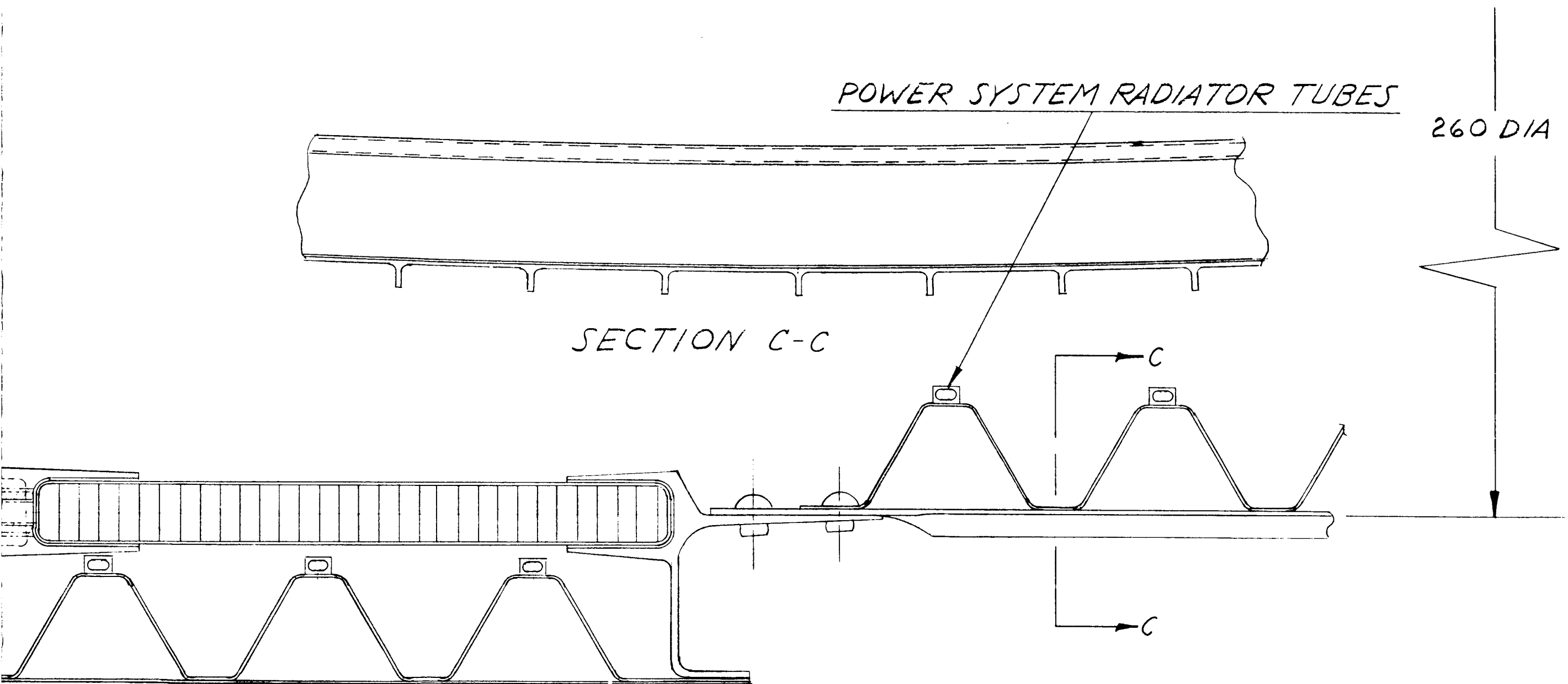


Figure 2-19. Structural Design - Synchronous Orbit Mission



68-4

2

68-5

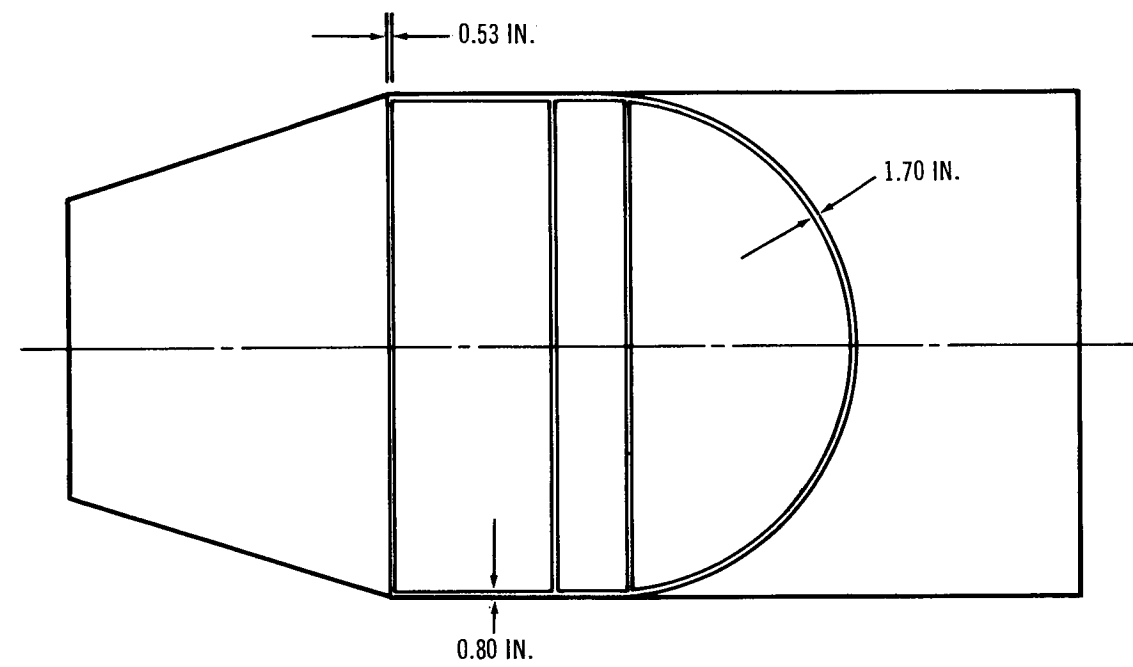


Figure 2-18. Synchronous Orbit Shield Thicknesses

The following sections describe the analysis used to substantiate the structural design.

A design-pressure differential of 17.5 psi was selected for the flat compartmenting bulkhead between the hangar and operations decks. The maximum stress in a 45° segment which is simply supported on all sides by the support beams is given by

$$S_t = \frac{0.114 p a^2}{t^2} \quad (\text{Reference 5}) \quad (2-1)$$

The required monocoque thickness is

$$t = 130 \sqrt{\frac{0.114 \times 17.5}{67,000}} = 0.71 \text{ in.} \quad (2-2)$$

Since this is greater than the thickness required for shielding, a sandwich construction must still be used. The required core thickness is estimated by equating the I/C for the sandwich with that required for the monocoque bulkhead.

$$I/C = 2 \left(\frac{t_f}{2} + \frac{h}{2} \right)^2 t_f \times \frac{1}{\frac{h}{2} \times t_f} = \frac{t^2}{6}$$

$$= \frac{(0.71)^2}{6} = 0.084$$

$$t_f = \frac{0.53}{2} = 0.265$$

$$h = 0.224 = \text{minimum required core thickness} \quad (2-3)$$

To provide an increased margin of safety at a very small increase in weight, the aft face of the sandwich-compartmented bulkhead for the synchronous orbit mission is machined from 0.750-in. plate, so that the core thickness used is 0.750 minus 0.265, or 0.485 in.

The 0.80-in. thickness specified for the cylindrical portion of the pressure shell can be readily power-brake-formed to the cylindrical contour. To facilitate welding of this thickness, the most weldable aluminum alloy that

is available in large plate sizes can be selected. Since the working stress level is so low (1,140 psi), the alloy strength is of little consequence except in the area of the bolted end joints. For this reason, 6061-T651 plate is used for the cylindrical portion of the pressure shell for the synchronous orbit mission instead of 2014-T651.

If the shield material is added to the pressure shell, the resultant weight is beyond the axial load capability of the cylindrical portion of the pressure shell; it is therefore impractical for this mission to suspend the pressure shell within a load-carrying outer shell. The cylindrical part of the pressure shell is 204.13 in. long. The resulting surface area is adequate for the reduced EC/LS radiator requirements on the synchronous orbit mission. The flight loads are therefore carried through the thick monocoque pressure shell. A fairing, spaced away from the pressure shell, serves as the mounting surface for the radiator tubes and protects the aluminized Mylar insulation around the pressure shell from the boost environment. The super insulation is still required with this revised structural arrangement, to keep the temperature of the pressure shell walls from falling below the dew point of the laboratory atmosphere.

The hangar portion of the pressure shell is unchanged from the baseline design, being bolted to the compartmenting bulkhead.

The conical portion of the outer shell is not required for radiator area for the synchronous orbit mission. A sandwich construction, with 0.020-in. aluminum faces and a truss-grid aluminum honeycomb core is therefore used.

The loads on the aft interstage are significantly increased over those imposed by the baseline configuration because of the increased launch weight. No flight loads analysis has been conducted for this configuration for the synchronous orbit mission. However, it is safe to assume that the load will not exceed the design load for the Saturn IVB forward interstage (1,318 lb/in.) since the synchronous orbit payload capability of the C-5 booster (60,000 lb) is slightly less than for the lunar mission, and the S-IVB forward interstage is designed to accommodate the loads imposed by the

lunar mission payload. An interstage design with this load-carrying capability, and which efficiently integrates the power systems radiator with the interstage structure, is shown in Figure 2-19.

The total length of the MORL configuration for the synchronous orbit mission is the same as the length of the baseline configuration. Since the requirement for radiator area is reduced for this mission from the baseline configuration, the radiator was removed from the conical portion to simplify the structure. If more radiator area is desirable than is available on the present 29.5 ft of cylinder length, it can most easily be incorporated into the meteoroid shield, which closes off the end of the aft interstage, or into the conical section.

The hemispherical shape used for the aft dome on the baseline configuration was selected to minimize the weight of the pressure shell and to make use of existing tooling and a developed manufacturing process. However, the 1.7-in. dome thickness specified as a radiation shielding requirement for the synchronous orbit mission makes these reasons no longer valid. The stress is maximum at the center of a flat monocoque bulkhead that is substituted for the hemispherical aft bulkhead. The maximum stress is given by

$$S = 1.24 p \left(\frac{a}{t} \right)^2 \quad (2-4)$$

If this thick flat bulkhead is designed for 17.5 psi, which seems reasonable because of the great damage resistance of this bulkhead, the required thickness is

$$t = 130 \sqrt{\frac{1.24 \times 17.5}{67,000}} = 2.38 \text{ in.}$$

Since this is greater than the 1.7-in. thickness required for radiation shielding, some means of support must be provided if a flat aft bulkhead is to be used. Four support beams are used for the flat compartmenting bulkhead. These beams can also be used to support the flat aft bulkhead, by employing a single tension member extending aft from the center of the compartmenting

bulkhead to the center of the aft bulkhead. In this case, the support beams will experience their maximum load when both the hangar and the main compartment are pressurized, and will be unstressed when the hangar is pumped down. The design load in the tension member can be estimated by equating the deflection 20 in. from the center of the bulkhead caused by a uniform pressure differential of 17.5 psi, to the deflection from a uniform load applied on a concentric ring 20 in. in radius (see Figure 2-18). Then, from Reference 5:

$$\frac{pa^2}{3Et^3} \left[2a^2 + \frac{r^4}{2a^2} - 2.5r^2 \right] = \frac{4w}{3\pi Et^3} \left[1.25(a^2 - r^2) - 2r^2 \log \frac{a}{r} - \frac{r^2(a^2 - r^2)}{4a^2} \right] \quad (2-5)$$

by taking $m = 3$ ($\gamma = \frac{1}{3}$) and combining Cases 1 and 3

$$p = 17.5 \text{ psi, } a = 130 \text{ in., } r = 20 \text{ in.}$$

$$\text{from which } w = 400,000 \text{ lb}$$

If 160,000-psi heat-treated titanium is used for the tension member, its cross-section area will be

$$\frac{400,000}{160,000} = 2.50 \text{ in.}^2$$

and its weight, less the weight of the end fittings, is given by

$$2.50 (204) 0.16 = 81.5 \text{ lb}$$

The maximum shear load in each of the support beams is

$$\frac{400,000}{8} = 50,000 \text{ lb}$$

and the shear flow, which is now constant, is

$$\frac{50,000}{42} = 1,190 \text{ lb/in.}$$

A corrugated shear web, brake-formed from 0.045-in. sheet with a b/t of 40, is selected. From Figure 3-4,

$$h/t = \frac{42}{0.045} = 934$$

the allowable stress is 29,000 psi, and the allowable shear flow is:

$$29,000 \times 0.045 = 1,300 \text{ lb/in.}$$

Because the beams must still be designed for the loading condition which results from evacuating the main compartment while maintaining the hangar pressurized, 0.050 must still be used for the outboard 8 in. of each beam shear web, as shown on Page 126. With both the hangar and the main compartment pressurized, the maximum bending moment in each support beam is

$$50,000 \times 130 = 6.50 \times 10^6 \text{ in. /lb}$$

Since this is considerably higher than the design condition for the baseline configuration (2,520,000 in. /lb) a new weight must be estimated for the beam caps. The required cross-sectional area at the center (with 7075-T6 caps) is:

$$\frac{6.5 \times 10^6}{42 \times 77,000} = 2.01 \text{ in.}^2$$

A straight-line taper to 0.1 in.² at the end is used and the resulting weight for one beam cap is:

$$\left(\frac{2.01 + 0.1}{2} \right) 260 \times 0.1 = 27.5 \text{ lb}$$

The total weight of the beam caps is

$$2 \times 27.5 \times 4 = 220 \text{ lb}$$

The weight of one beam shear web is $0.1 \times 42 \times \frac{4}{3} (0.045 \times 244 + 0.05 \times 16) = 66.1 \text{ lb}$. The total weight of the support beams for the synchronous orbit

mission is thus $220 + 4 (66.1) = 484$ lb. The weight of the support beams for the baseline configuration was 347 lb, so that 137 lb must be added to the beams to permit the use of a flat aft bulkhead for the synchronous orbit mission.

The maximum stress in the 1.7-in. -thick flat bulkhead will occur at the support ring, and can be calculated by again combining Cases 1 and 3 (Reference 5).

Maximum stress (S_r) with $r = 20 = r_o$, is given by:

$$S_r = \frac{w}{2\pi t^2} \left[1 + 4 \log \frac{a}{r_o} - \frac{r_o^2}{a^2} \right] - \frac{1.25p}{t^2} [a^2 - r^2]$$

where

$$a = 130$$

$$p = 17.5 \text{ psi}$$

$$w = 400,000$$

$$t = 1.7$$

from which

$$\max S_r = 57,000 \text{ psi (at ultimate pressure)}$$

and maximum working stress is

$$\frac{7}{17.5} (57,000) = 22,800 \text{ psi.} \quad (2-5)$$

2.3 DESCRIPTION OF BASELINE CHANGES--INTERNAL

Earlier studies in the MORL program placed special emphasis on providing a large laboratory volume to accommodate a diversified experiment program within the 260-in.-diam envelope restriction. During this phase of the study, the interior was evaluated more fully with respect to the expanded experiment program. In certain areas, the laboratory was inadequate; however, for the most part, the Phase IIa MORL was satisfactory. The philosophy of separation of living and working areas is compatible with the experimental program requirements and, for this reason, the major laboratory layout was not revised despite the extensive nature of the revision to the Hangar/Test area. The primary revisions expanded the console and experimental test facilities; major changes were restricted to the Hangar/Test area and the operations deck.

2.3.1 Hangar/Test Area

The Hangar/Test area is shown in Figure 2-1. It was completely revised as indicated by the following items:

1. Conversion of the common pressure bulkhead from a dome to a flat floor.
2. The incorporation of eight deep-section beams to support the pressure bulkhead and the logistics vehicle stowage ports.
3. The addition of six radial Apollo and MMM stowage ports.
4. The addition of an experiment bay.
5. Installation of an equipment mounting beam for experiments and operating equipment.
6. The addition of two experiment console work stations.
7. Conversion of the toroid pumpdown tank to two tapered cylindrical tanks.
8. Relocation of the control moment gyros to the hangar from the under floor area of the operations deck.
9. The addition of a handling system for the maneuver of large or heavy items in the hangar area.
10. Deletion of the cryogenic atmospheric supply tanks.
11. Complete rearrangement of the Hangar/Test area and installation of miscellaneous storage and handling equipment.

The flat beam-supported common bulkhead is necessitated by the addition of the experiment bay and the radial stowage ports which would interfere with the domed bulkhead. No changes are necessary to the external outline, or the pressurized volume. The annular space between the operations deck floor and the domed common bulkhead is effectively relocated in the Hangar/ Test area. This enables the relocation of the control moment gyros and other equipment to the space between the floor beams, where it is more accessible. Crawlway space for entry into each radial stowage port has to be maintained, but there is space for storage of items or installation of equipment on either side of the stowage ports and in the central floor region.

The experiment bay is located longitudinally along the nose belly. It retains the equipment airlock for exchange of smaller items into the space environment; the experiment bay door must be open for experiment airlock use. The equipment mounting beam is integral with the experiment bay and is used for mounting equipment which must maintain close accuracy and alignment with the MORL inertial reference and/or with each other. Several items are permanently installed on the beam because of their frequency of use or because of the difficulty of installation; among these items are the stellar and horizon attitude reference sensors, the inertial reference platform, the pointing and tracking telescope, and the experiment airlock. Mounting pads which extend through the pressure shell are used for numerous experiments. Assembly and alignment of the experiment is accomplished in a shirt-sleeve environment. Access to the experiment bay is provided by two methods: (1) through a hatch located in the operations deck, or (2) through the opened external doors. The former method is used for smaller items and the latter method is used for large or preassembled items; final adjustment and alignment is conducted from the pressurized shirt-sleeve environment of the experiment bay in either case. However, the initial installation must be accomplished extravehicularly if access through the external door is used.

Two individual console work stations are located adjacent to the experiment bay, one on each side of the experiment airlock. Thus, excellent accessibility and flexibility is available for the installation, maintenance, and control of experiments in either the airlock, the experiment bay, or the hangar.

One of the consoles is located directly beneath the scientific test console in the operations bay to provide short wire runs and other advantages for experiments which require close coordination or communication with the operations deck.

The consoles will be used primarily for experiments and, therefore, they must provide flexibility for multiple installations of control, test, and experiment support equipment, such as power supplies or IR cryogenic coolants. Electronic cooling will be provided by the standard laboratory system. Control of certain hangar equipment, such as the experiment airlock, will be conducted from one console or the other. The two consoles provide approximately 16 sq ft of panel space and 55 cu ft of volume for experiment installations.

Support equipment for the operation of the Hangar/Test area is located adjacent to one of the two pumpdown tanks. The support equipment is typified by the hangar EC/LS system and the pumpdown equipment for the experiment bay, airlock, or hangar.

The central core of the hangar remains essentially open for the maneuver of large experiments into position at the experiment airlock, and for preassembly and checkout prior to their being moved into the space environment through the 60-in. diam nose logistics port. A crane assembly (not shown in Figure 2-1) is used to assist in maneuvering the larger and heavier items, or to hold them for preassembly and erection. Transfer of large items from the hangar to the nose experiment boom for external installation is possible by this method. Experiment control and connections to experiments set up in the hangar is possible from either of the consoles.

Large storage facilities are provided along the side of the nose, opposite of the experiment bay; it is anticipated that the major storage for both laboratory supplies and experiments will be also provided in the multimission modules because permanent access is provided through the radial stowage ports.

2.3.2 Operations Area

The baseline operations deck is revised by the addition of an auxiliary scientific test console and an auxiliary maintenance bench. The enlarged test station is located in the scientific and maintenance bay. The auxiliary maintenance console is located at the side wall; it hinges at the outer corners to simplify installation of equipment and experiment apparatus, and to enable inspection and access to the pressure shell. Space is available for two crewmen working simultaneously, although one crewman at a time will be the usual arrangement. The original experiment control console is retained.

The auxiliary test console will house experimental apparatus and control equipment. It must, therefore, be capable of complete revision from time to time; this requires that wiring, coolant lines, and other connections be accessible. Approximately 18 sq ft of panel space and 50 cu ft of volume are available for experiment installations.

The auxiliary maintenance bench hinges from the back side of the operations console. It is intended to be a maintenance and repair station, and no particular connections or apparatus are provided. It is an auxiliary work space in which apparatus will be readily set up and torn down.

A pressure hatch into the experiment bay is located in the scientific bay; it is the same size hatch as the airlock hatches used throughout the laboratory. The hatches leading to the control moment gyros beneath the floor are deleted because the CMG's are relocated to the hangar deck.

2.3.3 Crew Living Quarters

Crew support systems were revised to add provisions for nine men. The provisions were largely restricted to increasing the EC/LS capacity and the galley facilities. The number of crew sleeping quarters remains unchanged (six) and no increase in hygiene equipment or toilet facilities is provided. With a crew of nine men, it is felt that at least three crewmen will always be awake and, therefore, the six bunks, if shared, are satisfactory. Should the actual crew be increased to nine men, additional supplies and equipment will be furnished simultaneously with the men.

The detailed changes to the EC/LS system are noted in Book 2, Douglas Report No. SM-48816. They consist primarily of increasing tank sizes for consumables and enlarging processing systems such as the water electrolysis, cabin conditioning, radiator area, and heat transport system to take care of the larger crew. Therefore, the living quarters do not show a configurational change. The same is true of the galley changes because these changes are associated with more frequent use of the existing systems rather than the addition of different facilities.

Hygiene and toilet facilities are used singly; effect of a crew of nine on these systems is, therefore, an increase of utilization time rather than a requirement for additional facilities. The waste processing system was changed from a thermal-vacuum drying system to one of vacuum only. Furthermore, the waste products are retained in a waste container in the toilet rather than being moved to the drying containers after each use. The waste container is retained in the toilet until it is filled, at which time it is sealed and stored in an MMM prior to discard of the MMM. The effect of a nine-man crew on the toilet system results in a larger storage requirement for waste containers. The laboratory and laundry facilities, like the toilet, are used more often, but the waste products of these systems are largely water borne; the electrolysis system changes to the EC/LS system have been sized to account for the added burden of nine men.

Since the baseline crew size continues to be six men, investigation into a complete revision of the crew living quarters arrangement was not attempted. A review and full explanation of the baseline living quarters may be found in Reference 3. Investigations into quarters for increased crew sizes of 9 and 12 were accomplished in a preliminary fashion.

The nine-man crew size could be accommodated by sharing the six-man crew compartments, or by converting three of the six single-crew compartments to two bunk compartments and retaining three single-man compartments for the crewmen with the longest tours of duty (Figure 2-20).

Twelve men could be accommodated by sharing three bunks of the latter nine-man arrangement above, or by converting all of the single-crew compartments

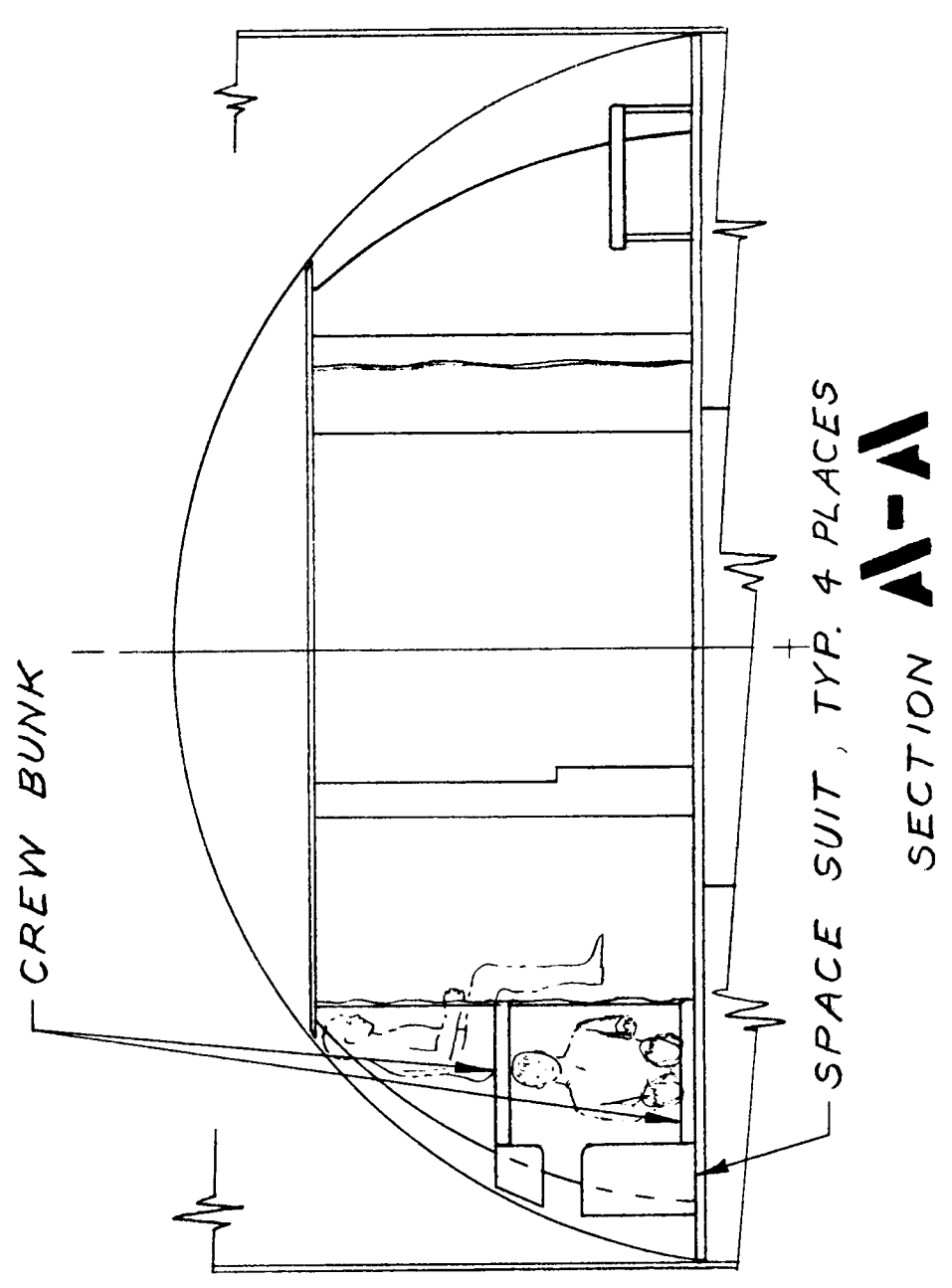
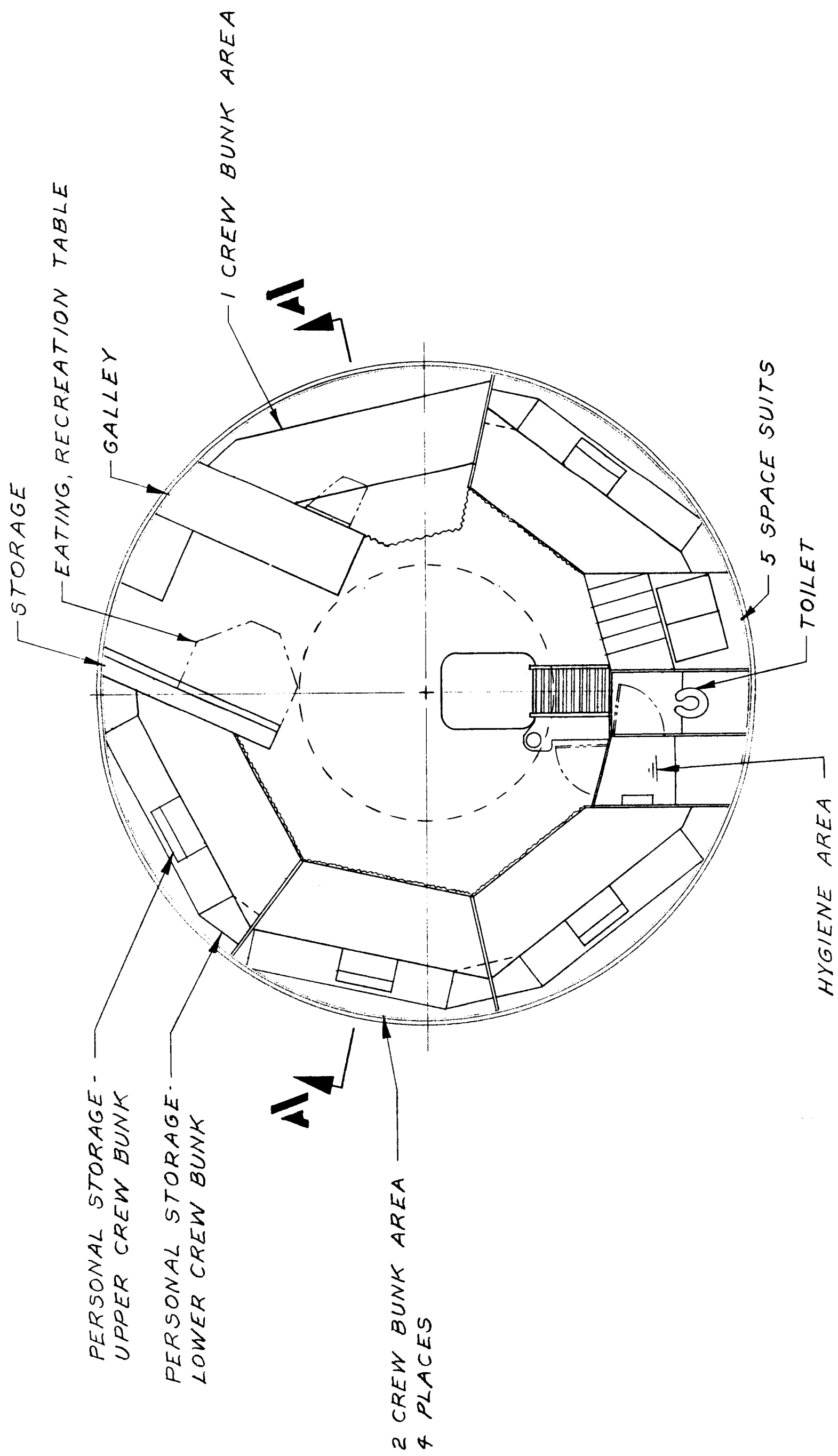


Figure 2-20. Living Quarters (Nine Crew Bunks)

into dual bunks; sharing of the six baseline single-bunk compartments is possible, but the ensuing rotation and asleep/awake schedule problems appear undesirable. A proposed 12-bunk arrangement is shown in Figure 2-21.

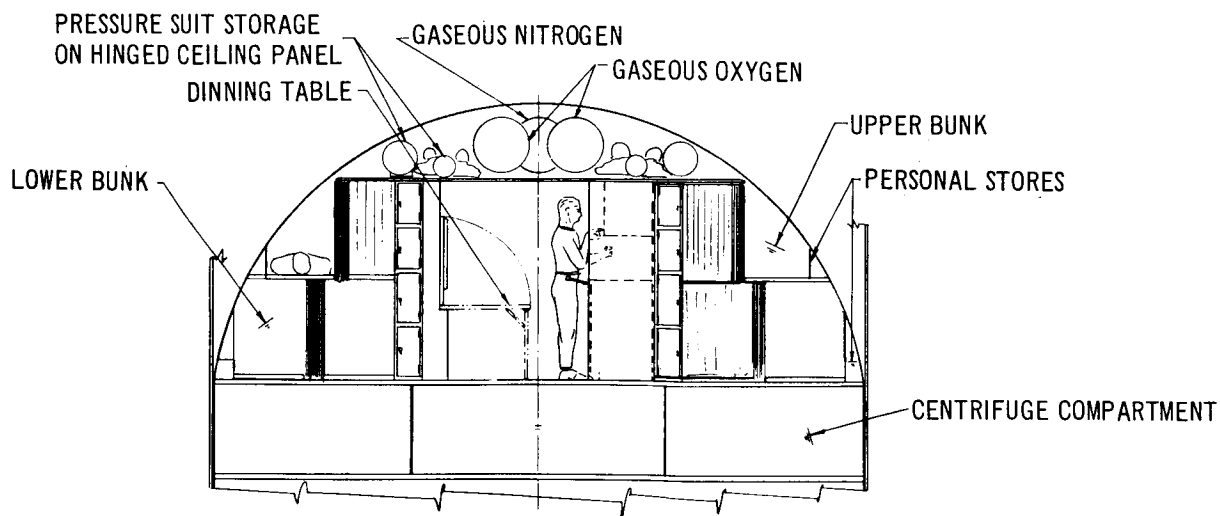
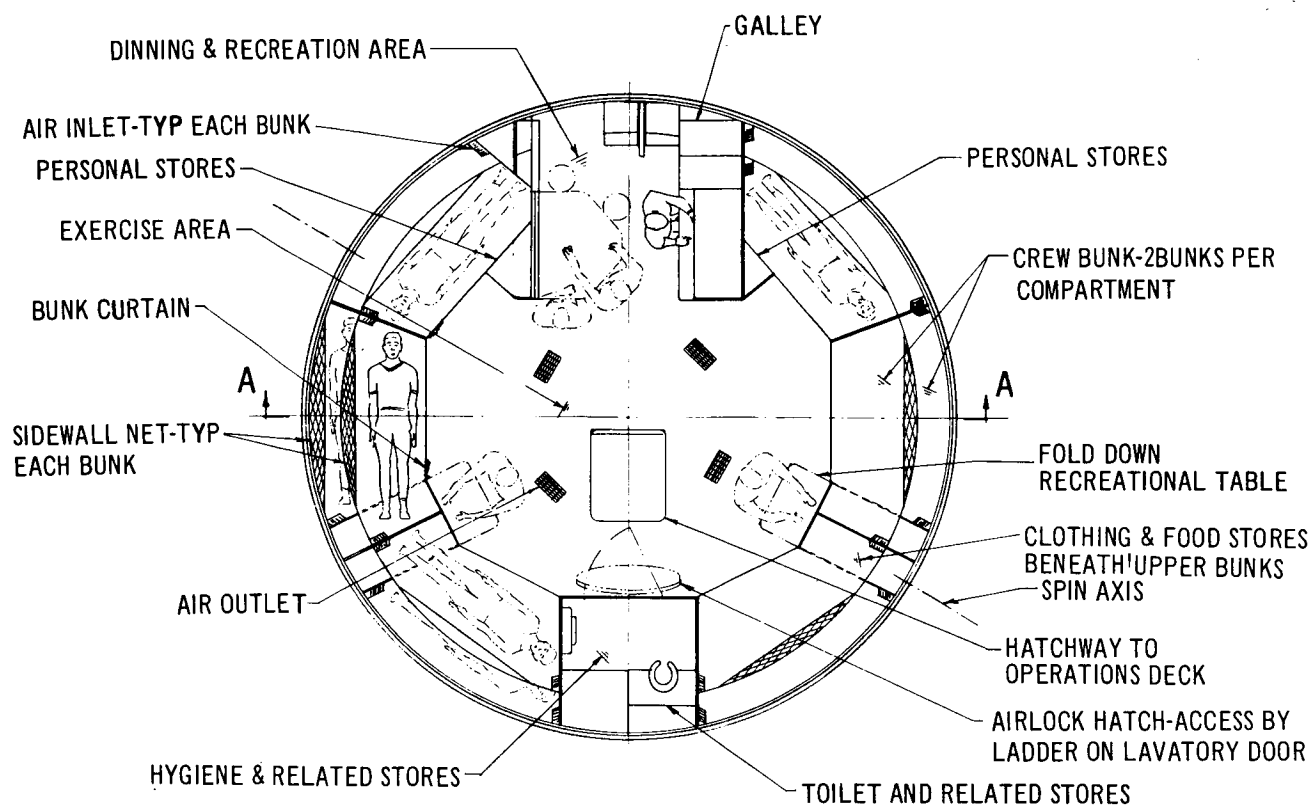
The nine-man configuration leaves approximately the same space for recreation, exercise, and personal upkeep as the baseline MORL. However, it was decided not to penalize the launch weight with the three additional bunks, but rather, for the present, to maintain the larger private area for the crewmen. Addition of the second bunk to the compartment is not difficult, and should nine-man crew requirements arise later, bunks could be added without major system changes.

The 12-man configuration noted in Figure 2-21 was selected because it retains the large central open area. The space-suit stowage area was removed into the overhead to allow for the six additional bunks. Each dual bunk is equipped with sound-deadening curtains which enclose the bunk area and allow privacy for sleep or recreation. The galley and bathroom facilities are the same as for the baseline arrangement; cabinets for storage of clothing and individual items are located beneath the upper bunks.

2.3.4 Displays and Controls

The operation control and subsystems displays station contains controls and displays for all vehicle operations. The panel is designed for a standing operator. A table-high bench and restraint system are provided. Related controls and displays are grouped by function to minimize operator movement and to facilitate rapid and reliable accomplishment of critical tasks. The console is designed so that one man can effectively monitor and control all routine functions.

The design also reflects the need for two-man operations during those instances when multiple or complex tasks occur. The controls and displays are mounted from the back of the panel to provide a clean, uncluttered panel with maximum space for descriptive nomenclature. The front panels are hinged to provide easy access to display fasteners from the front side of the console.



SECTION A-A
 0 50 100 150 200
 SCALE IN INCHES

Figure 2-21. Living Quarters (12 men)

The console is oriented so that Coriolis force effects on the operator are minimized. Immediately adjacent to the console are the items of equipment associated with the control and monitoring functions, including a periscope, typewriter/facsimile printer, and provisions for tape storage.

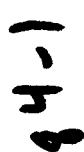
2.4 ALTERNATE CONFIGURATION STUDIES

The baseline laboratory configuration is described in Section 2.2 and 2.3 of this report. This section describes the following two alternate studies of configurational changes accomplished during Phase IIb: (1) an alternate MORL configuration which has an annular internal arrangement and (2) alternate methods of extending the zero-g experimentation capabilities of the MORL should artificial gravity be necessary.

2.4.1 MORL with Annular Interior

Figure 2-22 shows an alternate configuration which maintains external geometrical lines and size of the baseline configuration, but differs in internal configuration and structure. This configuration still retains two decks, a centrifuge, and a separately pressurizable Hangar/Test area which has the same equipment and arrangement as the baseline. The crew sleeping and living quarters are not as well isolated as in the baseline configuration, and a subsystem module is included rather than integrating the subsystems into the laboratory.

The structural concept, which is the primary change, utilizes two light-weight flat-pressure bulkheads with a central load-carrying core running between them. The beam-supported compartmenting bulkhead between the Hangar/Test area and the operational decks is identical to the baseline. Thus, when both the hangar and operations areas are pressurized, the pressure loads from the aft bulkhead are carried in tension through the core into the floor beams of the compartmenting bulkhead. When the hangar is depressurized and the operations deck pressurized, the pressure loads are bucked out against each floor by tension loads through the core. Also, when the hangar is pressurized and the operations deck depressurized, the loads are carried out by the compartmenting bulkhead floor



84-2

beams. Therefore, the central core is a tension member and may be perforated with access cutouts into equipment bays and consoles which are used for maintenance or equipment and experiment exchange. Flat floors and pressure bulkheads are then provided with lightweight tension structure.

The primary external structure may be either the baseline nonload-carrying or the alternate load-carrying pressure shell described in Section 3.

The intermediate floors are supported by the center core and by the pressure shell peripheral edges; the internal consoles, cabinets, and equipment installations are mounted either from the central core or suspended between the floors.

The central-core structure is used for the sleeping quarters; six, nine, or twelve bunks may be installed, depending on the crew size. Storage space for personal gear, clothing, and miscellaneous items is provided. The central core, used as the sleeping quarters, is better shielded from radiation by the equipment bays and surrounding structure than the baseline; it may be converted to a biowell for solar flare protection by adding shielding of a smaller weight than for the baseline because the surface area to be shielded is considerably smaller than the baseline area for living quarters. Surrounding the central core on both of the operational decks are bays for conducting experiments, laboratory control, and personal maintenance.

The floor adjacent to the hangar contains the scientific test station, the biological/liquids laboratory, the analytical station, and the maintenance console. Connections to other equipment or tests in the experiment bay or the hangar consoles are short.

The upper floor contains the laboratory operations station, the biomedical/behavioral test console, and galley equipment; excellent accessibility to the operating subsystems through ceiling panels is provided. The floor also provides a large open area for exercise and recreation.

The subsystem module which contains the laboratory operating subsystems and the centrifuge is located above the operations decks. Interconnecting lines and wiring to other equipment run through the central core.

The configuration offers advantages over the baseline. It has better radiation shielding, simplified internal structure, and additional volume. Against these advantages must be weighed the less luxurious living quarters, and a floor configuration which is less adaptable to rearrangement. Although no weight estimate of this configuration was made, there appears to be no reasons to deviate greatly from the baseline weights.

2.4.2 Artificial Gravity

The MORL baseline will continue to use two means for providing artificial gravity: (1) a centrifuge, and (2) provisions for a spin-deployment system. The two systems are described in Reference 6. The centrifuge is intended as a therapeutic/exploratory device to fully determine the gravity requirements of crewmen on board space vehicles; it is also intended to provide re-entry gravity simulation for the crewmen prior to return to Earth. The spin-deployment system is intended as a backup should manned space flight experience prove the necessity for continuous g; it is not intended for use until such necessity is conclusively established because of the complex laboratory operations and experiment program which result. The present uncertainty of continuous requirements, and the problems associated with the experiment program in a spinning configuration led to investigation into other methods of providing continuous gravity while still retaining zero-g for experimentation.

An analysis of the experiment program reveals that approximately 40% of the experiments require zero g, and that an additional 43% of experiments are complicated by the spinning mode. For example, all Earth-centered tests are drastically complicated by a spinning laboratory because the sensor must remain stationary with respect to the Earth while the laboratory is spinning. Thus, nearly 85% of the experiment program requires a stationary or zero-g laboratory portion, irrespective of the requirement for an artificial-g field for the crew.

The following two general methods for providing the combination zero- and artificial-g areas were investigated: (1) elaboration of the centrifuge principle, and (2) insertion of a zero-g laboratory between the MORL and its

spin-counterweight; the investigation was not detailed, but was carried to sufficient depth to give an insight into the potential problems.

2.4.2.1 Artificial-g by Centrifuge Methods

The modification of the baseline centrifuge by the addition of operating equipment and crew convenience items is an attractive method of providing artificial-g for the crew while the majority of the laboratory is at zero g. This enables crewmen to spend a significant amount of time in a g environment while they operate the laboratory and experiments. The concept is predicated on the basis that interrupted gravity levels are beneficial to the crew, and that such periods need not be of the same length. For example, if 12 hours are spent in artificial g on a given day and only 2 or 3 hours on another day, the cumulative effect is still beneficial.

The following four concepts were examined:

1. A spin room plus the baseline centrifuge.
2. A spin hall within the centrifuge compartment.
3. Two consoles added onto the existing centrifuge.
4. A single console added to one of the existing centrifuge cabs.

Spin Room

The spin room is shown in Figure 2-23. It contains the baseline centrifuge to simulate the re-entry gravity environment and a separate, 60-in. -wide rotating room. The room has a 24-in. -wide walkway or hall located alongside, which is used for access to the individual radial bays and for walking or exercise. The bays include a maintenance console, an experiment console, a galley with a recreational table and chairs, a toilet compartment, two sleeping bunks, and an entry ladder as well as limited storage volume. Access to the room is through the hub, which is initially counter-rotated until it is stationary with respect to the room, at which time the crewmen enters the room via the ladder. The room operates independently of the centrifuge and rotates continuously. A full crew of six men may inhabit the room simultaneously if all stations are occupied. It is the most elaborate of the centrifuge concepts and the MORL must be lengthened to incorporate this concept.

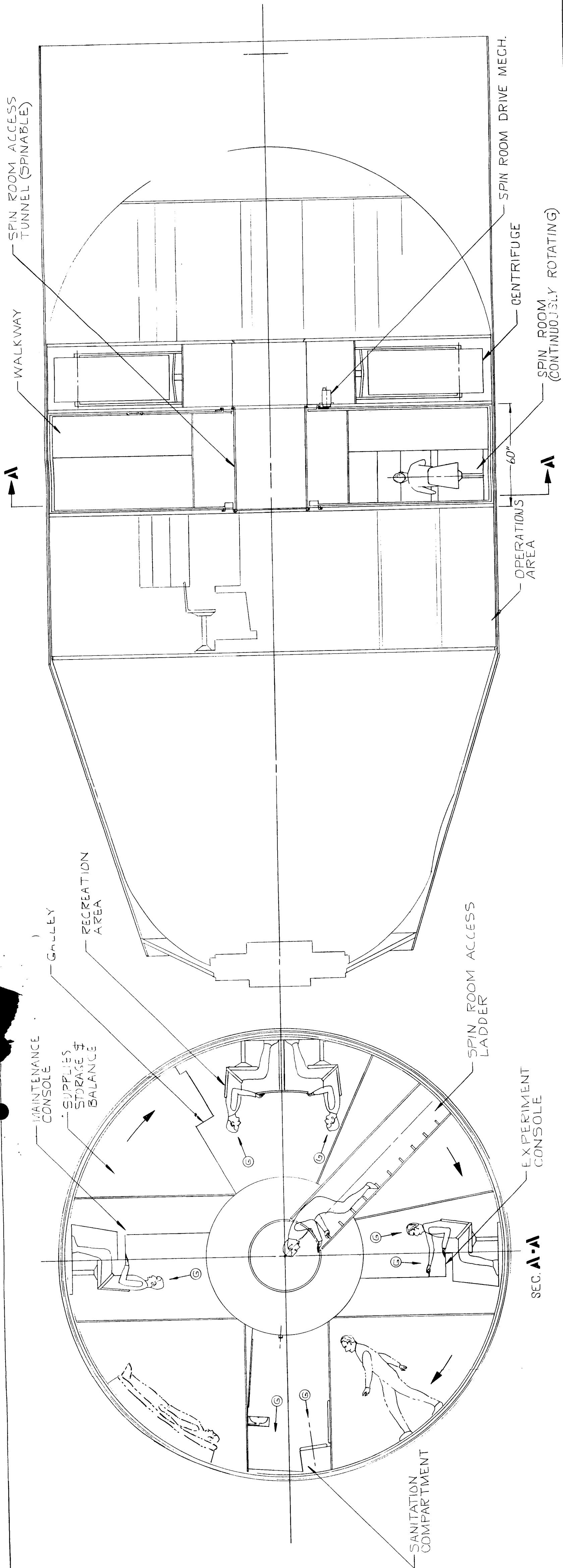


Figure 2-23. MORL Baseline Spin Room

88-3

88-2

88-1

Spin Hall

The spin hall is shown in Figure 2-24. This hall contains a maintenance console, an experiment console, two articulating chairs that can be converted to bunks, and space for exercise and storage. The hall occupies the 40-in. disc normally used for the centrifuge. This hall rotates continuously at the following two speeds: (1) slow speed for artificial g, and (2) fast speed for re-entry g simulation. The hall is accessible through a hub which operates in the same manner as the spin room. Normally, four crewmen would occupy the hall (one man at each console, and two men asleep). During re-entry simulation the hall is occupied by two crewmen. The exterior configuration of the MORL remains unchanged.

Dual Spin Console

The dual spin console concept is shown in Figure 2-25. It consists of the addition of two console cabs to the normal MORL centrifuge. The centrifuge operates intermittently; access to the cabs is through the normal centrifuge opening in the operations bay. The centrifuge must be maneuvered until entry into the desired cab is possible. Long-term exposure of the crew to a g field is possible while the crewmen operate the console equipment; however, the console cabs must be evacuated for the high-speed re-entry simulation runs. No particular configuration changes are necessary for this concept since the baseline 40-in. compartment and hub are used. Four crewmen can occupy this console.

Single Centrifuge Console

The single centrifuge console concept is illustrated in Figure 2-26. It consists of a small console added to one of the existing centrifuge cabs. Normal access to the cab is provided and no configurational changes are necessary. The concept is the simplest of the four; only two crewmen can use it at one time.

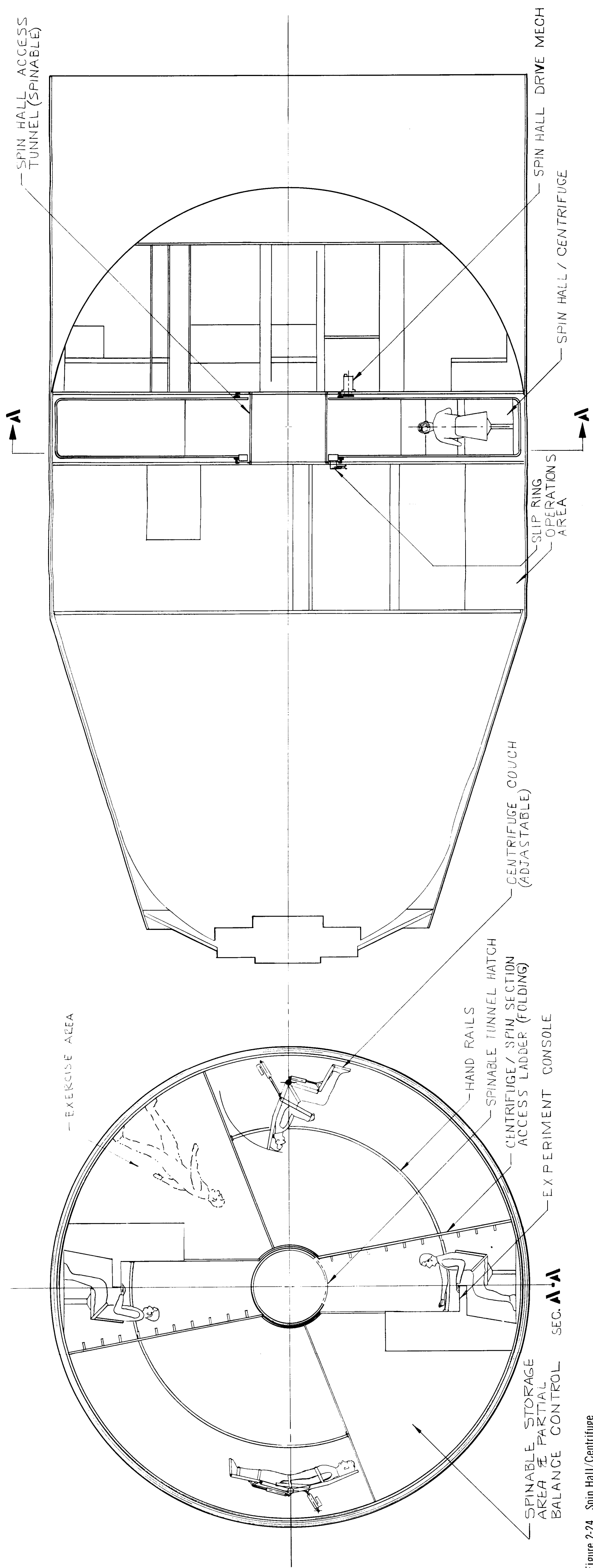


Figure 2-24. Spin Hall/Centrifuge

90-2

90-3

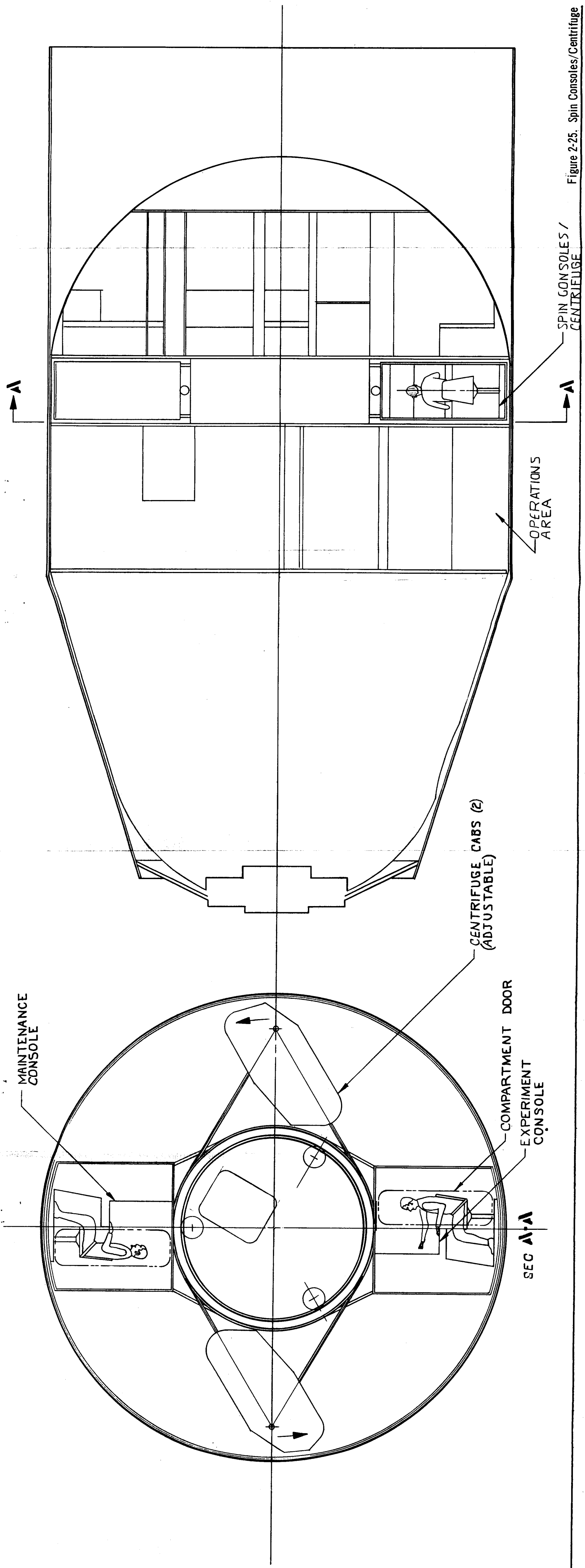


Figure 2-25. Spin Consoles/Centrifuge

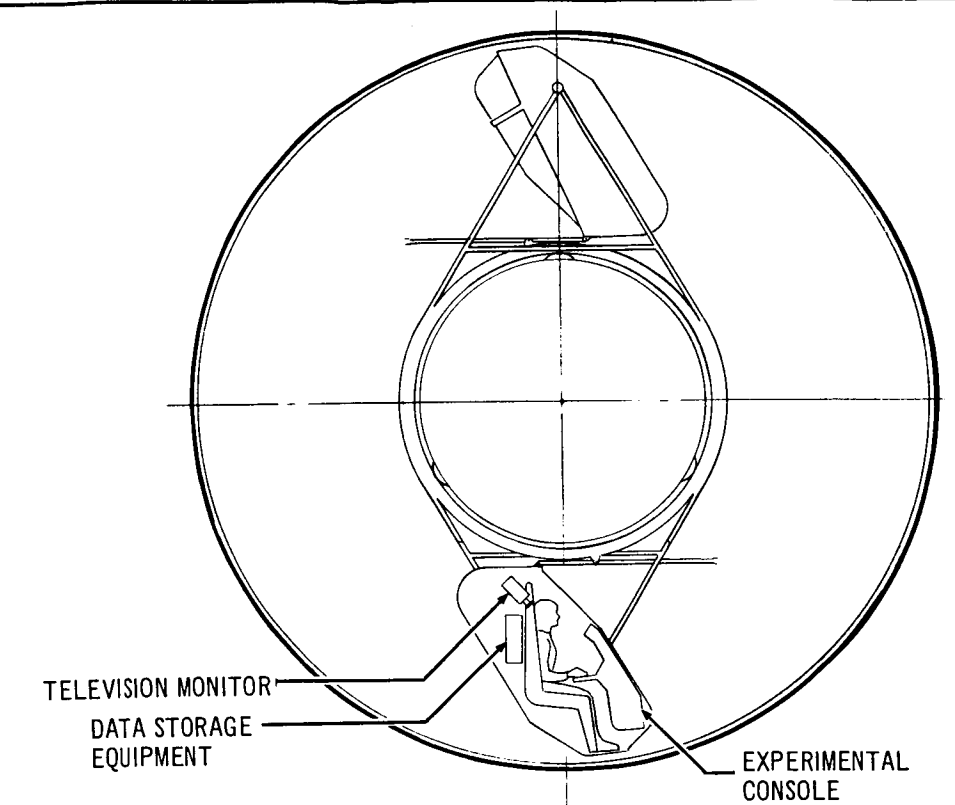


Figure 2-26. MORL Centrifuge Experimental Console Installation

Concept Evaluation

Because of the basic diameter of the MORL, all of the concepts are short-radius centrifuges. Therefore, evaluation must account for the requirements of short-radius centrifugation. A resume of these requirements follows. The evaluation is further compounded by the purposes for which the produced gravity is to be used. For example, a short-radius centrifuge, such as the baseline MORL, used to simulate high-g spacecraft re-entry conditions is considerably different from a centrifuge used to provide continuous low-g simulation, as in the concepts under evaluation. In the former case, the crewman's movements are restricted. In the latter case, the crewman is free to move about at will. The effects of centrifugation on a crewman may be summed up by noting that, for short-radius rotation, a restricted crewman may tolerate higher forces and rotational speeds without feeling nausea or discomfort than he can if he is unrestricted.

One reason for this is the Coriolis force effect. Travel to or from the center of rotation along a radius (radial motion) in a rotating environment will cause a variation in a man's local weight, and will produce a Coriolis force which acts at 90° to the direction of travel. This force gives a pitching or sidewise component to his direction of travel for climbing a ladder, standing up, or even nodding his head. The force acts in the rotation plane and, since it is dependent on radial velocity, its effect on a mobile crewman is uneven because the arms and legs go through larger velocity changes than the body trunk, which produces varying magnitudes of force on different parts of the body. The ratio of Coriolis force to local body weight must, therefore, be restricted to keep this awkward or perturbing force within tolerable limits.

A second problem is that of traveling along the circumference of a rotating device. Travel velocity along the circumference adds to, or subtracts from, the rim velocity which changes the centrifugal force. The sensation is somewhat analogous to walking up or down a variable inclined plane. Again, if the travel velocity (walking speed) approaches a large percentage of the rim velocity, the centrifugal force (artificial-g) change can become very large; furthermore, it is variable depending on the walking speed. Therefore, the ratio of walking speed to rim speed also must be restricted to keep this force within tolerable limits.

Other considerations are that the angular velocity (rotational speed) be kept below that which produces nausea, that the minimum artificial g be kept above that which produces traction, and that the maximum artificial g be kept below that which produces fatigue.

The foregoing considerations are summarized by the comfort envelope presented in Figure 2-27, which is used as design criteria for rotating stations whose occupants have unrestricted mobility (Reference 7). The boundary conditions are as follows:

1. Maximum angular velocity no greater than 4 rpm.
2. Minimum rim velocity 24 fps or greater.
3. Maximum Coriolis force to local weight ratio of 0.25 or less.
4. Minimum artificial g of 0.2 g.
5. Maximum artificial g of 1 g.

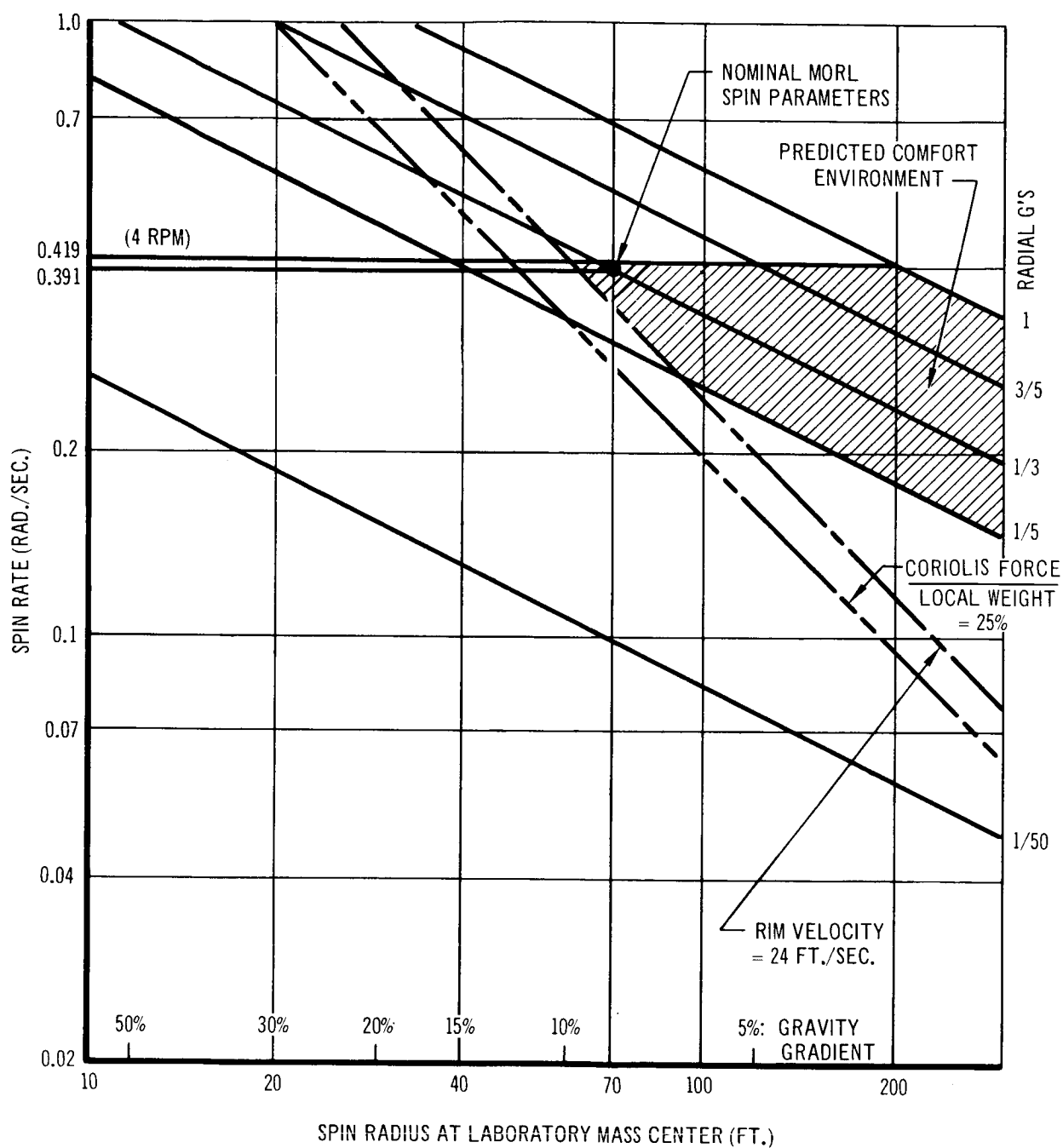


Figure 2-27. Artificial Gravity Parameters

The MORL radius is so small (10 ft) that all of the centrifuge configurations noted in Figures 2-22 through 2-25 are below the comfort envelope; if the maximum angular velocity of 4 rpm is accepted as the fastest the centrifuge can go without producing nausea, then a 10-ft radius results in a g force of less than 1/50, a Coriolis force to local weight ratio far above 25%, and a rim velocity considerably smaller than the 24 fps minimum. Furthermore, the 10-ft radius is at the outer limit of the rotating devices, and the intermediate radius distances at the head, arms, and so forth, are such that the above values are compounded further. On this basis the centrifuge methods for continuous artificial g are not acceptable. However, the data upon which the criterion are established has been evolved with the Earth's force superimposed, and has not been verified in a zero-g environment. Inclusion of these concepts into a space station is not recommended except perhaps for an experiment.

Other qualitative considerations are noted as follows:

1. Concepts 1 and 2 (spin room and spin hall) require crewmen's adaptation to two strange environments: zero g and some g intermediate between 0 and 1.
2. Concepts 3 and 4 (cab additions to the centrifuge) require the least motion on the part of the crewmen and should be investigated first should artificial g by a centrifuge method be desirable.
3. All of the concepts add complexity to the centrifuge. For example, complicated slip rings are necessary, and a great deal of power is required to move the large centrifuge mass; the effect on the stabilization and control system was not investigated.

2.4.2.2 Artificial G By Spin Deployment Methods

The baseline MORL is designed to have backup spin deployment capability. This capability is not installed on the first laboratory. Should artificial g be necessary, a backup laboratory with the spin-deployment system must be launched and transfer of long-term operations accomplished.

Because the baseline spin-deployment system has no facilities for zero-g experimentation, a method was examined for obtaining a zero-g or stationary laboratory when the spin-deployment system is used. The examination was conceptual in nature; a detailed analysis was not made. The concept

involves the insertion of an adapter section and a dual cable deployment system between the MORL and the booster. This MORL (No. 2) is then rendezvoused with the previous MORL (No. 1), which is already in orbit, and the deployment system is attached at the aft end of MORL No. 1; the two laboratories are then spun about each other with the adapter section located at the center of rotation. The zero-g laboratory portion is provided by inserting an MMM into the adapter, which is located at the CG, of the system then counter-rotating the module so that it is at zero g while the laboratories are rotating. For this method, it is required that the backup MORL be launched as specified in the baseline system.

The concept, shown in Figure 2-28, is similar to the baseline spin-deployment system except for the addition of the dual cable system and the adapter. The cable system is in two sections--the first section is attached between the laboratory and the adapter, and the second section is stowed between the adapter and the S-IVB booster. The S-IVB booster is discarded at orbit injection and the stowed cable system is attached to the MORL No. 1 upon rendezvous. The latter section is remotely controlled from the MORL No. 2 and, by adjusting the distances between the vehicles, the adapter may be kept at the CG location of the rotating system. Both cable systems have the same components as the baseline except for strut length; a payout and retraction system must be added for the adapter control and power leads. The adapter contains the deployment struts, the cable drive drums and pulleys, and the adapter to MMM airlock and counter-spin mechanism; the latter mechanism counter-rotates the MMM so that it remains at zero g while the two laboratories and adapter rotate. The adapter is 65-in. long x 260-in. in diam; it has space for two zero-g laboratories, although only one is shown in Figure 2-28.

The attachment of the cable terminals requires an extravehicular operation. Deployment of the two MORL's is similar to the baseline except that the RCS system is controlled directly from each MORL instead of remotely. However, remote operation of the adapter cable system is necessary.

A separation distance of 155 ft must be provided to allow a nominal MORL spin radius of 70 ft because of weight variations between the MORL No. 1 and the MORL No. 2. The artificial g for a 70-ft radius is $1/3$ g at a spin

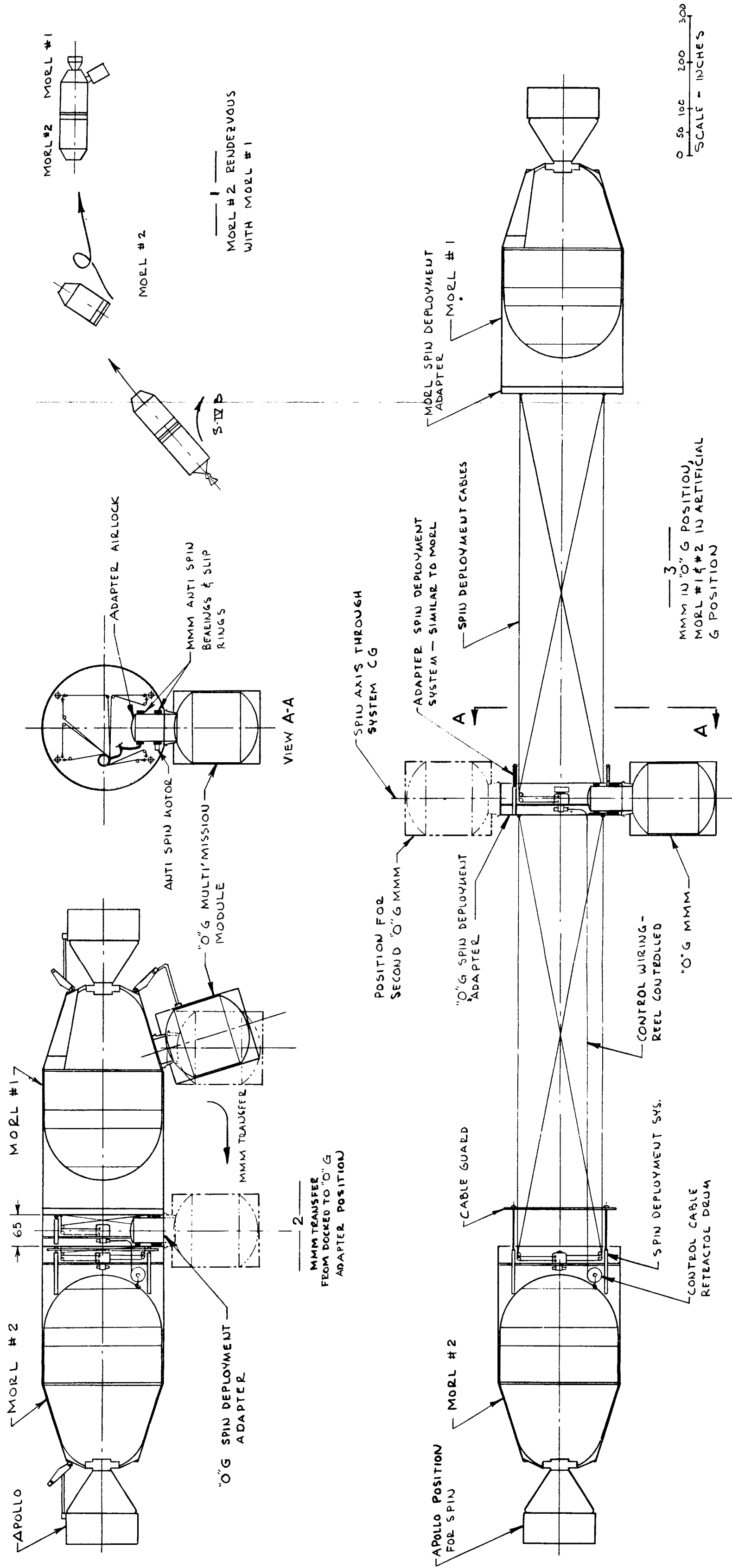


Figure 2-28. Dual MORL Artificial Gravity Spin Deployment Version

97-2

97-1

rate of 4 rpm, which is within the comfort envelope of Figure 2-27. Adjustment of the spin radius is possible by changing the spin rate, the cable separation distance, or the weight located on the MORL.

The concept has a distinct advantage over the baseline system because it provides for zero-g experimentation in the MMM. However, because the spinning system acts like a gyroscope, experiments which point at a local Earth vertical must be equipped with gimbals to keep from precessing the spinning MORL system. In addition, the MMM's would have to be modified to support the experiment program.

Because manned access to the central MMM is difficult, it is likely that remote operation of experiments would be necessary, which would add to the experiment complexity and lead to some unreliability. The MMM is accessible only when the system is retracted, unless an elevator assembly is added to the zero-g adapter which restrains the crewmen during transit from the MORL to the MMM. Free travel by the crewman from the MORL to the MMM is not considered feasible.

System complexity in the concept is increased by the remote operation of the adapter and the MMM. The system requires a MMM counter-spin system and attendant slip rings for multiple conductors, accelerometer sensing, and environmental support. A system for extending and retracting the conductors is also required.

The concept has the following three major advantages over the baseline:

1. The dual MORL system is lighter than the baseline because:
(1) the S-IVB does not have to be modified to add the spin RCS system, (2) the S-IVB does not have to be boosted into the circular orbit, and (3) the shorter span does not require as much wire and cable weight.
2. The zero-g MORL (No. 1), and all its system, is retained and used.
3. Laboratory space is increased by the volume of MORL No. 2.

The system weights for the concept and for the baseline deployment system are noted below:

	Dual MORL (lb)
1. Structure	
Single cable system	-
Dual cable system	695
Attachment adapter	62
Zero-g adapter	865
2. Electrical	
Control wire (for engines cables, experiment module, /and so forth)	520
3. RCS	56
4. Flight electronics	40
5. Booster models	-
6. On-board supplies	530
7. Growth contingency (20%)	450
8. Inject S-IVB booster into orbit	-
Total weight:	3,418

While the artificial-g concept considered in this study is advantageous because it provides zero-g experimental facilities, it also adds considerable complexity. The concept requires remote deployment, and multiple slip rings, bearings, and antispin equipment to support the zero-g laboratory. Accessibility to the MMM is also difficult, and the problem is compounded if an elevator system is installed. The dual MORL system does not require remote operation of the RCS. However, this advantage is not too beneficial because of the other systems that require remote operation.

PRECEDING PAGE BLANK NOT FILMED.

Section 3 STRUCTURES

The selection of a structural concept to satisfy the stringent requirements of the MORL mission is discussed in detail in Volume XII, Laboratory Mechanical Systems--Structures, of the Phase II Report on the Optimization of the Manned Orbital Research Laboratory (MORL) System. To avoid undue repetition, frequent reference will be made to that report with the emphasis placed on the changes to the baseline structure and the new or additional design features.

3.1 INTRODUCTION

Several wall configurations have been proposed for use on manned orbital space stations. Determination of the optimum configuration is dependent on the design criteria specified. This is particularly true in the case of the micrometeoroid penetration criterion. The shielding efficiency that is calculated for a wall configuration is dependent on the model assumed for the penetration process. It is in this area that the greatest controversy currently exists. Final resolution of this controversy must await the long-term exposure of various shield configurations of large surface area to the micrometeoroid environment in space. This data can perhaps best be gathered by the manned space station itself.

The structural concept which has been selected as the baseline meets the requirements for structural efficiency, producibility, ease of ground assembly, and checkout; the concept also provides maximum micrometeoroid shielding efficiency under the criteria specified by NASA Langley. A second structural concept has been documented as an alternate; this concept maintains the desirable features of the baseline approach and provides compatibility with an alternate model of the micrometeoroid penetration process which specifies the shield efficiency as a function of the separation between the bumper and the target.

3.2 SUMMARY

The baseline MORL structural subsystem is basically the same as described in Volume XII of the Phase II Report. It is composed of three major structural assemblies as follows:

1. An external shell which carries all the flight loads, protects the super insulation from the boost environment, and serves as the mounting surface for the radiator tubing. The outer shell also serves as a meteoroid shield for both the pressure shell and the radiator tubing.
2. A two-compartment pressure shell with welded longitudinal joints and flanged, O-ring-sealed, circumferential joints. The latter facilitate assembly as well as checkout and, provide for major internal equipment changes if the need arises after final assembly. The pressure shell is supported within the load-carrying outer shell at a single station plane by a short fiber glass insulating cylinder.
3. An internal equipment support structure which permits installation and checkout of the equipment on the support assembly prior to the installation of that assembly, as a complete unit, in the pressure shell.

The alternate concept for the MORL structural subsystem is also composed of three separate major assemblies. It differs from the baseline concept in that the flight loads are carried through the waffle-stiffened pressure shell rather than through the outer shell. The outer shell serves as a fairing for the super insulation during boost, as the mounting surface for the radiator tubing, and as a meteoroid bumper for both the pressure shell and the radiator tubing. Short cylindrical sections of sandwich construction with fiber glass honeycomb core and fiber glass faces are used to join the pressure shell to the aft interstage and nose cone.

The wall weight for the alternate concept is the same as that for the baseline, but a greater percentage of the total weight is in the pressure shell. Since both concepts employ the twin-shell approach, their thermal characteristics in orbit are identical. Manufacturing cost and complexity are similar for these concepts, both of which can be readily produced with present manufacturing methods. The chief area of difference lies in the micrometeoroid shielding efficiency. Assessment of the superiority of one concept over another requires a thorough understanding of the micrometeoroid environment and penetration process. It is in the latter area that no general

agreement currently exists. Either concept must be judged adequate, from the present understanding of the orbital environment, for use on the MORL.

The baseline structural concept is fundamentally the same as that established in Phase II and described in detail in Volume XII of that report. The principal changes that have been incorporated are as follows:

1. A radiator has been added in the conical section of the load-carrying outer shell. This additional radiator area was required to give oxygen regeneration capability to the laboratory system. To provide adequate heat transfer across the nose cone sandwich, a brake-formed corrugated core has been substituted for the truss grid honeycomb core. The bend lines of the axial corrugations coincide with elements of the cone. This construction is the same as that employed on the cylindrical portion of the load-carrying outer shell.
2. O-ring-sealed integral flanges, bolted together, have been substituted for the circumferential weld joints. To permit incorporation of integral flanges, the cylindrical and conical portions of the pressure shell are high-speed routed in the flat from 0.750-in.-thick plate. This process is employed on the S-IVB and has proved economical and practical.
3. The spherical section, honeycomb sandwich, compartmenting bulkhead between the experimental hangar and the control deck has been eliminated. This was made possible by increasing the face and core thicknesses of the control deck floor and by adding four transverse beams on the hangar side of the floor to divide the floor into eight 45° segments. These beams also provide support during boost for the equipment mounted in the hangar, and carry or support the loads imposed by the radially stowed vehicles.
4. A total of six radial stowing ports have been incorporated in the hangar. These ports permit continuous pressurized access to all stowed vehicles. The support structure has been sized to permit spin up to 1/3 g with a fully loaded cargo module. All six stowing ports are identical, to permit stowing either an Apollo command module or a multimission module at any port.
5. An experimental bay, encompassing 90° of the hangar circumference, has been incorporated. This bay permits pressurized access to the sensors for Earth-oriented experimental setup and alignment. The sensor mounting beam is supported on the laboratory structure so as to remain in a stress-free state at all times during the zero-g mode.

These changes were required to enhance both the orbital use potential and the flexibility to accommodate major internal equipment modification on the

ground. Because of experience gained since establishment of the Phase IIa structural approach, in the design and testing of elastomeric sealed interfaces, these changes do not appreciably alter the overall reliability of the laboratory nor do they appreciably increase the leak rate. The Phase IIa and Phase IIb baseline structural concepts and the alternate structural concept are shown in Figures 3-1, 3-2, and 3-3.

3.3 SYSTEM DESCRIPTION

The text, illustrations, and calculations in the following pages discuss and describe the structural considerations of the MORL system.

3.3.1 Structural Design

In the Phase IIa study, structural design criteria were selected to provide appropriately high reliability for the structural subsystem, so that crew safety, equipment integrity, and overall mission effectiveness would not be compromised. For all structure except the pressure shell, the yield factor of safety was selected as 1.10 and the ultimate factor of safety as 1.40 times the design load (which is defined as the maximum calculated load to which the structure will be subjected). Since all of the structure, other than the pressure shell, experiences its design load during boost, and since the laboratory is an integral part of the boost vehicle, it would not be reasonable to use one factor of safety for the booster and another for the laboratory. During boost, no single piece of primary structure can be judged more important than any other; all must function satisfactorily for successful completion of the launch phase. The selected factors of safety match those of the S-IVB and have been maintained.

For the pressure shell, the design limit pressure was selected as 10 psig, the maximum pressure differential to which the pressure shell would be subjected in space. Proof pressure was 1.5 times the design limit pressure, and burst pressure was 4 times the design limit pressure. It was considered essential that these factors be conservative because of the desired operating life of the laboratory and the comparative unknowns of the space environment

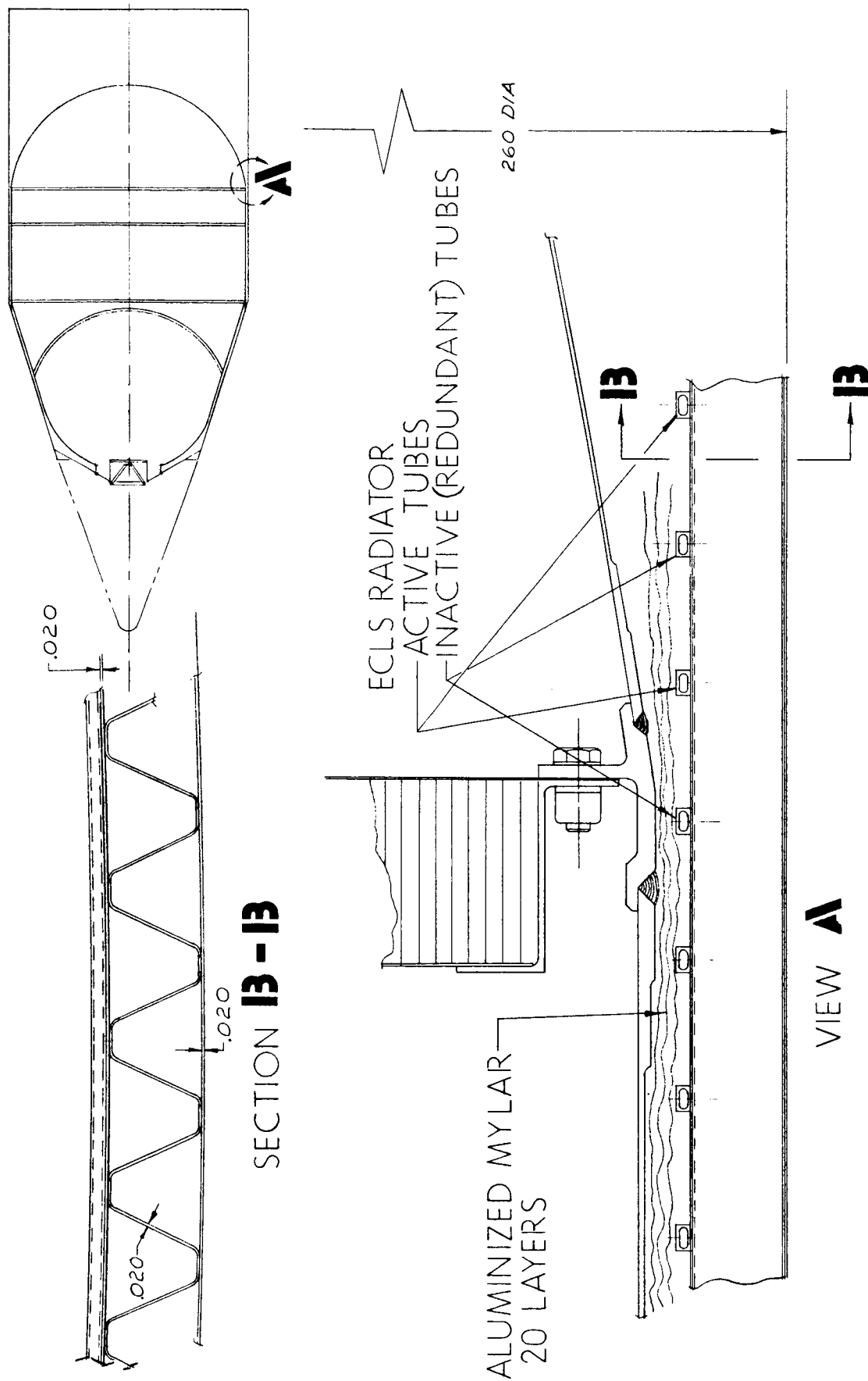


Figure 3-1. Structural Concept – Phase IIa MORL Baseline

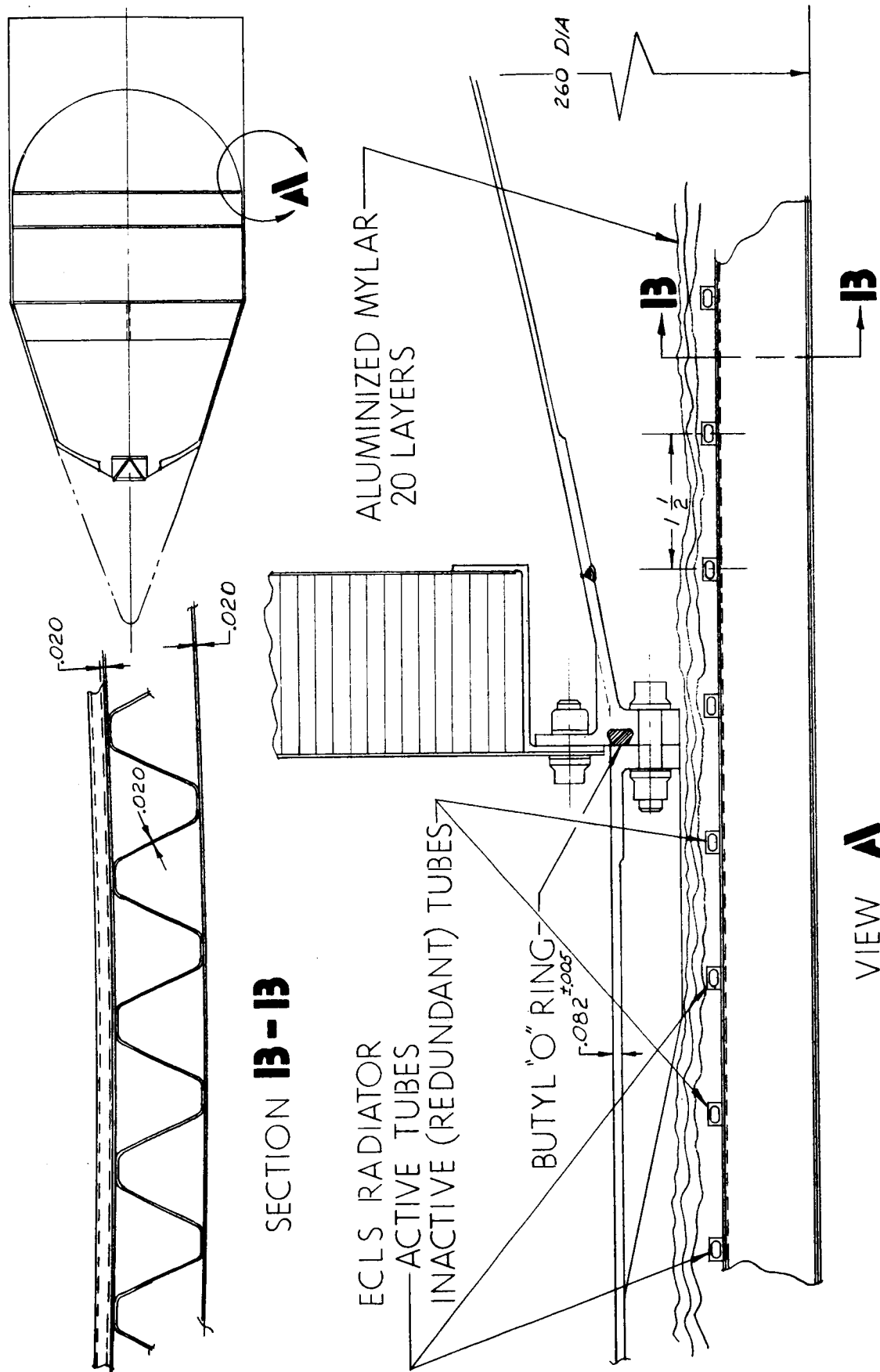


Figure 3-2. Structural Concept – Phase IIb MORL Baseline

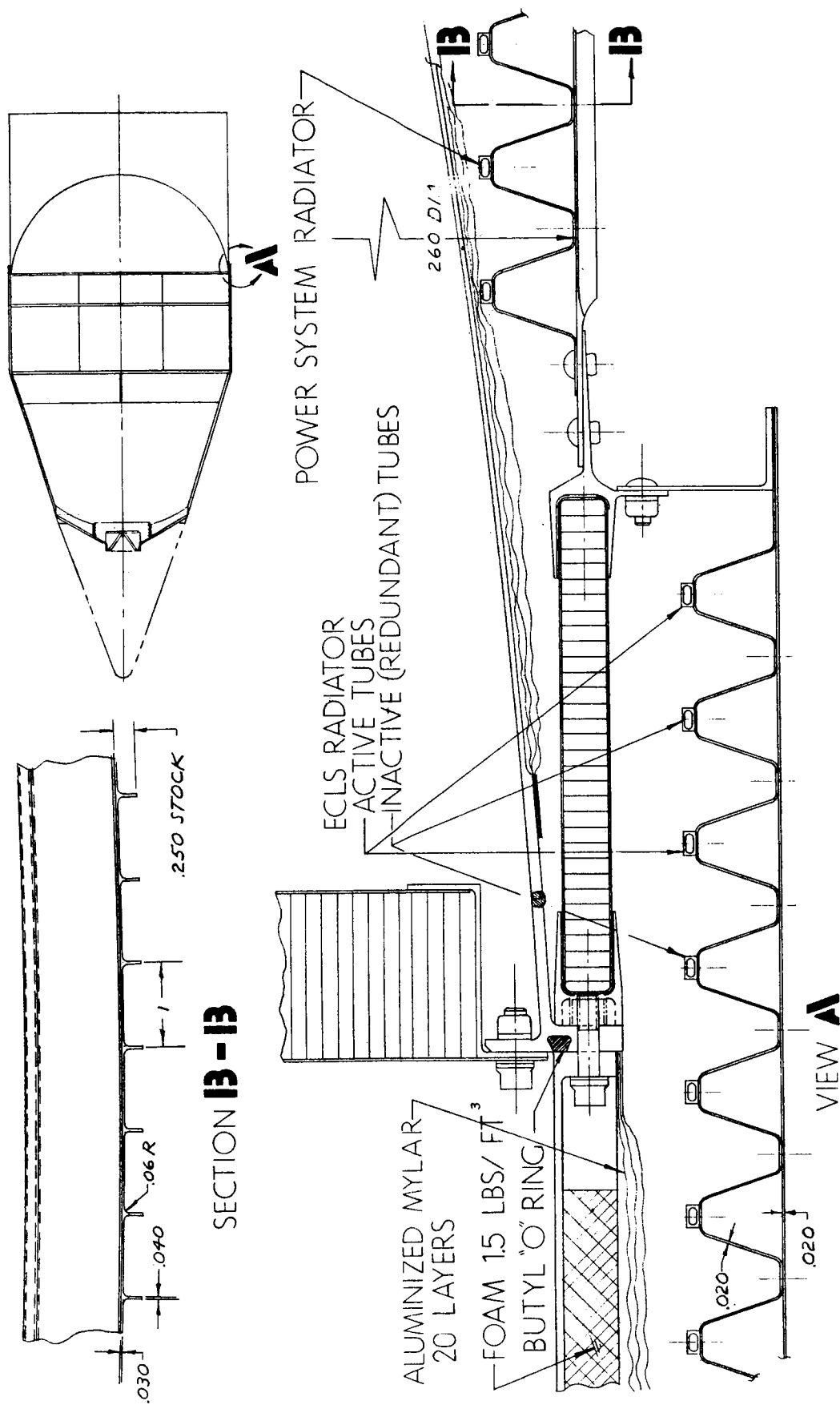


Figure 3-3. Alternate Structural Concept – MORL

They were derived primarily from an assessment of critical crack length as a function of stress level. Thus, they are most applicable to the membrane portions of the pressure shell.

Since the selection of 10 psig as the design limit pressure during Phase IIa, new data on aeroembolism makes the probability of ever operating at greater than 7 psig remote. In addition, the fracture factor, which was selected to give a critical crack length large enough to preclude fast crack propagation from any conceivable accident, cannot be reasonably applied to the design of bolted joints. Therefore, the bolted joints are designed for a burst of 17.5 psi (a burst factor 2.5 times the maximum operating pressure of 7 psi).

The pressure vessel wall thickness in the cylindrical section which resulted from the application of the factor of 4 to 10 psig design limit pressure was $t = 4(10)(128.5)/67,000 = 0.077$. To this was added 0.005 to account for the milling tolerance of ± 0.005 . The resulting nominal wall thickness of 0.082 was used in the Phase IIb radiation analysis, as were the pressure shell thicknesses in the hangar and aft dome, which were also established for a burst of 40 psig plus milling tolerances. This analysis showed that, to meet the specified dose rates, additional shielding was required for all missions, although for the baseline orbit inclination, an addition was required of only 0.020 in. to the dome thickness.

It is, thus, impossible to save structural weight through a re-examination of safety factors and a reduction in the pressure shell wall thickness. The weight saved would have to be returned in polyethylene or some similar shielding material. The pressure shell wall thicknesses established in Phase IIa will be maintained, except for the addition of 0.020 in. to the aft dome.

The flat interior compartmenting bulkhead must be considered part of the pressure shell. However, it is well protected from meteoroid impact and cannot be considered a part of the meteoroid shield because it contributes nothing to the puncture resistance of the pressure shell proper. It will be

in a stress-free condition most of the time. For these reasons, the flat compartmenting bulkhead has been designed for a burst pressure differential of 17.5 psig (a safety factor 2.5 times the maximum working pressure of 7 psig).

The critical crack length as a function of working stress was derived for the 2014-T6 MORL pressure shell noted in Volume XII of the Phase IIa Report. With the cabin shell stressed to 16,750 psi (1/4 of the tensile ultimate) the critical crack length in the cylindrical portion was shown to be 9 in. At 7 psig and with the nominal wall thickness of 0.082, the hoop tensile stress is

$$\sigma = \frac{7 \times 128.5}{0.082} = 11,000 \text{ psi}$$

The corresponding critical crack length is 13 in. in the cylindrical section. The critical crack length in the conical or hangar portion of the pressure shell will be approximately the same because the working stress level is the same. The aft dome thickness was

$$t = \frac{PR}{2\sigma} = \frac{10(130)}{2(16,750)} = 0.039$$

plus 0.005 in., which was added for the chemical-milling tolerance. The nominal aft dome thickness was 0.044. To this 0.020 in. has been added to meet the radiation shielding requirements. The stress level in the aft dome at 7 psig is thus

$$\sigma = \frac{7 \times 130}{2 \times 0.064} = 7,110 \text{ psi}$$

The resulting critical crack length is in excess of 16 in.

The flat, compartmenting bulkhead was sized for an ultimate pressure differential of 17.5 psi. The compressive yield of 2014-T6, 61,000 psi, was selected as the ultimate allowable stress because of the unpredictability of compressive crippling above the yield. Since the bulkhead must support the 17.5-psi pressure differential in either direction, both faces will work

to the same stress. At the maximum operating pressure of 7 psi, the working stress will be

$$\frac{7}{17.5} \times 61,000 = 21,200$$

Since the core and face thickness of the sandwich are maintained constant across the bulkhead, this stress will occur only at the maximum stress point of each of the eight quadrants. Thus, a fast crack, initiated by some accident on the tension side of the sandwich at the point of maximum stress, would have to propagate into lower stress regions. However, for the purpose of an approximate determination of the critical crack length in the bulkhead, it will be assumed that 21,200 psi is a uniform stress across the bulkhead. The relationship between critical crack length and working stress is

$$\frac{\sigma_r}{\sigma_u} = \frac{1 - \frac{l_c}{W}}{C_c \sqrt{1 + \frac{3 l_c}{R_P}}} \quad (3-1)$$

where

l_c = critical crack length

W = panel width

C_c = biaxial load correction factor

$C_c = 1.0$ for flat sheet analysis

R_P = plastic zone notch resistance factor

$R_P = 7$ for 2014-T6

σ_r = the applied stress

σ_u = the tensile ultimate stress

= 68,000 for 2014-T6

$$\frac{\sigma_r}{\sigma_u} = \frac{21,200}{68,000} = 0.312$$

W is assumed to be half the chord width for one 45° quadrant.

$$W = 53.5$$

$$\therefore 0.312 = \frac{1 - \frac{l_c}{53.5}}{\sqrt{1 + \frac{3 l_c}{7}}} \quad (3-2)$$
$$l_c = 12 \text{ in.}$$

Thus, a critical crack length of 12 in. is obtained; this is conservative, because of the neglected nonuniform loading of the bulkhead.

3.3.2 Material Selection

Early in the MORL study, 2014-T6 aluminum was selected as the material for the pressure shell of the MORL, and 7075-T6 aluminum was selected for the load-carrying outer shell. The background data and reasons for the selection of these materials, together with all the material properties, are presented in Volume XII of the Phase IIa Report. At the time of report preparation, it was believed that, to meet the low leak rate required for the MORL, the use of mechanical joints in the pressure shell would have to be held to an absolute minimum. Experience in the manufacture and testing of the NASA Langley two-man airlock, and data gathered from test programs in the vacuum facilities, together with recent testing of a new, Douglas-developed, inflatable seal configuration, negated this belief. Negligibly small leak rates have been achieved in mechanical joints simply through the exercise of reasonably careful design and manufacturing practice, with static, dynamic, and inflatable seals. Resin-cured butyl rubber is the sealing material currently selected. It has excellent stability at high vacuum and good resistance to weathering and ultraviolet radiation. In most of the sealing applications on MORL, with the exception of the seal at the hangar entrance, the sealing material is well shielded. Butyl rubber does not have good resistance to electromagnetic radiation, but a new polymer (epichlorohydrin), which has been developed by B. F. Goodrich, is currently

being evaluated by the Douglas Process Department. This elastomer is reported to have even lower permeability than butyl and it possesses good resistance to electromagnetic radiation; it may be used to replace butyl in the more exposed areas.

3.3.3 Flight and Ground Loads

The flight and ground wind loads were calculated for the MORL and were documented in Volume XII of the Phase IIa Report. Although the configuration now differs in several details from the configuration for which these loads were calculated, the changes were not sufficient to warrant reanalyzing the loads. This loads analysis showed that the loads induced by the MORL on the SIB launch vehicle are well within the current design limits of the launch vehicle. The ultimate compressive load at the interface between the MORL and the Saturn IB instrument unit is 1063 lb/in. The forward skirt of the Saturn IVB is currently designed for 1,318 lb/in., ultimate. The S-IVB as currently designed is, therefore, adequate for the loads imposed by the MORL.

3.3.4 External Shell

The structural design of the external shell is discussed in the following subsections.

3.3.4.1 Baseline

The baseline external shell is unchanged in the cylindrical section from the design established in Phase IIa, except for the addition of the isotope power system radiator in the aft interstage portion of the cylinder. A sandwich construction is used for this load-carrying shell. The inner and outer faces are spot-welded to the brake-formed corrugated core, with the corrugations running axially. The core maintains a 1 in. separation between the inner and outer faces. For both inner and outer faces, as well as for the corrugated sheet, 7075-T6 sheet, 0.020 in. thick, is used. The radiator tubes for both the EC/LS radiator and the isotope power system radiator, are

spot-welded to the inner sheet of the sandwich before that sheet is spot-welded to the corrugated core. The outer sheet is then blind-spot welded to the core.

The conical portion of the baseline external shell was changed to incorporate a radiator. Provisions for oxygen regeneration required an increase in the area of the EC/LS radiator. It was determined that 440 sq ft were available on the conical portion without using either a 3-1/2-ft section at the lower end of the cone which was reserved for radial stowing, or a 90° quadrant of the cone which was reserved for an experiment bay. Provision of a highly conductive path to ensure adequate heat transfer between the radiator tubes and the outer radiating face required a change from the bonded, truss-grid honeycomb core that was used on the sandwich conical portion. The honeycomb was replaced by a corrugated sheet, brake-formed in the flat, with the bend lines falling on elements of the conical inner and outer faces of the sandwich, which intersect at a common apex. The resulting sandwich is 3/4-in. thick at the forward 154-in. diam, and 1-1/4-in. thick at the 260-in. base diam. Aluminum sheeting (7075-T6), 0.020 in. thick, is used for both faces and the corrugated core. The spot-welding sequence for joining the radiator tubing, and the faces, to the core, is the same as employed on the cylindrical portion of the outer shell.

Calculations have shown that if minimum spacing, quality spot welds are achieved, the conduction will be adequate. However, a 1°F temperature drop between the radiator fluid and the radiating surface will cause a 2% reduction in the heat rejection rate. Since the heat transfer is across three spot-welded interfaces, careful quality control must be exercised with this design.

3.3.4.2 Alternate Concept

The outer shell for the alternate structural concept does not carry the axial loads. This function is reserved for the pressure shell. In this alternate concept, the nonload-carrying portion of the outer shell is suspended from a sandwich isolation band, with fiber glass laminate faces and a fiber glass honeycomb core. This isolation band transfers the compressive load imposed

by the outer shell (drag and inertia during boost) to the forward end of the conical hangar pressure shell. The nonload-carrying portion of the outer shell then extends aft to the isolation band at the aft end of the cylindrical portion of the pressure shell. Fiber glass spacer frames transfer the aerodynamic lift forces generated on the outer shell to the pressure shell, to prevent the accumulation of excessive shear or bending in the outer shell during boost.

In this alternate concept, the outer shell must serve three primary functions:

1. Provide the radiating surface for the EC/LS radiator.
2. Serve as a fairing during boost for the aluminized Mylar insulation.
3. Provide meteoroid shielding in space for both the radiator tubing and the pressure shell.

The design selected to meet these requirements uses a corrugated sheet with the 1-in. -high corrugations running circumferentially, to which is spot-welded an outer sheet. These corrugations provide the mounting surface for the radiator tubing and provide the hoop stiffness required for the shell to withstand the boost environment. In the cylindrical portion of the outer shell, the corrugated sheet can be easily fabricated by brake-forming in the flat, as on the baseline design, and then rolling or stretch-forming the circumferential corrugations to contour. In the conical portion of the outer shell, the circumferential corrugations must be formed in the flat pattern of the cone. This places each successive corrugation on a different radius and requires either a special rolling process, or a set of sequentially applied hydropress dies. The circumferential wraps of radiator tubing are spot-welded to the corrugated sheet prior to the spot-welding of the corrugated sheet to the outer sheet. All spot-welding is thus open and conventional and the blind spot-welded interface of the baseline design is eliminated.

Aluminum (6061-T6), 0.020-in. thick, is used for both the outer sheet and the corrugated sheet, for the nonload-carrying portion of the outer shell.

A very similar construction is used for the aft interstage, or load-carrying portion of the outer shell, in this alternate structural concept. The identical corrugated sheet and circumferential radiator tube configuration used on the nonload-carrying portion of the outer shell is used on the load-carrying or

aft interstage portion. The outer sheet is straddle-milled to a thickness of 0.030 from 0.250-in. -thick plate, leaving 0.040-in. -thick ribs 1 in. on center. This construction gives a positive margin with the ultimate loads applied during boost, with no load relieving, and stabilizing pressure differential across the interstage; however, (as is the case in the S-IVB interstages) the venting orifice would be sized to gain this advantage. The aft interstage of the alternate concept has the same weight per square foot as the load-carrying outer shell of the baseline design, but it improves the integration of the radiator with the structure. One spot-welded interface is eliminated and a more direct heat transfer path is achieved between the radiator tubing and the radiating surface.

3.3.4.3 Jettisonable Nose Cone

Both the baseline structural concept and the alternate concept make use of the same nose cone design. The jettisonable nose cone has a base diam of 154 in., a semiapex angle of 20° , and a tip radius of 15 in., and is of frame-stiffened monocoque construction. Three small solid propellant motors are installed in the nose cone, any two of which are sufficient to propel the nose cone clear after activation of a mild detonating fuse at the separation joint at first stage burnout.

3.3.4.4 External Shell Analysis

The outer shell experiences its maximum loading at maximum dynamic pressure, at which time the ambient pressure is 2.7 psia. The large volume of air in the nose cone and aft interstage will vent during boost to a low-pressure region behind a small fairing on the aft interstage. Careful selection of the size of the venting orifice can control the bleed-down rate and maximum pressure differential, to reduce the maximum load on the outer shell. This venting orifice will be sealed by a blowout plug to be released when the pressure differential reaches about 2 psig. This procedure would be used on either the baseline concept or the alternate structural concept. The stabilizing and load-relieving effects that this pressure differential provides have purposely been ignored in the preliminary structural sizing analysis, to provide a degree of conservatism.

The analysis of the outer shell for the baseline structural concept was documented in Volume XII of the Phase IIa Report. The corrugated core sandwich outer shell structure was analyzed for general and local instability and a small positive margin was demonstrated for the maximum loading condition, assuming no stabilizing pressure differential across the outer shell. Since the ambient pressure is 2.7 psi at the maximum loading condition, a large increase in margin of safety can be realized by careful sizing of the venting orifice, with no increase in weight.

In the alternate structural concept, the axial load-carrying portion of the outer shell is restricted to the aft interstage. The bending moment at the top of the S-IVB instrument unit is 26 million in.-lb, and the axial load is 220,000 lb. The resulting unit design load is

$$N_c = \left[\frac{26 \times 10^6}{\pi(130)^2} + \frac{220,000}{260\pi} \right] 1.4 = 1,063 \text{ lb/in.} \quad (3-3)$$

For the aft interstage of the alternate concept to be equal in weight per unit area to the corrugated core sandwich of the baseline outer shell, the rib-stiffened outer face must be equivalent in weight to a 0.040 monocoque sheet. Since all the axial load is carried in this rib-stiffened sheet, it will work to

$$\frac{1,063}{0.040} = 26,600 \text{ psi}$$

The buckling allowable for a flat-plate element under uniaxial load with all four edges simply supported is

$$F_{cr} = KE \left(\frac{t}{b} \right)^2 \quad (3-4)$$

Peery (Reference 8) gives the minimum value of the buckling coefficient, K (independent of panel dimensions) as 3.62. The rib spacing required to prevent buckling of the 0.030-in. sheet is therefore established by

$$26,600 = 3.62 \times 10^7 \left(\frac{0.030}{b} \right)^2 \quad (3-5)$$

$$b = 1.11 \text{ in.}$$

For preliminary design purposes a rib spacing of 1 in. will be used. The rib dimensions must now be established. The ribs can be analyzed as pin-ended columns, with the column length equal to the spacing between the circumferential corrugations. The column buckling load is given by

$$P_{cr} = \frac{\pi^2 EI}{l^2} \quad (3-6)$$

Since a 1-in. spacing has been assumed for the ribs, the column load is 1,063 lb.

$$1,063 = \frac{\pi^2 \times 10^7 \times I}{(1.5)^2} \quad (3-7)$$

from which the minimum moment of inertia is $I = 2.66 \times 10^{-5} \text{ in.}^4$. The rib cross-section area must be less than or equal to 0.010 for the weight of the alternate design to be less than or equal to the weight of the baseline outer shell. To check the compatibility of this restriction on rib cross-section area with the minimum moment of inertia requirement, assume a rib dimension of 0.040 in. thick by 0.25 in. high.

$$I = \frac{bh^3}{12} = \frac{0.04 (0.250)^3}{12} = 5.2 \times 10^{-5} \quad (3-8)$$

Since the true moment of inertia must take into account the 0.50-in. strip of 0.030-in. sheet on either side of the rib, it can be seen that the selected rib significantly exceeds the minimum moment of inertia required. The interstage of the alternate structural concept, designed for the same weight per unit area as the baseline outer shell, will thus be more than adequate for the maximum applied load.

3.3.5 Pressure Shell

The structural design and analysis of the pressure shell are discussed in the following text.

3.3.5.1 Baseline Design

All joints in the pressure shell are welded except the joint between the aft dome and the pressure shell cylinder, the joint between the conical experimental hangar and the cylinder, and the joint joining the forward dome to the hangar. O-ring-sealed, bolted joints are used in these three places to simplify initial assembly and checkout and to provide the flexibility after final assembly to easily incorporate internal equipment modification or the addition of extensive provisions for internally mounted experiments, if required.

All welded joints are a minimum of 2-1/2 times the parent sheet thickness for a distance of 1 in. on either side of the weld centerline. A thickness halfway between the parent sheet thickness and thickness in the weld area will be maintained for an additional 3/4 in. to smooth the transition in thicknesses. The weld joints so designed will exceed the strength of the sheet away from the weld area because proper chilling during welding will have restricted the heat-affected zone to well within the weld pad area.

The hemispherical aft dome is fabricated from nine stretch-formed, heat treated, chemical-milled segments. The segments are formed from 1/4-in. plate and stiffened by chemical-milling in an integral, full thickness, external waffle pattern. The shell thickness between the ribs is 0.064 ± 0.005 , which was established from radiation shielding requirements. The stiffening waffle pattern will enable the dome to support the aft airlock. A 2014-T6 aluminum frame incorporating an O-ring sealing groove is machined from a roll ring forging and butt-welded to the dome to provide a flange for bolting the dome to the cylinder. Facilities for fabricating roll ring forgings of this diameter are currently available.

The cylindrical portion of the pressure shell is high-speed-routed in the flat, on a vacuum table, from 0.750-in. thick plate, to provide the integral bolting flanges for joining the cylinder to the aft dome and to the conical portion. The conical portion is also high-speed-routed in the flat from 0.750-in. thick plate. After machining, the sections are rolled or brake-formed to contour and welded together. Aluminum plate, 130-in. -wide

by 260-in. long by 0.750-in. thick, is currently being purchased for use on the S-IVB. This method of manufacture permits integral reinforcing flanges to be incorporated for view ports, hatches, and all penetrations of the pressure shells, as well as the integral flanges for the bolted end joints.

The pressure shell is compartmentized by a flat sandwich bulkhead which separates the Hangar/Test Area from the remainder of the laboratory. This bulkhead is designed to support a pressure differential of 17.5 psi in either direction. It is supported by four transverse beams on the hangar side, which divide the bulkhead into eight 45° segments. Both faces of the sandwich bulkhead are machined from 0.750-in. -thick plate, to a thickness of 0.039 ± 0.005 . This permits integral ribs to be used for the riveted attachment of the corrugated shear webs of the support beams, without any penetrations of the bulkhead faces. The machined bulkhead faces serve as the aft beam cap for each of the beams. Integral ribs are also provided on the operations area side of the bulkhead for attachment of the front and rear faces of the consoles, to provide for their support during boost. Since the beams on the hangar side of the bulkhead have been sized to support the bulkhead with a 17.5-psi pressure differential across it, equipment doors and access covers in the consoles may be removed in orbit without jeopardizing the structural integrity of the compartmenting bulkhead.

The support beams in the hangar are bolted to the hangar wall to distribute the beam end load to the pressure shell. The through bolt pattern at the beam end does not penetrate the pressure shell, because of the 0.750-in. plate thickness from which the pressure shell is machined. A channel, which runs the length of the beam shear web, is machined in the pressure shell plate. Nut strips are installed on both sides of the channel and are held in place by single rivets at the ends of each nut strip. The gang channel nuts are counterbored to obtain full bearing for the bolts that attach an extruded T-section to the pressure shell. The T-section, which is riveted to the beam shear web, carries the pressure load across the open face of the machined channel. A 10-in. -deep frame, which inscribes 270° of the hangar circumference, is joined to the pressure shell in a similar manner. This frame is bolted to the forward caps of the bulkhead support beams, and serves to distribute the loads imposed by the radially stowed vehicles, with

the laboratory operating in the spin mode. With the laboratory operating in the zero-g mode, this structure provides a stiff support for the stowed vehicles that precludes dynamic coupling with the attitude control system.

3.3.5.2 Alternate Structural Concept

The pressure shell for the alternate structural concept is similar in all details to the pressure shell described for the baseline concept, except that an external, integral waffle pattern is superimposed on the conical and the cylindrical portions, to enable the pressure shell to carry all the flight loads. The weight added to the pressure shell in the form of integral stiffeners, plus the weight of foam that is added in the waffle pockets to improve the micrometeoroid shielding efficiency, is made just equal to the difference in weight between the baseline load-carrying outer shell and the nonload-carrying outer shell of the alternate concept. The pressure shell of the alternate concept, so designed, is more than adequate for the maximum flight loads imposed.

3.3.5.3 Pressure Shell Analysis

The structural analysis of the pressure shell is discussed in the following subsections, with illustrative sketches and formulas.

Waffled Cylinder of the Alternate Structural Concept

At Station 1890 (aft end of the pressure shell cylinder), the limit bending moment is 14,000,000-in. -lb, and the limit axial load is 211,000 lb at maximum dynamic pressure and angle of attack (max. $q\alpha$ --Volume XII, Phase IIa Report). At this time, the minimum pressure differential across the pressure shell is 6.5 psig (lower limit of the relief valve setting). The resulting design compressive load is .

$$\begin{aligned}
 N_c &= \text{S.F.} \left[\frac{M}{\pi R^2} + \frac{P}{\pi D} \right] - \frac{\rho R}{2} \\
 N_c &= 1.4 \left[\frac{14 \times 10^6}{\pi \times 130^2} + \frac{211,000}{\pi \times 260} \right] - \frac{6.5 \times 130}{2} \quad (3-9) \\
 N_c &= 310 \text{ lb/in.}
 \end{aligned}$$

The equivalent monocoque thickness of the nonload-carrying outer shell is 0.020 in. less than the baseline load-carrying outer shell (inner 0.020-in. sheet of the corrugated core sandwich removed in the alternate concept). If the heights of the pressure shell ribs are made equal to the plate stock thickness, the nominal depth of the waffle pockets will be

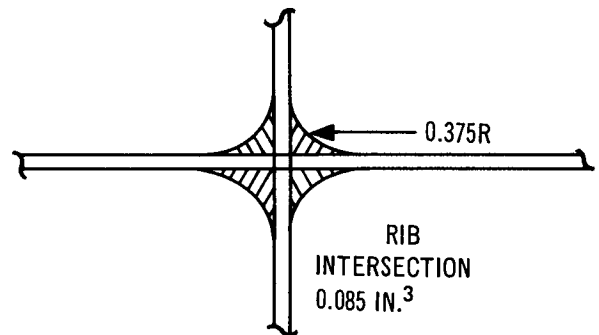
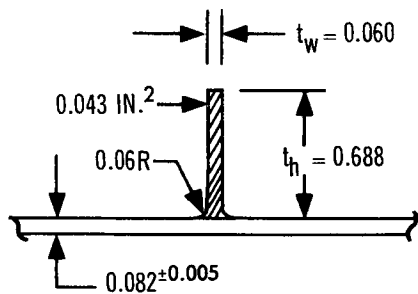
$$0.750 - 0.082 = 0.668$$

If the waffle pockets are filled with foam with a density of 1.5 lb/ft³, the aluminum sheet thickness that is equivalent in weight to the foam will be

$$0.668 \times \frac{1.5}{12} \times \frac{1}{14.4} = 0.0058 \quad (3-10)$$

This leaves $0.020 - 0.0058 = 0.0142$ equivalent thickness to be added in the form stiffeners to the pressure shell.

The nominal cross-section area of the selected stiffener is 0.043 in.²



If the longitudinal ribs are spaced 5.5 in. apart and the circumferential ribs are spaced 10 in. apart, the monocoque sheet that is equivalent in weight to the stiffeners is approximately

$$\frac{0.043}{5.5} + \frac{0.043}{10} + \frac{0.085}{55} = 0.0137 \text{ in. (sheet thickness)} \quad (3-11)$$

The rib spacing that is required to prevent skin buckling is given by the empirically determined expression

$$\sigma_{cr} = 8.47 E \left(\frac{t_s}{l_s} \right)^2 \quad \text{for a square pattern (Reference 9)}$$

$$l_s = t_s \sqrt{\frac{8.47 E}{\sigma_{cr}}}$$

$$t_s = 0.082 \pm 0.005$$

$$\sigma_{cr} = \frac{310}{0.077 + \frac{0.043}{5.5}} = 3,660 \text{ psi} \quad (3-12)$$

$$l_s = 0.077 \sqrt{\frac{8.47 \times 10^7}{3,660}} = 11.7 \text{ in.}$$

l_s = stiffener spacing required to prevent skin buckling with a square waffle pattern

The selected stiffener spacing is thus well below the required spacing.

The allowable rib stress (that is, the maximum stress at which local rib buckling will not occur) is given by the expression for a plate simply supported on one side with three sides free (Reference 9).

$$\sigma_{cr} = 0.416 E \left(\frac{t_w}{t_h} \right)^2$$

$$\sigma_{cr} = 0.416 \times 10^7 \left(\frac{0.06}{0.688} \right)^2 = 31,600 \quad (3-13)$$

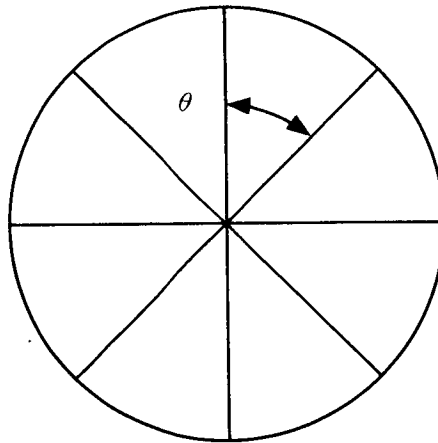
Since this is well above the working stress of 3,660 psi, local rib buckling will not occur.

The linearized buckling theory for stiffened cylinders developed in Douglas Report SM-47837 has been programmed in Fortran IV, and can be used to determine the load for the general instability and bay buckling modes of failure for a given design. It was not used in the analysis of the alternate concept, but, from the analysis of similarly stiffened shells, the margin of safety for this stiffened cylinder is large. The 0.014 in. added to the pressure shell in the form of stiffening ribs will in all probability enable the laboratory to be launched unpressurized, with the pressure

differential building up naturally until the relief valve opens at an altitude of approximately 17,000 ft. The maximum load condition (maximum $q\alpha$) occurs at 40,000 ft. Since the laboratory will have been at its full gage pressure from 17,000 ft, it is fairly obvious that the maximum $q\alpha$ condition is the critical design condition for the waffle stiffening. However, to remove all doubt, flight load as a function of altitude would have to be determined between liftoff and 17,000 ft, to compare the worst combination of flight load and internal pressure during this time, with the known conditions prevailing at maximum $q\alpha$.

Flat Pressure Bulkhead Analysis

The compartmenting bulkhead is designed to support a pressure differential of 17.5 psi. Four transverse beams divide the bulkhead into eight 45° segments, as shown below.



From Roark (Reference 5, page 212 3rd Edition), the maximum stress on a simply supported segment is given by

$$S_t = \frac{\beta \omega \alpha^2}{t^2} \quad (3-14)$$

for

$$\theta = 45^\circ$$

$$\beta = 0.114$$

$$S_t = \frac{0.114 \times 17.5 \times 130^2}{t^2} = \frac{3.37 \times 10^4}{t^2}$$

for

$$S_t = 61,000 \text{ (compressive yield for 2014-T651)}$$

$$t^2 = \frac{3.37 \times 10^4}{61,000} = 0.552$$

A sandwich bulkhead will work to the same stress as a monocoque bulkhead with the same I/C. Equating I/C for monocoque and sandwich

$$\frac{t^3}{12} \cdot \frac{2}{t} = \frac{t^2}{6} = \frac{h^2 t_f}{2} \cdot \frac{2}{h} = h t_f \quad (3-15)$$

h = core thickness

t_f = face thickness

$$h t_f = \frac{0.552}{6} = 0.092$$

$$t_f = \frac{0.092}{h}$$

For these preliminary design purposes, it will be assumed that one half the pressure load on the bulkhead is reacted at the ends of the support beams, and one-half is uniformly distributed between the beams. Assume a honeycomb core density of 4.4 lb/ft³ (a 5056 aluminum honeycomb core with this density has a typical shear strength in the L direction of 400 psi.)

The weight per square foot (W) for the sandwich panel is thus

$$W = 28.8 t_f + \frac{4.4}{12} h + 0.160 \quad (3-16)$$

where

t_f = face thickness (in.)

h = Core thickness (in.)

Glue weight = 0.160 lb/ft²

substituting $t_f = \frac{0.092}{h}$

$$W = \frac{2.65}{h} + 0.367 h + 0.160$$

differentiating and equating the differential to zero to determine the core thickness for minimum weight.

$$\frac{dw}{dh} = -\frac{2.65}{h^2} + 0.367 = 0 \quad (3-17)$$

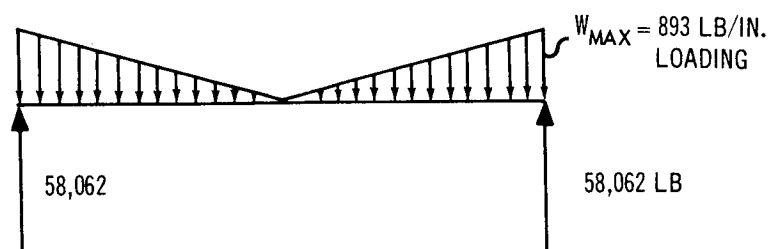
$$h^2 = \frac{2.65}{0.367} = 7.12$$

$$h = 2.67 \text{ in. (core thickness)}$$

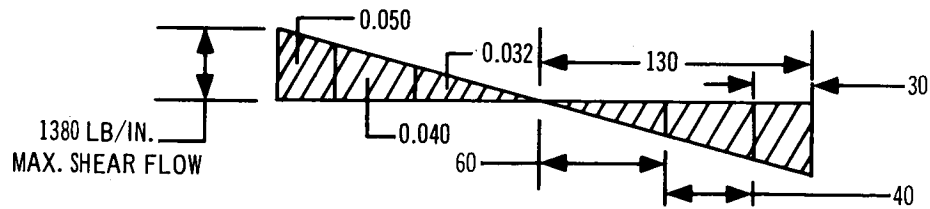
$$t_f = \frac{0.092}{2.67} = 0.0345 \text{ in. (face thickness)}$$

In this analysis, it was assumed the segment is simply supported along its edges. In actuality, since the bulkhead is continuous across the support beams, full fixity exists along the radial edges of the quadrant. The unit weight thus established for the sandwich is conservative, but a more detailed analysis must remain the object of a future study, because of the limited time available in Phase IIb for detail design and analysis. The nominal weight per unit area calculated for the pressure bulkhead sandwich is $28.8 \times (0.039) + 0.367 (2.67) + 0.160 = 2.26 \text{ lb/ft}^2$.

The total design load on the bulkhead is $P\pi R^2 = 17.5 \times \pi \times (130)^2 = 929,000 \text{ lb}$. Half of this load is assumed to be carried by the support beams. The beam end reaction, which must be distributed to the pressure shell is therefore $1/8 \times 464,500 = 58,062 \text{ lb}$. To develop the bending moment diagram, a triangular load distribution is assumed.



To allow space for the radial stowing ports between the compartmenting bulkhead and the deep ring frame, a 42-in. depth is selected for the support beams. The maximum shear flow in the beam web is then $58,062 \div 42 = 1320 \text{ lb/in.}$



A corrugated web of 7075-T6 aluminum has been used. The center section will be 0.032 in., the intermediate section 0.040 in., and the outboard section 0.05 in. The b/t will be 40 for each section.

For the center section:

$$h/t = \frac{42}{0.032} = 1,312$$

From Figure 3-4:

$$F_s = 20,000$$

$$q = 0.032 \times 20,000 = 640 \text{ lb/in.}$$

From the above sketch, using a proportion:

$$130 \times \frac{640}{1,380} = 60 \text{ in.}$$

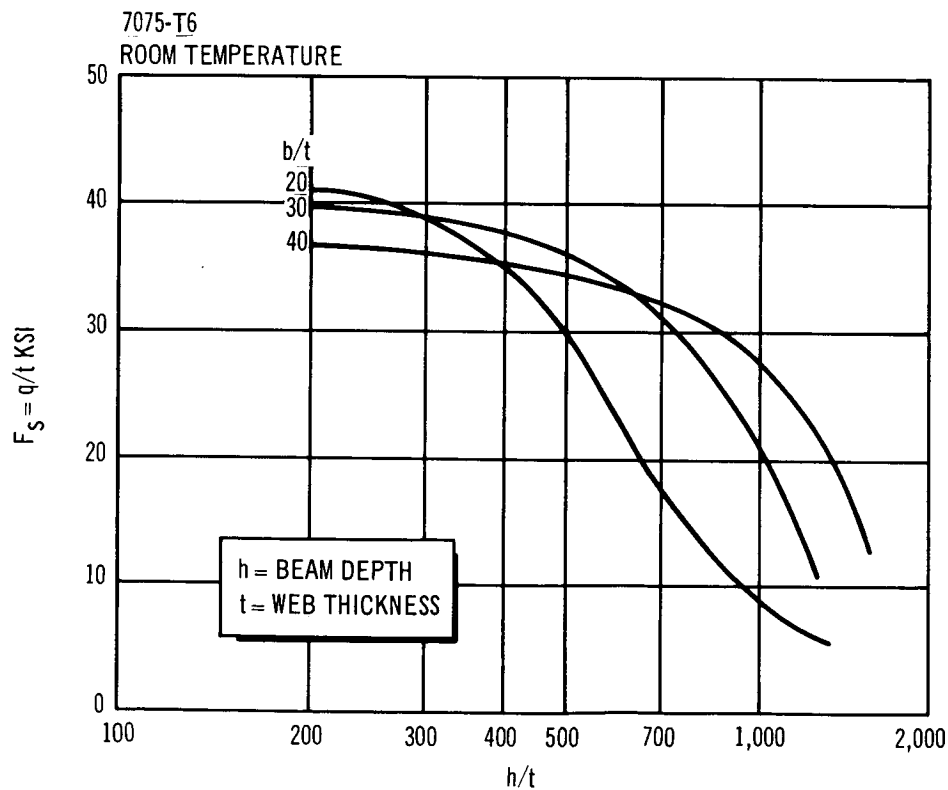


Figure 3-4. Corrugated Shear Webs

For the intermediate section:

$$\frac{h}{t} = \frac{42}{0.04} = 1,050$$

From Figure 3-4:

$$F_s = 26,600$$

$$q = 0.04 \times 26,600 = 1,060 \text{ lb/in.}$$

From the sketch:

$$130 \times \frac{1,060}{1,380} = 100$$

$$100 - 60 = 40$$

For the outboard section:

$$\frac{h}{t} = \frac{42}{0.05} = 840$$

$$F_s = 30,200$$

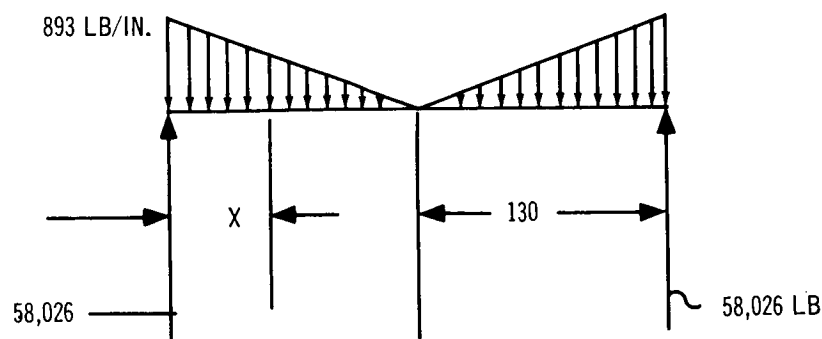
$$q = 0.05 \times 30,200 = 1510 \text{ lb/in.}$$

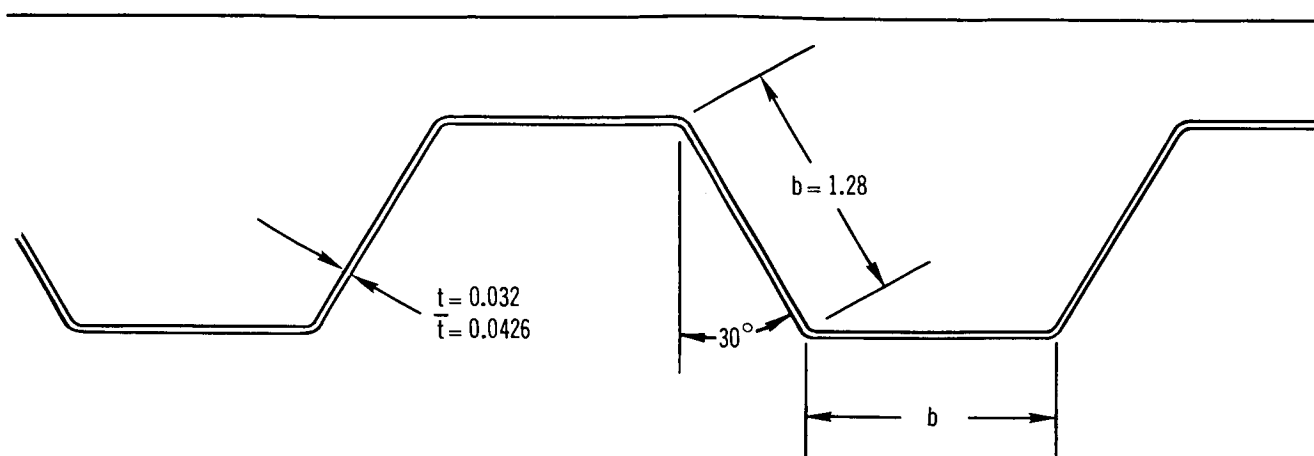
Shear Web Weight

For the 30° corrugations used $\bar{t} = 4/3 t$. Therefore, the weight of one beam shear web is

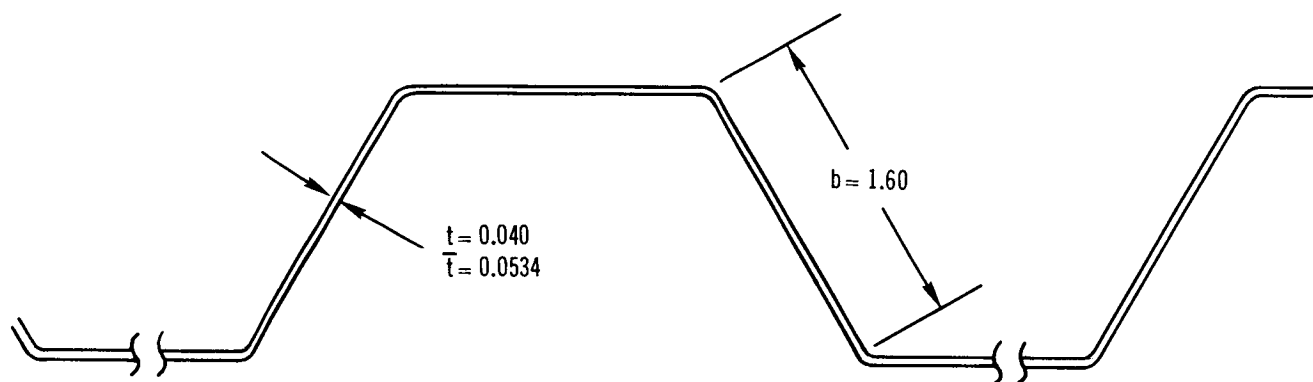
$$0.1 \times 42 (120 \times 0.0426 + 80 \times 0.0534 + 60 \times 0.0667) = 56.1 \text{ lb} \quad (3-18)$$

The weight of the shear webs for the four beams will be 224 lb. The three shear web sections are shown in Figure 3-5.





INTERMEDIATE SECTION



OUTBOARD SECTION

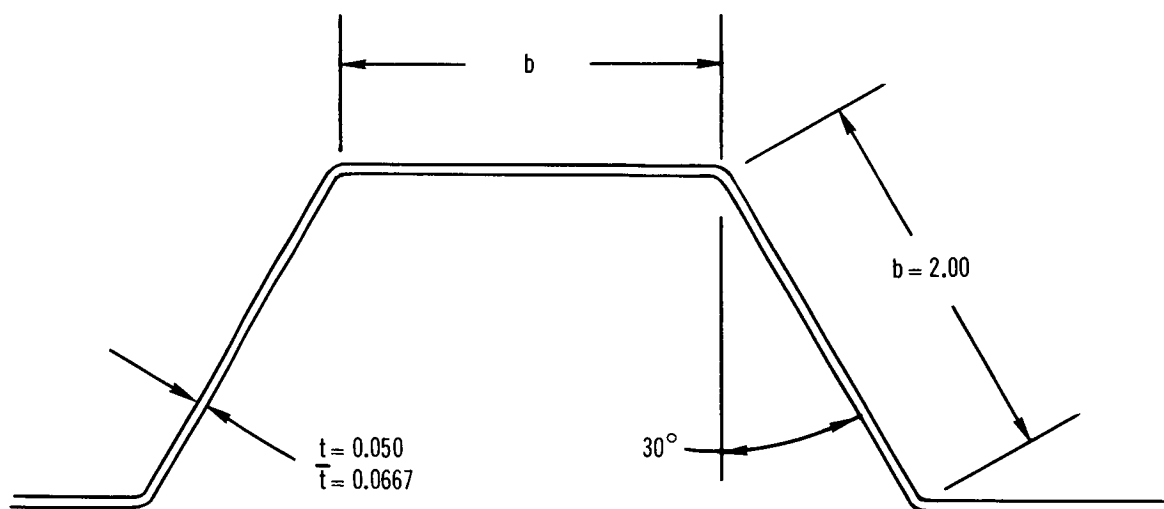


Figure 3-5. Beam Shear Web ($b/t = 40$) Center Section

The bending moment in the beam can be expressed as a function of the distance from the end of the beam by

$$M_x = 58,026X - \frac{893}{130} (65 X^2 - \frac{X^3}{6}) \quad (3-19)$$

The cap load is equal to M_x divided by the beam depth, and the cap area (A_c) is equal to the cap load divided by the allowable stress.

$$A_c = \frac{M_x}{42 (77,000)} = \frac{M_x}{3.23 \times 10^6} \quad (7075\text{-T6 bar}) \quad (3-20)$$

The total weight (W_c) is then

$$\begin{aligned} W_c &= 2\rho \int_0^{130} A_c dx = 0.2 \int_0^{130} \frac{M_x dx}{3.23 \times 10^6} \\ W_c &= \frac{0.2}{3.23 \times 10^6} \int_0^{130} \left[58,062 X - 446.5 X^2 + 1.144 X^3 \right] dx \\ W_c &= \frac{0.2}{3.23 \times 10^6} \left[\frac{58,062 X^2}{2} - \frac{446.5 X^3}{3} + \frac{1.144 X^4}{4} \right] \bigg|_0^{130} \\ W_c &= \frac{0.2}{3.23 \times 10^6} \left[29 \times 1.69 \times 10^7 - 32.7 \times 10^7 + 8.16 \times 10^7 \right] \\ W_c &= 6.2 (4.90 - 3.27 + 0.816) = 15.2 \text{ lb} \end{aligned}$$

The forward beam cap will weigh more than this because the cap area cannot taper to nothing at the beam end as the analysis assumes. The aft cap will be considerably lighter, however, because the faces of the sandwich bulkhead, for which the weight has already been accounted, will serve to carry part of the cap load. For this preliminary analysis, and to make the estimated weight conservative, the 15.2 lb will be assumed to be the average weight of the forward and aft beam caps. The total weight of the caps for the four support beams is then $2 (15.2) (4) = 121.6$ lb. The weight of the shear webs was calculated to be 224 lb, so the total weight of the support beams is 346 lb.

The unit weight of the sandwich bulkhead was calculated to be 2.26 lb/ft². The area of the bulkhead is $\pi (130)^2/144 = 368 \text{ ft}^2$, and the bulkhead weight is therefore 831 lb. The total weight, for support beams and bulkhead, is then $831 + 346 = 1177 \text{ lb}$.

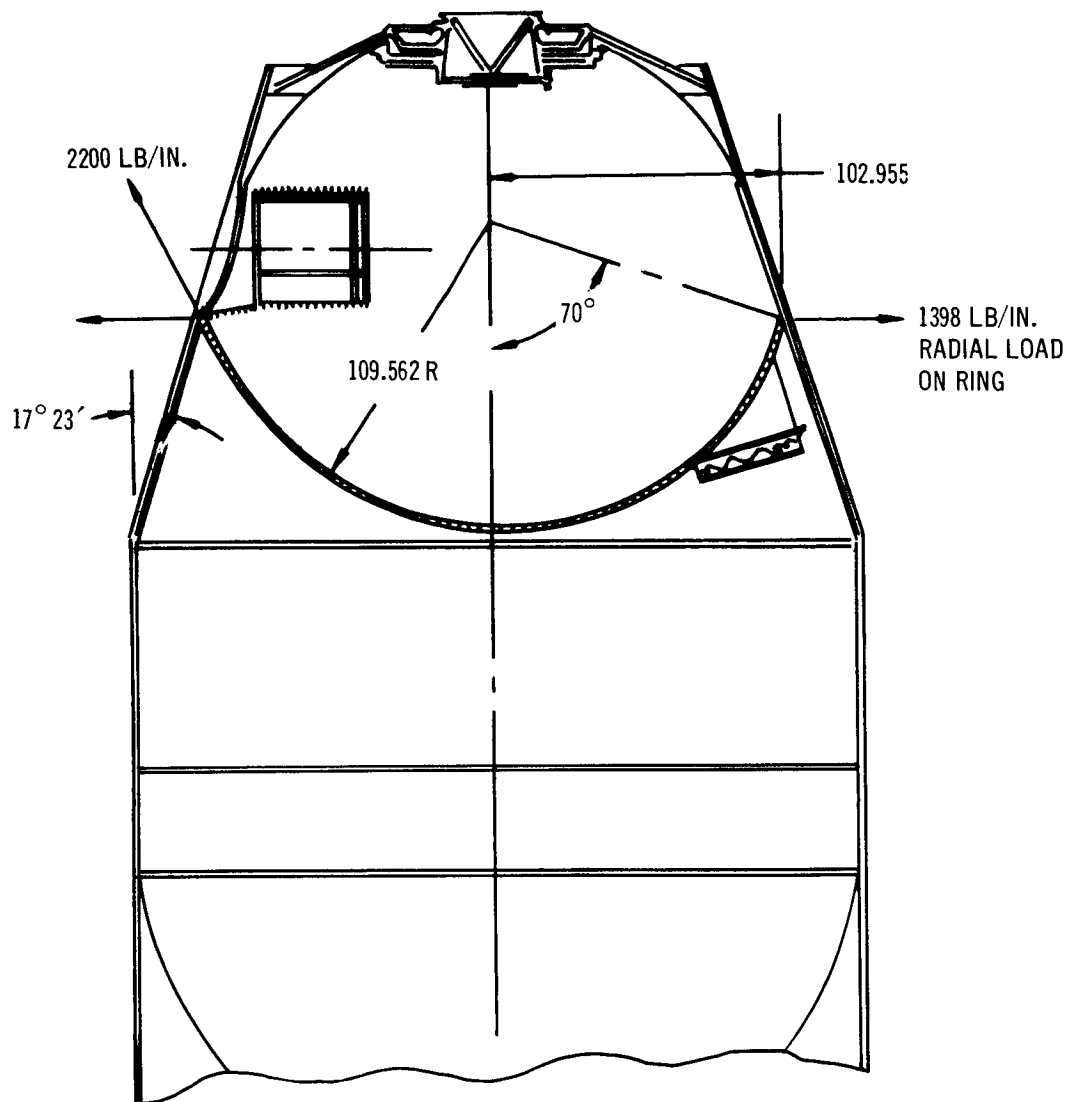
The preceding analysis for the beam-stiffened, compartmenting pressure bulkhead, is crude. The sandwich geometry was optimized for the maximum stress point in the segment, and the resulting core and face thickness was held constant over the whole bulkhead. The analysis assumed the segments were simply supported along the radial edges, when these edges are really fully fixed. The beam end reactions were established by estimating that one-half the pressure load on the bulkhead was carried by the beams. These simplifying assumptions should result in a conservative weight estimate. A more detailed analysis, which was considered beyond the scope of this study phase, can best be accomplished by the redundant force method.

The beam-stiffened, flat sandwich pressure bulkhead replaces the hemispherical segment sandwich bulkhead and the operations compartment floor, which were sized in the Phase IIa study. For the purposes of weight comparison, the weight of these items will be redeveloped.

The hemispherical segment sandwich bulkhead, which has been removed, was designed for a pressure differential of 40 psi in either direction. It had 0.025-in. faces and a honeycomb core with a density of 4 lb/ft³. The unit weight for this sandwich bulkhead was (faces + core + glue) $28.8 (0.025) + 0.667 + 0.260 = 1.647 \text{ lb/ft}^2$. From the bulkhead geometry, the radial load on the bulkhead attach ring is given by the following expression:

$$\frac{PR}{2} (\tan 17^\circ 23' + \tan 20^\circ) = \frac{40}{2} (102.955) (\tan 17^\circ 23' + \tan 20^\circ) = 1,398 \text{ lbs/in.}$$

Applicable sketch is shown on next page. The radial load in the ring which joins the hemispherical bulkhead to the cone is 1,398 lb/in. The resulting hoop load is $1,398 \times 103 = 144,000 \text{ lb}$. To allow for some reduction in material strength from welding the ring to the cone, 60,000 psi will be



assumed to be the allowable stress. The required ring cross-sectional area is then

$$\frac{144,000}{60,000} = 2.40 \text{ in.}^2$$

and the ring weight is $2\pi \times 103 \times 2.40 \times 0.1 = 155 \text{ lb.}$ The surface area of the spherical segment is

$$A = 2\pi R^2(1 - \cos\Theta) = \frac{6.28 \times 109.6^2}{144} (1 - \cos 70^\circ) \quad (3-21)$$

$$A = 344 \text{ ft}^2$$

The weight of the spherical segment bulkhead is thus $344 (1.647) + 155 = 721 \text{ lb.}$

The operations compartment floor had 0.016-in. faces and a 2-in. honeycomb core. The weight per unit area of this floor was $28.8 (0.016) + 0.500 + 0.160 = 1.121 \text{ lb/ft}^2$ and the total weight of the floor was then $368 \times 1.12 = 412 \text{ lb}$.

The combined weight of the floor plus hemispherical bulkhead was $412 + 721 = 1,133 \text{ lb}$. The weight calculated for the flat pressure bulkhead and support beams, that are used to replace the hemispherical segment bulkhead and the operations compartment floor, is 1,173 lb. An apparent weight penalty of 40 lb has thus accrued from this change, but this will be reduced by the simplification the flat bulkhead makes possible in the design of the hatch with the inflatable airlock. Provisions for this hatch can be integrally machined in one face of the bulkhead, eliminating the omni-mill-machined transition cylinder that was required with the hemispherical segment bulkhead.

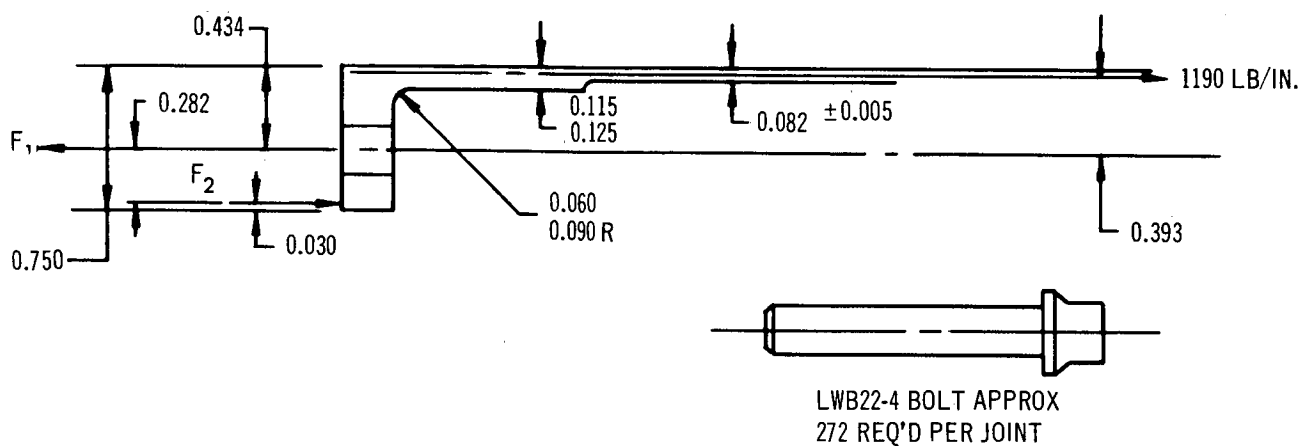
The weights that were calculated here for the purpose of comparison of the Phase IIa and Phase IIb configurations, do not include provisions for weld pads or joints, and so may not exactly match the weight statement which, of course, must go into much greater detail. However, they indicate the degree of weight penalty incurred by this change. The cryogenic tankage, and hangar pumpdown tank, can now be supported during boost by the bulkhead support beams. The same is true for the equipment mounted on the operations compartment side of the bulkhead. The structure required for support of tankage and equipment in the hangar, had not been detailed for the Phase IIa configuration. In all probability, if time permitted both configurations to be developed in complete detail, it would be found that these design changes had resulted in a weight saving. The selection of a more realistic design pressure differential for the compartmenting bulkhead is more responsible for this weight saving than the simplification, and multiplicity of purpose, which the flat, beam-stiffened, compartmenting bulkhead provides.

Bolted Joint Analysis

The O-ring sealed, bolted joints between the aft dome and cylinder, and between the hangar and the cylinder, have been sized for a pressure differential of 17.5 psi. The design pressure load across the joint is thus

$$\frac{PR}{2} = \frac{17.5 \times 130}{2} = 1,140 \text{ lb/in.}$$

Fifty lb/in. is added to this to conservatively account for the compressive load on the O-ring seal, giving 1,190 lb/in. The resulting bolt load is determined from the free body diagram of the integral flange.



$$0.282 F_2 = (0.393) 1,190$$

$$F_2 = 1,660 \text{ lb/in.}$$

$$F_1 = 1,190 + 1,660 = 2,850 \text{ lb/in.}$$

8,540 lb is the allowable load for the LWB22-4 bolt that is used.

The required bolt spacing is $8,540/2,850 = 3$ in. on center. This analysis neglects the small additional eccentricity due to the curvature of the joint and the external flange. This is, however, extremely small with this radius and bolt spacing. The bolt spacing actually used will be that which divides the bolt circle into an integral number of equal spaces, and so will be slightly less than the 3-in. maximum spacing permissible.

This analysis assumes the pressure shell is 260 in. in diameter which is the case for the alternate concept. The pressure shell diameter for the baseline concept is 255.5 in. in diameter, and so the maximum permissible

bolt spacing would be slightly larger. For the waffled cylinder of the alternate concept, the longitudinal rib spacing would be made an integral multiple of the selected bolt spacing. To keep the combined weight per unit area of the pressure shell and outer shell the same for both the baseline and alternate concept, a 5-in. rib spacing was selected for the alternate concept. A 6-in. spacing would be adequate for the maximum loading condition and is more compatible with the required bolt spacing.

3.3.6 Radial Stowing Ports

3.3.6.1 Baseline

The experimental hangar has been modified to incorporate six ports for radially stowing docked vehicles. These ports permit continuous pressurized access to the stowed vehicles as shown in Figure 3-6. The six ports are equally spaced 49° between centers at the aft end of the hangar cone. This permits the concentrated loads imposed by the stowed vehicles to be distributed by the support beams and flat pressure bulkhead, and leaves a 90° quadrant of the hangar free for the Earth-oriented experiments. A deep frame, which inscribes 270° of the hangar, is bolted to the caps of each of the support beams and to the hangar shell. A machined fitting, fabricated from either a hand-forged billet of 7079-T652 which is $38 \times 45 \times 3\text{-}5/8$ -in. thick, or an equivalent size piece of 7079-T651 plate, is bolted to the hangar pressure shell. This fitting, together with the bolting flange integrally machined in the 0.750-in. thick plate from which the pressure shell is fabricated, serves as the doubler around the 38-in. diameter stowing port hole in the pressure shell. A resin-cured, butyl O-ring (0.270 in. in diameter) is used to seal the bolted joint between the fitting and the pressure shell. Integral flanged ribs on the fitting are bolted to ribs on the pressure shell floor, and to the deep ring frame joining the beam caps, to react the loads imposed by the stowed vehicle. A large aluminum snap ring is installed in a machined groove in the fitting. This expandable ring is used to lock the stowed vehicle to the port. The locking ring is manually expanded and contracted from within the hangar by means of an acme threaded through shaft.

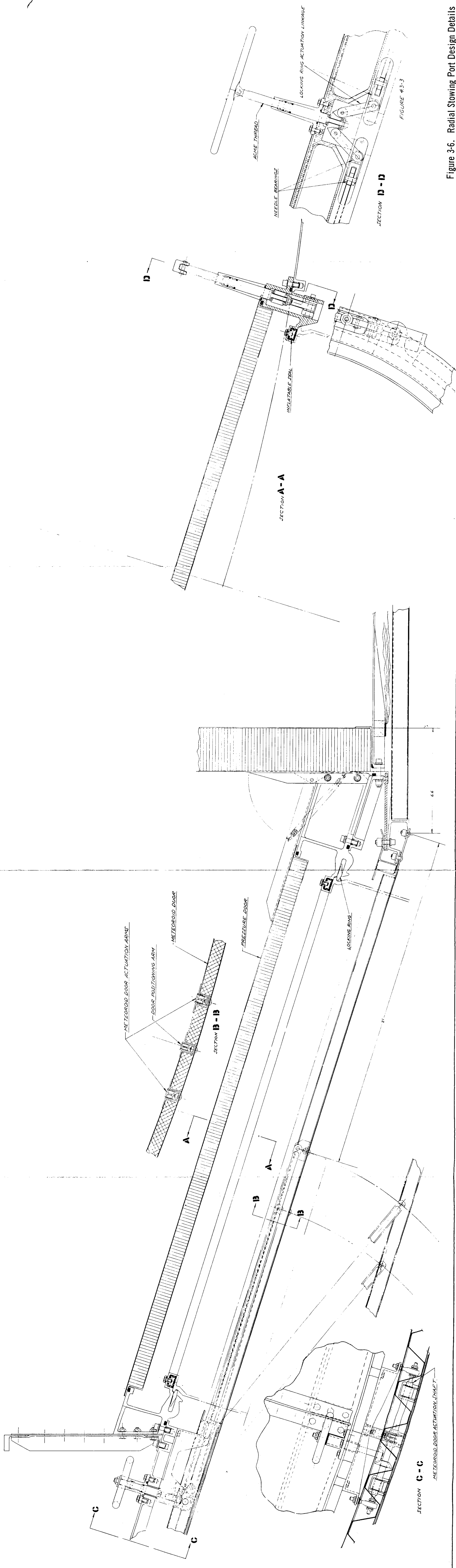


Figure 3-6. Radial Stowing Port Design Details

135-084

135-3

135-2

135-1

The shaft is rotated with a handle that swivels parallel to the shaft when not in use. The through shaft is sealed by two O-rings with the annular space between the two O-ring grooves filled with silicone grease for lubrication. A similar rotatable shaft and sealing arrangement was used on the Langley two-man airlock; this arrangement was satisfactory. A fitting on the outboard end of the shaft engages inner and outer thrust bearings on the shaft. Each side of this fitting is joined to a pair of links. A needle bearing is mounted on the outboard end of the first link to react the component force in the link that is parallel to the drive shaft. The normal component is transmitted through a pin joint to the second link, which is connected to a slot in the lock ring through a second needle bearing. Rotating the shaft moves it in or out enabling the low friction linkage to expand or contract the locking ring. By removing the swivel handle and threaded support fitting, the O-ring seals and silicone grease can be replaced. The leak rate during this operation is kept small by minimizing the clearance of the shaft in the through hole.

The joint between the stowed vehicle and the stowing port is sealed by an extruded, inflatable seal of butyl rubber. A lathe-turned, internal retainer ring that clamps the seal in position is bolted to the seal mounting slot, with sealing washers under the bolt heads. This seal design is currently under test at Douglas and gives promise of being a long-life, low-leak arrangement.

The inflatable seal can be designed to maintain a sufficiently small leak rate when pressurized to the 7 psi hangar pressure, so that the seal retainer bolts can be removed without a large loss of hangar atmosphere. A leaking sealing washer can thus be replaced while a vehicle is stowed in the ports by deflating the seal from its 50 psi normal operating pressure to 7 psi. The leaking washer can be found by coating the sealing washers with a soap solution while the seal is pressurized to 50 psi.

The inflatable seal can be replaced by removing the retainer bolts while a vehicle is stowed in the ports, by closing the port pressure door and removing the stowed vehicle. The seal must be removed and replaced from the outside, which requires EVA. However, the seal retain bolts can be installed from the pressurized hangar after the stowed vehicle is replaced in the port.

Replacement of any of the stowing port seals may never be required in the 5-year life of the laboratory because of the expected stability of the sealing material in the space environment.

A circular pressure door is used to seal the port when no vehicle is stowed in it. A sandwich construction is used for this door, with 0.031-in. faces and an aluminum honeycomb core with a density of 3.1 lb/ft³. The flange and one face of the door are integrally machined from a piece of 1-in. plate, so that no leak can occur through a bonded joint in the door. The door flange engages a butyl O-ring that is mounted in a lathe-turned bevel groove in the stowing port fitting. The pressure differential across the door is used to supply the sealing force and no latching mechanism is required. An over center spring holds the hinged door in the closed or open position when no pressure differential exists across it. The hinge is placed so that the door lies flat against the compartmenting bulkhead when in the open position.

A door is provided in the outer shell to serve as a fairing for the stowing port during boost, and as a micrometeoroid shield for the inflatable seal and pressure door when no vehicle is stowed in the port. The inner face of the micrometeoroid door is lined with aluminized mylar to minimize thermal cycling of the port when no vehicle is stowed in it. A sandwich construction is used for the micrometeoroid door with a 2 lb/ft³ truss grid aluminum honeycomb core, and 0.020-in. 6061-T6 aluminum faces.

The cargo modules are supplied with an adapter, the end of which is identical with the stowing flange on Apollo. This adaptor is removable so that a clear opening 60 in. in diameter can be maintained for unloading cargo at the hangar mouth. Because the adaptor must clear the door at the hangar entrance when the cargo module is stowed there for off loading, the distance that the adaptor can extend past the 60-in. diameter sealing flange is limited. With the cargo module stowed in the radial port there is thus very little clearance between the 60-in. diameter flange and the surface of outer shell. For the stowing port micrometeoroid door to clear this 60-in. diameter flange, it must lie flush against the outer shell when in the open position, with its curvature in the same direction as the curvature of the

outer shell. Stowing the door in this position is accomplished by a pair of hinge arms and idler link that maintains the door parallel to the surface of the outer shell. The pair of hinge arms are splined to a shaft which is positioned inside the outer shell by two rod end bearings. The rod end bearings are mounted on a fitting that is bolted to the pressure shell. The splined shaft is driven through a pair of bevel gears by a through shaft into the hangar. The rod end bearings permit adjustment of the bevel gear engagement. The through shaft is sealed by two spaced O-rings with silicone grease in the annular space between the O-ring grooves, similar to the shaft actuating the locking ring. These O-rings and the silicone grease can be replaced in orbit by removing the shaft handle and the guide fitting. Leakage is limited during this operation by the fit of the shaft in the guide bushing.

The shaft mounting the hinge arms is fabricated in two sections which are joined by two splined crank fittings and a crank pin. A spring, which goes over center when the door is opened, is attached at the crank pin, and holds the micrometeoroid door in either the open or the closed position in orbit. Two explosive bolts are used to secure the door in the closed position during boost.

To maximize reliability, the hardware associated with the stowing operation has been designed to be manually operated. This required two through shafts at each of the six stowing ports. From the experience gained on similar through shafts in testing the Langley two-man airlock, the increase in leak rate from this feature will be negligible. A similar case can be made for the O-ring sealed pressure hatches and inflatable seal joints between the stowed vehicles and the ports. With reasonable care in the detail design, the total leak rate at any port, whether a vehicle is stowed there or not, can be held to a maximum of 50 cm^3 per day. This will give a maximum of $300 \text{ cm}^3/\text{day}$ for the six ports. At this rate, it will take 3.4 years for the six ports to leak 1 lb.

In the stowing port design that has been described, it is assumed that provisions for damping both bending and torsional oscillations in the stowing arm will be a design feature of the arm. A detail design of the stowing arm has not been accomplished. If incorporation of this design feature should

prove difficult, the stowing port can be modified to permit stowing a vibrating vehicle. A short, conical, lead-in section lined with butyl, or a similar material suitable for serving as a bumper, can be added to the stowing port fitting. Adding this lead-in section requires enlarging the hole in the outer shell which requires moving the stowing port hole forward on the cone. This has the following undesirable effects:

1. The clearance between the stowed vehicles is reduced.
2. The depth of the support beams must be increased, at least locally, to provide for attachment of the deep frame which would have to be moved forward to clear the stowing port hole.
3. Since the separation between the deep frame and the floor is increased, the depth and weight of the stowing port fitting is increased.

A design tradeoff study will have to be made to determine whether provisions for stowing a vibrating vehicle should be included in the design of the stowing port, or whether an oscillation damper should be a design feature of the stowing arm.

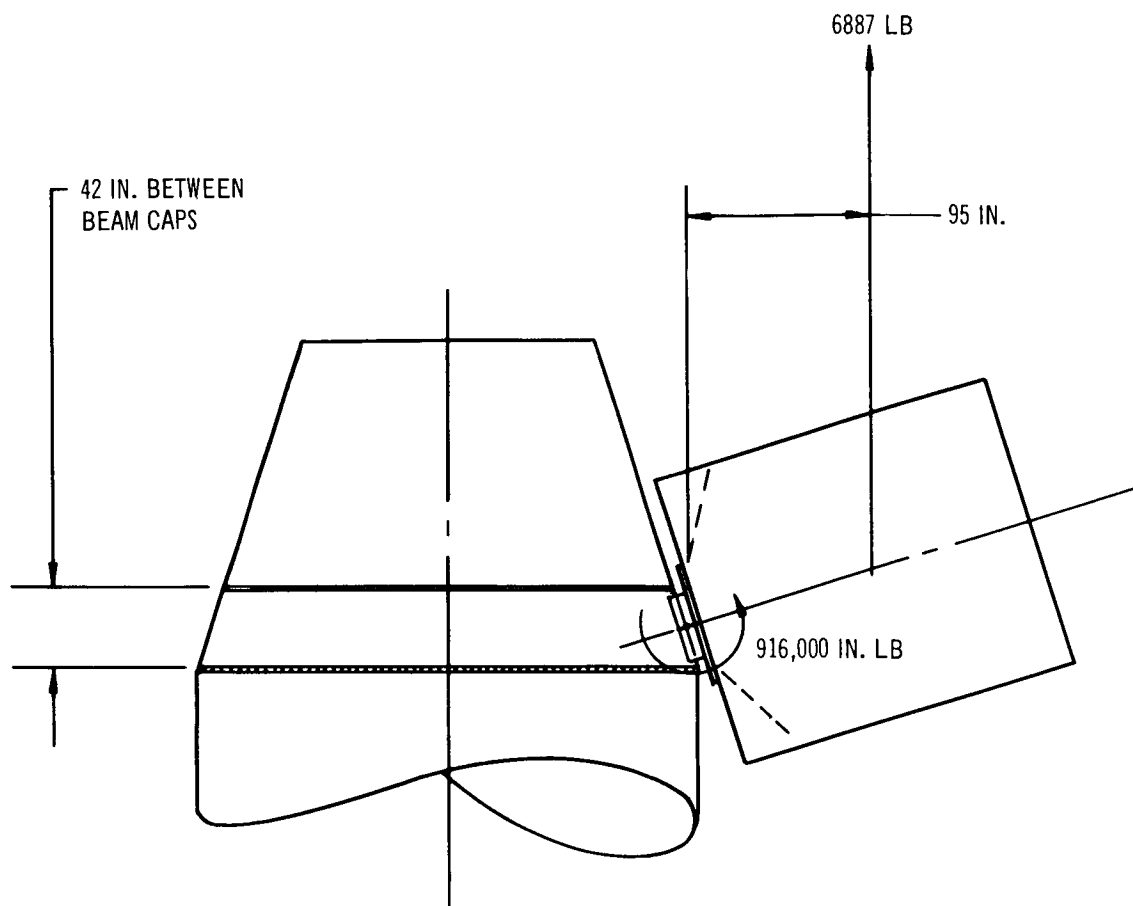
3.3.6.2 Alternate Concept

The stowing port design for the alternate concept would be identical to that described for the baseline. In both cases the hangar pressure shell is high-speed routed in the flat from 0.750-in. plate, so that integral provisions for attachment of the stowing port fitting can be made.

3.3.6.3 Stowing Port Analysis

The stowing port structure has been sized to permit spin up to $1/3 g$ at the center of mass of a fully loaded cargo module. The loaded cargo module weighs 20,660 lb. Its center of mass is approximately 95 in. from the stowing port. The resultant bending moment at the port is $1/3 (95)(20,660) = 654,000$ in.-lb. The design moment is $1.4 (654,000) = 916,000$ in.-lb. The load on the latching ring from spin up is

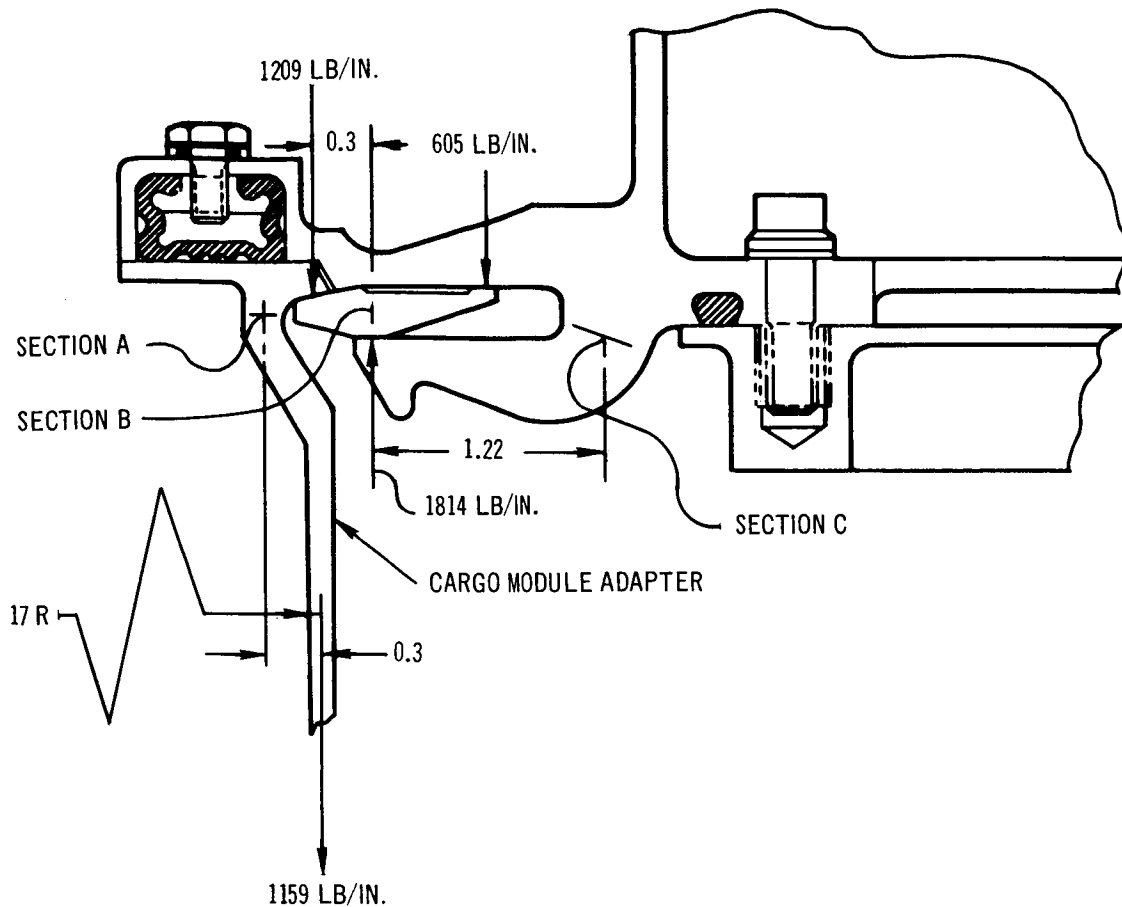
$$\frac{Mc}{I}t = \frac{M}{\pi R^2} = \frac{916,000}{\pi (17)^2} = 1,010 \text{ lb/in.}$$



The design pressure load on the latching ring is

$$\frac{PR}{2} = \frac{17.5 (17)}{2} = 149 \text{ lb/in.}$$

A load of 50 lb/in. is added to account for the inflatable seal. On the tension side of the neutral axis these loads are added to give a total design load on the latching ring of $1,010 + 149 + 50 = 1,209$ lb/in. The resultant stress at various sections of the joint is as noted.



At Section A

$$f = \frac{MC}{I} + \frac{P}{A} = \frac{6 \times 1,159 \times 0.3}{(0.2)^2} + \frac{1,159}{0.2} = 57,500 \text{ psi} \quad (3-22)$$

At Section B

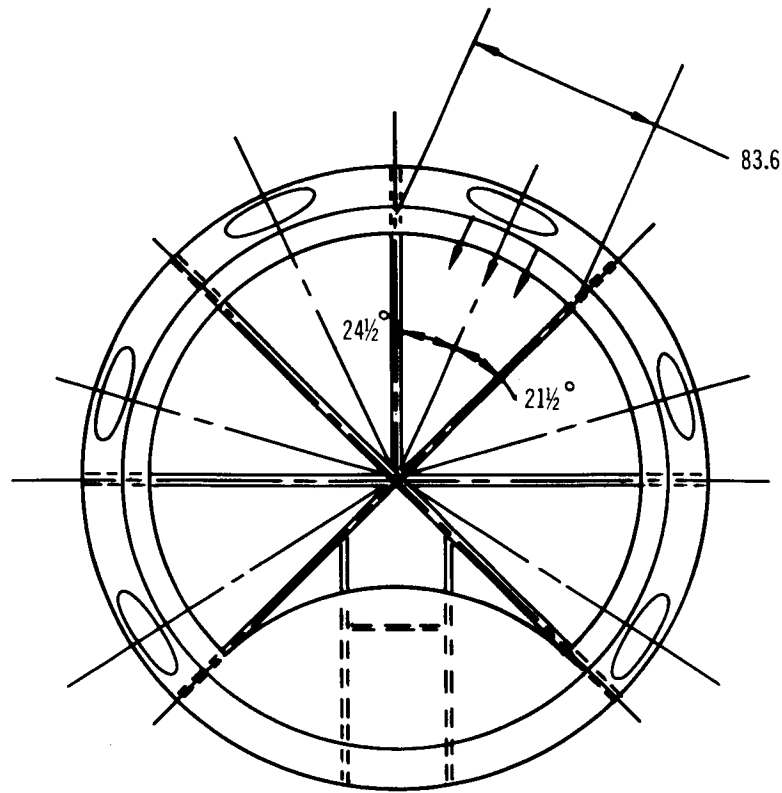
$$f_b = \frac{MC}{I} = \frac{6M}{h^2} = \frac{6 \times 1,209 \times 0.3}{(0.250)^2} = 34,800 \text{ psi} \quad (3-23)$$

At Section C

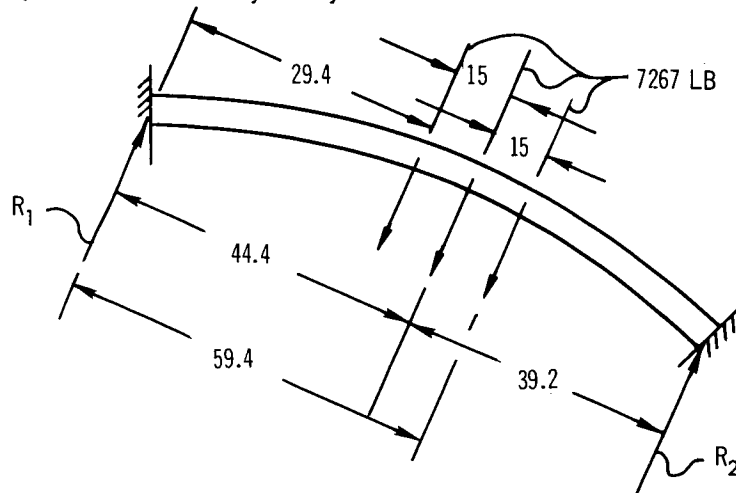
$$f_b = \frac{MC}{I} = \frac{6M}{h^2} = \frac{6 \times 1,814 \times 1.22}{(0.5)^2} = 53,100 \text{ psi} \quad (3-24)$$

The reactions introduced in the planes of the floor and deep ring frame are

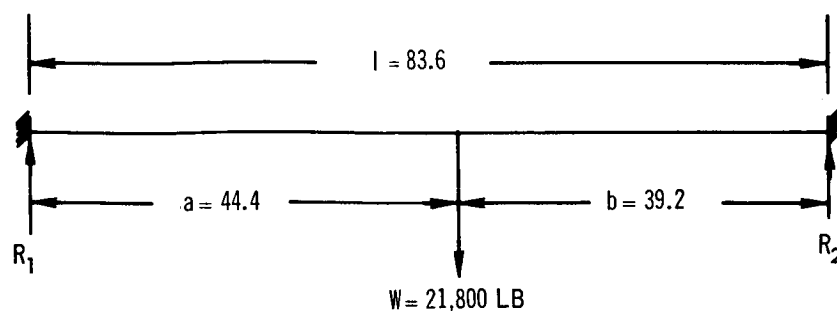
$$\frac{916,000}{42} = 21,800 \text{ lb}$$



It is assumed for the purposes of this preliminary analysis, that this reaction is equally divided between the three ribbed flanges on the stowing port fitting. These flanges are located on the centerline and 15 in. either side of the centerline of the stowing port fitting. The maximum bending moment in the deep ring frame will occur on the centerline of the most centrally located stowing port. The loading diagram for the ring frame in this quadrant is as shown. Since the ring frame is continuous over the beam caps, full end fixity may be assumed.



A conservative quick approximation to the resultant maximum bending moment is estimated by neglecting the curvature and approximating the loading as shown.



$$R_1 = \frac{Wb^2}{l^3} (3a + b) = \frac{21,800 (39.2)^2}{(83.6)^3} [3 (44.4 + 39.2)]$$

$$R_1 = (57.4 (172.4)) = 9,900$$

$$R_2 = 21,800 - 9,900 = 11,900$$

$$\text{Max. } M = \frac{-Wab^2}{l^2} + R_1 a \quad (3-25)$$

$$\text{Max. } M = \frac{-21,800 (44.4)(39.2)^2}{(83.6)^2} + 9,900 (44.4)$$

$$= -213,000 + 436,000 = 223,000 \text{ in. /lb}$$

For a 10-in. frame depth, the maximum cap load is 22,300 lb. The required cap area is $22,300/67,000 = 0.333 \text{ in.}^2$ (2014-T6 caps). The weight of the two frame caps is $3\pi (0.333)(107)(0.1) = 33.6 \text{ lb}$. The actual cap weight will be a little less than the cap weight calculated above because the pressure shell can serve as part of the frame outer cap. An additional saving over that calculated, can be achieved by tapering the frame caps.

The maximum shear in the web is 11,900 lb. With the 10-in. frame depth, this gives a shear flow of 1,190 lb/m. Assume a shear web thickness of 0.032. The maximum shear stress is $1,190/0.032 = 37,200 \text{ psi}$. The H/t for the web is $10/0.032 = 310$. From Figure 3-4 it can be seen that if a corrugated shear web is used with a b/t of 20, the allowable shear stress is

in excess of 38,000 psi. The \bar{t} for the shear web is $4/3 \times 0.032 = 0.0426$, and the weight of the shear web is $3/2 \pi (107)(0.0426)(10)(0.1) = 21.4$ lb. A conservative weight estimate for the frame is $33.6 + 21.4 = 55$ lb.

3.3.6.4 Stowing Port Hatch

The hatch required to seal the radial stowing port when a vehicle is not stowed there, is 36 in. in diameter. It has been sized for a 28 psi burst pressure (factor of four on maximum operating pressure of 7 psi).

From Roark, page 194, Case I

$$S_{\max} = 1.24 p \left(\frac{a}{t} \right)^2$$

$$t^2 = \frac{1.24 (28)(18)^2}{60,000} = 0.1875 \quad (3-26)$$

A sandwich plate will work to the same stress as a monocoque plate with the same I/C.

Equating I/C

$$\frac{t^3}{12} \times \frac{2}{t} = \frac{t^2}{6} = \frac{h^2 t_f}{2} \cdot \frac{2}{h} = h t_f$$

$$h t_f = \frac{0.1875}{6} = 0.0312 \quad (3-27)$$

Use 0.031 faces and a 1-in. aluminum honeycomb core.

$$\frac{PR}{2h} = \frac{28 \times 18}{2} = 252 \text{ psi} = \text{max. core shear.}$$

Use a 3.1 lb/ft³ core density.

3.3.7 Experimental Bay

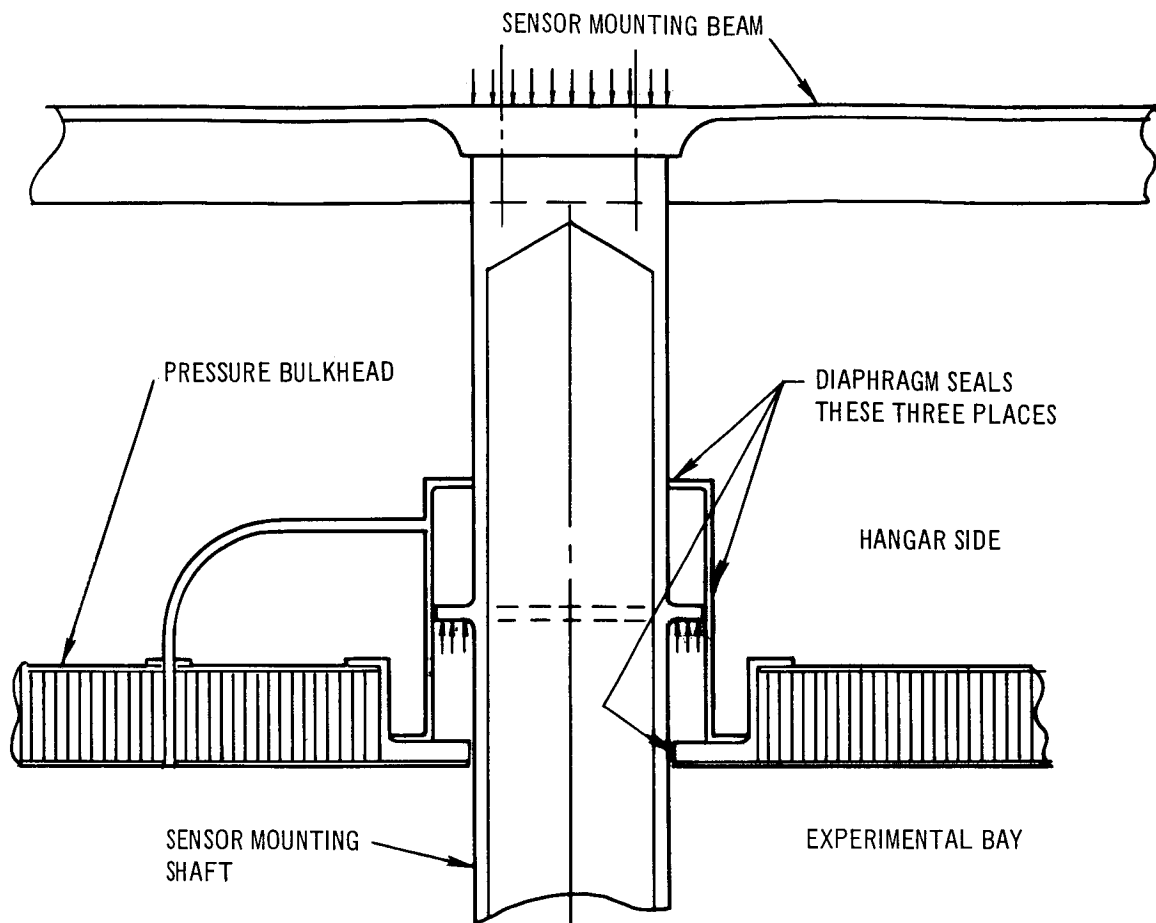
To permit the installation and alignment, in a pressurized environment, of sensors on the sensor mounting beam, an experimental bay will be provided in the hangar portion of the laboratory. The principal use for the bay will be the setup and alignment of Earth-oriented sensors. Several configurations

for the bay have been investigated. Insufficient time was available in this study phase to accomplish the design tradeoffs that will be required to select the optimum configuration for the bay. Two configurations that established the feasibility of the concept are described, and a preliminary design-type stress analysis is written for each.

The six radial-stowing ports have been arranged around the hangar so that a 90° quadrant is left clear for the experimental bay. With the laboratory flying in the belly-down mode, the bay (except for the small angle between the approaching horizon and the local horizontal) is shielded from micro-meteoroid impact by the Earth and the remainder of the laboratory.

One configuration of the experimental bay has been designated as baseline. This is not meant to infer that this configuration has been optimized; this was merely the first configuration investigated and received the greatest amount of detail effort.

In the baseline configuration, the experimental bay is separated from the remainder of the hangar by a flat, sandwich, pressure bulkhead which intersects the hangar pressure shell along straight-line-conical elements. The sensor mounting beam is mounted on the inboard, or pressurized, side of the flat bulkhead. The sensor mounting shafts extend through the bulkhead into the bay. To prevent the accumulation of bending stresses in the sensor mounting beam, which must be maintained in as nearly a stress-free condition as possible to meet the accuracy required for sensor alignment, a load-balancing flange is provided on the sensor mounting shaft. This arrangement is schematically shown below. The surface area of the load-balancing flange is made equal to the cross-sectional area of the shaft where it penetrates the pressure bulkhead. With the venting arrangement shown, the pressure differential across the load-balancing flange balances the pressure end load on the shaft. Diaphragm-type seals permit the pressure bulkhead to move, relative to the sensor mounting beam, without introducing appreciable load in the beam.



With this scheme and the venting arrangement shown, the pressure end load on the sensor mounting shaft is balanced, no matter what the magnitude, or the direction, of the pressure differential between the hangar and the experimental bay.

The experimental bay is exposed to space by opening a large pressure door in the hangar. This door spans 90° of the hangar circumference and extends the full length of the bay. The edges of the door lie along straight-line elements of the conical hangar shell. Both the door and the hangar pressure shell are machined in the flat from 0.750-in.-thick 2014-T6 plate. This thickness permits integral, flanged lips to be machined into both the door and the door jamb. These lips are interlocked when the door is in the closed position. With the hangar and the experimental bay both pressurized, the hoop load is carried through the interlocked lips.

After machining in the flat, the door and the flat pattern segments of the conical hangar pressure shell are rolled to contour. The door is sealed by

an inflatable seal similar to the seal used on the radial-stowing port, which forms a seal between the stowed vehicle and the stowing-port fitting.

Provisions for this seal are integrally machined into the door jamb. An inflatable seal is used to minimize the door latching force and to accommodate tolerances in machining and forming.

The interlocking lips extend along the full length of the sides of the door, and across the 90° of circumference at the forward end of the door. A locking ring segment, extending across the 90° of circumference at the aft end of the door, engages an integrally machined groove in the door and locks it in the closed position.

To open the door, the experimental bay is pumped down. Residual pressure differential across the door is eliminated by venting the inflatable seal to vacuum. The locking ring at the aft end of the door is retracted. The hinge mechanism at the forward end of the door slides the door 2 in. forward in the plane of the conical elements at the sides of the door. At this time, the interlocking lips are fully disengaged. The hinge mechanism then rotates the door forward until the centerline of the door lies in the plane tangent to the approaching horizon.

The portion of the load-carrying outer shell that faces the experimental bay pressure door is joined to the edges of the door by fiber glass stringers, and along the forward and aft ends by fiber glass frame sections. Additional fiber glass spacers, between the outer shell and the pressure door, will be provided as required. Aluminized mylar is installed in the space between the outer shell and the door to prevent the door from falling below the dew point of the hangar atmosphere when the door is in the closed position. Flight loads are carried through a butt joint at the aft end of this section of the outer shell. The pressure door maintains the position of the outer-shell segment.

The hinge mechanism, which slides the door assembly forward and then rotates it, is attached to the outer-shell segment. The outer-shell door, along with the Earth and the remainder of the laboratory, protects the pressure door from micrometeoroid impact.

Temperature differential between the door and jamb, which could be appreciable when the door is first rotated into the closed position, will be reduced by holding the door in this position until the interlocking lips can be freely engaged. The locking ring at the aft end of the door, which will be manually actuated, cannot be extended with the interlocking lips partially engaged. A view port will be provided in the pressure bulkhead to monitor the position of the door prior to actuation of the locking ring segment. Also, this port can be used for inspection of the door surface. In the open position, the door is protected from meteoroid impact (except for the very small angle between the surfaces from the door to the points of tangency on the laboratory and on the trailing horizon).

The baseline configuration of the experimental bay permits continuous pressurized access to the sensor mounting beam, and pressurized access to the sensors when the bay is pressurized. The experimental airlock, part of the sensor mounting beam, in this configuration extends through the pressure bulkhead into the experimental bay. A load-balancing flange, identical to that described for the sensor mounting shafts, is provided on the experimental airlock to balance the end load from pressure differential across the airlock.

Three disadvantages of the baseline configuration which have been identified are as follows:

1. The airlock can only be used when the experimental bay door is open. Because the time for sensor setup, alignment, and change may be small, this disadvantage may not be serious.
2. The large flat pressure bulkhead is structurally inefficient. If support beams are added across this bulkhead on the experimental bay side to reduce the bulkhead weight, they reduce the already limited working space in the bay; if added on the hangar side of the bulkhead they force an increased separation between the sensor mounting beam and the bulkhead.
3. Access to the bay must be gained through the operations/experimental area of the laboratory because of the arrangement of the sensor mounting beam and experimental airlock. This arrangement requires a circuitous route for sensors off loaded in the hangar.

3.3.8 Alternate Experimental Bay

An alternate concept for the experimental bay was developed in an attempt to eliminate the three disadvantages of the baseline concept noted above. This concept is shown in Figures 3-7 through 3-10. To minimize the structural weight penalty imposed by the bay, a conical bulkhead was used to replace the flat pressure bulkhead that separated the experimental bay from the rest of the hangar. This conical bulkhead has the same shape as the hangar cone. Straight-line elements along its edges intersect straight-line elements of the hangar shell. The kickload that is developed at the intersection of the two cones, when the experimental bay is evacuated, is reacted by titanium tie rods which extend across the center of the bay in the same plane as the flat bulkhead in the baseline concept. The tie rods, which are 18 in. on center, feature pin joints at the center and each end so that they can be easily removed when it is necessary to increase the clear working space in the bay. They are not required, of course, when the bay is pressurized.

The sensor mounting beam is in approximately the same location as in the baseline concept. But, because of the conical shape and resultant increased depth of the bay, in this concept the beam is on the experimental bay side of the bulkhead. Since the sensors and the sensor mounting beam now share the same environment, the need for load-balancing features on the sensor mounting shafts is eliminated, and the sensor installation is considerably simplified. Because the sensor mounting beam is exposed to the space vacuum along with the sensors, it must be insulated so that no appreciable temperature gradients can be created. The beam will be supported by a pin joint at one end and a hinged link at the other end; therefore, changes in the mean temperature of the beam are of no consequence. However, the beam must be sufficiently insulated so that the rate of temperature change is sufficiently slow to ensure that no appreciable temperature gradients can accrue to bow the beam. Since the sensor mounting beam will be fabricated from either aluminum or beryllium, both of which are excellent conductors, the beam insulation problem should be trivial.

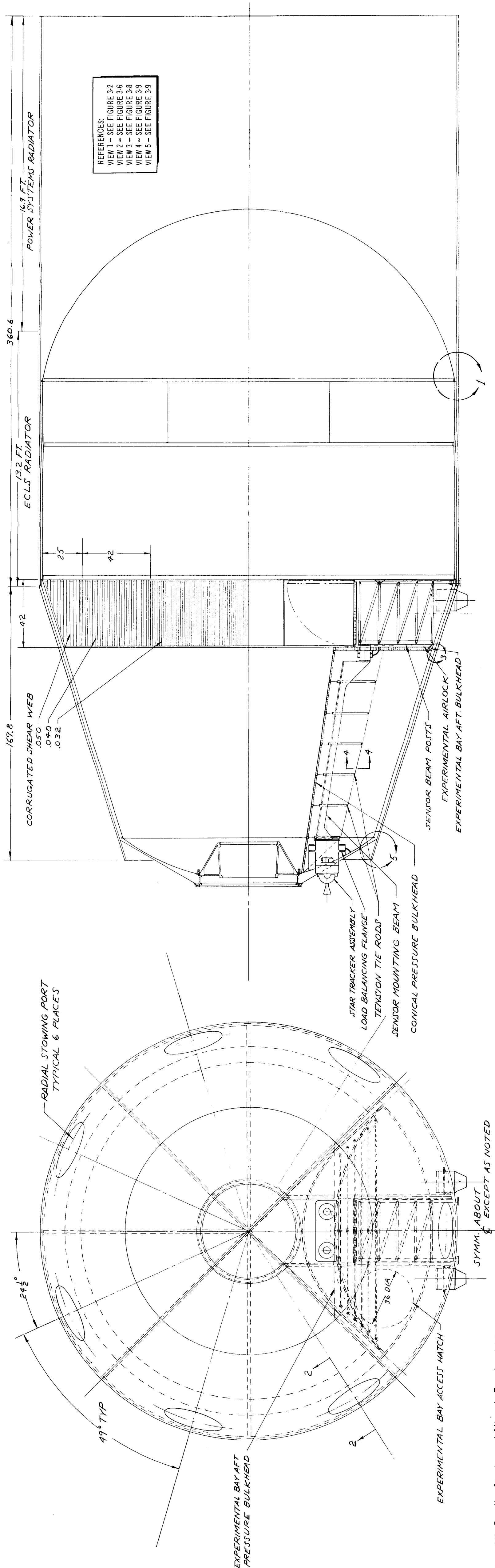


Figure 3-7 Baseline Structure and Alternate Experimental Bay

150-2

150-2 3

150-4

150-0-5

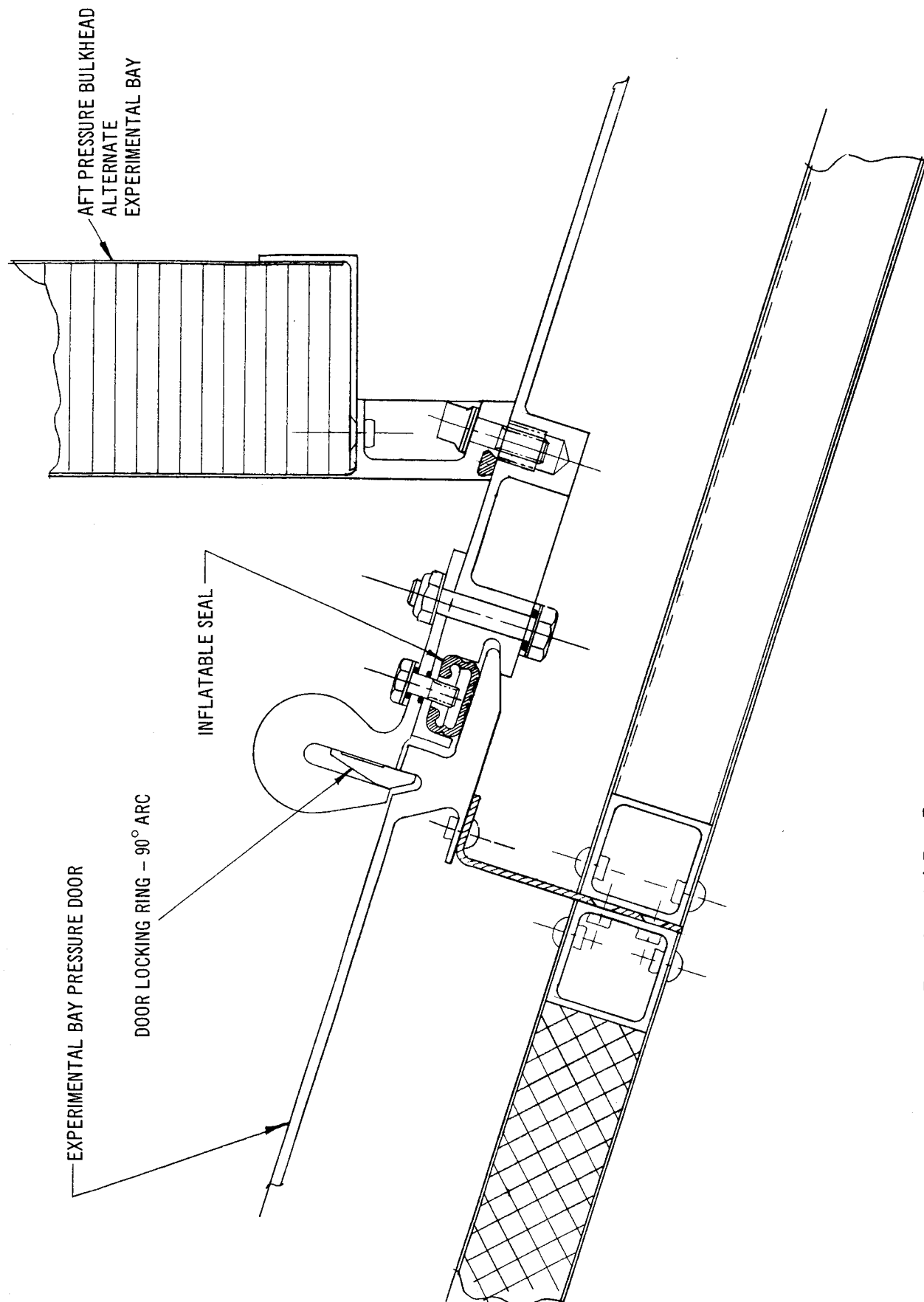


Figure 3-8 Aft-End View of Experimental Bay Door

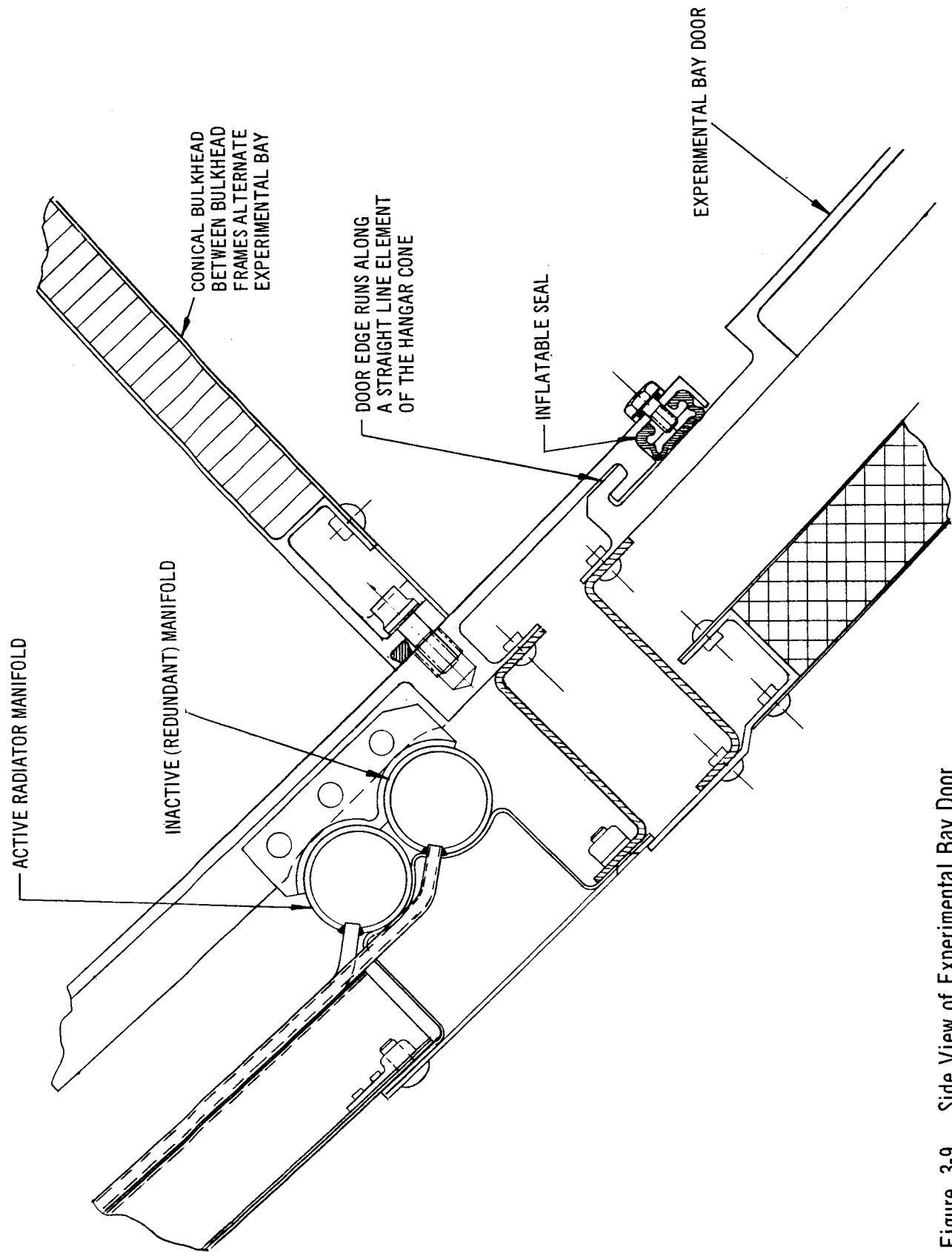


Figure 3-9. Side View of Experimental Bay Door

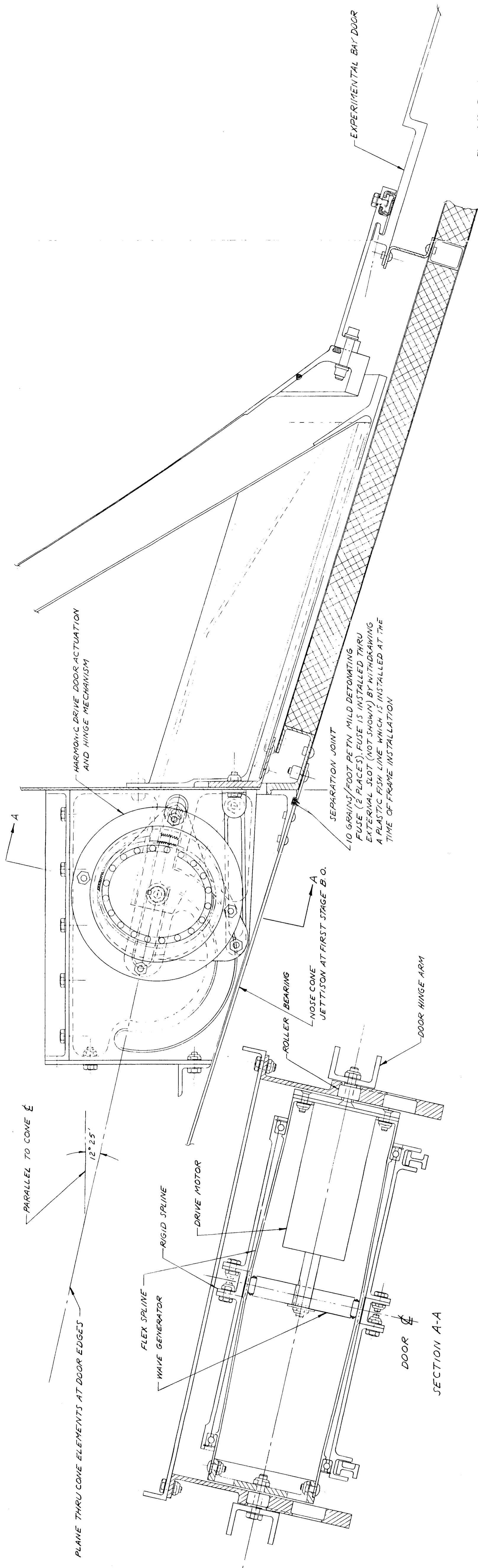


Figure 3-10. Experimental Bay Door Section

153-884

153-83

153-2

153-1

153-85

The whole experimental bay is moved forward, in this concept, from the position it occupied in the baseline concept. The aft end of the bay is closed by a flat sandwich pressure bulkhead which ties into the forward caps of the bulkhead support beams. The end of the bay is, thus, 42 in. forward of the main compartmenting bulkhead. The bulkhead support beam, which lies in the plane of the centerline of the experimental bay, is divided into two beams 40 in. apart for a little less than half of its length. These beams are pressure-tight sandwich bulkheads that are bolted to both the main compartmenting bulkhead and the experimental bay end bulkhead. These bolted joints are made pressure tight with O-ring seals. The 42-in.-high by 40-in.-wide rectangular experiment airlock that is formed by this arrangement is closed off at its inboard end by a rectangular hatch that hinges against the main compartmenting bulkhead. This hatch features an O-ring seal and is held it either the open or the closed position by a spring that goes over center when the hatch is opened. A circular hatch, 38 in. in diameter, closes off the outboard end of the airlock.

The airlock portion of the sensor mounting beam features four posts that are positioned in the four corners of the airlock. Truss members between the posts keep them rigidly positioned relative to each other. Machined pads on the two forward posts are rigidly bolted to cylindrical extensions of the sensor mounting beam in the experimental bay. Load-balancing flanges, identical with those used on the sensor mounting shafts in the baseline concept, are used where the cylindrical extensions penetrate the experimental bay end bulkhead. This arrangement prevents end load on the sensor mounting beam no matter what pressure differential exists between the airlock and the experimental bay. The two aft posts, which are supported from the airlock by a pin joint, extend out through the pressure shell. Load-balancing flanges are also incorporated where these posts penetrate the pressure shell. Machined pads are provided on the outboard ends of these posts for attaching an external sensor mounting beam for those sensors too large to be accommodated in the experimental bay. An additional pad is provided on one of the posts for mounting the horizon scanner assembly. A load-balancing flange arrangement is provided on the horizon scanner shell

where it penetrates the pressure shell, so that continuous pressurized access to the horizon scanner is maintained without introducing any load in the sensor mounting beam.

The forward end of the sensor mounting beam is supported by a hinged link in the experimental bay. The pinned joint in the airlock reacts fore and aft and lateral loads on the beam during launch, and the hinged link, which features ball joint sockets, reacts load only along its centerline. This arrangement maintains the sensor mounting beam in as stress-free a condition in orbit as possible.

The forward end of the sensor mounting beam penetrates the hangar forward bulkhead. The same load-balancing flange is provided. A machined pad on the end of the beam is provided for mounting the star tracker assembly. The section of the sensor mounting beam outboard of the end bulkhead is made pressure-tight, so that access to the back face of the star trackers is maintained from within the experimental bay.

Screw jacks are positioned on the centerlines of each of four sensor beam posts in the experimental airlock. The screw jacks are synchronously actuated by a bicycle chain which engages a spur gear at the top of each one of the jacks. One of the jacks is driven by an O-ring-sealed crank which extends into the hangar. A threaded fitting is provided on each of the screw jacks for attaching the sensor mounting plate. Machined pads on the sensor beam posts position the sensor mounting plate when it is cranked to the outboard position.

To change sensors, the sensor mounting plate is cranked in until the sensors clear the circular pressure door on the airlock. This door is then closed and latched, and the seal is inflated. Provisions will be made for manually closing and latching this door, similar to those provided for the radial stowing port. The airlock can now be pressurized and the inboard, rectangular pressure door can be opened. The sensor mounting plate is then detached from the screw jack fittings and taken into the hangar for replacement of the sensors.

Access to the experimental bay is provided by a hatch close to the experimental airlock at the aft end of the bay. This concept eliminates the three disadvantages listed for the baseline concept and also provides greater working space in the experiment bay for the installation and alignment of sensors on the beam. On the other hand, the hatch provides only limited access to the experimental airlock because of its location between the support beams. Furthermore, a load-balancing flange assembly must be provided if a camera or a telescope is to be mounted on the sensor mounting beam in the airlock, and extend into the hangar. In the baseline concept, since the airlock shell is itself an integral part of the sensor mounting beam, a sealing flange on the camera or telescope could be bolted directly to a sealing flange on the airlock. In this case, the load-balancing flange is between the airlock and the flat bulkhead, rather than between the camera or telescope and the airlock, and so need not be disturbed each time the camera or telescope is replaced with another sensing element. Lastly, more space is required in the hangar experiment compartment for this installation, making operations in that area potentially more difficult.

An optimum configuration for the experimental bay has not been developed. To do so will require a greater understanding than currently exists of the details of all the sensors that may be employed. However, the two configurations which have been described demonstrate the feasibility of the experimental bay concept.

3.3.9 Experimental Bay Analysis - Baseline

From Figure 3-11:

$$\begin{aligned}
 S_b &= \frac{0.75 w b^2}{t^2 (1 + 1.61 \alpha^3)} = \frac{0.75 \times 28 \times (114.3)^2}{t^2 [1 + 1.61 (0.792)^3]} = \frac{152,000}{t^2} \\
 S_b &= S - \frac{PR \cos 45^\circ}{2 t_f} = 67,000 - \frac{28 \times 102 \times 0.707}{2 t_f} = 67,000 - \frac{1,010}{t_f} \\
 t^2 &= \frac{152,000}{67,000 - \frac{1,010}{t_f}}
 \end{aligned}
 \tag{3-28}$$

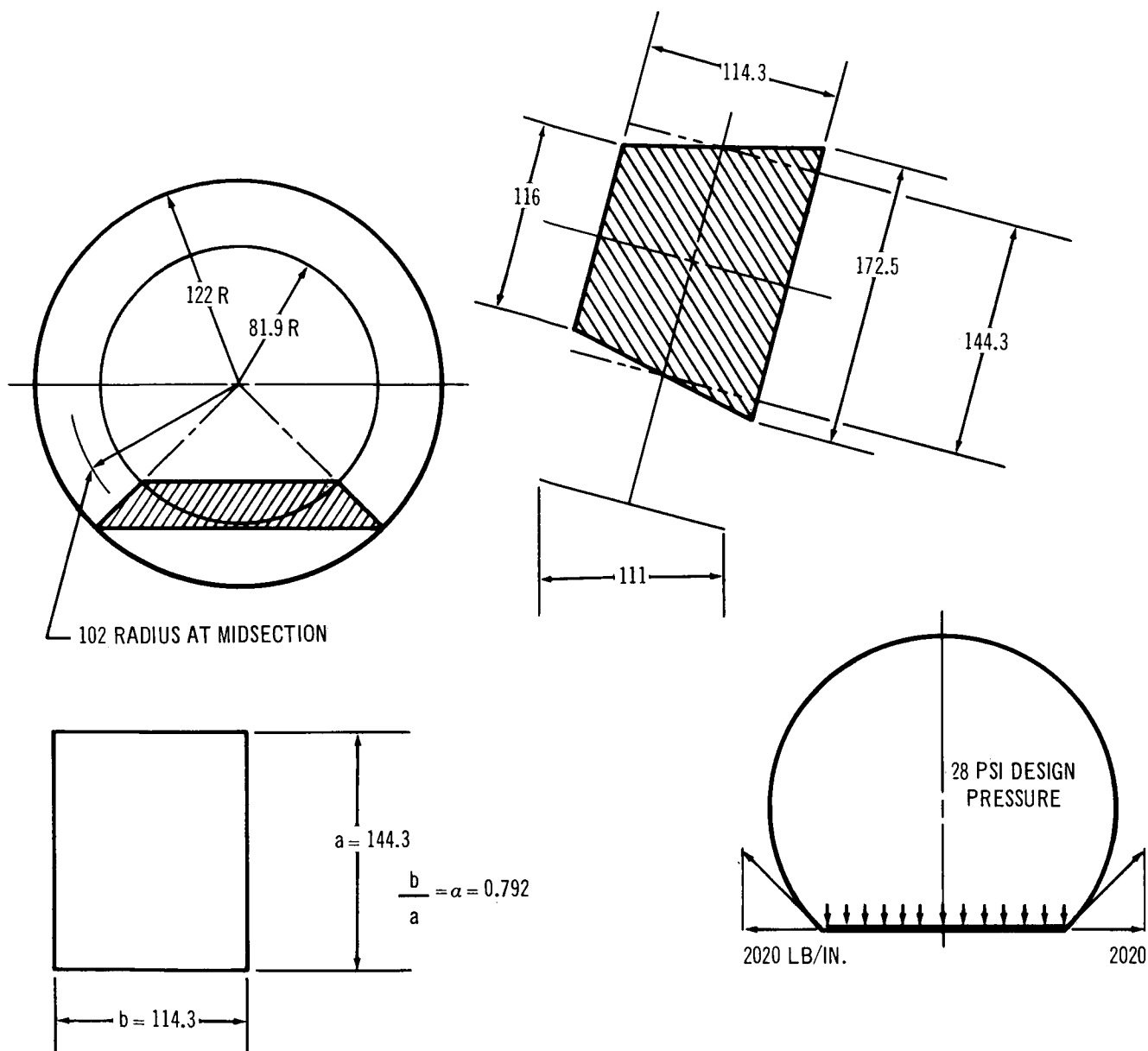


Figure 3-11. Experimental Bay Details – Baseline

Equating I/C for monocoque and sandwich

$$\frac{t^2}{6} = \frac{25,300}{67,000 - \frac{1,010}{t_f}} = h t_f$$

h = core thickness

t_f = face thickness

$$25,300 = 67,000 h t_f - 1,010 h \quad (3-29)$$

$$t_f = \frac{25,300 + 1,010 h}{67,000 h} = \frac{25.3 + 1.01 h}{67 h}$$

$$\text{sandwich wt/ft}^2 = W = \underset{\text{faces}}{28.8 t_f} + \underset{\text{core}}{\frac{3.4 h}{12}} + \underset{\text{glue}}{0.160} \quad (3-30)$$

$$W = 28.8 t_f + 0.283 h + 0.160$$

substituting for t_f

$$W = \frac{28.8 (25.3 + 1.01 h)}{67 h} + 0.283 h + 0.160$$

$$W = \frac{10.9}{h} + 0.434 + 0.283 h + 0.160$$

$$\frac{dW}{dh} = \frac{10.9}{h^2} + 0.283 = 0$$

$$\text{for minimum weight } h^2 = \frac{10.9}{0.283} = 38.5$$

$$h = 6.2 \text{ in.}$$

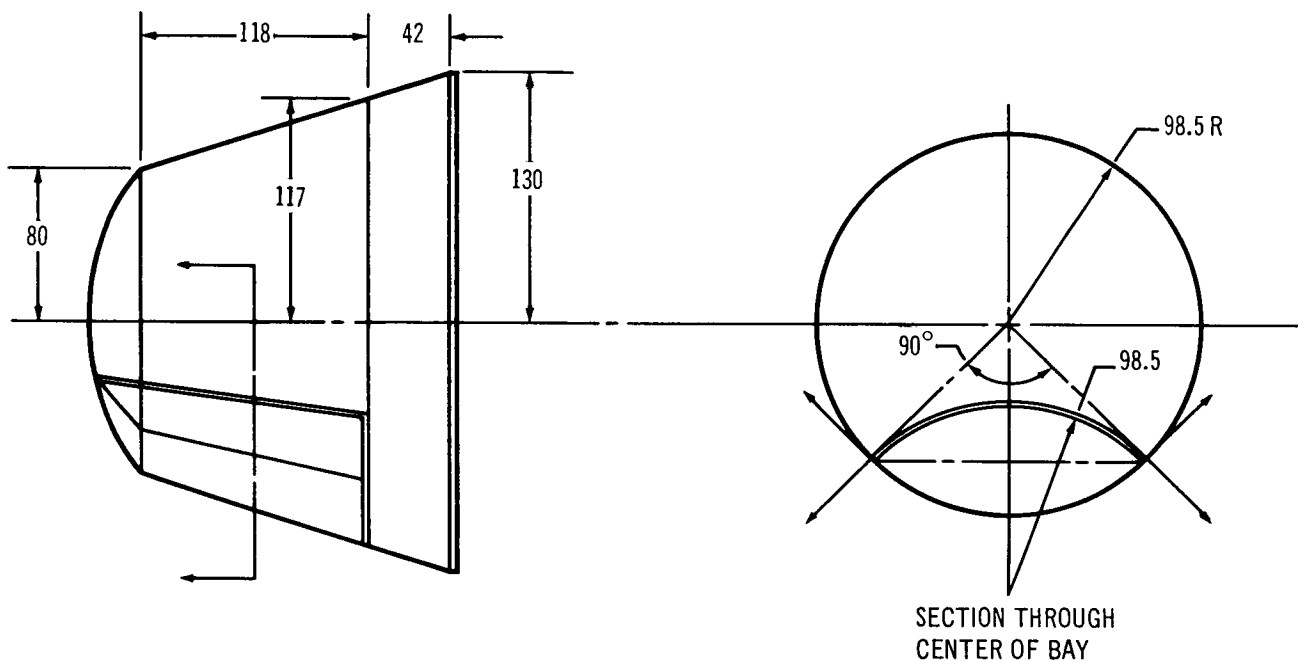
$$t_f = \frac{25.3 + 6.26}{67 (6.2)} = \frac{31.6}{415} = 0.076$$

$$W = 28.8 (0.076) + 0.283 (6.2) + 0.160 = 4.10 \text{ lb/ft}^2$$

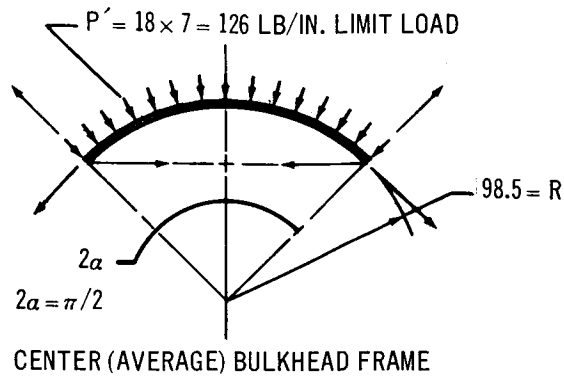
W = weight per unit area for flat pressure bulkhead of baseline experimental bay

3.3.10 Alternate Experimental Bay Analysis

Rapid sizing analysis (necessary to obtain a conservative weight approximation for the conical pressure bulkhead of the alternate experimental bay) requires the following assumptions. The tension tie rods are spaced 18 in. on center. The bulkhead frames in the planes of the tie rods carry all the pressure load (this assumption is used for the frame sizing). The panels between the bulkhead frames are analyzed as short, complete cylinders under radial pressure and axial load. The total weight of the bulkhead frames is obtained by sizing the center frame and assuming that it represents the average frame.

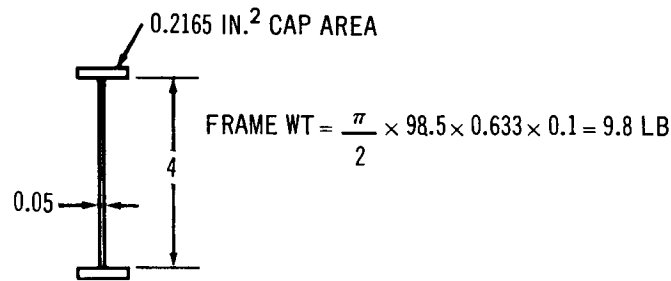


At center of bay $PR = 7 \times 98.5 = 689.5 \text{ lb/in. (limit)}$. Design tension load in center tie rod equals $2.5 \times 18 \times 689.5 \times 1.414 = 43,900 \text{ lb}$. Using 160,000 H. T. titanium $A_c = 274 \text{ in.}^2 = \text{average cross-section}$. Total tie rod weight (6 rods) = $0.274 \times 98.5 \times 1.414 \times 6 \times 0.16 = 36.6 \text{ lb}$. Use 40 lb for tie rod weight to allow for pins and end fittings.



$$P' = \frac{EI}{R^3} \left(\frac{\pi^2}{\alpha^2} - 1 \right) = 15 \frac{EI}{R^3}$$

$$I = \frac{R^3 P'}{15E} = \frac{(98.5)^3 \times 126 \times 2.5}{15 \times 10^7} = 2.0 \text{ IN.}^4$$



$$\text{TOTAL WT OF BULKHEAD FRAMES} = 6 \times 9.8 = \underline{58.8 \text{ LB}}$$

Panel section between bulkhead frames is analyzed as a short cylinder under radial pressure and axial load. The critical radial pressure and the critical axial load are calculated separately and are then combined by the method of stress ratios.

Radial pressure

$$P' = 0.807 \frac{E t^2}{1 r} \sqrt[4]{\frac{1}{(1 - u^2)^3}} \frac{t^2}{r^2} \text{ (Reference 5, page 318)}$$

$$P' = \frac{0.807 E t^{5/2}}{1 r^{3/2} (0.91)^{3/4}} = \frac{0.864 E t^{5/2}}{1 r^{3/2}} \quad (3-32)$$

$$\sigma_{cr} = \frac{P' r}{t} = \frac{0.864 E t^{3/2}}{1 r^{1/2}}$$

assume 0.030 faces for the sandwich bulkhead

$$\sigma_{cr} = \frac{p r}{2 t_f} = \frac{28 \times 117}{0.06} = 54,600 \text{ psi}$$

$$t^{3/2} = \frac{\sigma_{cr} 1 r^{1/2}}{0.864 E} = \frac{54,600 \times 18 \times 117^{1/2}}{0.864 \times 10^7} = 1.245 \quad (3-33)$$

$$t = (1.245)^{2/3} = 1.157$$

equating radius of gyration squared for monocoque and sandwich

$$\frac{t^2}{12} = \frac{h^2}{4}$$

$$h = \frac{t}{\sqrt{3}} = \frac{1.245}{1.732} = 0.719$$

(3-34)

to account for combined axial load, use a 0.750 core and 0.04 faces

$$t = \sqrt{3} h = 1.732 (0.750) = 1.3$$

$$\sigma_{cr} = \frac{0.864 E t^{3/2}}{1 r^{1/2}} = \frac{0.864 \times 10^7 \times (1.3)^{3/2}}{18 \times 117^{1/2}} = 65,900 \text{ psi}$$

$$P'_{\text{allowable}} = \frac{2 t_f \sigma_{cr}}{r} = \frac{0.08 (62,000)}{117} = 42.4 \text{ psi critical radial pressure} \quad (3-35)$$

(the compressive yield is assumed to be the critical buckling stress rather than the calculated 65,900)

Allowable axial load calculation for a sandwich cylinder with 0.030-in. faces and a 0.750-in.-honeycomb core is now made.

$$t = \sqrt{3} h = 1.732 (0.75) = 1.3$$

(this assumes that sandwich and monocoque cylinders with the same radius of gyration will buckle at the same stress, the lengths and diameters being equal)

$$\frac{l^2}{rt} = \frac{18^2}{117 (1.3)} = 2.13 \text{ transition range}$$

$$\sigma_{cr} = K_c \left(\frac{\pi^2}{12(1 - u^2)} \right) \left(E_s E_t \right)^{1/2} \left(\frac{t}{l} \right)^2$$

$$Z_1 = \frac{l^2(1 - u^2)^{1/2}}{rt} = \frac{18^2(0.91)^{1/2}}{117(1.3)} = 2.03$$

$$\frac{r}{t} = \frac{117}{1.3} = 90$$

from Reference 10, Figure 6

$$K_c = 4.0$$

$$\sigma_{cr} = \frac{K_c \pi^2 E}{12(1 - u^2)} \left(\frac{t}{l} \right)^2 = \frac{4 \times 3.14^2 \times 10^7}{12(0.91)} \left(\frac{1.3}{18} \right)^2 = 188,000 \text{ psi} \quad (3-36)$$

since this is over the compressive yield, the compressive yield is used as the bulking stress.

$$\sigma_{cr} = 62,000 \quad N'_c = \text{allowable axial load}$$

$$N'_c = 2 t_f \sigma_{cr} = 0.08 (62,000) = 4,960 \text{ lb/in.}$$

$$N_c = \frac{pr}{2} = \frac{28 \times 117}{2} = 1,640 \text{ lb/in.}$$

$$\frac{N_c}{N'_c} + \frac{p}{p'} = \frac{1,640}{4,960} + \frac{28}{42.4} = 0.33 + 0.66 = 0.99$$

Because the panels only subtend a 90° arc, this crude preliminary analysis must be considered conservative.

$$MS = \frac{1}{0.99} - 1 = 0.01 \quad (3-37)$$

An approximate weight comparison between the baseline and alternate experimental bay pressure bulkheads is made below.

baseline 4.10 lb/ft² (flat bulkhead)

$$\text{area} = \frac{144.3 \times 114.3}{144} = 115 \text{ ft}^2$$

flat bulkhead weight = 4.10 x 114 = 471 lb

conical bulkhead - 0.040 faces 0.750 core 3.1 lb/ft³

$$\text{wt/ft}^2 = 14.4 \times 0.08 + \frac{3.1 \times 0.750}{12} + 0.160 = 1.50 \text{ lb/ft}^2 \quad (3-38)$$

$$\text{conical bulkhead area} = \frac{\pi l (d_1 + d_2)}{8}$$

$$\text{area} = \frac{3.14 \times 124(234 + 160)}{144 \times 8} = 133 \text{ ft}^2$$

conical bulkhead weight = 1.5 x 133 = 199 lb

bulkhead	199
frames	59
tie rods	<u>40</u>
Total	298 lb

471 - 298 = 173 lb saved with conical bulkhead

This weight comparison does not account for the discontinuities in the flat bulkhead or the weight of the attaching joint for either bulkhead. The joint weight is comparable for the two concepts.

3.3.11 Internal Equipment Support Structure

The internal equipment support structure has been described in considerable detail in Volume XII of the Phase IIa Report. The design changes which have been described do not make necessary any reconfiguration of the laboratory interiors, except as already described for the experimental hangar. However, changing to the flat, beam-stiffened compartmenting bulkhead does permit

some simplification and lightening of the consoles in the operational experimental area. The equipment consoles, partitions, and transverse floor and ceiling bulkheads have been integrated to minimize the weight of the internal equipment support structure. The front and rear faces of the consoles are aligned with each other to provide shear paths. Each console has been designed so that the operating panels, equipment doors, and access covers support the shear loads applied during boost, with the lateral bulkheads serving as cap material. Since the flat, beam-stiffened compartmenting bulkhead can support all the equipment during boost, an opportunity exists for simplification of the design of the consoles. The loads which the equipment can impose, during boost, on the compartmenting bulkhead are small compared to the pressure load for which the bulkhead has been designed. No attempt was made during this study phase to redesign the equipment consoles, because of the limited time available. However, the opportunity now exists to reconfigure the operations/experimental area, because of the incorporation of the flat compartmenting bulkhead.

3.4 THERMAL BALANCE

The thermal analysis for the MORL baseline structural subsystem is described in Volume XII of the Phase IIa Report. Since the alternate structural and baseline structural subsystems are very similar from a thermal standpoint, the analysis is equally applicable. In each structural concept, the aluminized Mylar between the outer shell and the pressure shell maintains the pressure shell essentially at the temperature of the laboratory atmosphere. In each concept, thermal cycling and cyclic thermal stresses are virtually eliminated in the pressure shell. In the baseline concept, the pressure shell is suspended within the load-carrying outer shell by a fiber glass cylinder which minimizes heat transfer between the pressure shell and outer shell. In the alternate concept, the load-carrying pressure shell is joined to the aft interstage, and to the nose cone, by short, fiber glass sandwich cylinders, which serve the same purpose.

The design and performance of the thermal radiators, which are integral with the outer shell, are also similar for the two concepts. In the baseline

concept, the power system's radiator tubing runs in fore and aft loops on the inside face of the aft interstage portion of the outer shell sandwich. The EC/LS radiator tubing runs in single circumferential loops between the inlet and return manifolds which are side by side in the cylindrical portion of the outer shell, and on opposite sides of the experimental bay in the conical portion. In the alternate concept, the radiator tubing for both the EC/LS and the power systems radiator runs in single circumferential loops. The efficiency of the radiator is slightly improved in the alternate concept because of the improved conduction between the radiator tubing and the radiating surface. This improvement is brought about by the elimination of one spot-welded interface and the more direct heat transfer path. However, in both concepts the available radiating surface area appears adequate to accommodate the maximum anticipated heat loads.

Since the entire surface area of the laboratory is now utilized for the radiation of heat (except for the area of the experimental bay), an appreciable increase in heat load will require either an improved radiator efficiency, an increased inlet temperature, or an enlargement of the radiating area. In a strictly zero-g mode with no backup spin capability, the 368 sq ft of the meteoroid shield that is exposed when the S-IVB is jettisoned could be used as additional radiator area, with a large increase in the margin between the maximum heat rejection capability and the maximum anticipated heat load.

In both the baseline and alternate structural concepts, manifolds will be used around access hatches and any other required discontinuities in the outer shell, to minimize the surface area lost to the radiator.

3.5 METEOROID PROTECTION

A meteoroid hazard analysis was completed for the baseline structural concept in Volume XII of the Phase IIa Report, using the penetrating micrometeoroid flux that was specified by NASA. This analysis showed that the baseline structural system, which provides a multiple bumper meteoroid shield, gives a very low probability of micrometeoroid puncture to the pressure shell. The penetrating micrometeoroid flux was specified as

$$P = 4 \times 10^{-10} t^{-3} \quad (3-39)$$

where

P = penetration flux in penetrations per square foot per day
t = effective thickness in inches

The effective thickness used in this equation is the armor-plate thickness of aluminum that will resist the penetration of an impacting micrometeoroid. The effective thickness of structures other than armor plate can be obtained by dividing the total thickness of the structural components by an efficiency factor which was also specified by NASA. The typical structural arrangements and their corresponding efficiency factors are shown below.

<u>Structure</u>	<u>Efficiency Factor</u>
Armor plate	1.0
Two-spaced sheets	0.29
Three-spaced sheets	0.27
Two sheets, with the space between filled with foam	0.25

It has been assumed that a 1-in. separation between the spaced sheets is required to give the specified efficiency factors. It has also been assumed that the minimum required foam density is 1.5 lb/ft³.

With the Phase IIa baseline structural concept, an efficiency factor of 0.27 was used for the conical- and aft-dome portions of the pressure shell. An efficiency factor of 0.29 was used for the cylindrical portion of the pressure shell because of the small separation (1/2 in.) between it and the inner face of the load-carrying outer shell.

The efficiency factors were not specified as a function of the separation between the spaced sheets. But, if it is assumed that the efficiency factor does not improve with increased separation beyond that specified for 1 in., the alternate structural concept can be compared with the Phase IIa baseline, using the factors specified by NASA Langley.

The monocoque sheet thickness that is equivalent in weight to the corrugated core sandwich, load-carrying outer shell of the baseline concept, is 0.076 in.

The pressure shell thickness is 0.082 in. in the cylindrical portion. The equivalent armor plate thickness is

$$\frac{0.158}{0.29} = 0.545 \text{ in.}$$

in the cylindrical section of the Phase IIa baseline concept. In the alternate concept, the inner face of the outer shell sandwich is removed. This 0.020-in. face is replaced by an integral waffle pattern filled with foam. The waffle pattern on the pressure shell will support the flight loads, and the foam improves the shielding efficiency. The combined weight of the waffle pattern and foam is equivalent to that of the inner face that was removed. The aluminum sheet thickness that is equivalent in weight to 1 in. of 1.5 lb/ft³ foam, is

$$\frac{1.5}{12(144)(0.1)} = 0.00868 \text{ in.}$$

The remaining 0.01132 in. is adequate for the required waffle pattern. The armor plate equivalent of the alternate concept is then

$$\frac{0.056 + 0.082}{0.25} = \frac{0.138}{0.25} = 0.552 \text{ in.}$$

This is comparable to the 0.545 in. equivalent armor plate thickness that was calculated for the Phase IIa baseline structural system.

When the Phase IIa baseline structural system was modified to incorporate O-ring sealed, bolted joints at both ends of the pressure shell cylinder, the separation between the inner face of the load-carrying outer shell and the pressure shell was increased to 1.1 in. to provide room for the integral bolting flanges. With this increased separation, an efficiency factor of 0.27 can be used. So the equivalent armor plate thickness of the Phase IIb baseline structural system is

$$\frac{0.158}{0.27} = 0.585 \text{ in.}$$

in the pressure shell cylinder.

Another method of evaluating the micrometeoroid hazard for MORL is specified in the Air Force sponsored Report NO. TOR-269(4560-40)-2

titled "Aerospace Meteoroid Environment and Penetration Criterion" by V. C. Frost; as a cross check the following calculations were made.

The efficiency factors for double plate wall construction are noted below:

With no foam between the plates

<u>Separation (in.)</u>	<u>Efficiency Factor</u>
1. 0	0. 50
1. 5	0. 35
2. 0	0. 27

With foam between the plates

<u>Separation (in.)</u>	<u>Efficiency Factor</u>
1. 0	0. 33
1. 5	0. 25
2. 0	0. 20

If in the alternate structural concept, a 2-in. separation is maintained between the outer shell fairing and the load-carrying pressure shell, but only 1 in. of this separation is foam filled, it would seem reasonable to use an efficiency factor half way between the listed 0.27 and 0.20, or 0.235. Based on this criterion, the equivalent armor plate thickness for the cylindrical portion of the pressure shell is

$$\frac{0.138}{0.235} = 0.587 \text{ in.}$$

The referenced report cannot be used directly to evaluate the baseline structural concept because the efficiency factors are only listed for double plate wall construction.

It can be used, however, if the baseline structure is evaluated in two steps: (1) obtaining an armor plate equivalent thickness for the outer shell, (2) using this thickness with the pressure shell thickness to obtain an equivalent armor plate thickness for the combination. The armor plate equivalent of the outer shell is

$$\frac{0.076}{0.50} = 0.152 \text{ in.}$$

The armor plate equivalent of the combination is

$$\frac{0.152 + 0.080}{0.50} = 0.464 \text{ in.}$$

This calculation is considerably more optimistic than the referenced report intended because it does not take into account the relative thickness of the outer plate. The thickness of the outer plate should be from 0.15 to 0.25 of the total thickness to be compatible with the efficiency factors specified in the report.

According to the penetration criterion specified in the referenced report (which is based on work done at NASA-Ames, NASA TND-94 (1959), by J. L. Summers), the shielding efficiency of the alternate structural concept is better than that which can be calculated for the baseline concept. This criterion is by no means universally accepted, however, and more data on the mechanics of particle impact at micrometeoroid velocities is required to settle the controversy. This is the reason that the newer structural concept is documented as an alternate only. Both the baseline and the alternate structural concepts appear to have acceptably low puncture probabilities. The probability of encountering no punctures of the pressure shell in 1 year in orbit was shown to be 0.99486 in Table 6-2 of Volume XII of the Phase IIa Final Report. This is slightly improved to 0.99498 by changing the efficiency factor for the cylindrical part of the pressure shell from 0.29 to 0.27.

The internal equipment has been arranged to permit complete in-flight inspection and puncture repair, and the pressure shell has been divided into two pressure-tight compartments, each with its own life support system. The hazard that the micrometeoroid environment presents to the MORL mission has been minimized so that either structural system, baseline or alternate, must be judged adequate for the micrometeoroid shielding requirement.

3.6 STUDY CONCLUSIONS AND RECOMMENDATIONS

Two structural concepts, baseline and alternate, have been described for the MORL structural subsystem. The baseline system, in which the flight loads are carried in a corrugated-core-sandwich outer shell, has been shown to be equivalent in weight to an alternate system. In the alternate system, the flight loads are carried in the waffle-stiffened pressure shell, with the outer shell serving as an aerodynamic fairing during boost and a micro-meteoroid bumper and radiator in orbit. An interesting variation to the alternate system would be to have the outer shell carry the flight loads in the conical portion, and serve as a fairing in the cylindrical portion. This is a compromise between the baseline and alternate concepts, which would permit the separation between the outer shell and the pressure shell to be varied at will, as with the alternate concept, yet would maintain the conical portion of the load-carrying outer shell unchanged. The optimization of the structural subsystem must be a continuing process, with design improvements being incorporated as new data on the environment and on the mission are obtained. The subsystem which efficiently meets all the requirements, as they are currently specified, and yet maintains sufficient flexibility to efficiently accommodate new or changed requirements that future knowledge may dictate, must be judged best. For this reason it is recommended that the design and performance evaluation of alternate structural configurations be a specified part of any future study of the MORL.

Section 4

ELECTRICAL POWER SYSTEM

In addition to providing power to all MORL subsystems, the MORL power system must furnish power for the on-board experiments, and must maintain the Apollo logistic spacecraft in a standby condition. The average electrical loads for the operating MORL subsystems are divided between ac and dc in the following proportions: (1) 2.4 kW of square wave ac, (2) 0.3 kW of sine wave ac, (3) 2.6 kW of 56 ± 28 Vdc. Recomputing these loads in terms of 1,067 cycle ac, at which power is generated and allowing 3 kW for the expanded experimental program as well as 1.3 kW for contingencies, leads to a total power requirement of 11 kW at the alternator terminals. Both power sources considered in this document are designed to fulfill the above power requirements adequately.

4.1 SUMMARY

A summary comparison of the characteristics of the solar cell/battery and the Pu-238 Isotope Brayton Cycle (PBC) system is shown in Table 4-1. The PBC system exhibits a clear advantage with respect to the performance and operational aspects of the mission by eliminating the large solar cell panels which constitute an impediment to extravehicular as well as experimental activities. While the nuclear safety aspects of the PBC system add an element of risk to program development, it is anticipated that timely launch approval will be obtained for a major program with the national significance attached to an orbiting research laboratory.

The difference in launch weight between the PBC and the solar system is not considered significant at this time. On the basis of preliminary cost estimates, the solar cell system shows an advantage over the PBC system.

Table 4-1
POWER SOURCE COMPARISON SUMMARY
(11 kW system*)

Characteristics	Solar Cell Battery	PU-238 Brayton Cycle
Total launch weight penalty (lb)	4, 781	4, 967
Resupply weight (lb/year)	1, 345	1, 308
Development cost (5-year mission)	\$77 x 10 ⁶	\$104 x 10 ⁶
Development risk	Slip rings (Rot. MORL) (H) Deploy and gimbal mech (L) RCS impingement (L)	Pu availability (NASA-AEC problem) (M) Gas bearing (L) Radiator coating (L) Fuel block life (L)
H = high M = medium L = low		
Reliability/maint ease	Solar panel - exc/poor Gimbal mech - good/good	PCS - fair/exc Radiator - exc/poor
Growth potential limits	Stow and deploy Launch weight Cost	Pu availability Radiator area
Miscellaneous problems	Operational hazard Operational interference Experimental interference	Nuclear Safety

*Both systems rated equivalent to 11 kW_e at alternator of Pu-238 system.

The resupply penalties are small for both systems, and are not significant during the 1971 to 1975 time period; however, during the subsequent years of higher atmospheric density, an increase in solar cell/battery resupply weight as well as a small increase in launch weight, would occur.

The launch weights assumed in Table 4-1 for the Isotope Brayton Cycle system are predicted on the use of the purified fuel form (Reference 11), and the use of a helium-xenon mixture as the Brayton cycle working fluid. The launch weights assumed for the solar cell/battery system are an extrapolation of the baseline system, and have assumed the use of the following technological advances: (1) larger area solar cells, (2) thinner solar cells, (3) integral cover slides, (4) wrap-around cell contacts, (5) improved substrate panel structure, and (6) silver-cadmium batteries. These systems are felt to be both achievable and compatible with the MORL system.

The biggest unresolved problem with the PBC system is the availability of adequate quantities of Pu-238 for MORL and its contemporary space programs. Information available to Douglas indicates that the quantities of Pu-238 resulting as a by-product of weapons production are adequate to meet an early (1971) launch date assuming MORL is given priority on all Pu-238 available from this source. The lead time for additional quantities (produced as a prime product) is estimated to be 5 to 6 years. NASA and the AEC are currently formulating plans to alleviate the isotope availability problem, and it is therefore assumed that adequate supplies will be provided for recognized national programs such as MORL.

The ultimate use potential of the PBC system, which is unaffected by orbital parameters and long lunar nights, might be expected to be broader and provide greater flexibility and growth potential to support alternate missions.

In view of these factors, it was recommended to NASA that a PBC system of 11 kW nominal capacity be used as the baseline power system for the MORL, replacing the solar cell/battery system. This PBC system has allowed supplemental changes to other MORL subsystems, some of which

are potentially very beneficial to the MORL mission; these are discussed as appropriate in conjunction with the affected subsystems.

4.2 LOAD ANALYSIS

A revision of the electrical load analysis was accomplished during the MORL Phase IIb study. The purpose of this analysis was to include all of the subsystem changes and to reflect the power available from the PBC system. Table 4-2 is a summary of the load analysis. A detailed breakdown of the electrical power requirement for each item of equipment is shown in Appendix D. The loads lead to the requirement of 11 kW of high-frequency ac at the alternator terminals of the PBC system.

The connected loads shown in Table 4-2 represent the total load requirement of each system if it is assumed that all equipment items are operating simultaneously. These values are, therefore, indicative of the size of the distribution branch circuits and buses. The average power is an integrated average of the load requirements of each system, taking into account an approximate duty cycle associated with each item of equipment over a 24-hour period.

Table 4-3 accounts for all of the power from the alternator for the PBC system. The values shown in this table are reflected values to the alternator buses and, therefore, include conversion and distribution efficiencies. The total power requirement is 9.1 kW, excluding the reserve for contingencies and parasitic losses. The systems, thus, provide approximately 1.3 kW for subsystem growth and contingencies.

As shown in Table 4-3, approximately 3 kW of alternator bus power (1,067 cps) are available for experiments. This corresponds to approximately 2.5 kW of regulated bus power. In the MORL Phase IIa study, an average of 2 kW were allocated for the experimental requirements.

Table 4-2

HOUSEKEEPING LOAD ANALYSIS SUMMARY--NORMAL OPERATION*

System	Square Wave ac**		Sine Wave ac**		56 (± 28) Vdc**	
	Connected	Average	Connected	Average	Connected	Average
Guidance and control	99	77	89	68	421	236
Communications and data acquisition	100	100	115	115	1,435	572
Environmental control and life support	1,593	1,225			1,658	1,510
Display, control and instrumentation					760	311
Logistics vehicle and maintenance	780	740	2,368	87		
Lighting and miscellaneous	1,063	268				
Propulsion					2,688	1
Totals	3,635	2,410	2,572	270	6,962	2,630

*Does not include experimental loads.

**In watts

Table 4-3
POWER SOURCE REQUIREMENTS

Power Requirement	Magnitude (W)
Reflected square wave ac*	2,692
Reflected sine wave ac*	308
Reflected 56 ±28 Vdc*	3,190
Subtotal	6,190
Experiments**	2,953
Subtotal	9,143
Contingency (15%)	1,371
Parasitic losses	486
Total	11,000

*Reflected to alternator bus power
**Experimental power at alternator bus

The PBC and the solar cell/battery power systems are designed to deliver power to the respective buses in accordance with the data in Tables 4-2 and 4-3.

4.3 ISOTOPE BRAYTON CYCLE SYSTEM

This section describes the PBC system and specifies its characteristics, design parameters, launch weight, installation in the MORL vehicle, and overall performance. A more detailed description of the system is presented in Reference 11 through 16.

4.3.1 System Description

The MORL PBC electrical power system is shown in simplified schematic form in Figure 4-1. The principal elements and subsystems are given in Table 4-4, along with their function.

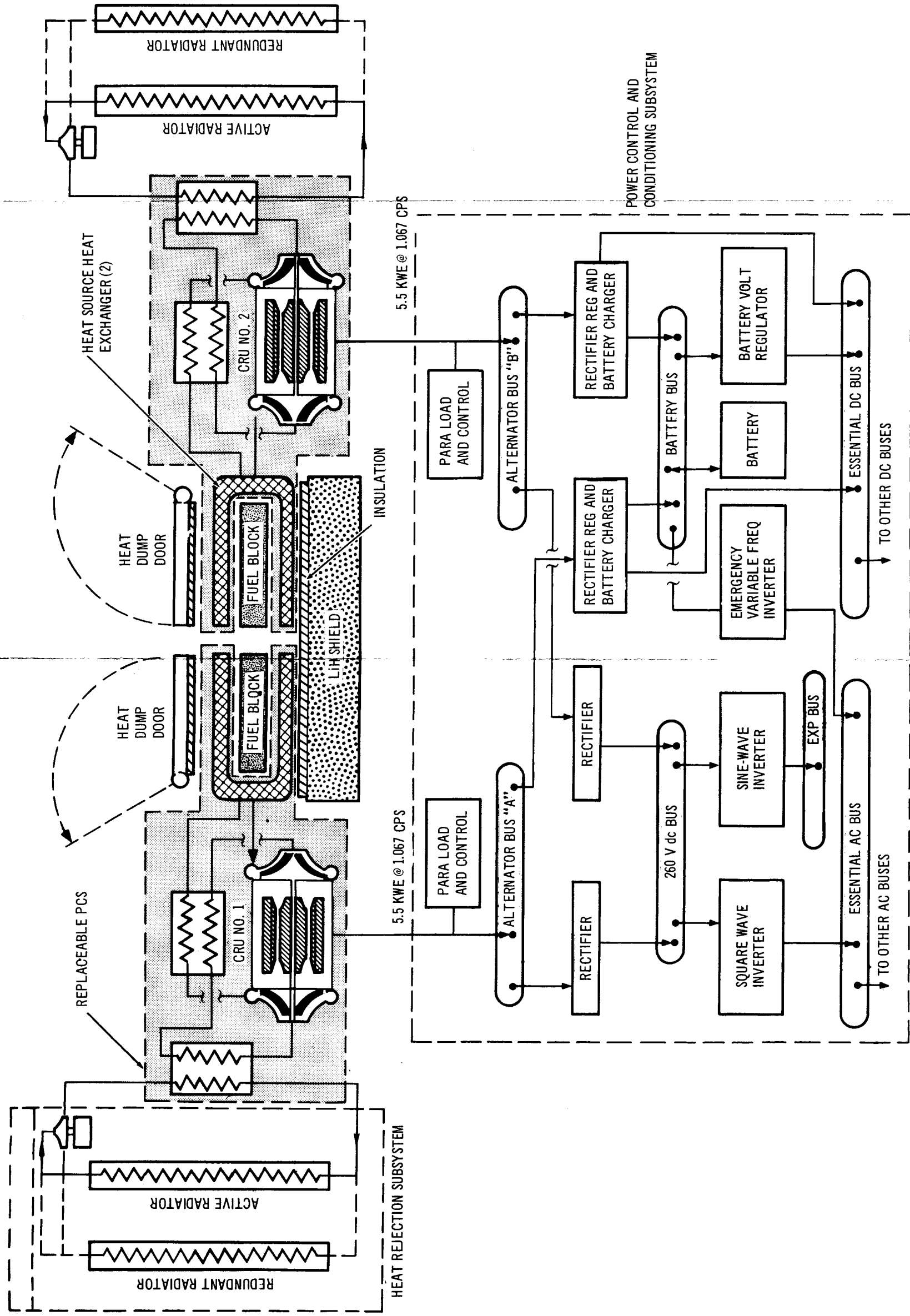


Figure 4-1. Pu-238 Brayton Cycle System Schematic

Table 4-4
PBC SUBSYSTEM FUNCTIONS

System Element	Function
Pu-238 fuel block	Provides heat (energy) source for the system
Shield	Attenuates fuel block neutron radiation to the crew compartment
Brayton cycle power conversion system (PCS)	Converts fuel block thermal power to electrical power
Power conditioning and control subsystems	Converts alternator 1,067 cps ac power to: (1) ± 28 Vdc, (2) 400 cps square wave, (3) 400 cps sine wave, and (4) provides an Ag-Cd battery to accommodate peak loads
Heat-rejection subsystem	Rejects system waste heat through a liquid loop space radiator; also cools the system during launch and prelaunch when the radiator is not effective
Heat-dump door	Provides for emergency fuel block cooling by direct heat dump to space

The PBC system installed within the MORL interstage area is designed to produce a total of 11 kW at the alternator terminals. The total fuel block heat load is shared by two identical power conversion systems. In each system, the Pu-238 isotope is contained within fuel capsules, which are inserted into a fuel block assembly. Heat is transferred by radiation to the surrounding U-shaped heat exchanger of the associated power conversion system. The heart of the closed-loop recuperated Brayton cycle power conversion system is a 64,000 rpm turbo-alternator-compressor unit, which is supported on gas bearings using the power conversion system working fluid, helium-xenon.

Waste heat is rejected to the liquid radiator loop through a helium-xenon to liquid heat exchanger. The radiator is an integral part of the MORL vehicle interstage structure. Each PCS is serviced by two identical heat-rejection loops, one of which is normally on standby. The two operating heat-rejection loops share a total effective radiator surface of 920 sq ft. FC-75 fluid is used as the heat-rejection loop coolant.

Should the normal heat-removal capability of either PCS be lost, the heat source is maintained within safe temperature limits by opening its associated heat-dump door, which permits direct thermal radiation to space. A lithium hydride (LiH) biological shield shadows the occupied compartments of the vehicle from the neutron emission of the isotope source and maintains radiation exposure of personnel within acceptable limits.

The two power conversion systems, under normal conditions, operate at constant load to produce three-phase, 1,067 cps, 112/194 Vac power at the alternator terminals. A parasitic load is provided for each system to dissipate power in excess of the load demands, according to a programmed frequency control. Power conditioning to satisfy load requirements is accomplished by initial rectification to 260 Vdc for inversion and ultimate use by the ac loads, and by rectification to 56 ± 28 Vdc power for ultimate use by dc loads.

Paralleling of the ac portion of the system is accomplished through the 260 Vdc bus. All ac loads are supplied through a sine wave inverter for high-quality 400-cps power on the experimental bus, and through a square-wave inverter, for unfiltered, 400-cps power on the other ac bus. The dc loads are supplied at 28 V by a three-wire circuit from the 56-V essential dc bus. A battery is provided to meet peak load and emergency power demands on both the essential dc and ac buses. Battery charging is accomplished from either or both power conversion system sources through the battery bus. An emergency inverter, supplied from the battery, is provided to supply emergency power to essential ac loads. This inverter is designed to supply variable-frequency, variable-voltage power to start either power conversion system.

Besides supplying electrical loads, the power system serves as a direct source of thermal power to satisfy the requirements of the EC/LS system. Heat transfer for this purpose is provided from PBC system waste heat.

4.3.2 PBC System Design Parameters

The basic design parameters for individual components, which evolved from cycles optimization, are shown in Table 4-5.

Each of the two fuel blocks is designed to produce a thermal power output of 20.35 kWt at the end of a 5-year mission, which corresponds to an initial installed capacity of 21.15 kWt when isotope decay is considered. The fuel block surface operates at a maximum temperature of 1,800°F; radiative heat transfer across an effective heat transfer surface area of 9.5 sq ft (each fuel block) raises the helium-xenon gas temperature from 1,203 to 1,640°F in its passage through the heat-source heat exchanger. The combined rotating unit (CRU) design is based on a turbine of 87.3% and a compressor efficiency of 80%. Operation of the CRU at 64,000 rpm results in an optimum pressure of 17.7 psia at the compressor inlet. Gas expansion through the turbine expends about 88% of the total heat developed by the compressor, with the remainder allotted to pressure drop through heat exchanger components and ducts.

The gas flow from the recuperator enters the heat sink heat exchanger at 347°F, where provisions are made for removing up to 2.42 kWt by the EC/LS coolant; the remainder of the waste heat load is transferred to the heat rejection system.

After passage through the compressor, the gas flow is regeneratively heated from 265° to 1,203°F in the recuperator. The high recuperator effectiveness (0.92), combined with optimized cycle operating conditions, results in a cycle efficiency of 27%.

The reference PCS design parameters are based on operation with no heat extraction for the EC/LS system. The total waste heat rejected by the radiator is 27.4 kWt and the resulting overall PCS cycle efficiency is 27%. The corresponding total output power at the alternator terminals is 11 kWe, for end-of-mission design conditions. With the removal of a total of 1.8 kWt to satisfy EC/LS system requirements, the radiator heat load is reduced to 25.6 kWt and overall cycle efficiency increased to 27.3%. Consequently, output power is increased to 11.1 kWe.

Table 4-5 (page 1 of 3)
PLUTONIUM BRAYTON CYCLE SYSTEM
DESIGN PARAMETERS

Parameter	Requirement
Output power (total, two PCS units at alternator terminals) (kWe)	11
Overall system efficiency (cond power at load bus ÷ 40.7 kWt)	21.6%
Heat source	
Fuel block thermal power, both fuel blocks (kWt)	
End of mission	40.7
Beginning of mission	42.3
Total heat loss (fuel blocks and PCS) (kWt)	2.3
Fuel block surface temperature, operating maximum (°F)	1,800
Fuel block effective heat transfer surface area (sq ft) each block, both sides	9.5
Fuel block--heat exchanger temperature differential, nominal (°F) (gas outlet end)	110
Maximum radiation dose, power source (Rem/man/90 days)	10
PCS	
Working fluid	Helium-Xenon
Gas-flow rate, lb/sec, each PCS	0.334
Turbine inlet temperature (°F)	1,640
Heat-source heat exchanger, inlet temperature (°F)	1,203
Compressor inlet temperature (°F)	65
Shaft speed (rpm)	64,000
Recuperator effectiveness	0.92
Recuperator pressure loss ($\Delta P/P$)	0.04
Heat-source heat exchanger pressure loss ($\Delta P/P$)	0.04
Heat-sink heat exchanger pressure loss ($\Delta P/P$)	0.02
Total system pressure loss (r_t/r_c)	0.88
Compressor inlet pressure (psia)	17.7
Compressor pressure ratio	1.95
Compressor efficiency	0.80

Table 4-5 (page 2 of 3)

Parameter	Requirement
Turbine pressure ratio	1.716
Turbine efficiency	0.873
Type of alternator	Rice
Frequency (cps)	1,067
Nominal alternator electromagnetic efficiency	0.90
Initially assumed bearing losses, each PCS (W)	500
Alternator windage losses, each PCS (W)	190
Control circuit losses, each PCS (W)	20
Coolant pump power requirement, each PCS (W)	135
Heat losses, each heat source area (W)	958
Heat losses, each PCS package (W)	189
Overall cycle efficiency (*%)	27.0
Heat-rejection system	
Heat load, total (two PCS packages) (kWt**)	27.4
Radiator surface area (sq ft)	920
Number of loops	4
Number of redundant loops	2
Coolant fluid	FC-75
Coolant flow rate, each loop (lb/min.)	13.85
Coolant inlet temperature (°F)	266
Coolant outlet temperature (°F)	51
Absorptivity/emissivity ratio (max.)	0.25
Design orbital sink temperature (°F)	-20
Reliability (two of four radiator segments)	0.9999

*Alternator output power at terminals divided by thermal input power at end of mission, assuming no heat extraction for EC/LS system; 27.3% with 1.8 kWt total extracted for EC/LS system.

**Allowance for EC/LS thermal load (amounting to 1.8 kWt) is not deducted here.

Table 4-5 (page 3 of 3)

Parameter	Requirement
Electrical power control and conditioning efficiencies	
High frequency (1,067 cps) and parasitic circuits	95.5%
Power conditioning system (alternator bus to load bus)	83.4%
Dc conditioning subsystem	79.8%
Ac conditioning subsystem	91.3%
Sine wave subsystem	90.3%
Square wave subsystem	92.4%
Power distribution to loads	97.0%
Electrical power system (alternator to loads)	77.3%
Power quality	
General characteristics	MIL-STD-704
Electromagnetic-interference (EMI)	MIL-STD-826
Voltage	
Alternator bus	112/194 V $\pm 3\%$
Dc loads	56 V, (51 to 57 V), or ± 28 V, (25.5 to 28.5 V)
Ac, square wave loads	115/200 V $\pm 5\%$
Ac, sine wave loads	115/200 V, (108.5 to 117.5 V)
Frequency	
Alternator bus	1,067 cps $\pm 1.25\%$
Ac, square wave bus	400 cps $\pm 1\%$
Ac, sine wave bus	400 cps $\pm 1\%$

In each of the heat rejection systems, the FC-75 coolant removes waste heat from the heat sink heat exchanger and the alternator. Flow through the radiator reduces coolant temperatures (by thermal radiation), the range of which is between 266° and 51°F to heat-sink temperature of -20°F.

4.3.3 Launch Weight

A launch weight summary of the PBC system is shown in Table 4-6. These weights include a purified fuel form and a helium-xenon mixture as the Brayton cycle working fluid. All changes in the baseline configuration of the MORL vehicle occasioned by application of the PBC system are considered in the launch weight. The weight includes an extension of the interstage length by 38 in. over the Phase IIa baseline length to accommodate the power system radiator.

The vehicle integration weight penalties occur in the vehicle structural and mechanical systems primarily because of the installation of the heat dump doors, structural beef-up, internal handling aids, PCS supports (including those for spares), and radiator optical coatings. The launch weight does not include the provision of spare power conversion systems or other spare modules and components.

4.3.4 Installation

The basic physical arrangement of the PBC is shown in Figure 4-2 and its installation within the MORL interstage area is illustrated in Figure 4-3.

The MORL interstage is extended to provide the required additional radiator surface area, and to accommodate the internal installation of the power system in a relatively compact and readily accessible arrangement. Two adjacent fuel block assemblies are situated near the perimeter of the interstage, with one heat transfer surface of each fuel block facing the vehicle surface. The two identical PCS units are packaged within sealed enclosures which are mounted inboard of the fuel blocks on the opposite side of the shield assembly, with their respective U-shaped heat exchangers extending around both sides of the fuel blocks.

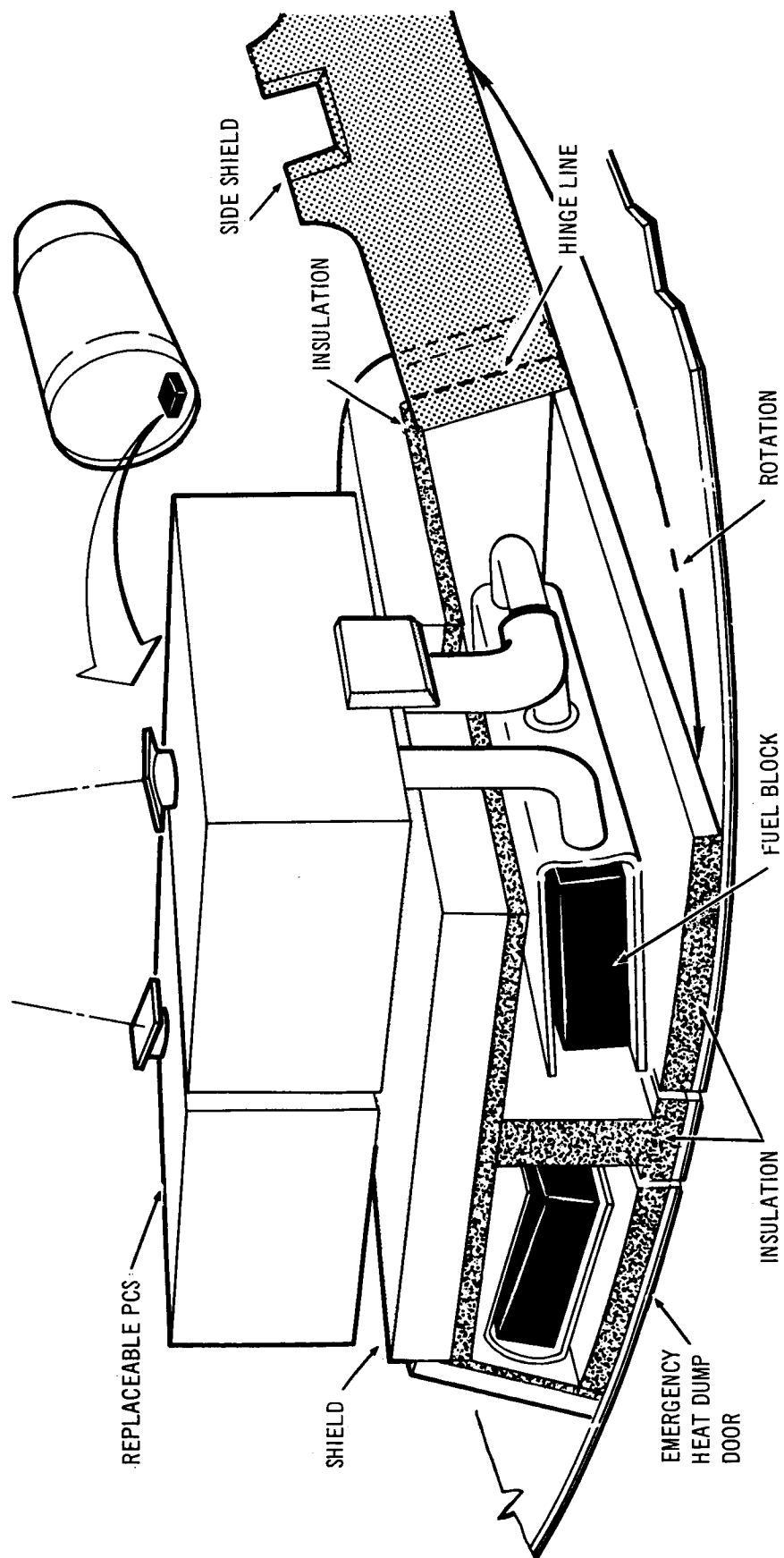


Figure 4-2. Pu-238 Brayton Cycle System

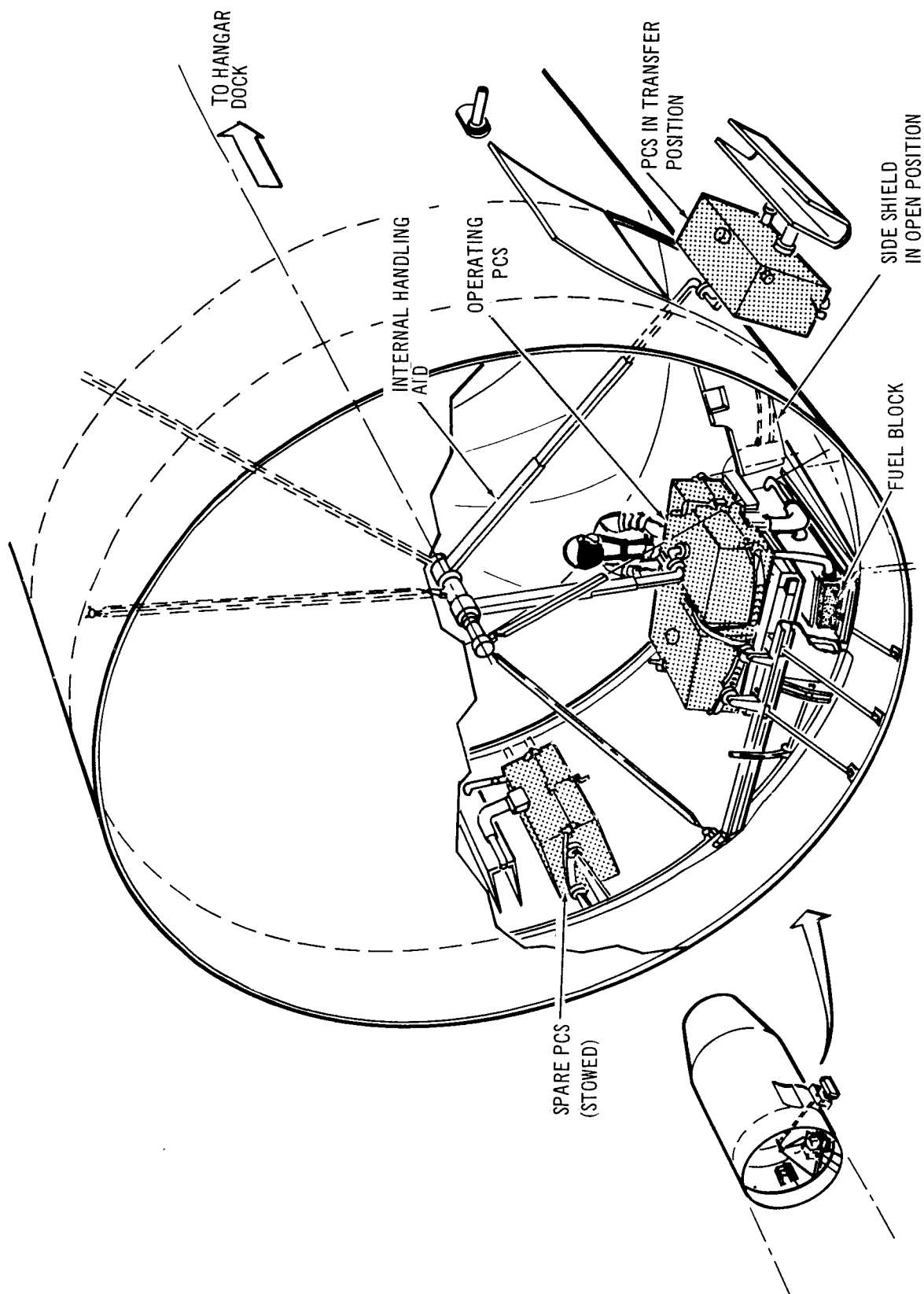


Figure 4-3. Pu 238 Brayton Cycle System Installation, MORL Interstage

Table 4-6
PBC SYSTEM WEIGHT SUMMARY

System	Weight (lb)	Weight (lb)
Fuel block and radiation shield		1,353
Power conversion unit		1,308
Brayton cycle PCS	924	
Radiator	164	
Coolant motor assembly	40	
Pump assembly	50	
Evaporator subsystem	130	
Power conditioning and energy storage		1,089
Parasitic load and control	90	
Transformers and rectifiers.	116	
Inverters	119	
Relays, circuit breakers and misc	134	
Variable frequency inverters	200	
Battery and case	384	
Battery controls	46	
Vehicle integration		1,217
Interstage extension	355	
Structural changes	665	
EC/LS system	64	
Insulation and attachments	133	
Total system weight penalty*		4,967

*Does not include 519 lb for distribution and protection equipment

The fuel blocks are initially installed in the vehicle through the heat-dump doors and are supported in a fixed position by the reinforced interstage structure. The two heat-dump doors are positioned in line with the respective fuel blocks to allow emergency heat removal from the fuel blocks

if PCS failure occurs. Each heat-dump door contains an emergency panel in case of primary mechanism failure. The inside surface of these doors, the separation panel between fuel blocks, and the inside shield surface are insulated to minimize heat loss and to maintain system external surfaces at temperatures within acceptable levels for maintenance personnel.

The shield to attenuate neutron radiation from the isotope consists of an inverted L-shaped fixed section that extends over the top and inboard surfaces of the fuel blocks in a position to completely shadow the occupied compartments of the vehicle and maintenance personnel in the interstage area. Side shields are hinged at the forward ends of the main shield and rotated forward to permit insertion or removal of the PCS units. To provide a partial-power capability if a single unit fails, the two PCS units are identical and interchangeable and each provides half the total power requirement of 11 kWe. The PCS unit is replaced in the following manner. First, the following elements are disconnected: (1) the four small radiator liquid-line quick disconnects, (2) two electrical connectors, and (3) the structural supports. Then, the PCS units are swung from the vicinity of the fuel-block assembly by using one of the two manually activated internal handling aids, pivoted at the vehicle axis.

4.3.5 PBC System Performance

The performance characteristics of the power system are discussed in the following sections.

4.3.5.1 Performance Criteria

The maximum thermal power and minimum absorptivity-to-emissivity ratio at the start of the mission results in the highest cycle efficiency and a single PCS output power level exceeding the 5.5 kWe design basis throughout the orbit. Although the maximum variation below rated power is approximately 7% for the least favorable combination of operating conditions, the integrated average output power of one PCS over the complete orbit period exceeds 5.5 kWe at the alternator terminals under all conditions. The

minimum total electrical power available at the load buses is 8.78 kWe, and the minimum total power at the load terminals is 8.52 kWe.

The turbine inlet temperature varies between the extremes of approximately 1,615° and 1,680°F as a function of orbital position and mission duration. Although the interval above the design value of 1,640°F is relatively short for the most plausible combination of operating parameters, the turbine design includes sufficient margin to accommodate this nominal increase in temperature without penalizing performance or reducing reliability.

The compressor inlet temperature varies as a function of orbital position and mission duration between the extremes of approximately 30° and 75°F. To preclude the effects of a decrease in system efficiency, the range above the design value of 65°F is relatively small.

4.3.5.2 Performance with Single PCS in Service

PBC system operation with only one power conversion system in service results in a somewhat higher unit output power than the normal operating condition in which both power conversion systems are functioning. Under these conditions, the heat dump door for the system that is out of service is opened to maintain the associated fuel block within safe temperature limitations. The temperature distribution in the fuel block and heat source heat exchanger of the operating system remains essentially the same as for normal operation with both systems functioning.

4.3.5.3 Reduced Power Rating

The reference power system design provides a margin for growth in the MORL electrical loads that is consistent with development of more sophisticated life support systems and larger crews; the system design also provides sufficient latitude for a comprehensive experimental program. A reduction in output power by reducing compressor inlet pressure for a system operating at design speed is achieved by reducing the amount of working fluid in the system. This results in a decrease in thermal power

input for a given turbine inlet temperature. A high temperature ratio is maintained, and the overall system pressure loss and heat exchanger efficiency is improved with the reduced flow, resulting in an increase in overall cycle efficiency.

Reduction of power output by lowering the turbine inlet temperature is achieved through a reduction in isotope loading in the fuel blocks, with the design compressor inlet pressure level held constant. However, this alternative will result in a considerably lower cycle efficiency.

The PBC system performance at reduced power ratings for the two above conditions will be as shown in Table 4-7.

Table 4-7
PBC SYSTEM PERFORMANCE AT REDUCED POWER RATING

Parameter	Reference Design ¹	Operation at Reduced Compressor Inlet Temperature ²	Operation at Reduced Turbine Inlet Temperature ³
Output power, alternator terminals (kWe)	11	8	8
Turbine inlet temperature (°F)	1,640	1,640	1,430
Compressor inlet pressure (psia)	17.7	9.5	17.7
Overall cycle efficiency	27	31	23
Thermal power required, end of mission (kWt)	40.7	25.8	34.8

1. Reference PCS component designs remain unchanged
2. Compressor inlet pressure is reduced at constant turbine inlet temperature
3. Turbine inlet temperature is reduced at constant compressor inlet pressure

4.3.5.4 PBC System Performance During Ground Operation

During ground operation of the power system, waste heat is transferred by the heat rejection system coolant (FC-75) to a ground source of chilled water at 40° to 45°F, which circulates at 15 lb/min. through the evaporative cooling system associated with each PCS and is discharged overboard to the ground facilities. The system is capable of operation for an indefinite time while the flow of cooling water is sustained. The selected cooling water inlet temperature maintains the corresponding PCS compressor inlet temperature approximately equal to the nominal design value of 65°F.

4.3.5.5 PBC System Performance During Launch and Ascent

Immediately prior to launch, the ground water supply is removed, and waste is removed by the evaporative cooling system using an on-board supply of chilled water throughout the launch, ascent, and orbital injection phases. For this purpose, a supply of 16.6 lb of stored water (for each PCS), precooled to 45°F by the ground cooling supply, is expended over a period of 1,400 sec until orbit is attained and normal heat rejection through the radiators is effective. The cooling water is heated to the saturation temperature corresponding to existing ambient pressure, flashed into vapor, and discharged from the evaporator to the atmosphere.

From the time the on-board supply of cooling water flow is initiated until the initial ascent phase is completed, power conversion system compressor inlet temperature increases because the cooling water boils at a higher temperature (as a function of ambient pressure) than normal heat rejection system coolant temperatures. However, after approximately 2 min., when ambient pressure has been reduced to a high vacuum, boiling occurs at a sufficiently low temperature that compressor inlet temperature and, consequently, output power are restored to rated operating values. The minimum output power level during launch and the initial period of ascent will exceed 3 kWe for each of the operating power conversion systems. The power available, therefore, is well in excess of anticipated power requirements during this period.

4.3.6 Fuel Block Recovery

Since completion of the MORL power system study, questions have been raised at some NASA centers on the feasibility of attaching the fuel blocks to the outside of the Apollo command module (CM). These questions have been based on the acceptability of perturbations to the CM's center of gravity. A meeting was held on 9 November 1965 at the NASA Manned Spacecraft Center in Houston, Texas, to review the initial design concepts and several alternates. The major conclusions are covered below.

The basic body recovery concept included in the MORL power system study is feasible, although final positioning of the fuel blocks will require a detailed study; it was indicated that this study is not justified at this time.

The modification to the CM should be minimized; however, it is recognized that modifications will be required to allow extended vehicle life either for the extended missions or standby operations associated with either Apollo applications flights or orbiting research laboratories.

4.4 SOLAR CELL/BATTERY SYSTEM

The solar cell/battery system is discussed in the following sections.

4.4.1 Solar Cell/Battery Description

The solar cell/battery system described herein is an updated solar cell system, as compared to the baseline system; it produces and distributes to the load buses equivalent power to that delivered by the Isotope Brayton Cycle system. The updated solar cell/battery system differs from the MORL baseline system defined in Reference 17 as shown in Table 4-8 and as follows:

1. The dimension of each solar cell has been increased to 2 cm by 2 cm.
2. The thickness of the solar cells has been reduced to 0.010 in.
3. Integral cover slides are being used in place of the conventional cover glasses.
4. Solar cells with wrap around contacts are being used.

Table 4-8
 BASELINE AND UPDATED SOLAR CELL/BATTERY SYSTEM CHARACTERISTICS

	Baseline Solar Cell/Battery System	Updated Solar Cell/Battery System
Panel area	1, 704 sq ft	2, 676 sq ft
Panel specific weight	0. 85 lb/sq ft	0. 65 lb/sq ft
Panel design power	13. 9 kW	23. 0 kW
Average to busses	6. 0 kW	9. 6 kW
Solar cell thickness	0. 018 in.	0. 010 in.
Cell efficiency (AMO-bare)	11. 25%	11. 25%
Batteries		
Type	Hermetically sealed nickel-cadmium	Hermetically sealed silver-cadmium
Cells per battery	24	30
Ampere hour capacity	107	173
End of discharge voltage	1. 0 V/cell	0. 9 V/cell
End of charge voltage	1. 50 to 1. 55 V/cell	1. 55 to 1. 60 V/cell
Ampere hour efficiency	80%	95%
Weight (lb)		
Solar cell panels	1, 448	1, 740
Battery system (four batteries)	924	1, 124
Deployment mechanism	400	600
Total	2, 772	3, 464

5. The substrate structure of the panels has been improved.
6. Silver-cadmium batteries are being used in place of nickel-cadmium batteries.

A simplified diagram of the solar cell/battery system is shown in Figure 4-4. The solar-cell system is made up of N on P silicon solar cells attached to four flat solar panels that are oriented toward the sun by a gimbaling mechanism. During the illuminated portion of the orbit, the solar cell panels provide electrical power for all of the electrical load requirements and for recharging the batteries that provide the vehicle power during periods of solar eclipse and peak power demands. The battery system consist of four batteries, each made up of 30 hermetically sealed, alkaline, silver-cadmium secondary cells connected in series, and the associated battery charging circuitry. Charging of the batteries is controlled by the charging circuitry so that excessive overcharge and gassing of the cells does not occur.

The dc regulation and distribution subsystem is not shown in Figure 4-4 but it is schematically similar to the ac system.

The improvements in the uprated solar cell/battery system are a result of a later launch date and each item will be briefly discussed in this section.

4.4.1.1 Larger Area Solar Cells

Most of the solar cell manufacturers are manufacturing single-crystal silicon solar cells with dimensions of up to 3 cm by 3 cm at no sacrifice in efficiency. The larger area cells were made possible when switching from P on N to N on P solar cells. This increase in solar cell size and area allows the designer of solar cell systems to use fewer cells, interconnections, and cover slides, as well as reduces the cost per unit area of active surface. The decrease in the number of interconnections will increase the system reliability.

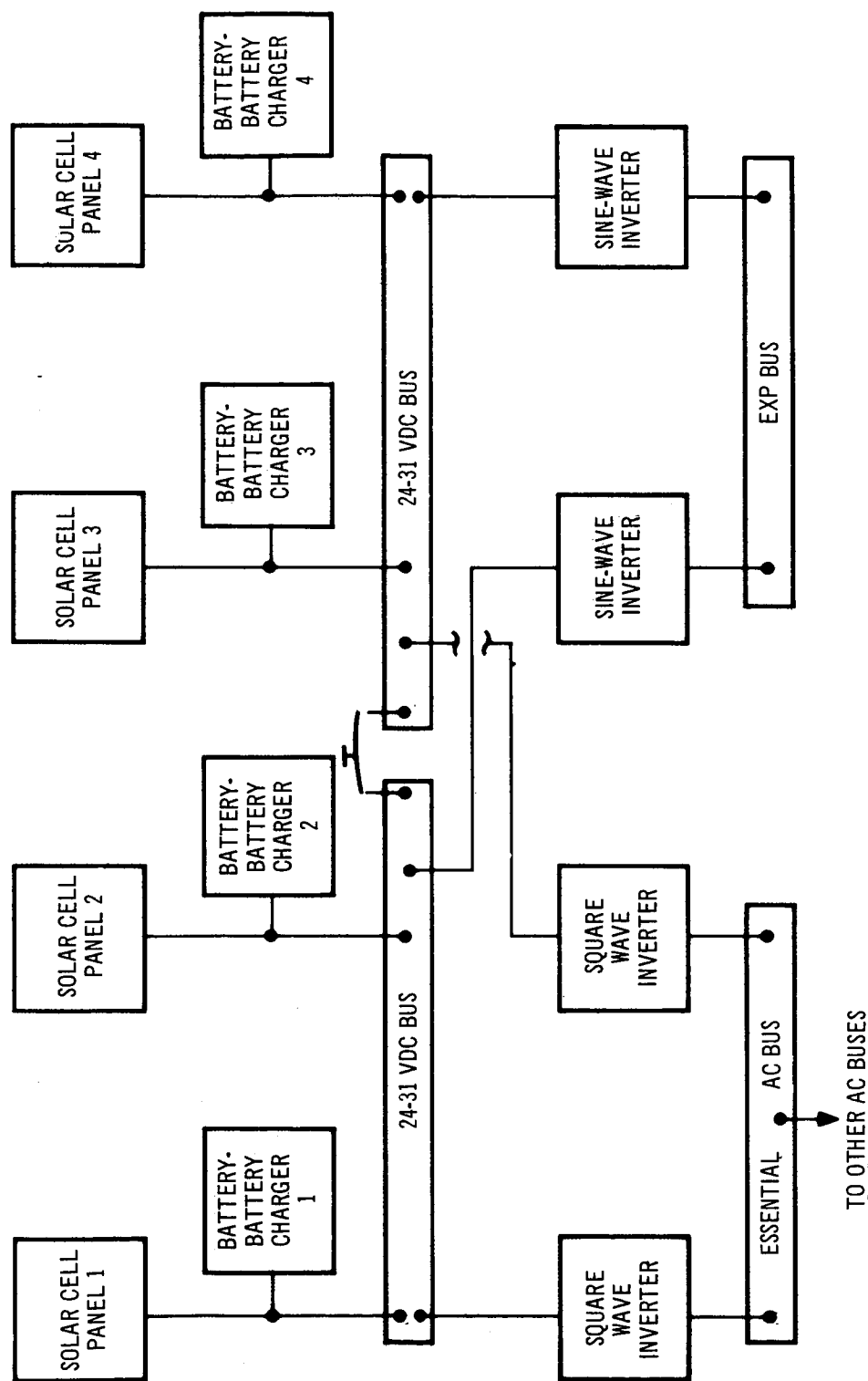


Figure 4-4. Simplified MORL Solar Cell/Battery System

The cost of the fabrication of the 3 cm by 3 cm cell is not currently competitive with the smaller size cells and, therefore, the 2 cm by 2 cm cell have been chosen for this system. This size of solar cell is being used on the fourth interplanetary monitoring platform, IMP-D (Reference 18).

4.4.1.2 Thinner Solar Cells

Several of the solar cell manufacturers have fabricated silicon solar cells of various thickness, down to 4 mils thick (Reference 19 and 20). Tests have shown that at about 8 mils thickness, the efficiency of cell begin to drop off rapidly. The radiation resistance has been shown to be greater for the thinner solar cells. A solar cell thickness of 10 mils has been selected for the uprated system and it results in a large decrease in solar cell weight. The conventional solar cells have a thickness of approximately 18 to 20 mils and, therefore, the solar cell weight, which contributes at least one-fourth of the total panel weight, is cut in half by use of 10-mil solar cells.

4.4.1.3 Integral Solar Cell Covers

The ultraviolet filter on the solar cell cover glasses is a cause for the large cost in solar cells because the ultraviolet filter requires many vacuum deposited metal coatings of exact thicknesses and each cover glass must be attached by hand to the solar cells. At least one manufacturer (Reference 21) has developed an integral glass coating that performs the same function as the conventional cover glass and can provide simpler fabrication and lighter cell weights. The covers are fused to the cell to form an integral coating, this shows a good thermal match between the cell and the cover. The thicknesses of the integral covers are 2 to 3 mils (cutting the weight of the covers in half) and are designed for use where the radiation environment consists mainly of low-energy particles. Cells with integral cover slides are not available in quantity at the present time; however, they could be available for the MORL and will offer potential savings in weight and cost.

4.4.1.4 Wrap-Around Cell Contacts

Another advancement in solar cell technology which has a potential application on the MORL solar-cell panels are solar cells that are constructed with contact grids on the bottom of the cell (wrap-around contacts). This arrangement provides a 5% increase in power for a given area because of the increased cell effective area (Reference 19). The wrap-around contacts permit the solar cells to be sweat soldered to printed circuit boards and eliminate the unreliable wire connections. The only disadvantages of this type of cell are slightly higher costs and the difficulty of inspecting the solder joints. Full production of these cells could reduce or eliminate the increased cost. Proper inspection methods could be developed to eliminate the latter problem. Solar cells with wrap-around contacts are being used on the IMP-D satellite which is to be launched in 1966 (Reference 18).

4.4.1.5 Improved Substrate Structure

Methods to improve the structure of solar cell panels are being conducted by several companies (Reference 19). Solar cell panels with densities of less than 0.45 lb/ft have been reported, but they have not been constructed. Programs for developing solar cell arrays are currently in progress at Ryan Aeronautical Co., (Reference 18), Hughes Aircraft Co., and Boeing Co. (Reference 19). It is expected that larger area solar-cell arrays can be constructed in the MORL time period to achieve at least the design value of 0.65 lb/ft. The solar cell improvements discussed previously have been a large factor in making this reduction in weight possible.

4.4.1.6 Silver-Cadmium Batteries

A parametric evaluation of a sealed nickel-cadmium and a sealed silver-cadmium battery was conducted, the batteries were compared, and a silver-cadmium battery was selected for the uprated energy storage subsystem (Reference 16). The selection of the silver-cadmium battery was based on the battery and system weight savings over that of the nickel-cadmium battery, and advancing technology of the silver-cadmium cells. A comparison of the nickel-cadmium battery characteristics is shown in Table 4-9.

Table 4-9
NICKEL-CADMIUM AND SILVER-CADMIUM
BATTERY CHARACTERISTICS

Characteristic	Nickel-Cadmium	Silver-Cadmium
Number of batteries	4	4
End of discharge voltage	1.0 V/cell	0.9 V/cell
End of charge voltage	1.5 V/cell	1.6 V/cell
Weight per cell	13.7 lb	7.6 lb
Cells/battery	24	30
Battery system weight (four batteries)	1,644	1,124
Amp-hour capacity	173	173
Depth of discharge		
Peak	70%	70%
Overloads	35%	35%
Estimated design life	1 year	1 year

4.4.2 Solar-Cell Panel Shadowing

A study was conducted to investigate the effects and the extent of shadowing on the MORL solar-cell panels, because the shadowing of the solar cells can reduce the solar-cell panel output more than proportionately to the amount of panel shaded. A detailed discussion of this study is presented in Appendix B.

The amount of shadowing that occurs in a belly-down orientation can be reduced by using single rectangular solar-cell extension panels. The single rectangular extension panels are achieved by moving the rectangular extension panels nearest the laboratory on each of the four main panels, and joining them with the rectangular extension panels located farthest away from the laboratory. Figure 4-5 shows the time power variation for a 50° launch inclination using the modified panel and shows that the average power-available, with shadowing, is always greater than the average power required.

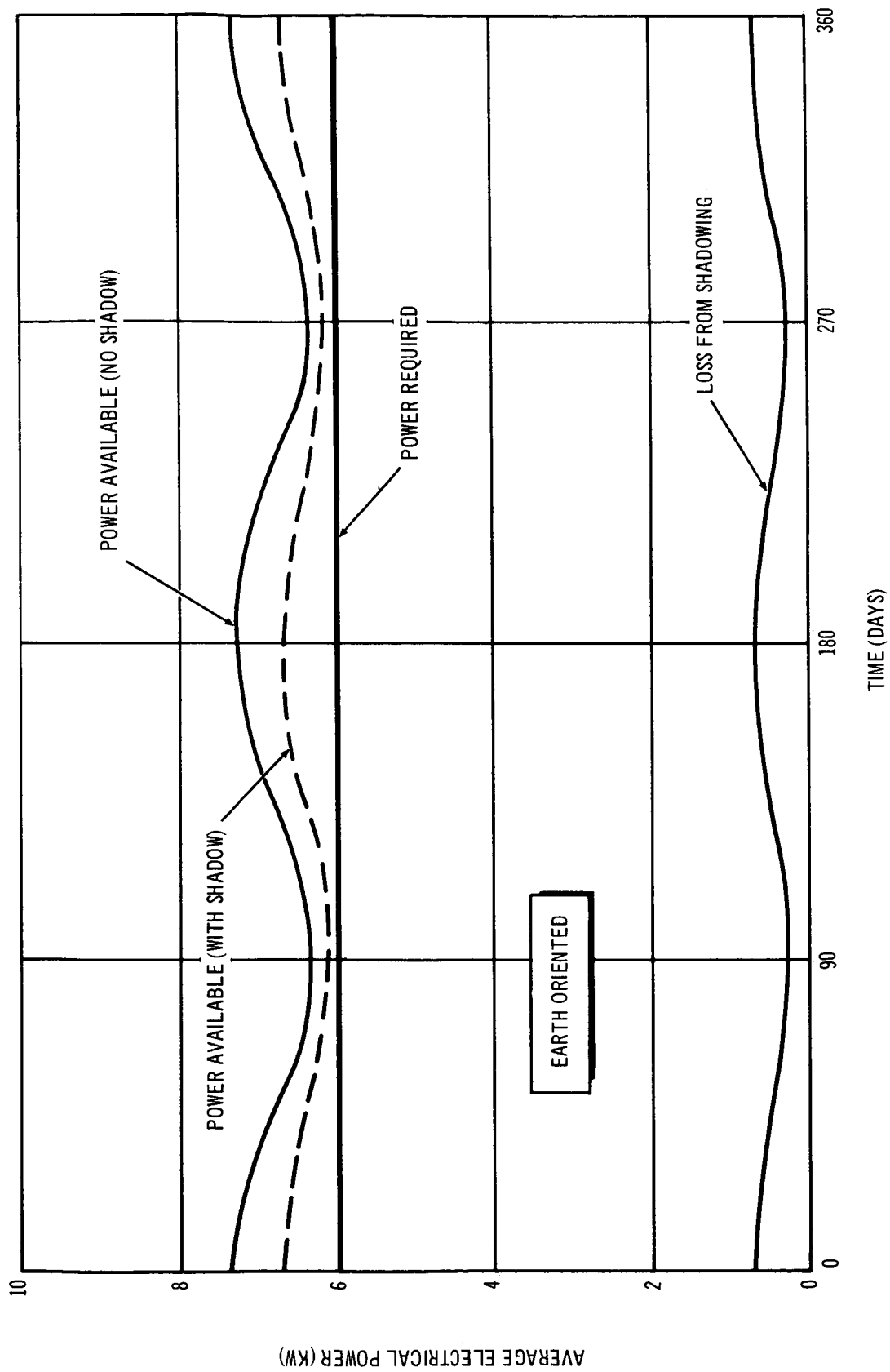


Figure 4-5. Time-Power Variation (50° Launch Inclination) Single Rectangular Extension Panel

With a roll solar orientation, the shadowing is reduced from 18.5 to 5.5% with the use of single rectangular extension panels and the shadowing can be eliminated by rotating the laboratory 180°

The shadowing of the solar-cell panels is not a serious problem. The rotating of the laboratory 180° in the roll solar orientation and/or the use of single rectangular solar-cell extension panels will assure continuous normal operation of the laboratory.

4.4.3 Solar Cell Technology Requirements

The technology requirements of a solar cell/battery system that are to be implemented in support of MORL development were investigated and a flow chart of the requirements was prepared. The flow chart appears in Appendix C. Each of the development items was defined from its general function and functional requirement through its performance requirements, area of investigation, studies and analysis, and tests. Also included were subsystem orbital test requirements which could be demonstrated by AAP mission and technology items that are potential improvements to the baseline system.

4.5 COMPARISON OF ISOTOPE BRAYTON CYCLE AND SOLAR CELL/BATTERY POWER SOURCES FOR MORL

This section presents a comparative evaluation of the two primary candidate electrical power sources for the MORL vehicle discussed in the previous sections, and to make appropriate recommendations concerning the baseline MORL system. The systems compared are: (1) the Pu-238 Isotope Brayton Cycle system evaluated under a parallel study, and (2) the solar cell/battery system, which was the MORL baseline system during Phase I, Phase IIa, and most of Phase IIb. Both systems are scaled to provide equivalent power to the using loads and are extrapolated, in so far as possible, to a common technology supported time scale.

Discussed in this section are the relative merits of the two power systems under consideration, with respect to the following system selection criteria: (1) launch weight penalty, (2) resupply weight, (3) total mission cost, (4) development risk, (5) reliability and maintenance, (6) growth potential, (7) safety, (8) operational flexibility, and (9) miscellaneous vehicle integration penalties.

4.5.1 Launch Weight Penalty

Table 4-10 summarizes the launch weight aspects of the improved Pu-238 Isotope Brayton Cycle system and the uprated solar cell/battery power source. This table includes the weight of each power source and the attendant weight penalties in other subsystems that interface with the power subsystem. For example, installation of a solar cell/battery system requires that the MORL interstage area be lengthened 3 ft, at a weight penalty of 216 lb, to provide space for solar-panel stowage. These weight and length penalties are relative to a hypothetical MORL without an electrical power source. The total weight penalty represents the total increase in MORL weight with the addition of the indicated power source, relative to the hypothetical MORL.

4.5.1.1 Pu-238 Isotope Brayton Cycle System

The total Pu-238 Brayton Cycle energy source weight is 2,661 lb. The weight of the battery and power conditioning equipment is 1,089 lb, bringing the total weight of the power source to 3,750 lb. A weight saving of 78 lb can be realized in the EC/LS system by using 1.8 kWt of Brayton Cycle waste heat for various heating functions. This heat is now provided by a special Pu-238 heat source and some associated equipment which may be eliminated.

The MORL vehicle is not long enough to provide the area required for an optimum radiator design. A weight optimization study, on the basis of minimum vehicle weight, showed that 58 in. of interstage should be added to the vehicle. This is the removal of 20 in. of interstage length used for solar-panel stowage and the addition of 58 in. or a net increase of 38 in. in

Table 4-10
MORL LAUNCH WEIGHT

System	Pu-238 Isotope Brayton Cycle (lb)	Solar Cell/ Battery (lb)
Power source		
Primary energy source	2,661	2,591
Battery and power condition	<u>1,089</u>	<u>1,685</u>
Power Source Total	3,750	4,276
Vehicle integration penalties		
EC/LS		
Isotope heater removal	- 78	---
Regenerative heat exchanger and control	- 16	---
Nonoptimum radiator	+ 130	---
Miscellaneous	+ 38	+ 178
Structure		
Interstage extension	+ 355	+ 216
Shield insulation and attachments	+ 133	---
Additional structural changes	+ 665	---
RCS (drag propulsion)	Negligible	+ 43
Communications (antenna)	<u>---</u>	<u>+ 68</u>
Total Vehicle Penalty	4,967	4,781

interstage length. This optimum length vehicle, however, requires that the EC/LS radiator operate at a nonoptimum point, Figure 4-6. Accordingly, a 130 lb penalty is charged to the isotope system. The area represents a 355 lb structural penalty. The shield insulation and attachments represent a 133 lb penalty. Another structural penalty of 665 lb is incurred to beef-up the interstage and provide special supports and mechanisms. The use of waste heat from the power system to satisfy the thermal-load requirements of the EC/LS system results in a weight reduction of 78 lb through

NOTES:

1. 10.5 KWE OUTPUT WITH A SINGLE FUEL BLOCK
2. HEAT TRANSFER FROM ONE SIDE OF FUEL BLOCK
3. ABSORPTIVITY-TO-EMISSIVITY RATIO (α/ϵ) = 0.20
4. HEAT LOAD OF 25.3 KWT
COOLANT $T_{IN} = 220^\circ\text{F}$; $T_{OUT} = 60^\circ\text{F}$
5. EC/LS HEAT LOAD OF 12.2 KWT
COOLANT $T_{IN} = 105^\circ\text{F}$; $T_{OUT} = 35^\circ\text{F}$
6. T_T = TURBINE INLET TEMP
 \triangle SELECTED OPTIMUM SYSTEM FOR $T_T = 1,540^\circ\text{F}$
 \square SELECTED OPTIMUM SYSTEM FOR $T_T = 1,340^\circ\text{F}$
7. EC/LS AREA SHOWN INCLUDES 78 SQ FT PENALTY FOR NONUSABLE SURFACE

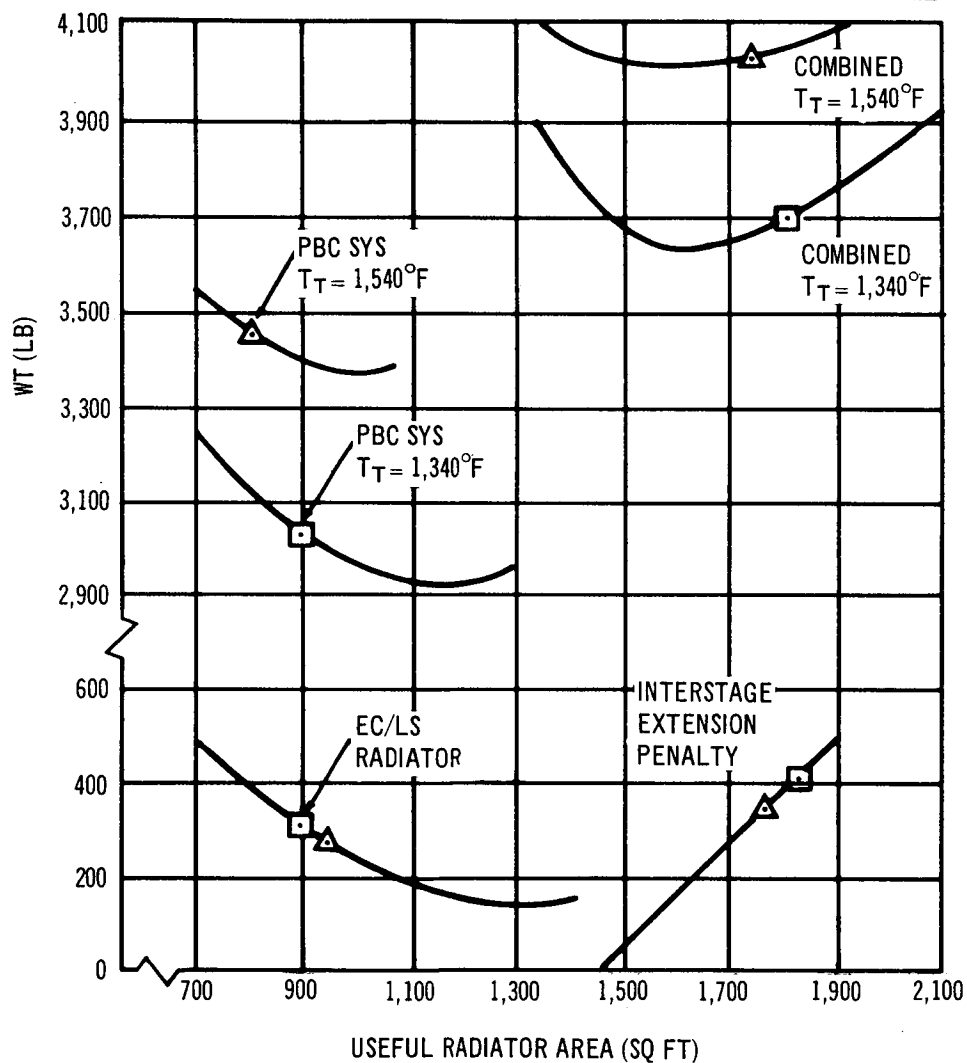


Figure 4-6. Radiator Optimization

elimination of a separate isotope source initially provided for this purpose. The drag penalty for this power system is negligible, despite the increased vehicle length, because the long-term orientation is belly down. The system is sized to provide rated power in the belly-down orientation (worst case). Performance may be improved a few percent by more optimum orientations.

4.5.1.2 Solar Cell/Battery System

The total weight of the power source is 2,591 lb and the weight of the battery and power conditioning equipment is 1,685 lb. Included in the power conditioning weight is 52 lb of increased wire weight for the distribution system of the low-voltage, high-current solar cell/battery source as compared to a high-voltage, low-current Brayton Cycle source. The 216 lb structure penalty results from the need to increase the length of MORL to stow the solar cell panels, as previously discussed. The increased length of the communication antennas and the use of rotating RF joints results in a penalty of 68 lb to this power system.

Table 4-11 summarizes the yearly propellant consumption chargeable to the solar cell/battery system. The variation from year to year is the result of the changing atmospheric density. The increased RCS propellant tankage (to hold the fuel required to overcome the solar-cell panel drag) and a 20 -day supply of propellants results in a 43-lb weight penalty using tanks sized to hold a 147-day supply of propellant during the 1976, the worst portion of the 1972 to 1976 time period.

4.5.2 Resupply Weight

Table 4-12 summarizes the resupply requirements for the Isotope Brayton Cycle and the solar cell/battery sources. The replacement period for the Brayton Cycle power conversion system (PCS) is assumed to be 1 year. The life of the PCS units cannot be accurately predicted at the present time; however, the life of these units may be well in excess of 1 year because the only

Table 4-11
SOLAR CELL SYSTEM DRAG PROPELLANT

Year	Propellant Consumption (lb/year)
1972	204
1973	132
1974	132
1975	204
1976	<u>432</u>
Average	221

Table 4-12
RESUPPLY WEIGHT

Item	Pu-238 Isotope Brayton Cycle (lb/year)	Solar Cell/ Battery (lb/year)
Power source replacement	924	- -
Battery replacement	384	1,124
Drag propellant	<u>Negligible</u>	<u>221</u>
Total	1,308	1,345

identified wearout mode (turbine creep) results in a life of more than 5 years. The duty cycle of the battery for the Brayton cycle system is such that the life should be more than 1 year.

The batteries are the major resupply items on the solar-cell battery source. The batteries for this source have been designed with a duty cycle such that their life should be approximately 1 year. All four batteries are assumed to be replaced each year. Table 4-12 also includes the drag propellant requirements, which have been discussed previously.

4.5.3 Total Mission Cost

The program costs chargeable to the power system for a solar cell/battery system and PCS are shown in Figure 4-7, assuming that the isotope is recoverable. The intercept of these cost curves at launch includes: (1) the total nonrecurring costs and (2) the procurement of two flight systems and the long-lead-time items for the third system. The isotope cost which is included in Figure 4-7 is calculated in Appendix E. The slope of the curves in Figure 4-7 represent the yearly resupply requirements multiplied by the logistic cost of \$3,000/lb delivered to orbit. The \$3,000/lb cost is the result of the Phase IIa system analysis studies.

Mission success probabilities are such that there is an excellent chance that the backup systems need not be launched. This situation does not usually help the economics because the hardware is already fabricated and it is so special that a refund cannot be obtained if it is released for another application. However, this is not the case with the Pu-238 inventory allocated for the flight vehicles because any unused isotope will always be a valuable commodity. Thus, post-mission recovery of the isotope can help the economic picture.

The nonrecurring costs of Figure 4-7 include an expected isotope cost, and the probability of actually requiring launch of the backup vehicles as well as mission recovery. The expected cost of the isotope is made up of the cost of lost isotope, based on the probability of launch and post-mission recovery, and a rental charge. The rental charge is made up of a charge for the usage of a valuable commodity (Pu-238), a charge for the decay of the isotope, and a charge for reprocessing the isotope so that it is available for other applications. A detailed discussion of the isotope costs is given in Appendix E.

4.5.4 Power Rating Increase

The growth potential of the solar-cell battery system is limited primarily by stowage and deployment of the large-area solar cell panels. Figure 4-8 shows the deployment sequence and relative size of the panels for the

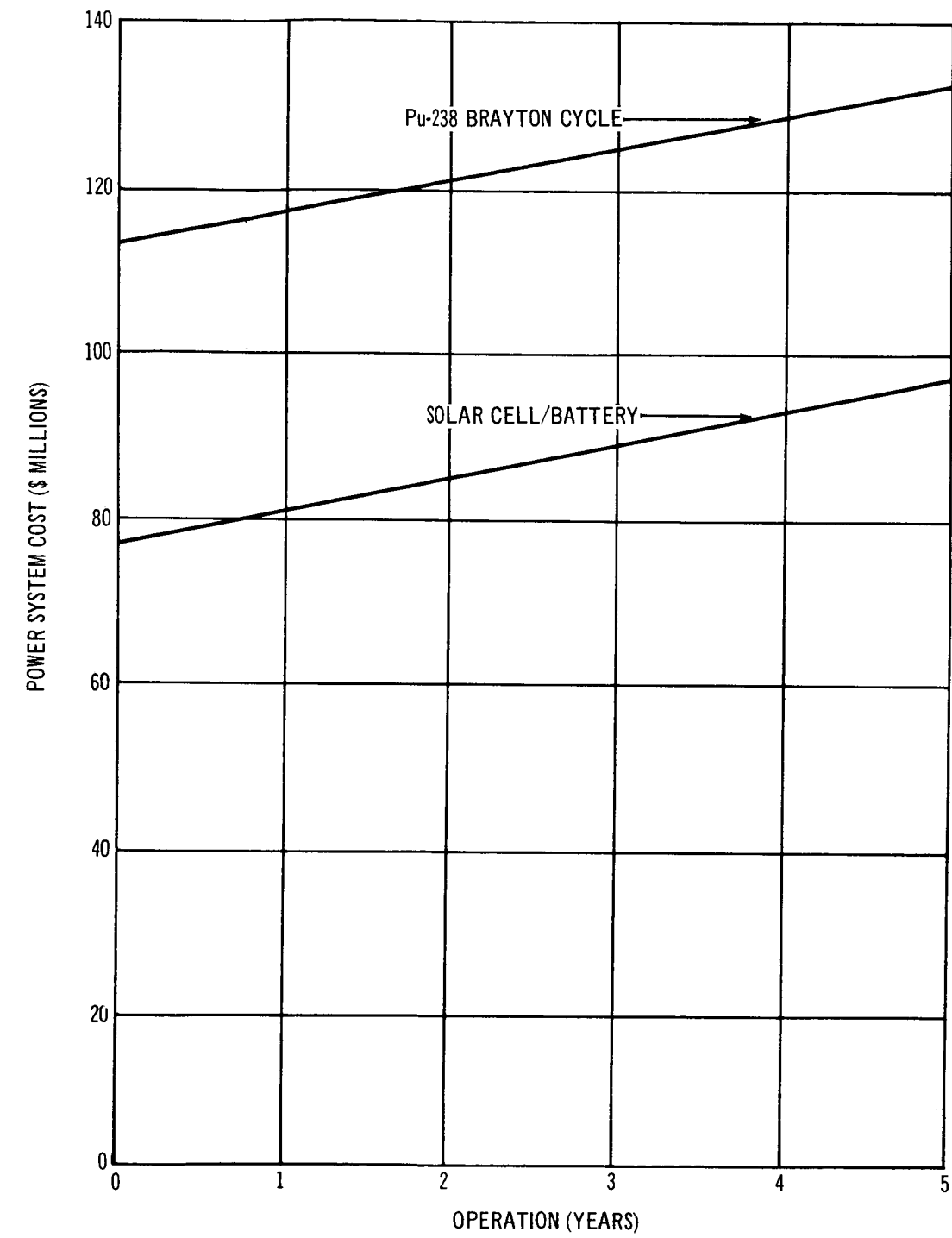
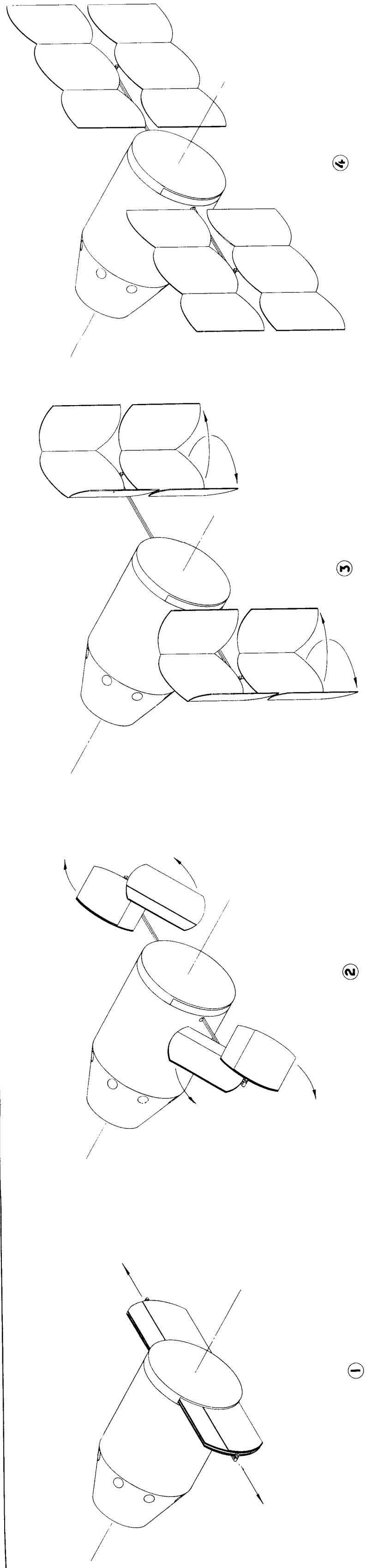


Figure 4-7. Power System Cost Comparison



SOLAR PANELS DEPLOYED (267% SQ. FT.)

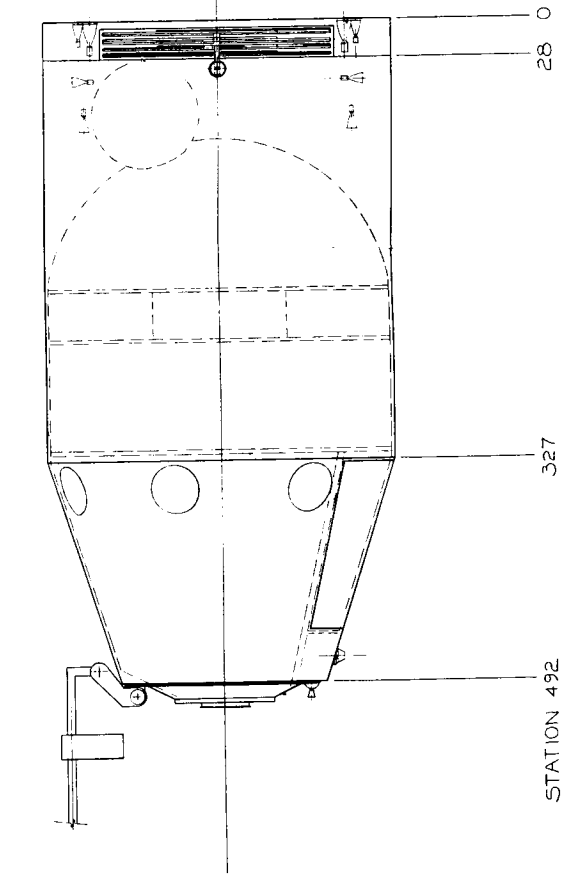
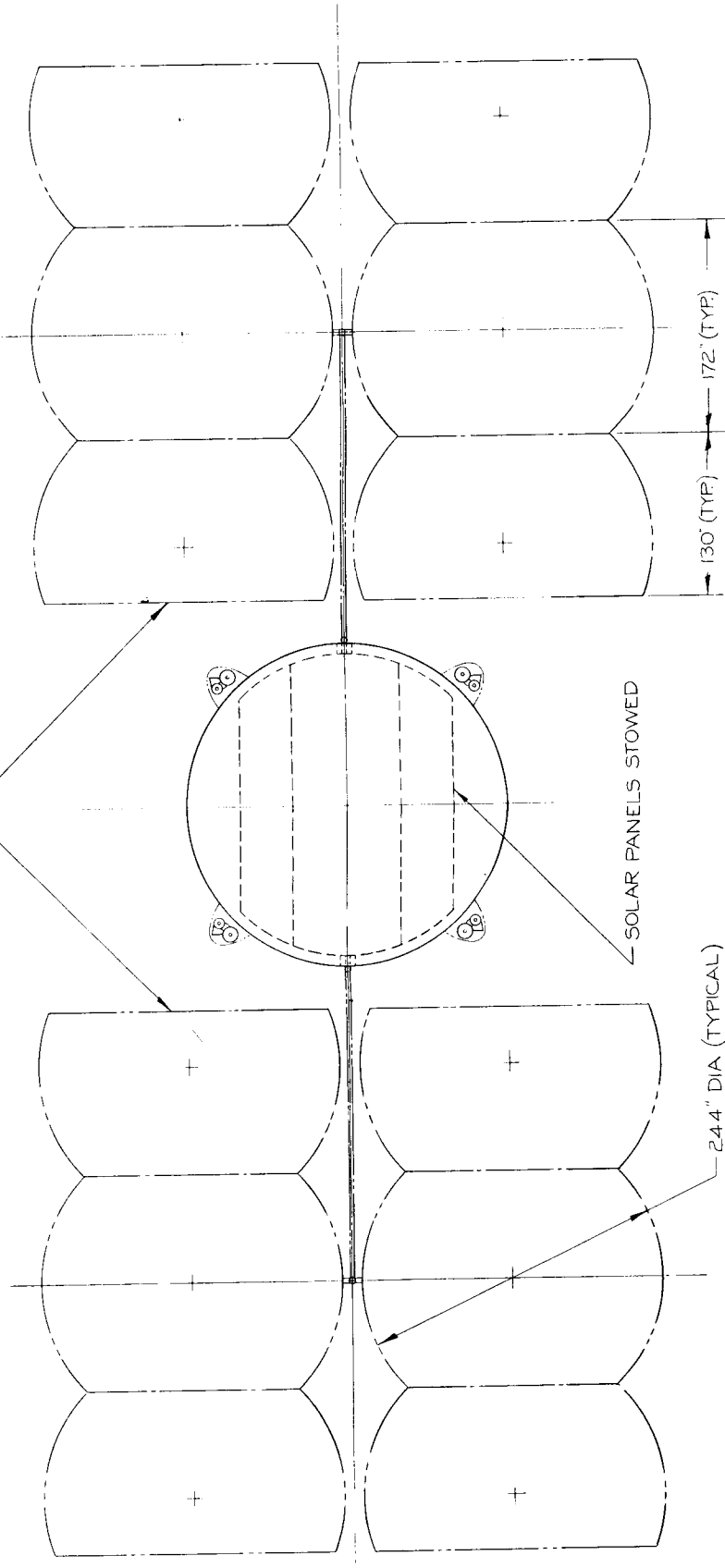


Figure 4-8. Solar Cell Panel Deployment Sequence

solar-cell system described in Section 4.4.1. Stowage and deployment of a panel of this size is feasible, although difficult; increased panel sizes make the problem increasingly difficult.

The availability of Pu-238 and vehicle radiator area are the two factors that tend to limit the growth potential of a PCS.

The availability of Pu-238 has been discussed previously; increased power requirements would aggravate the situation. The 11 kW reference isotope system requires a 5-ft extension to the MORL interstage to provide increased radiator area; thus, further increase in power requirements would require: (1) deployable radiators, (2) further additions to the interstage, or (3) lowered cycle efficiency associated with less than optimum radiator area. The upper practical limit is on the order of 15 to 20 kW because of radiator area limitations.

4.5.5 Life Extension Potential

The primary factor limiting the life of the PCS is the cladding material creep and the consequent stress in the fuel block. The extension of life beyond the 5-year design point requires either increased cladding material capsule thickness or slightly reduced system temperatures. A small increase in the size of the solar-cell panels, to allow for the increased total solar-cell degradation over a longer period of time, is required to extend the life of the solar-cell battery system. Thus, neither system is severely penalized by life extensions beyond the present 5-year design point.

4.5.6 Alternate Mission Capability

The alternate missions that are presently considered for MORL are polar orbit and synchronous orbit missions. The applicability of the isotope and solar-cell systems to these alternate missions is discussed in the following sections.

4.5.6.1 Polar-Orbit Mission

Both of the systems designed for the baseline 50° mission are suitable for the polar-orbit mission with virtually no changes. The weight of the two systems is unchanged for this mission.

4.5.6.2 Synchronous Orbit Mission

The referenced PCS is compatible with the synchronous orbit mission with no changes; in fact, the system output power is increased a few percent because of the reduced radiator sink temperature.

Table 4-13 compares the characteristics of a solar-cell battery system for the baseline and synchronous mission. The values shown in Table 4-13 are for a system optimized for each specific mission. The synchronous orbit is characterized by a favorable light/dark cycle for a solar-cell battery system. MORL is continuously in the sun, except for two 18-day periods each year; during these periods the maximum dark time is only 1.2 hours per orbit (day). The resulting long-light periods lead to a large decrease in solar-cell panel area requirements and weight. In addition, the vehicle integration penalties are reduced because of: (1) reaction control propellants are not required to overcome drag and (2) reduced antenna penalty. However, the battery weight must be increased because of the longer dark period.

In summary, the PCS offers improved flexibility for alternate missions, without requiring system redesign. Overall, the two systems are equal with respect to growth potential.

4.5.7 System Safety

The solar-cell battery is a safe system; possible exceptions are a potential collision hazard between resupply vehicles and the large extended solar cell panels and the remote possibility of battery rupture caused by excessive gassing. The battery gassing problem is also common to the isotope system.

Potential safety problems for the PCS include turbomachinery rupture, caused by excessive overspeed, and nuclear safety problems with respect to the civilian population. The system is designed so that the possibility of

Table 4-13
SOLAR CELL/BATTERY COMPARISON*

Item	Synchronous Mission	50° or Polar Mission
Solar panel area	1,285 sq ft	2,676 sq ft
Weight (lb)		
Power source	1,897	3,152
Battery	1,556**	1,124
Integration penalty	462	505
Total	3,915 lb	4,781 lb

*To provide same power to buses as isotope system

**Based on 50% depth of discharge

turbomachinery rupture is extremely low; if it occurs, pieces are contained within the system, thereby precluding the possibility of damage to MORL.

The PCS was designed to minimize nuclear safety problems with respect to a MORL crew and the civilian population. Nevertheless, nuclear safety is a political problem that will not be fully resolved until launch approval is obtained at the Secretary of State/Presidential level. It is expected that launch approval can be obtained for MORL because of the consideration given to safety in the system design and the significance of a MORL program to the nation.

4.5.8 Operational Flexibility

Freedom of vehicle orientation and noninterference with experiments and other extravehicular activities are discussed in the following sections.

4.5.8.1 Vehicle Orientation Freedom

The demands of MORL experimental program may require random inertial orientation for extended periods; thus, any power system used for MORL

must have the capability of providing essentially rated output with any vehicle orientation. These requirements are inherently incompatible with a simple solar-cell system because the solar-cell panels require orientation to the sun within $\pm 10^\circ$ to 20° . The necessary vehicle freedom of orientation is obtained with a solar-cell system by two axis gimbaling of the solar-cell panels. In addition, the rotating MORL requires slip rings to transfer electrical power from the solar-cell panels to the vehicle. Thus, freedom of orientation can be obtained with a solar-cell system, at the expense of increased complexity in the stabilization and control subsystem as well as the inherently simple power system. The principal disadvantage of this approach appears to be the increased development risk in the power system, the impact of which has been discussed previously.

The performance of the PCS is essentially independent of vehicle orientation, except for minor variations in the radiator sink temperature, which is a function of vehicle orientation. The PCS discussed in this report was designed to provide rated power at essentially the worst conceivable orientation; consequently, this system's output will increase a few percent with more favorable vehicle orientations. In summary, there is a slight advantage for the PCS with respect to freedom of vehicle orientation, neglecting the development risk of the solar-cell panel gimbal and slip-ring system.

4.5.8.2 Extravehicular Space Utilization

The large gimballed solar-cell panels require a large volume of extravehicular space at the aft of MORL to be maintained free of obstructions. This precludes the use of this space for experimental purposes and limits the ability to accommodate large stowed modules. Thus, the capability for growth to accommodate large special-purpose experimental modules is limited by the solar-cell battery system. In addition, solar-cell panels represent a hazard to extravehicular activities, as well as a collision hazard during resupply operations.

4.5.9 Miscellaneous Integration Penalties

Some of the miscellaneous integration problems and penalties not previously considered for the two power sources are discussed in the following sections.

4.5.9.1 Experiments

The neutron emission from the isotope system may affect the results of a number of the MORL experiments unless the experiments are properly placed and are designed with the necessary shielding. Several of the experiments require the measurement of the neutron spectra and flux distribution. However, it is expected that the isotope neutrons will be at a higher energy level than the natural space neutrons. The neutron flux from the isotope system may also affect some of the biological experiments. Therefore, it is recommended that studies be conducted to determine the effect of the isotope system on the experiments after the experiments become more fully defined.

4.5.9.2 Resonant Frequencies

A potential problem area that has not been investigated is the possible resonant frequencies of the thin, larger-area, solar-cell panels caused by perturbations on the MORL vehicle. The major perturbation would be caused by impulses of the RCS and by docking vehicles. This effect could result in panel stiffeners with a resulting increase in solar-panel weight.

4.5.9.3 Communications and Data Acquisition

The antenna patterns must be satisfactory for all exterior appendage variations. The variations are caused by docked logistic vehicles, cargo and experimental vehicles, and the large area of moving solar-cell panels. The use of the isotope system eliminates a large unknown effect and, therefore, development and test time. The antenna will shadow the solar-cell panels; however, the extent and effect of the shadowing has not been determined. The placement of the antenna at the rear of MORL and in the plane of the panel deployment arms will eliminate all shadowing. The change in antenna location will cause an increase in weight because of increased coaxial length and the need for rotating rf joints. Rotating rf joints are required because of the rotating panels. The isotope system does not place a limitation on the communications subsystem. Table 4-10 summarizes the weight penalty imposed on the communications system by the solar-cell panels.

4.5.9.4 EC/LS Subsystem

The large area requirements of the Brayton Cycle and EC/LS radiators will alter the thermal balance of the vehicle with the isotope power source. However, this will result only in a change in the insulation requirements, which will not significantly alter the vehicle weight.

4.5.9.5 Reaction Control Subsystem

The isotope system allows a 42% reduction in the duty cycle for some of the RCS engines, resulting in increased life. Also, the use of the isotope system permits a greater freedom of engine location because the solar-cell panel impingement constraint is removed. This may result in reduced attitude control propellant consumption.

Section 5

LOGISTICS SYSTEM

5.1 SUMMARY

The selected MORL logistics system consists of three vehicle configurations to satisfy the requirements imposed by the three MORL missions. These systems use the following building blocks:

1. Baseline 50° mission--the modified Apollo command module, the MORL logistics service pack, the multimission module, and a Saturn IB booster.
2. Polar mission--the modified Apollo command module, the MORL logistics service pack, the multimission module, and a Saturn V booster.
3. Synchronous mission--the modified Apollo command, the modified Apollo service module, the MORL multimission module suspended within the LEM fairing and, a Saturn V booster.

Cargo capacity for each configuration is about 10,500 lb delivered into the specified orbit in addition to three crewmen carried in the Apollo. The payload capacity of the selected logistics vehicle is adequate for each of the mission requirements. The first three launches for the 50° orbit utilize about 85% of the available cargo capacity; only 57% of the capacity is used in subsequent flights. The larger payload of the initial three launches is caused by a requirement for nearly 3/4 of the total experimental equipment (by weight) within the first 45 days. This results from common equipment usage by a considerable portion of the experiments. Should the logistics systems capacity become marginal due to growth, adjustments may be required in the experimental program to ease the need for the large initial cargoes.

5.2 INTRODUCTION

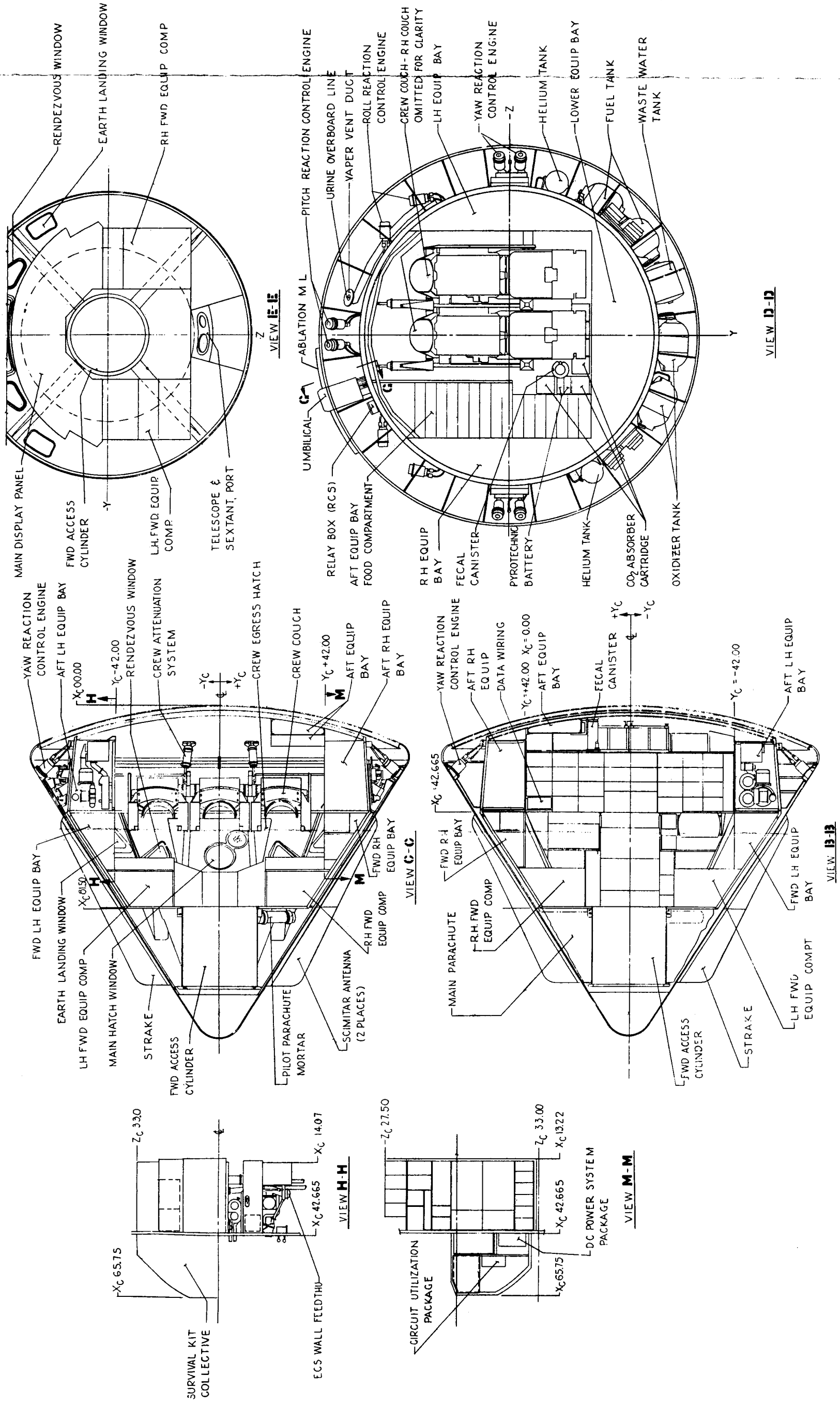
Logistics system requirements for the three missions, and various alternate vehicle configurations which meet the requirements, are discussed in the

Task III Responsiveness Analysis (Reference 4). The 50° mission requires that three 3-man Apollo flights be made in the first 45-day period. The first launch is to activate and check out the laboratory; the next two, about 45 days later, are to rotate the checkout crew and fully man the laboratory. Crew rotation and resupply follow at regular 90-day intervals thereafter. The total logistics weight necessary on these flights, from the requirements for 147 days of housekeeping supplies, is approximately 1,500 lb on initial spares; the experimental gear required in the first 90 days is 26,000 lb; thus, a little less than 9,000 lb per flight is necessary for the 50° mission. The cargo requirements for the remainder of the flights for the 50° mission are less (about 6,000 lb), but 10,500 lb will be used as the design number to allow for growth.

The requirements for experimental cargo on the polar and synchronous missions are not clearly identified at this time since experimental program requirements for these missions have not been developed. The consumables necessary on the latter missions are 1,850 lb/month and 1,580 lb/month for the polar and synchronous missions respectively. In the absence of a clearly defined experimental cargo weight on these two missions, the same design number of 10,500 lb per flight as determined for the 50° mission will be used. The baseline logistics vehicle configuration is shown in Figure 5-1. Description of the baseline MORL service pack, multimission module (MMM), and necessary modifications to the Apollo command module are noted in the Phase IIa MORL Logistics System Final Report (Reference 22) and will not be covered further in this report; only changes to the MORL Phase IIa baseline system required by the MORL missions are discussed. Subsequent sections describe the selected system and the changes necessary for each mission.

5.3 MISSIONS

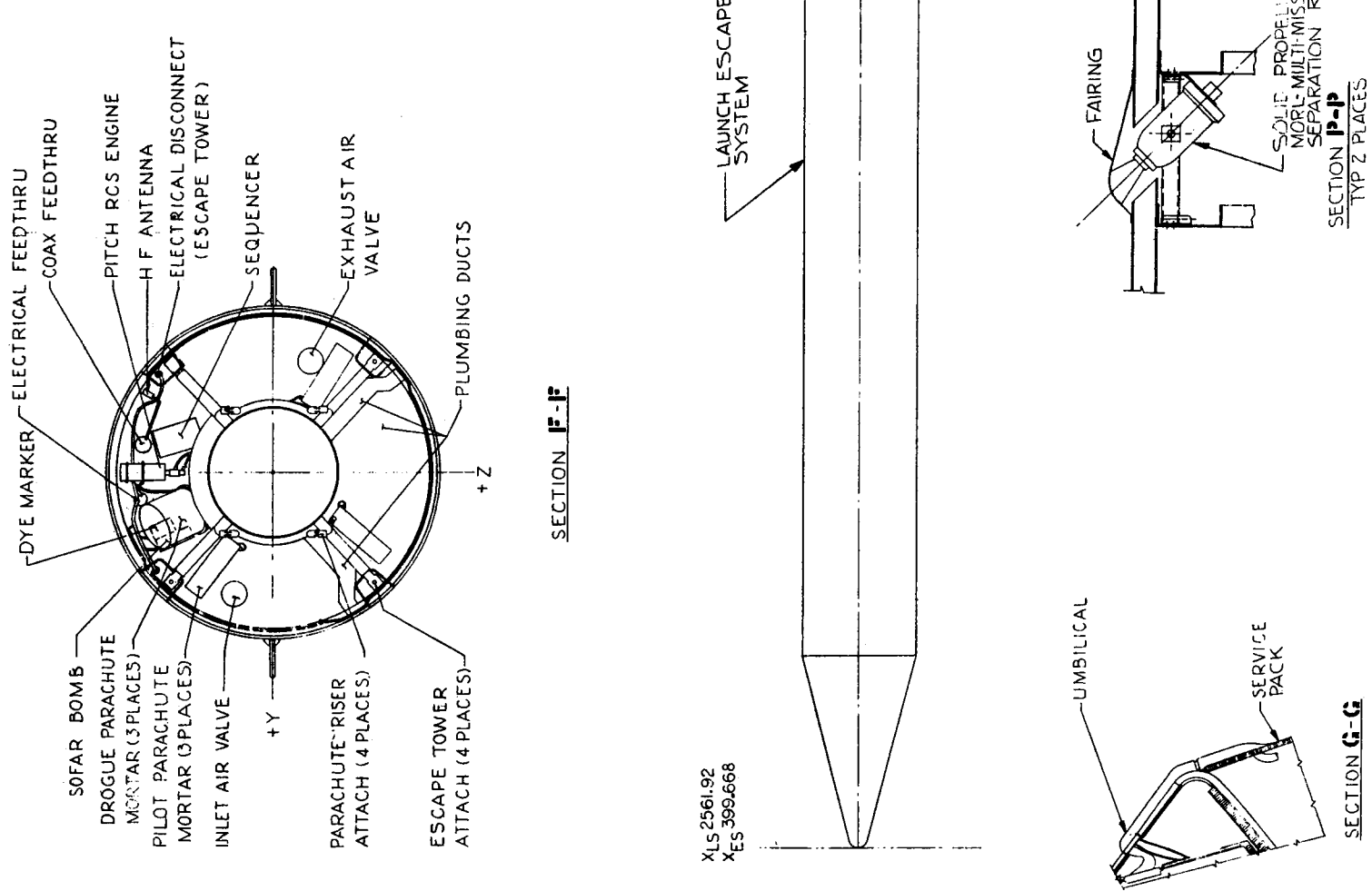
Logistics requirements for the various missions are discussed in the following subsections.



217-1

217-2

217-3



5.3.1 The 50° Inclination Mission

The baseline logistics system noted in Reference 22 and Figure 5-2 was derived for an orbit inclination of 28.7°. Essentially the same system is satisfactory for the 50° inclination orbit since the only significant change is the orbit inclination with a resulting minor payload degradation. Necessary changes are enlargement of the EC/LS oxygen and water supplies and an increase in electrical capacity to account for the longer mission time to rendezvous (approximately 3 days as compared to 1 day for the 28.7° orbit); both of these changes are minor and no configurational changes were made in this study. This system carries approximately 10,500 lb per flight to orbit, while offering flexibility of the multiple mission module concept and requiring only minimum change to the Apollo Command Module.

5.3.2 The Polar Mission

The polar mission will utilize essentially the baseline logistics spacecraft boosted by a Saturn V. The polar orbit requires about a 10% increase in fuel for the multimission module RCS to accommodate the longer rendezvous. If orderly progression from the 50° to polar missions were assumed, the logistics vehicle RCS could be sized for the polar mission originally at a small penalty (approximately 100 lb) which would then make a universal logistics vehicle except for the booster; otherwise the extra capacity must be added to the multimission module RCS system. The change is not large enough to perturb the configuration defined in Reference 22. (Also see Figure 5-1.) This system results in a payload of approximately 10,200 lb per flight.

An alternate logistics vehicle for the polar orbit could be a modified Apollo CSM, plus a multimission module suspended in the LEM adapter, launched by a Saturn V at an azimuth of 146° from ETR. This configuration would have a larger cargo capacity than the preferred logistics system because of the added volume available in the Apollo service module. However, since the cargo capacity of the baseline multimission module exceeds that required by the MORL for either the 50° or the polar orbits, no real benefit accrues from the larger capacity; in reality, it causes handling and stowage problems at the MORL because both the multimission module and the Apollo

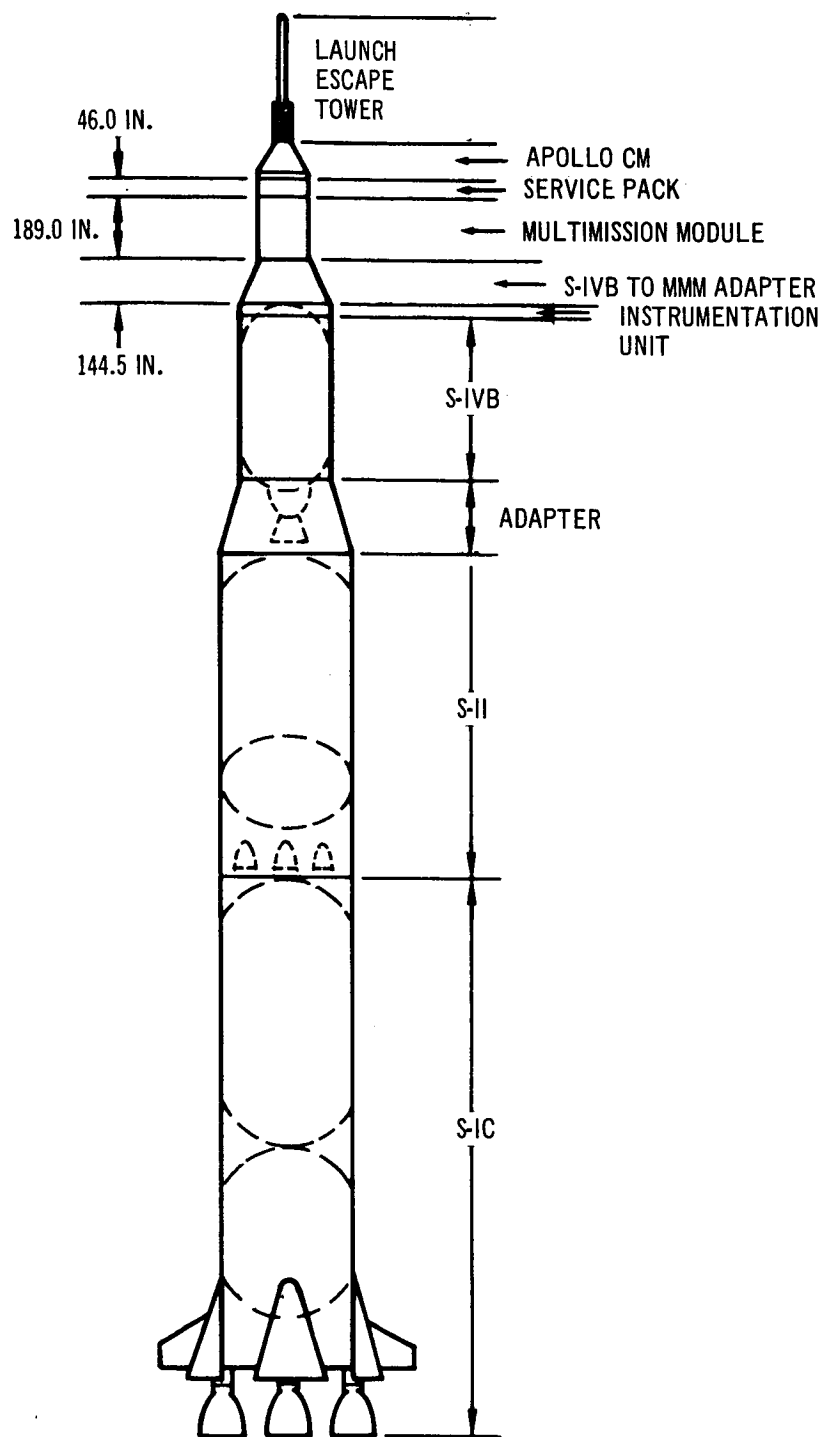


Figure 5-2. Polar Orbit Logistics Vehicle

command and service module must be handled after docking. In addition, the launch azimuth required may cause range safety problems because of overflight and instantaneous impact points (IIP) across Cuba and Panama. Lastly, the added weight of the service module plus multimission module would make a less attractive configuration should an upgraded S-IB be developed or should launch from the WTR with the present S-IB prove to be desirable.

5.3.3 Synchronous Mission

Because the deorbit velocity required for the Apollo command module exceeds that of the baseline service pack, the only logistics vehicle configuration considered for the synchronous mission includes the Apollo service module to provide the deorbit velocity. The cargo capacity of the modified Apollo service module is insufficient for the mission requirements, and therefore a baseline multimission module is also necessary; the MMM also provides the flexibility of the add-on modules. The system results in a payload of 19,000 lb per flight.

The three-man lunar Apollo command module must receive essentially the same modifications that were required for the baseline MORL logistics mission (Reference 22). Exceptions are that the command module may be exposed to space for up to 6 months and no retro pack is needed for deorbit. The 4.5 gm/cm^2 (average) shielding of the command module structure and permanent equipment results in approximately 1 rad of radiation on transit through the radiation belts, which is considered acceptable.

Modifications to the Apollo service module for the synchronous logistics mission include the following:

1. The service module systems must be adapted to a stay time in orbit of up to 6 months.
2. The fuel cells must be replaced with batteries for the Apollo CSM ascent and descent power requirements. This also forces modifications to the EC/LS system.
3. EC/LS consumables must be furnished for a three-day duration ascent phase and a two-day maximum duration descent phase.

4. The service propulsion system must be kept to provide deorbit impulse. The propellant tanks could be resized to the 11,600 lb of propellant required for deorbit (the lunar mission requires about 37,000 lb of propellant). However, the expense of modification was not considered worth the 1,000+ lb of tank and pressurant system weight that could be saved, and the SPS was left unmodified.
5. Some modification to the service module electronics is also required because of the new mission.

An attachment structure between the service module and the multimission module is required. This logistics vehicle configuration will require redesign of the MORL handling arms to enable storage of the multimission module as well as the combination Apollo command and service modules. Figure 5-3 shows the logistics vehicle docked and stowed at the MORL. The multimission module from the baseline configuration can be used without modification.

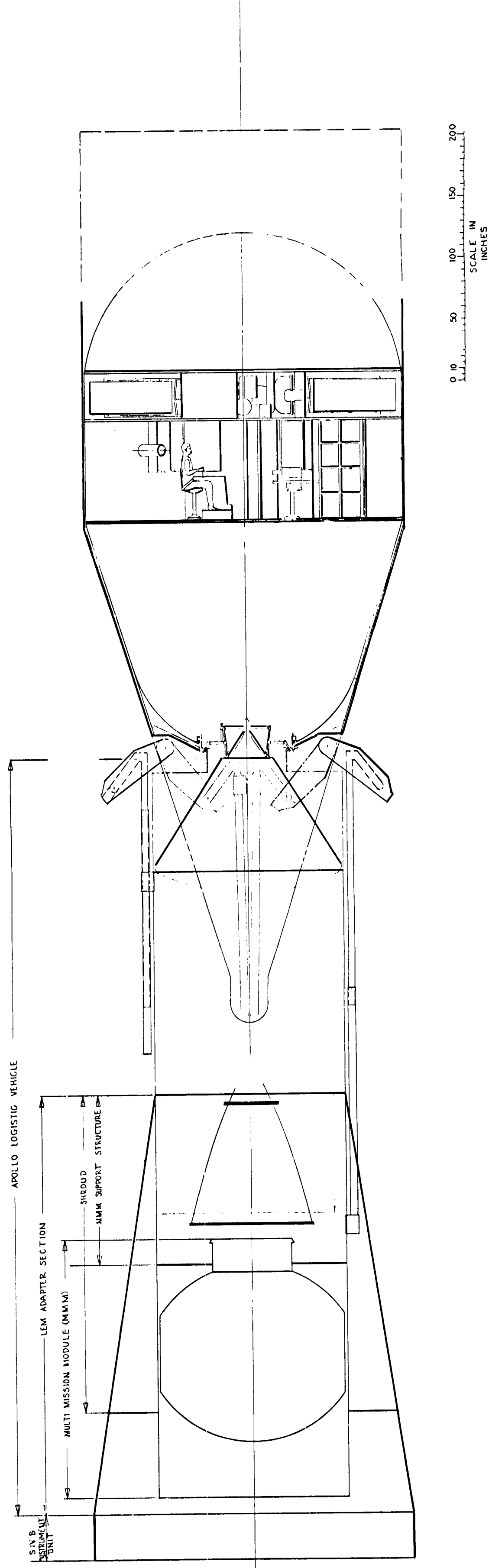


Figure 5-3. MORL 260 In. Diameter Laboratory, Synchronous Orbit

222-2

222-3

Section 6
PERFORMANCE OF THE MORL SYSTEM

The performance of the MORL system is improved through weight control measures designed to maximize the discretionary payload within the capability of the launch vehicle and to reduce the demands on the logistics system. Reduction of logistics requirements involves primarily the optimum use of laboratory propellant, the selection of a minimum drag profile which is consistent with propellant usage and the mission experiment requirements, and the selection of an optimum altitude for MORL operations.

During the Phase IIb study, many changes have been made to the baseline system. Those changes which affect the discretionary payload have been divided into two classes and are summarized as follows:

1. Changes derived from mission requirements--These changes include the following:
 - A. Change of baseline orbit inclination from 28.72° to 50° .
 - B. Change to belly down orientation from roll solar orientation.
 - C. Changes to the laboratory system--These include the following:
 - (1) Additional radiation protection.
 - (2) Separate air ventilation circuit in the Hangar/Test area.
 - (3) Additional experimental console provisions.
2. Changes stemming from the MORL improvement analysis--These include the following:
 - A. Change to an Isotope Brayton Cycle power supply.
 - B. Electrolysis of water for providing oxygen for breathing.
 - C. Incorporation of provisions for an experiment bay in the Hangar/Test area.
 - D. Change to a flat interior bulkhead utilizing bolted joints to separate the Hangar/Test area from the operations deck.
 - E. Deletion of the rendezvous radar interrogator aboard the MORL.
 - F. Change to a two arm stowing system for logistics spacecraft modules.

- G. Change to a radial stowage technique for logistics spacecraft.
- H. Incorporation of a combined waste management device.
- I. Added radiator provisions in the conical section to accommodate an oxygen regeneration system for the MORL.

Most of these items result in changes to the basic laboratory dry weight, generally an increase. A few, however, when combined with a MORL launch date in late 1971 or 1972 affect the payload requirements of the laboratory. These two subjects, payload requirements, and laboratory weight, are discussed in Sections 6.1 and 6.2, respectively. The resulting discretionary payload is presented in Section 6.3.

6.1 PAYLOAD REQUIREMENTS

Several changes made to the baseline MORL system had a considerable impact on the orbital characteristics of the laboratory. The more important changes were the substitution of the Isotope Brayton Cycle system for the solar cell/battery system as the primary power source, the change from roll-solar to belly-down orientation, and the change in launch date to late 1971 or 1972. Each of these three changes reduced the propellant requirements for maintaining the laboratory attitude and altitude. The decrease in the demand for in-orbit consumables lead to a review of the operating orbit altitude payload trade-off analysis to determine if a change in the optimum altitude had occurred. That review clearly indicated that the optimum operating altitude had dropped considerably. The following paragraphs discuss the changes which result in a new altitude selection and the net effect on launch vehicle payloads.

6.1.1 Effect of Changes to the MORL System

The effect of the three changes to the MORL system are presented in the paragraphs below.

6.1.1.1 Change of MORL Launch Date

The change of the MORL launch date from 1970 to late 1971 or 1972 causes the spacecraft to be exposed to a different solar flux pattern. Figure 6-1

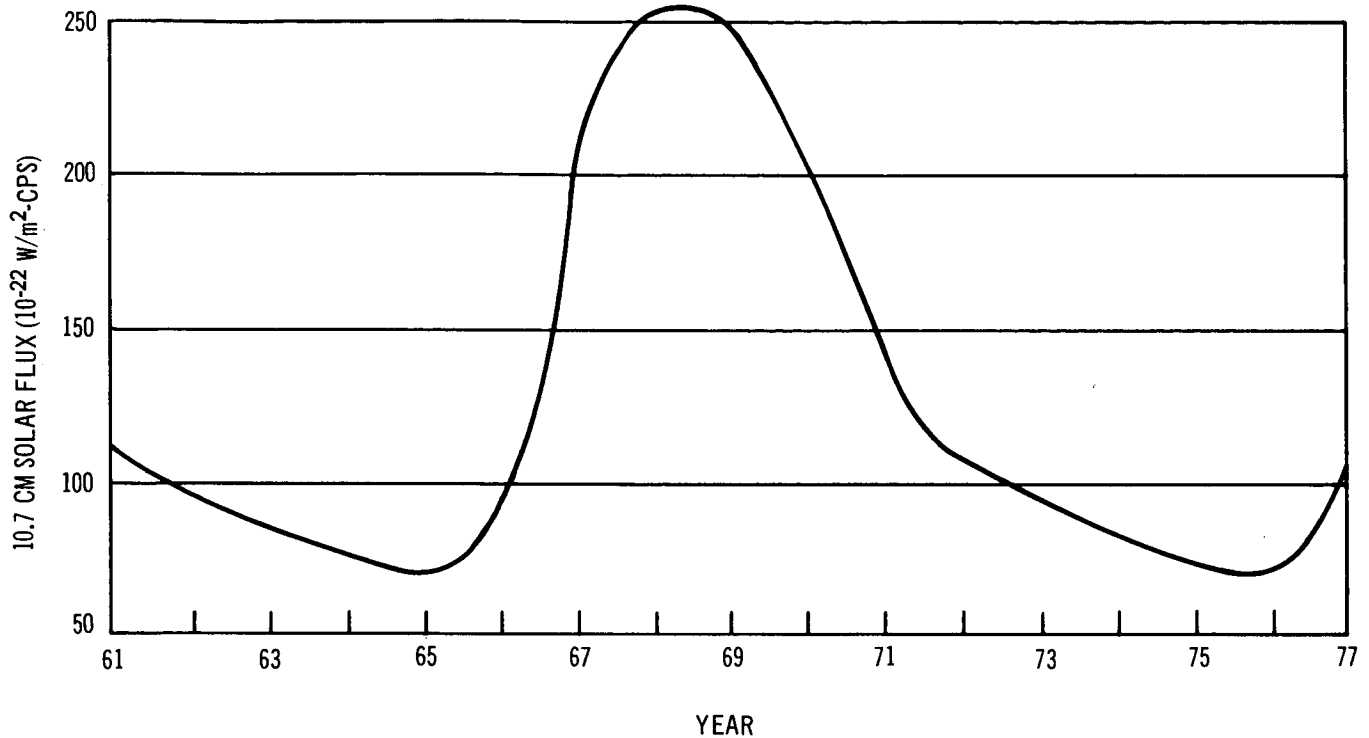


Figure 6-1. Long-Term Solar Cycle

shows the average yearly solar flux level as a function of calendar year. These data are based on extrapolations of the standard eleven year solar cycle and are in agreement with Reference 1. From this figure it is readily observable that a laboratory operating in the 1972 to 1977 period will be in the minimum solar flux region.

The effect of solar flux on high altitude atmospheric density is illustrated in Figure 6-2. These data were obtained from Reference 1. Note the marked reduction in effective density during periods of minimum solar flux. By launching the laboratory in 1972, the entire orbital life will be spent at the low density level. This reduces the effective dynamic pressure which in turn lowers the drag force and aerodynamic moment on the laboratory. The net result of these reductions is to decrease the laboratory propellant requirements at any given altitude.

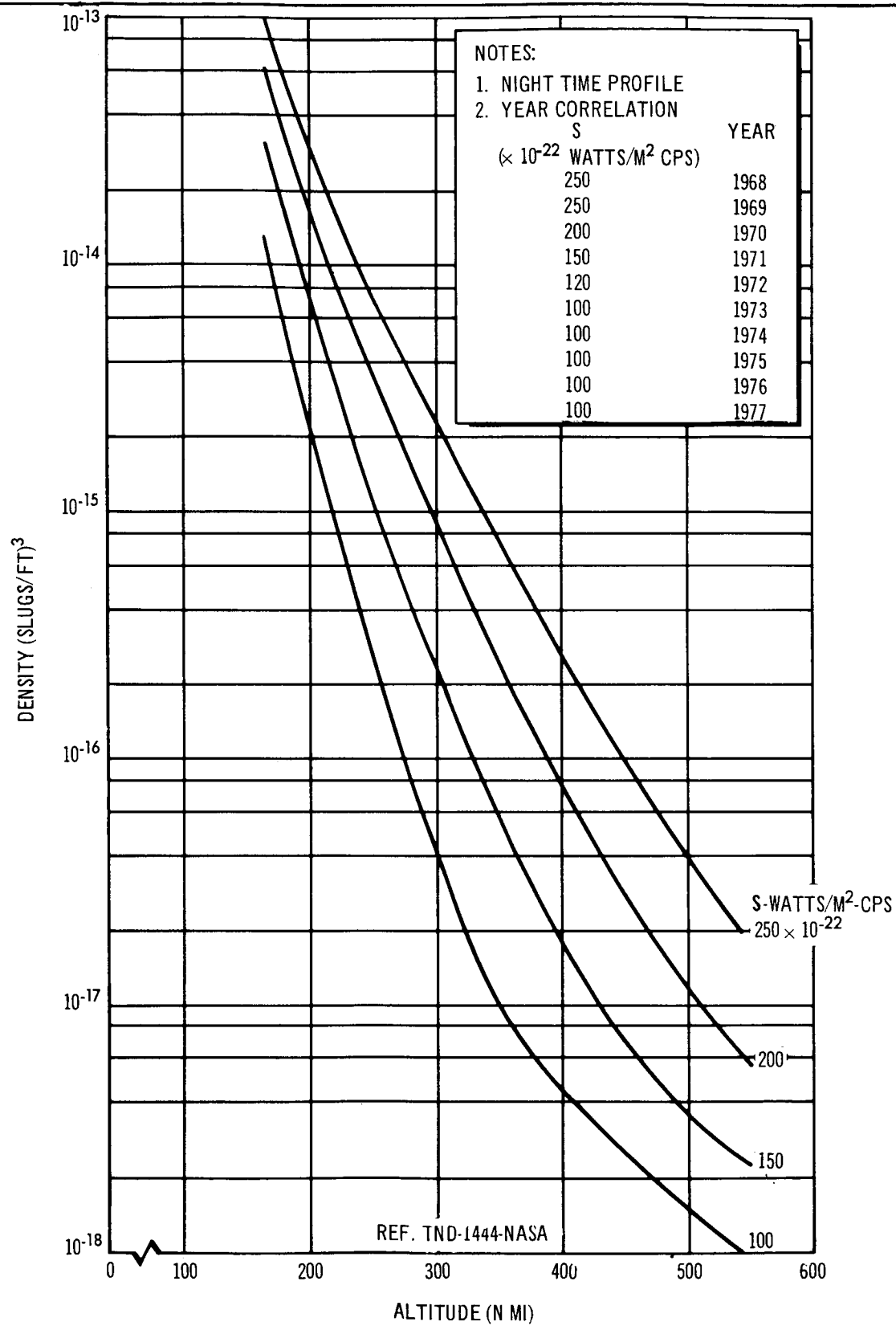


Figure 6-2. Average Density Profiles

6.1.1.2 Change to the Isotope Brayton Cycle Power System

The substitution of the 11 kWe isotope power system for the 6 kWe solar cell/battery system has a dramatic effect on the orbital configuration of the laboratory. 1,750 sq ft of solar panels have been removed from the baseline MORL leaving a clean, cylindrically shaped laboratory. The effects of this deletion on the orbital aerodynamic coefficients are shown in Figure 6-3 (drag), and Figure 6-4, (pitching moment). The significant reduction in both the drag and pitching moment coefficients decreases the propellant required to maintain altitude and orientation control of the laboratory in any given orbit. The effect of solar panel removal becomes even more significant when an equivalent 11 kWe solar/battery system is considered because in this case 2,680 sq ft of solar panels would be involved.

6.1.1.3 Change to the Belly-Down Laboratory Orientation

As a result of the increased emphasis on Earth-oriented experiments and with the deletion of solar panels, the long term operating orientation of the laboratory was changed from roll solar to belly down. In addition to reducing the aerodynamic coefficients to lower levels, this change permitted attitude control propellant to be used to provide orbit keeping impulse. This advantage of the belly-down orientation is illustrated in Figure 6-5. As can be seen, the attitude control propellant is sufficient to supply all the orbit keeping requirements above an altitude of 160 nmi.

These changes provide the basic justification for the revision in performance estimates for the MORL. They apply to any low altitude orbit regardless of inclination.

6.1.2 Analysis of the MORL Altitude

6.1.2.1 Payload Trade-Off

A 5-year mission with 20 Saturn IB/Apollo logistics appointments was postulated. The payload data for the Saturn IB launch vehicles were derived from Reference 23. The propellant consumables over a 5-year period were derived from Figure 6-5. The net result of these payload fluctuations are

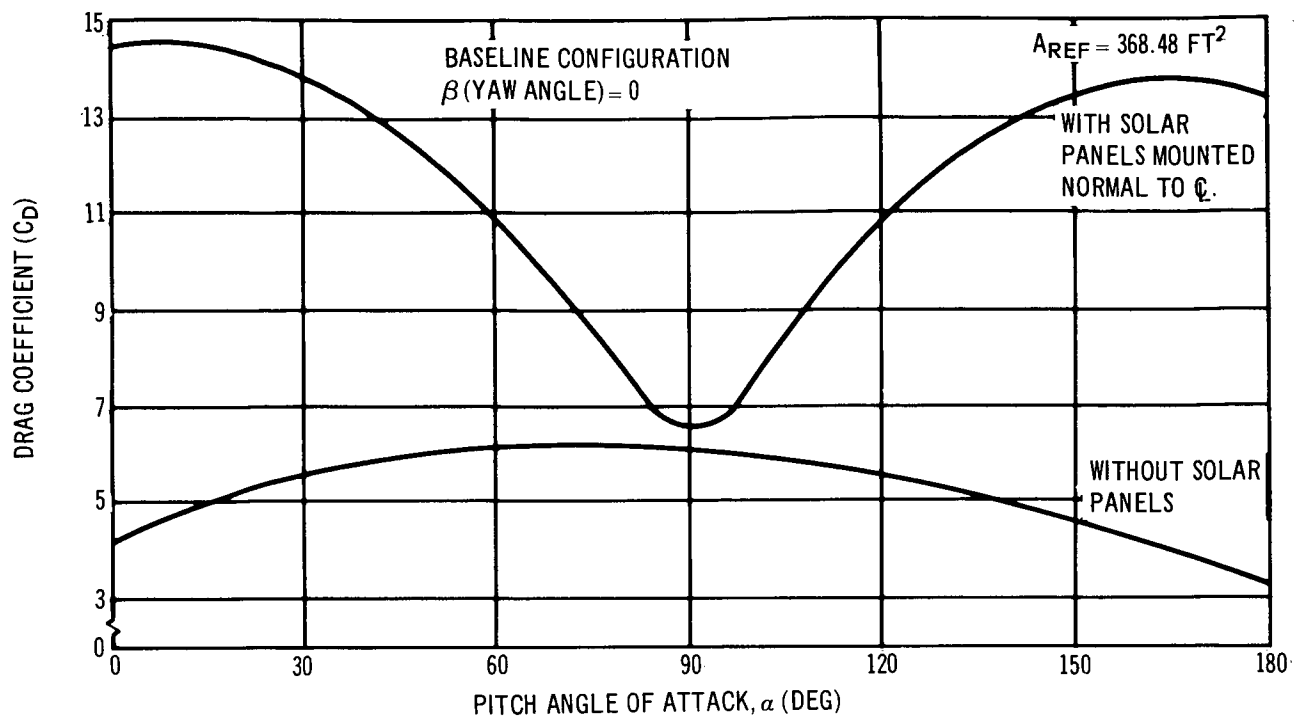


Figure 6-3. MORL Orbital Drag Coefficient as a Function of Angle of Attack

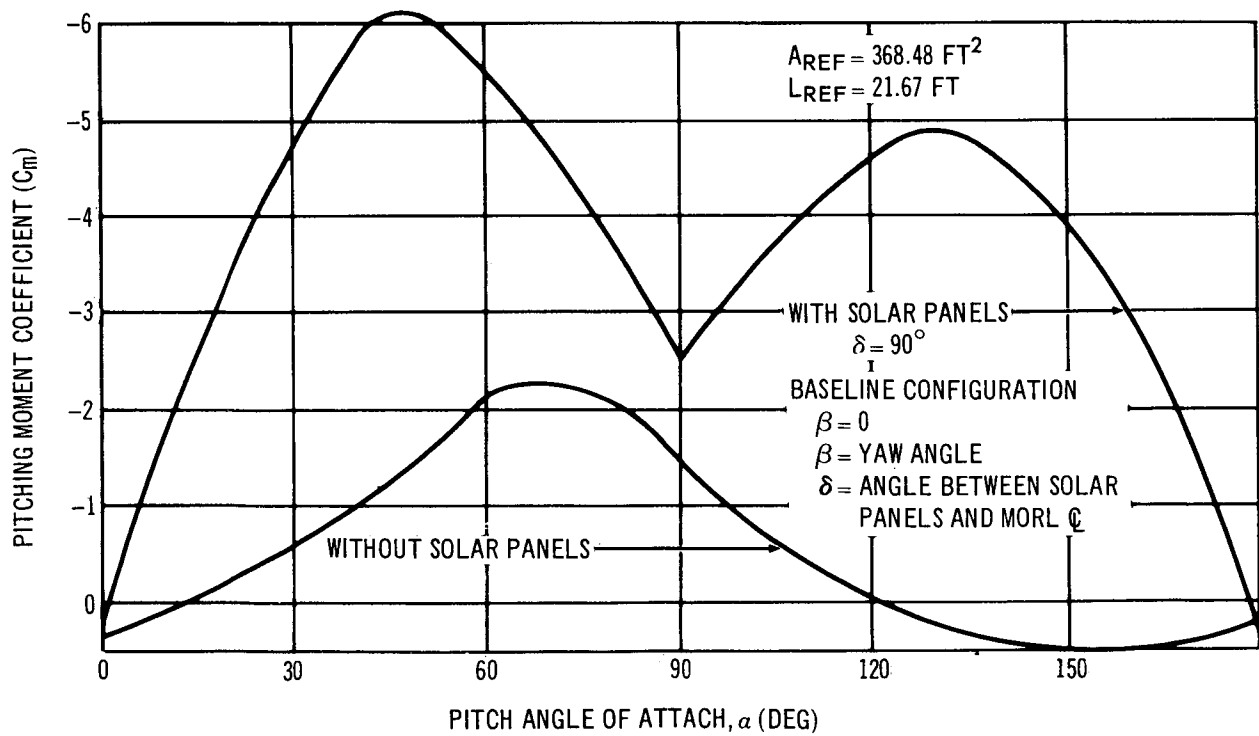


Figure 6-4. MORL Orbital Pitching Moment Coefficient

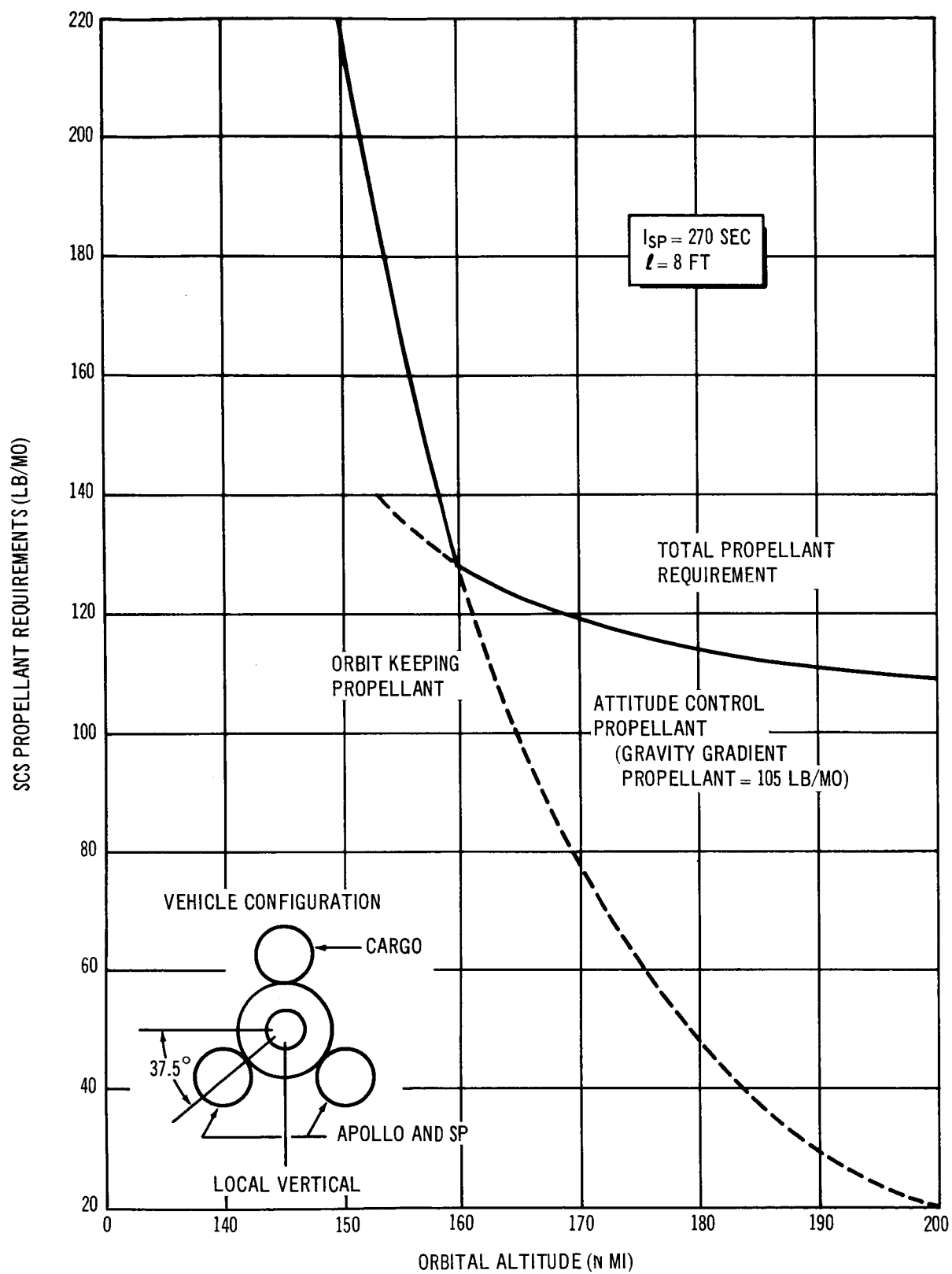


Figure 6-5. SCS Propellant Requirement as a Function of Orbital Altitude for 1972

shown in Figure 6-6 as a function of the laboratory operating altitude. A maximum positive change occurs around 155 nmi. An operating altitude in the range between 145 and 165 nmi is acceptable from a payload consideration standpoint.

6.1.2.2 Orbital Characteristics

A restricted combination of altitudes and inclinations can produce a subsynchronous orbit. A subsynchronous orbit is a class of orbits in which the spacecraft periodically retraces its path over the Earth. The combinations of altitude and inclination that yield this property are shown in Figure 6-7. For example, a satellite at an altitude of 275 nmi and a 50° inclination will retrace its path over the Earth's surface daily; a satellite with the same inclination at an altitude of 192 nmi will retrace its path every second day. In the altitude range of interest there exists an orbit at 164 nmi altitude and 50° inclination that is 3-day subsynchronous. A periodically repeatable orbit accrues some mild benefits for the experiment program and ground operations. Those experiments that require repeated coverage of the same surface areas over long time periods will automatically have this requirement fulfilled. The work schedules and rendezvous launch missions in support of the laboratory can be planned on a regularly scheduled basis.

6.1.2.3 Selection of Operational Altitude for 50° Inclination Mission

The long-term operating altitude for a MORL module in a 50° inclination orbit is recommended at 164 nmi. This altitude is in the region of optimum payload utilization for the mission and provides a subsynchronous orbit with a 3-day period. A typical ground trace covering a 24-hour period of this orbit is shown in Figure 6-8. Launch vehicle payload capability is increased 300 lb. For the MORL/Saturn IB launch, payload in orbit becomes 32,900 lb.

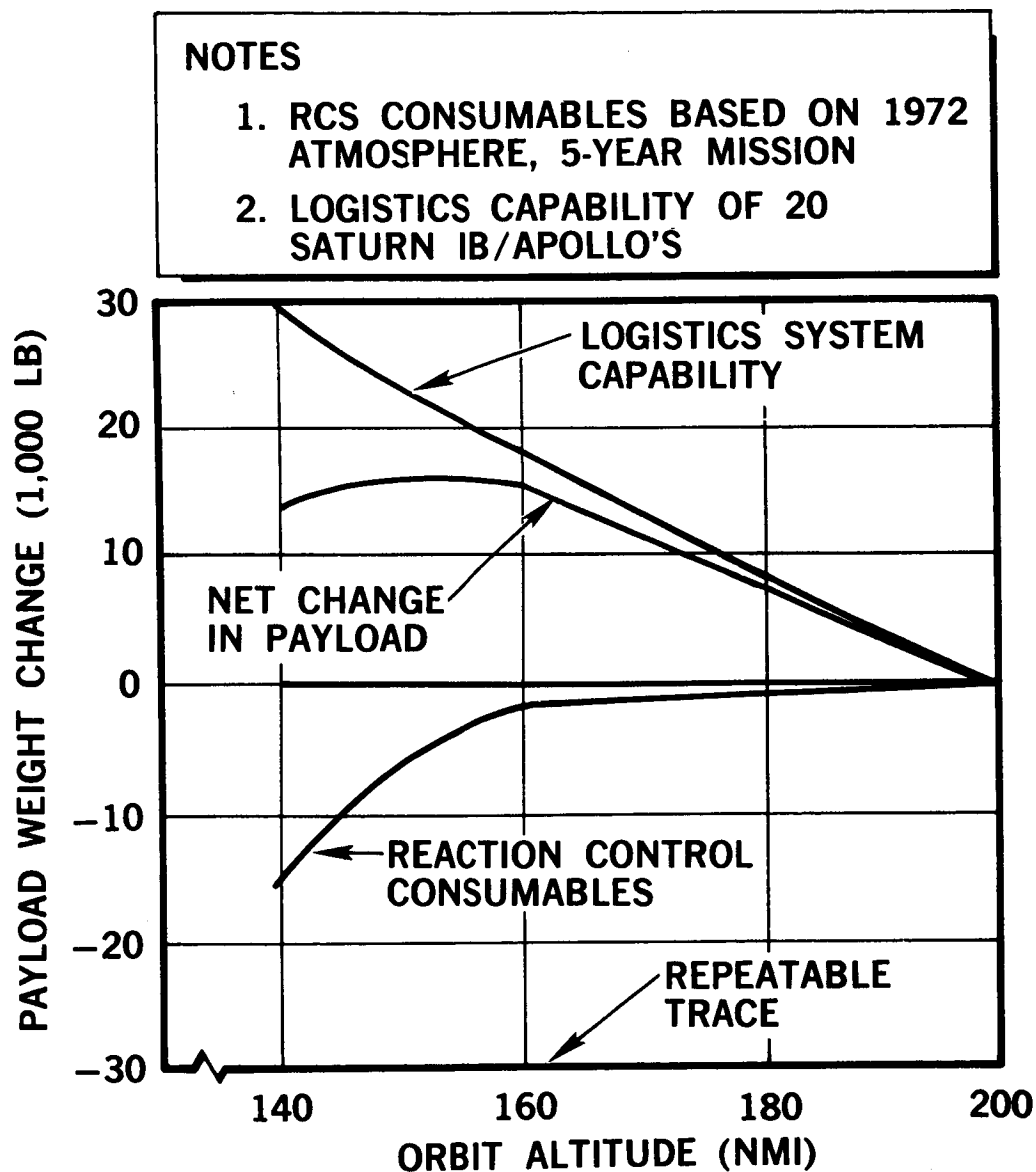


Figure 6-6. Optimum Operating Altitude

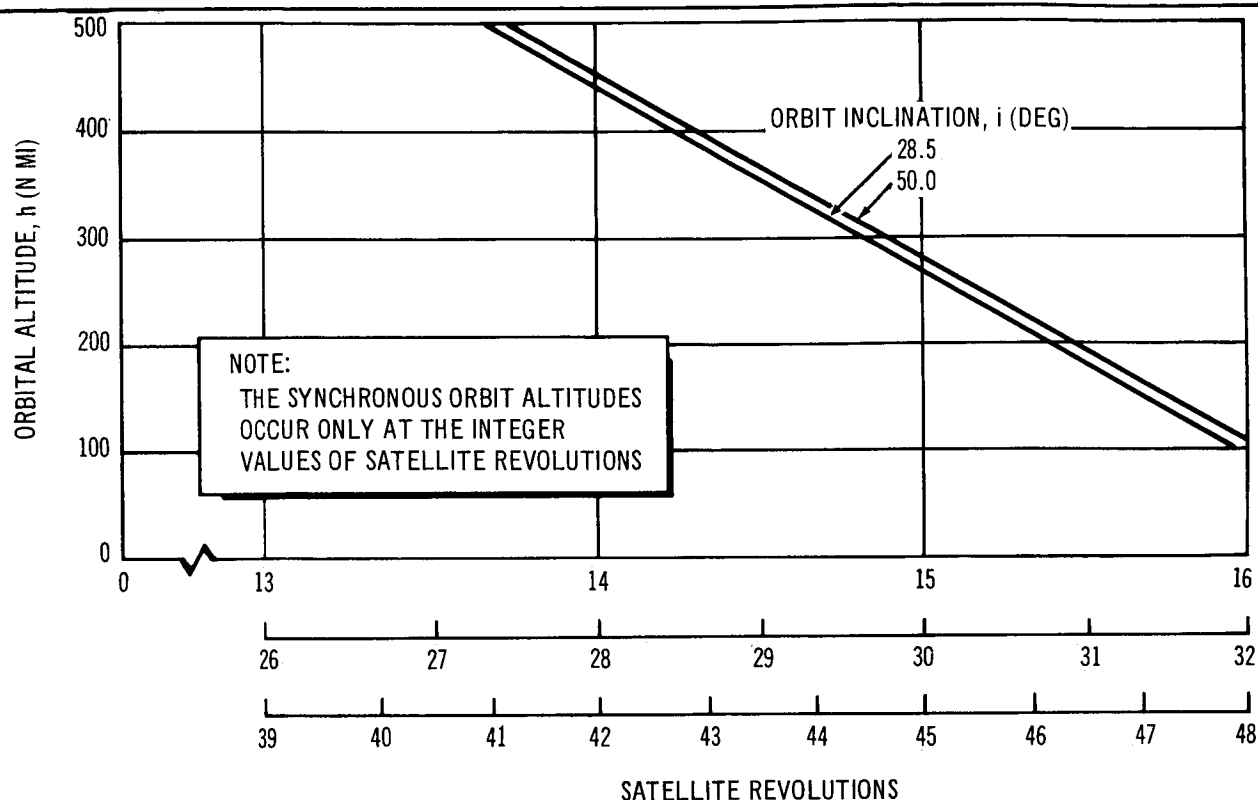


Figure 6-7. Synchronous Orbit Altitudes

The baseline rendezvous profile will be maintained; however, the change in altitude will result in an increase of 570 lb in logistic vehicle payload. This increase is due to a reduction in energy requirements, a decrease in required Apollo de-orbit velocity, and a reduction in the rendezvous impulse error component.

6.2 LABORATORY WEIGHT

The weights of the laboratory and its subsystems are based on the requirements for a 50° inclination 164 nmi altitude mission (baseline). These

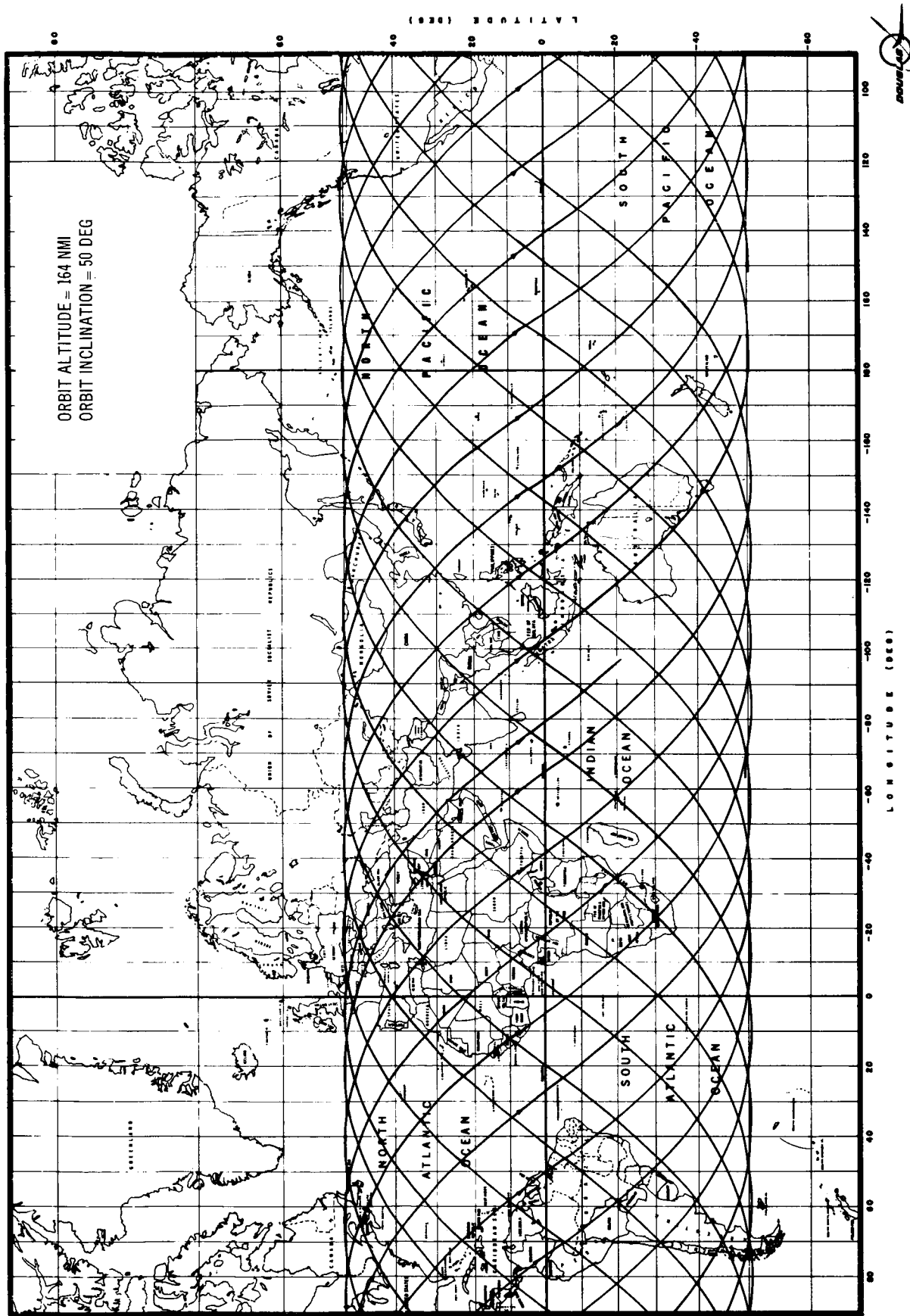


Figure 6-8. Typical MORL Ground Trace

values are presented in Table 6-1. Discrepancies between subsystem weights contained in the summary volumes and in the individual subsystem volumes are noted and accounted for. The summary weight statement contained on pages 2 to 24 of Volume II, Systems Analysis - Mission Analysis and Results, SM-46073, is used to represent the Phase IIa reference weights.

The weight contingency is again taken at 20% of the basic laboratory weight and is intended to account for items erroneously omitted as well as to provide for weight growth. The laboratory dry weight represents the basic laboratory weight without experiments but does include the experimental equipment built into the laboratory, that is, consoles, airlock, and so forth. The laboratory system weight is the weight of the MORL on the launch pad less the discretionary payload, which will, of course, be utilized in the form of additional experiments, supplies/spares. The laboratory effective weight is a term used to compare to the launch vehicle capability to determine discretionary payload; it is the system weight corrected for the nose fairing which is jettisoned after first stage burnout.

6.3 DISCRETIONARY PAYLOAD

The discretionary payload for the baseline MORL mission (50° inclination) is derived as shown in Table 6-2.

Table 6-1 (page 1 of 7)

LABORATORY AND SUBSYSTEM WEIGHTS--BASELINE 50° INCLINATION MISSION

Item	Current Weight (lb)	Reference Weight Phase IIa (lb)	Change in Weight (lb)	Remarks
Structure	13, 841	11, 182	+2, 639	
Laboratory vessel	6, 146			Error in Phase IIa report, -240 lb; changed from curved common bulkhead to a flat bulkhead, +257 lb; changed from a welded to a bolted joint at bulkhead/cylinder interface, +120 lb; increased thickness of aft dome to provide additional radiation protection for 50° inclination mission, +165 lb; increase in length of cylindrical section and added provisions to accommodate isotope power supply, +1, 020 lb.
Hangar/Test area	3, 520			Change from a seven arm to a two arm logistics vehicle stowage-arm system, -572 lb; changed to a radial stowage concept, +104 lb; added an experiment console (less equipment), +15 lb; added an experimental bay, +1, 231 lb; added provisions for Apollo docking omitted in the Phase IIa report, +876.
Meteoroid shield	3, 424			
Airlocks, windows, and hatches	303			

Table 6-1 (page 2 of 7)

Item	Current Weight (lb)	Reference Weight Phase IIa (lb)	Change in Weight (lb)	Remarks
Nose fairing (effective)	65			
Separation provisions	20			
Attaching parts	270			Reduced allowance from 6% to 2% of basic structure and adjusted for above changes, -337.
Thermal protection	93			
Reaction control subsystem	436	789	-353	Changes to the isotope power system, control logic, and propellant (IRFNA/MMH to NTO/MMH) result in lower system weight, -353 lb.
Pressurization system	69			
Propellant feed and leak detection system	76			
Engines	96			
Fairings	9			
Tank Assembly	196			
Environmental control/life support subsystem	2,507	2,374	+133	Error in Phase IIa report, +115 lb; weight changes noted below include corrections for this error and other minor revisions
Atmospheric supply system	848			Changed to H ₂ O electrolysis for O ₂ supply.

Table 6-1 (page 3 of 7)

Item	Current Weight (lb)	Reference Weight Phase IIa (lb)	Change in Weight (lb)	Remarks
Atmospheric purification system	665			Added CO ₂ collection system and reduced heating requirements, +120 lb.
Water management system	228			Added capability for 9-man operation, +68 lb.
Waste management system	45			Combined collection, processing and storage functions, +22 lb.
Compartment conditioning system	129			Added separate air ventilation circuit to Hangar/Test area, +5 lb.
Cooling circuit	131			Decreased radiator tube size and increase radiator area, -142 lb.
Heating circuit	0			Deleted heating circuit because of waste heat availability from isotope power supply, -96 lb.
Heat transport circuit	68			Add heating functions, +28 lb.
Atmospheric pumpdown system	393			Increased storage tank capacity to accommodate additional Hangar/Test area volume generated by the change to a flat bulkhead, +79 lb.

Table 6-1 (page 4 of 7)

Item	Current Weight (lb)	Reference Weight Phase IIa (lb)	Change in Weight (lb)	Remarks
Crew subsystem	714	686	+28	Added required built-in provisions to accommodate a 9-man crew.
Stabilization and control subsystem	770	770	0	
Sensors and associated structure	33			
Momentum storage device	490			
Control electronics	90			
Displays	62			
Inertial platform and electronics	25			
Wire and connectors	70			
Test subsystem	200	200	0	
Communications and telemetry subsystem	733	801	-68	
Telemetry system	55			
Tape recording system	70			
Voice communication system	39			
EVSTC system	16			
Data processing and computing	180			

Table 6-1 (page 5 of 7)

Item	Current Weight (lb)	Reference Weight Phase IIa (lb)	Change in Weight (lb)	Remarks
Television system	119			Deleted rendezvous radar interrogator, aboard the laboratory, originally required for use with an unmanned resupply spacecraft and subsequently retained for back-up capability with the Gemini spacecraft.
Tracking aid system	18			
Digital command system	26			
Facsimile system	30			
File and photo processing	7			
Rendezvous and docking	30			
Antenna system	114			
Displays	23			
Orbit keeping	6			
Miscellaneous electronics	1,174	1,039	+135	
Wire and connectors	595			
Cold plates	40			
Consoles	539			Added provisions for an experimental console in the Hangar/Test area.
Electrical power subsystem	4,402	3,410	+992	Changed from a 6 kW solar cell/battery system to a 11 kW Isotope Brayton Cycle power system.

Table 6-1 (page 6 of 7)

Item	Current Weight (lb)	Reference Weight Phase IIa (lb)	Change in Weight (lb)	Remarks
Fuel block and radiation shield	1,353			
Power conversion unit	1,308			
Power conditioning and energy storage	1,089			
Distribution and protection equipment	519			
Radiation shield insulation	133			
Contingency (20%)	4,955	4,130	+825	Adjusted contingency for above changes
Laboratory dry weight	29,732	25,382	+4,350	
Required payload	2,787	3,080	-293	
Experiments	470	(470)		
Spares	0	(0)		
Onboard supplies	2,317	(2,610)		Decreased propellant requirements due to atmospheric density change, -264 lb; corresponding decrease in pressurant required, -68 lb; increased EC/LS provisions, +15 lb; error in Phase IIa report, +68 lb; reduced laboratory drag, higher impulse propellant and improved control logic, -329 lb.
Laboratory system weight	32,519	28,462	+4,057	

Table 6-1 (page 7 of 7)

Item	Current Weight (lb)	Reference Weight Phase IIa (lb)	Change in Weight (lb)	Remarks
Laboratory effective weight*	32,099	28,042	+4,057	

*The aerodynamic nose fairing, weighing 480 lb, is jettisoned after first stage burnout. As a result of this staging sequence, the fairing has an effective weight of only 60 lb in relation to launch payload weight. This results in a laboratory effective weight that is 420 lb less than the actual laboratory weight.

Table 6-2
DISCRETIONARY PAYLOAD FOR BASELINE MISSION
(164 NMI--50° INCLINATION)

Parameter	Magnitude (lb)
Saturn IB launch vehicle payload capability	32,900
Laboratory effective weight	<u>32,100</u>
Discretionary payload (difference)	+800

The discretionary payloads for the two alternate missions investigated during this study are shown in Tables 6-3 and 6-4.

Table 6-3
DISCRETIONARY PAYLOAD FOR POLAR MISSION
(164 NMI--90° INCLINATION)

Parameter	Magnitude (lb)
Saturn V launch vehicle payload capability (launch azimuth of 44.5° out of ETR)	33,000
Laboratory effective weight*	<u>33,755</u>
Discretionary payload (difference)	-755

*Includes 1,820 lb of radiation shielding.

As described in Task III, Book 1, the preferred launch trajectory for the polar mission involves a launch into a 50° inclination with subsequent orbit plane changes to achieve a 90° inclination. A positive discretionary payload can be obtained without modifying the MORL by using a 146° launch azimuth out of ETR; the Saturn V payload is about 160,000 lb. This trajectory involves a double dogleg with overflights of Cuba and Panama. The operational Saturn IB launch vehicle launched from PMR provides about 33,300 lb capability.

Table 6-4
DISCRETIONARY PAYLOAD FOR SYNCHRONOUS MISSION
(19,350 NMI--28.3° INCLINATION)

Parameter	Magnitude (lb)
Saturn V launch vehicle payload capability	60,625
Laboratory effective weight*	<u>73,935</u>
Discretionary payload (difference)	-13,310

*Includes 42,000 lb of radiation shielding required to sustain the crew for 90 days.

An acceptable solution to provide the required radiation protection for the synchronous mission has not been identified in this study. However, such a solution does exist and can be developed through further analysis. The current uncertainty of the environment at synchronous altitude is about an order of magnitude and the determining factor in shielding requirements. The corresponding variation in required shield weight is 4,400 to 110,000 lb.

PRECEDING PAGE BLANK NOT FILMED.

Appendix A
AXIAL HANDLING AND STOWAGE SYSTEM
(ALTERNATE STUDY)

The axial handling and stowage systems provide facilities for the storage and handling of the logistic vehicle and its two separate components, the Apollo spacecraft and the multimission module. Seven stations for stowing components of the logistic vehicle are provided.

A.1 SYSTEM DESCRIPTION

The axial stowage and handling configuration is shown in Figure A-1 and A-2. In Phase IIa baseline, clearances between the stowed vehicles were less than 2 in. when the logistic vehicles were left attached to the stow arms and stowed next to the hangar shell. Using the two-arm stow system, the rotary ring movement tolerance may increase the misalignment in the placement of the vehicles at the stow station, and longer stow arms will increase the arm deflections at the end of travel. Therefore, the distances between the stowed vehicles should be increased to provide sufficient clearances and reduce the possibilities of contact. To increase the clearance between the stowed vehicles, it is necessary to move each stowed vehicle a longer distance from the longitudinal axis. Adding pads on the large diameter of the MORL and on the side of the logistic vehicle increases the storage position diameter, resulting in added clearance between the stowed vehicles. By placing the MORL pad at the beginning of the 260-in. diameter, it is possible to extend the hangar shell cone to the top of the pad; this results in a faired contour that relieves the necessity of providing a fairing during the launch phase. To secure and hold the logistic vehicle during storage, a four-latch cluster is installed in each MORL pad, and corresponding catches are structurally attached to each logistic vehicle pad. These are shown in Figure A-3, Sections D-D, M-M, and P-P. An electrical jack screw actuator is provided to lock and open the latch cluster. For the launch phase of both the MORL

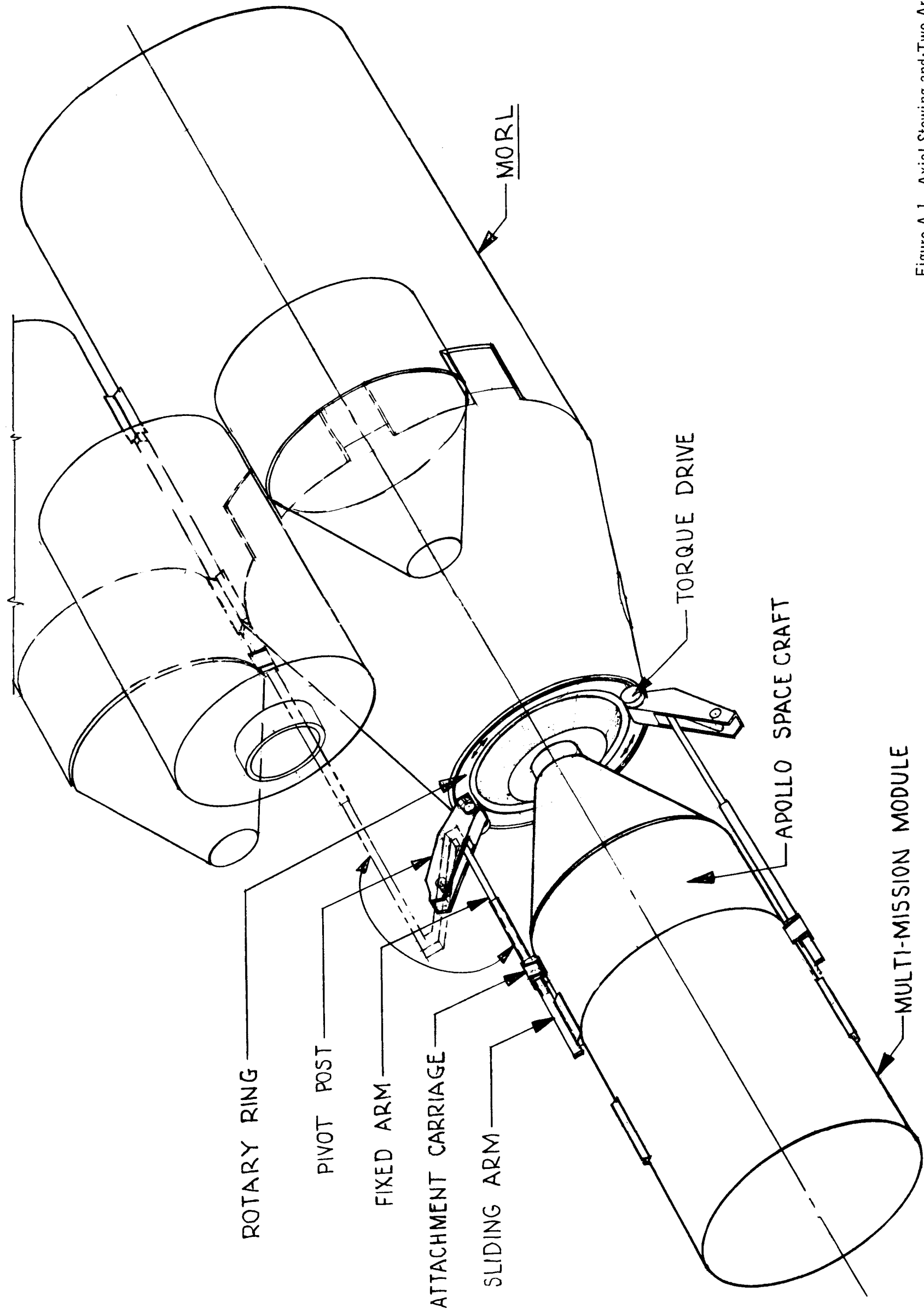
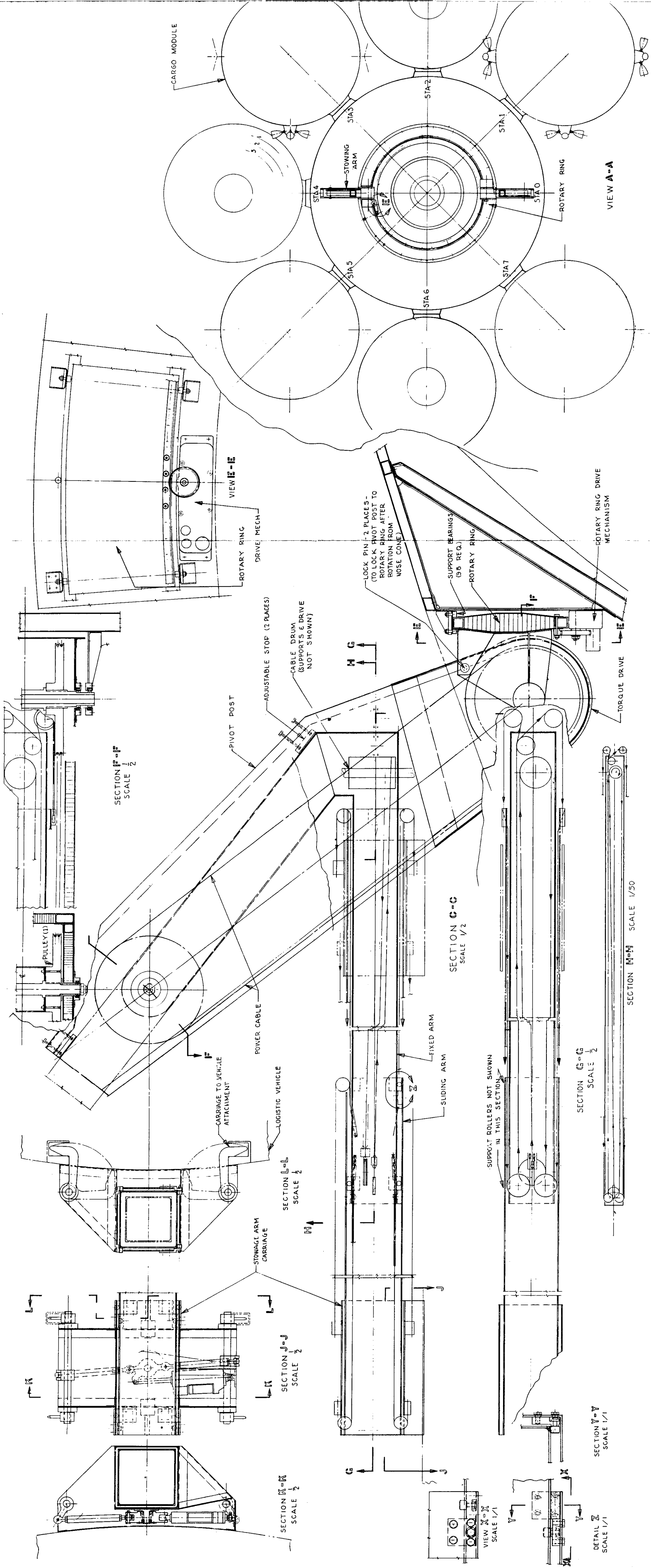


Figure A-1. Axial Stowing and Two-Arm Handling System

2462



247-2

247-1

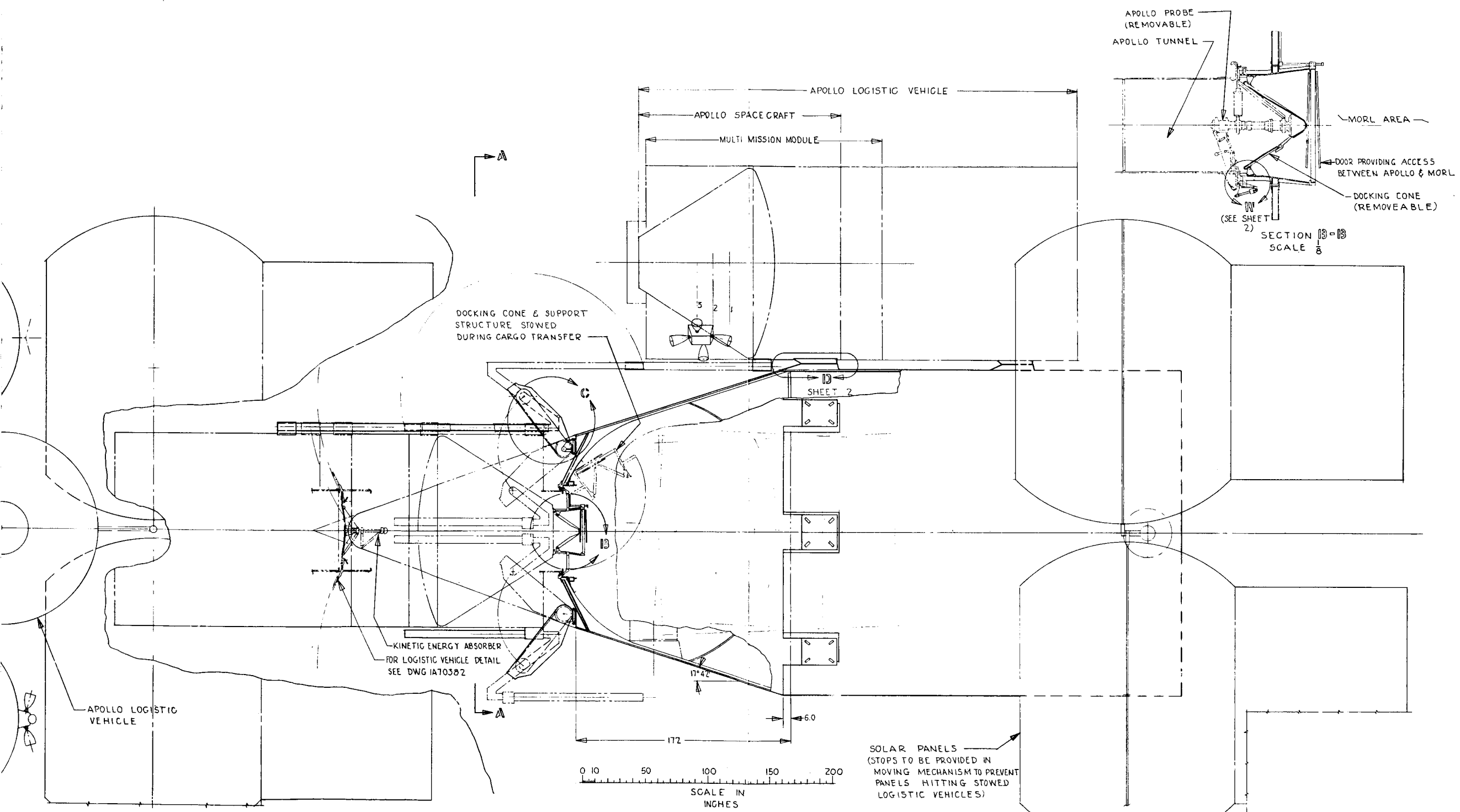


Figure A-2. Two Arm Handling System Details

247-#39



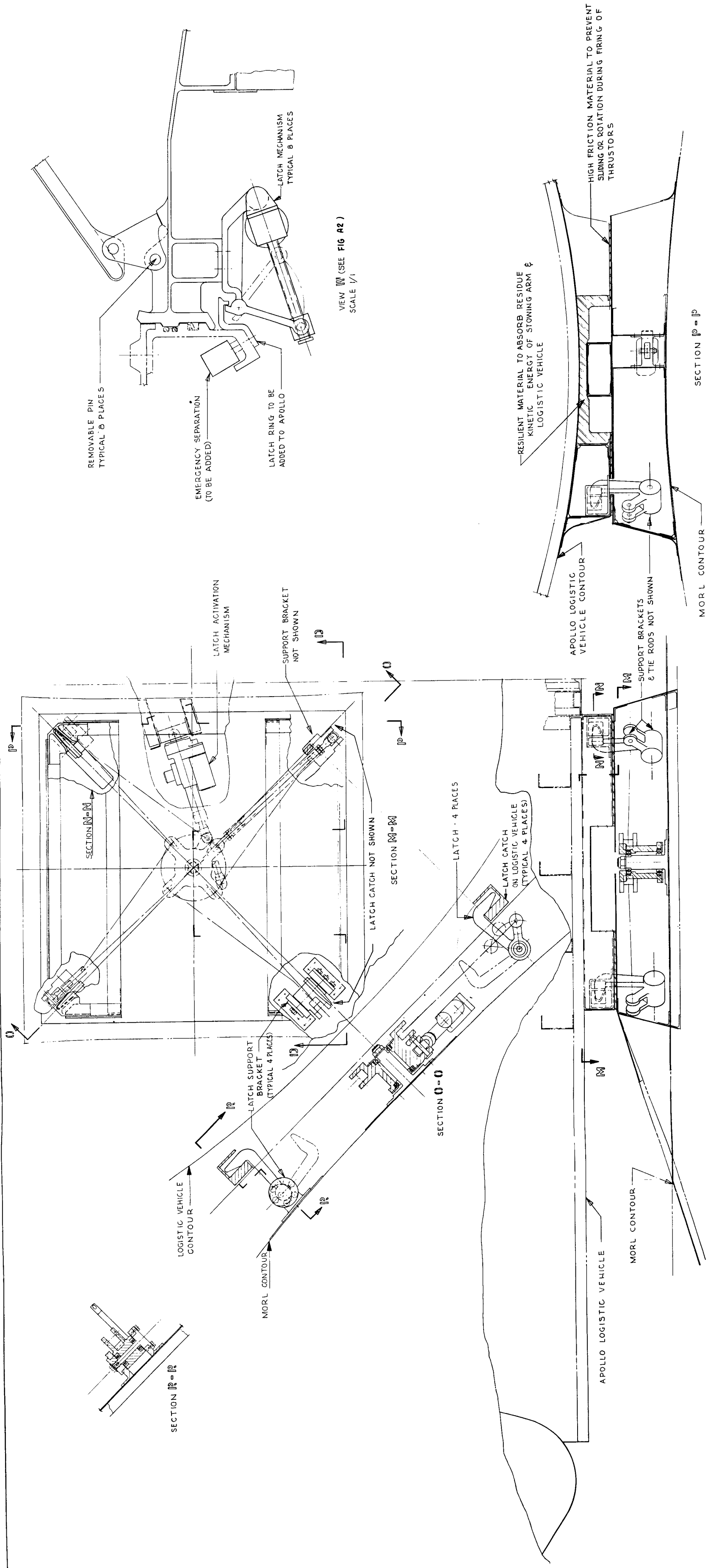


Figure A-3. Apollo Logistic Vehicle Stowing Details

248-1

248-2

248-3

and the logistic vehicle, covers are provided for each pad to provide a smooth aerodynamic form. These are jettisoned, along with the nose cone and the other fairings, shortly after first stage burnout to provide maximum launch capability.

Essentially the components of the baseline handling system, discussed in Section 2.2.2, and the axial handling concept are the same, except for the sliding arm, nonrotating sliding carriage, and method of achieving the rotary motion.

In this concept, to place the Apollo spacecraft in the storage location requires a long arm, while for the multimission module only a short arm is needed. Conversely in both cases, return of the arm for the next transfer operation requires that the arm be shortened still further, to clear the stowed vehicle. To meet the conditions of maximum and minimum length, an outer arm sliding over a fixed arm is provided. The stow arm assembly consists of a fixed arm pivoted at the pivot posts, a movable arm free to slide over the fixed arm, a powered cable system to extend and retract the movable arm, and a fixed cable system to move the carriage as the movable arm is extended or retracted.

In this system, the carriage does not have to be revolved or rotated about the arm centerline. Both the movable arm and the carriage are fitted with bearings, adjusted to minimize the play between the two sliding surfaces. Carriage latches are used to attach the arm assembly to the logistic vehicle. Located on the front face of MORL is the rotary ring with two attached arm assemblies, held in position by cam-follower bearings. Rotation is achieved by a spur gear driving a large gear attached to the rotary ring. To provide a high degree of reliability, two redundant drive units will be installed.

For relationship and arrangement of the above items to the balance of the system, see Figure A-2, Section C-C.

A. 2 STOWING SEQUENCE

Basically, except for minor variations, the handling or stowing sequence for this concept is the same as that described for the baseline system in Section 2.2.2

Differences in the two concepts that change a few steps in the procedure are:

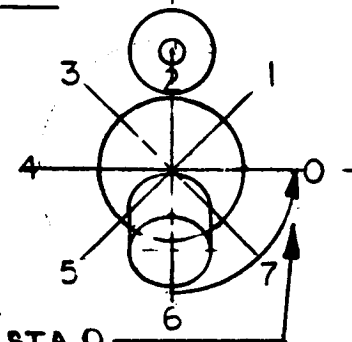
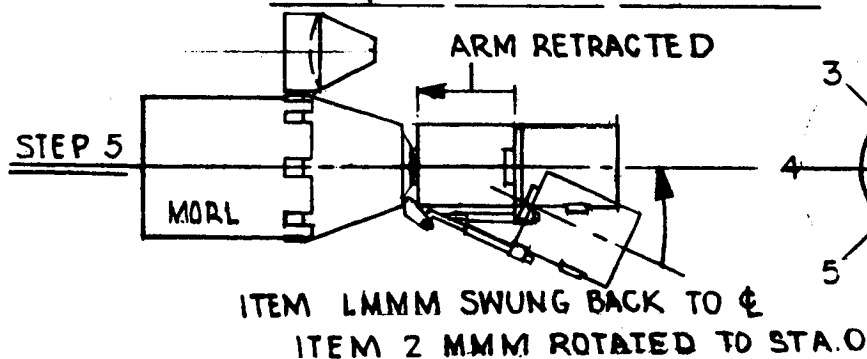
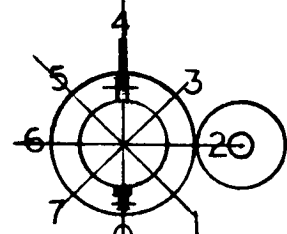
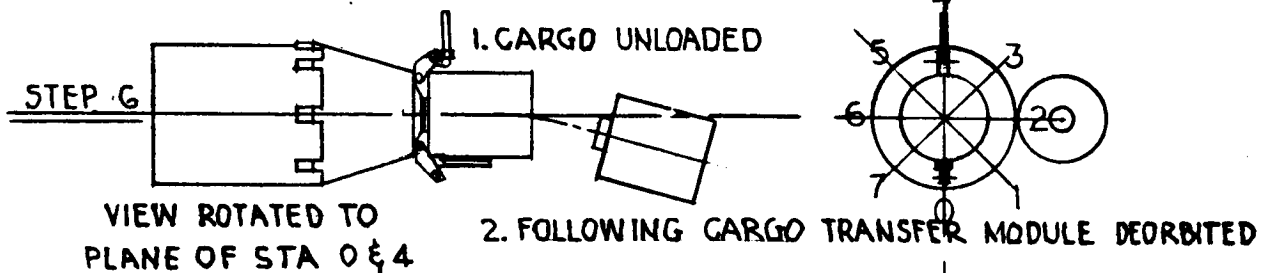
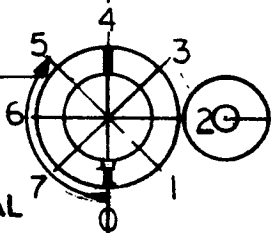
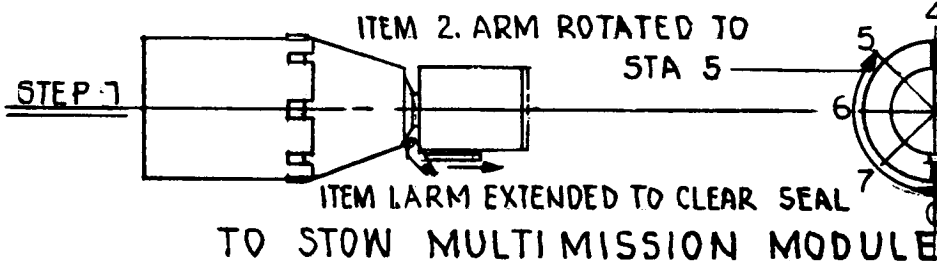
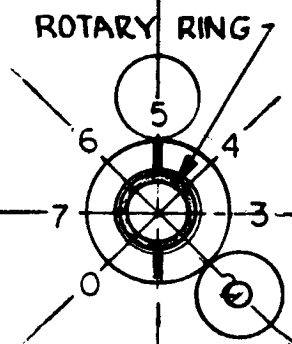
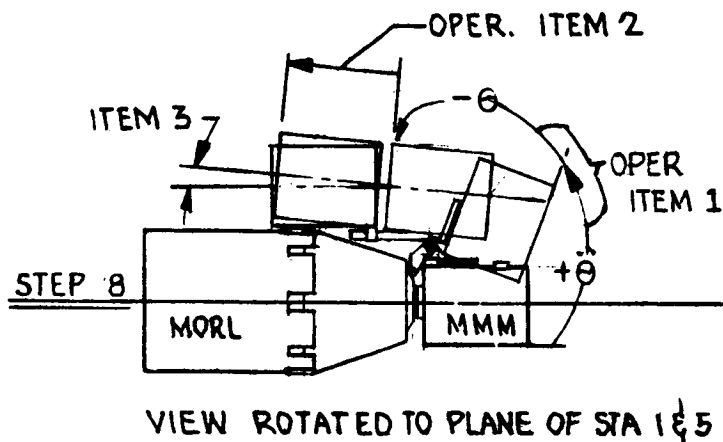
Baseline	Alternate
1. Radial stow Requires opening of meteoroid door before stowing	1. Axial stow No advanced preparation after fairings are jettisoned
2. Multimission module A. Requires Apollo docking ring adapter to tie to stow station B. Smaller door openings C. Adapter cone and ring must be removed before unloading large packages at docking station	2. Multimission One door for entrance to interior
3. Single stow arm	3. Telescoping stow arms
4. Attaching carriage Rotation around centerline axis of arm	4. Attaching carriage No rotation capability needed
5. Movable dolly Each carriage has independent motion	5. Rotating tracks Both arms fixed and rotate together

The stowing sequence is illustrated in Figure A-4. Steps to be followed are the same as described in Section 2.2.2, except for the following modifications:

Steps 1 and 2

Same as Section 2.2.2. As the stow pads are located on the exterior of MORL and access to the interior of the hangar area is not provided,

- OPERATION - STEP 8
 ITEM 1. MMM SWUNG
 ↓ 2. ARM EXTENDED TO MATE MMM TO MORL
 ↓ 3. MMM SWUNG TO LATCH TO MORL



OPERATION STEP 4

- ITEM 1. JOINT BETWEEN SPACECRAFT & MMM SEPARATED
2. MMM SWUNG TO CLEAR SPACE CRAFT
3. SPACECRAFT SWUNG
4. ARM EXTENDED TO MATE SPACECRAFT TO MORL
5. SPACECRAFT SWUNG & LATCHED TO MORL

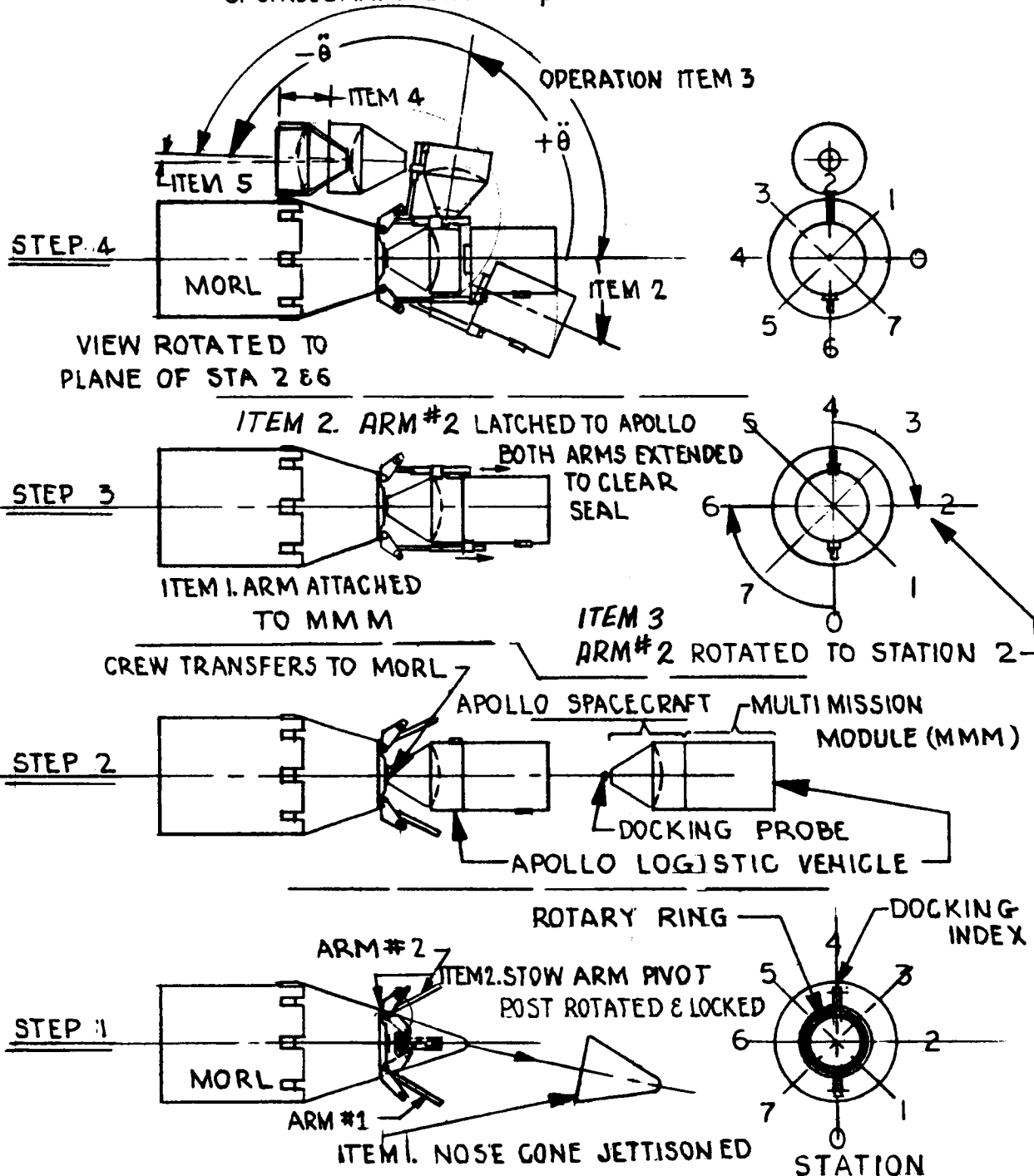


Figure A-4. Axial Stowing and Handling System Sequence

To unload cargo, the MMM is returned to the docking port. Again, in Figure A-3, steps to be followed are the same as described in Section 2.2.2, with the following differences:

Step 5

- Item 1 and 2. Same as Section 2.2.2. In the baseline system, an Apollo adapter ring was added to the MMM. In this concept, all that is required to enter the pressurized cargo section of the MMM is to open the hatch door.
- Item 3. The door in the MMM passageway leading to the cargo space is opened (not shown).

Step 6

- Item 1. Same as Section 2.2.2.
- Item 2. Same as Section 2.2.2.

Step 7

To stow the multimission module after cargo unloading, the sequence is similar to the baseline operation, except for the elimination of the procedure of removing the Apollo adapter ring and cone from the MMM, the elimination of the need to rotate the attaching carriage about the centerline of the arm and the adding of the operation of extending the movable arm to mate the MMM to the stow pad.

- Item 1. Starting with the MMM at the docking station. MMM internal door swung closed and locked. MMM passageway depressurized. MORL pressure seal deflated and lock ring holding MMM to MORL released. Arm No. 1, telescoping portion extended, moving the MMM to clear the MORL seal and latch ring.
- Item 2. Rotary ring rotates Arm No. 1 and MMM to plane of stow station No. 5.

Step 8

- Item 1. Arm No. 1 torque motor is activated and swings the MMM away from the MORL docking and unloading station.

- Item 2. At approximately 55° of swing, the telescoping arm is extended to place MMM in the proper position to mate with the stow attachments.
- Item 3. Arm swing continued until the MMM is mated to the stow station.
- Item 4. Latches are activated, latching the MMM to MORL (not shown).
- Item 5. Arm attaching carriage unlatched (not shown).
- Item 6. Telescoping arm retracted to shortest length and swung to clear stowed vehicle (not shown).

A.3 DESCRIPTION OF OPERATIONAL CYCLE

This procedure is similar to the operational cycle described in Section 2.2.2. The change in the position of the stow locations has created some basic differences in the stow cycle. With the baseline system, the final length of the stow arm is considerably shorter than with the alternate system. However, the problems of the elastic body, the natural frequency of vibration, and the dissipation of kinetic energy are similar. As shown in Figures A-5 and A-6, a bumper strip of resilient material has been installed on the stow vehicle and a bumper post has been installed on the MORL platform. With the end of the arm and logistic vehicle stopped just clear of the MORL platform, but vibrating or moving with a natural frequency, the next step is to dissipate this kinetic energy. First, the logistic vehicle is moved closer to the MORL stow platform. Depending upon the type of disturbances, the resilient material will strike the bumper post either on the sides or top. To dampen the oscillations, the friction surface of the logistic platform is dragged or rubbed over the surface of the MORL platform. After all oscillations have stopped and the kinetic energy of the system has been absorbed, the resilient material, which has acted as the deflection agent, will now be resting on the top of the bumper post.

The final operation of stowing is to actuate the stow latches on the MORL platform. As the latches contact the catches on the logistic vehicle, the resilient material will be compressed, allowing the two vehicles to be locked together.

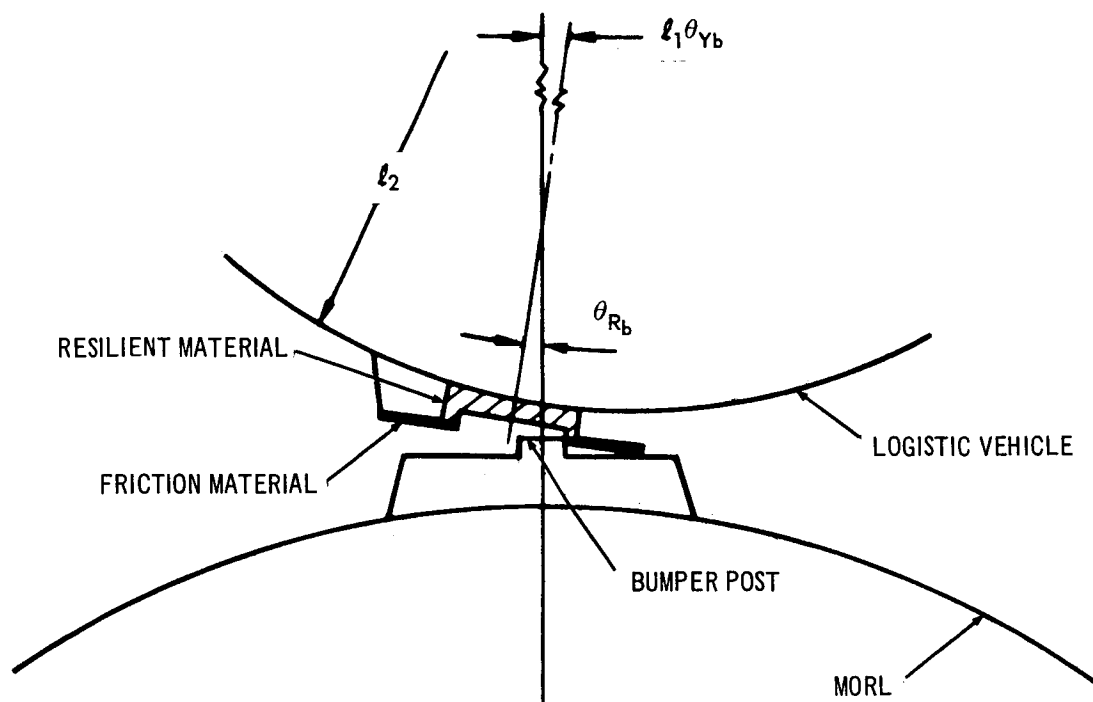


Figure A-5 Vehicles Being Stowed

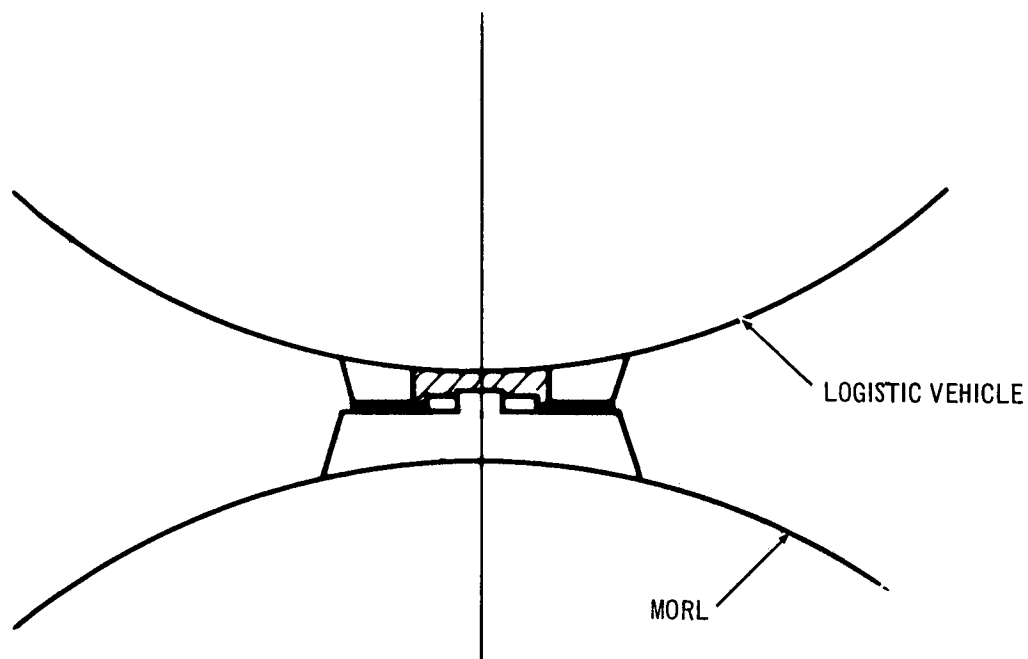


Figure A-6. Vehicles in Stowed Position

A. 4 DYNAMIC ANALYSIS

The following text, equations, and illustrations describe the dynamic analysis problems and solutions.

A. 4.1 Stowing Arm Load Requirements

For the analysis of the stowing arm load requirements, the multimission module is rotated from the docked position to the stowed position about an axis parallel to the MORL pitch axis. The pivot point is located on the front end of the frustum cone of MORL, off the longitudinal axis.

For any yaw or roll disturbance, the stowing arm is (effectively) rigidly attached to the MORL and resupply craft, since the pivot has only one degree of freedom. In the pitch plane, the stowing arm is attached to the resupply craft but pivoted at the MORL connection. By using a reversible torquer to drive the arm, the largest pitch disturbance that can be transmitted is the torque capacity of the torquer motor.

With the reaction control system maintaining the orientation of MORL, the stowing of the logistic vehicle becomes a pure rotational movement. The equation to determine the torque requirements is:

$$\begin{aligned} T &= I_1 \ddot{\theta} + \Delta f \\ I_1 &= I + Md^2 \end{aligned} \quad (A-1)$$

where

Δ_f = torque resulting from friction in rotating parts and torquer internal losses.

I_1 = inertia of resupply craft about the pivot post in slug-ft².

I = inertia of resupply craft about its CG in slug-ft².

M = mass of resupply craft in slugs (= 932 slugs).

d = distance between resupply craft CG and pivot point of the stowing arm (= 18 ft).

$\ddot{\theta}$ = acceleration in radians/sec².

θ = transfer angle in radians.

$$\begin{aligned} I_1 &= 92,000 + 932 \times 18^2 \\ &= 0.4 \times 10^6 \text{ slug-ft}^2 \end{aligned}$$

For an operation time of 5 min. the transfer cycle would be broken down into approximately 130 sec for the initial angular movement over the first 90°, 130 sec to slow the unit to zero velocity, and the remaining time to dampen the natural frequency of the beam.

$$\theta = 1/2 \ddot{\theta} t^2$$

$$\ddot{\theta} = \frac{2\theta}{t^2}$$

$$\theta = \frac{2 \times \frac{90^\circ}{57.3}}{130^2} = 1.86 \times 10^{-4} \text{ rad/sec}^2$$

$$\begin{aligned} T &= 0.4 \times 10^6 \times 1.86 \times 10^{-4} + \Delta f \\ &= 74 \text{ lb ft} + \Delta f \end{aligned}$$

use of a 100 lb-ft torquer provides up to 26 lb-ft for the Δf function.

The largest yaw and roll disturbances (1,600 lb-ft), are due to firing of the attitude control thrusters. The disturbances caused by crew motion, aerodynamic forces, and gravity-gradient torques were found to be much smaller than that of the attitude control thrusters.

The dynamic equations for the yaw motion are as follows (also see Figure A-7):

$$T_Y = I_1 \ddot{\theta}_{Y1} + K (\theta_{Y1} - \theta_{Y2}) \quad (\text{A-2})$$

$$0 = I_L \ddot{\theta}_{Y2} - K (\theta_{Y1} - \theta_{Y2}) \quad (\text{A-3})$$

where

$$\ddot{\theta} = \text{acceleration in rad/sec.}^2$$

$$M_2 = \text{mass of resupply craft in slugs}$$

$$I_2 = \text{inertia of resupply craft about its CG in slug-ft}^2.$$

$$I_L = I_2 + M_2 d^2 = 0.4 \times 10^6 \text{ slug-ft}^2.$$

$$d = \text{distance between resupply craft CG and pivot point of the stowing arm.}$$

$$I_1 = 0.2 \times 10^6 \text{ slug-ft}^2 \text{ (inertia of MORL about its CG).}$$

$$M_1 = \text{mass of MORL in slugs.}$$

$$T_y = \text{yaw torque} = 1,600 \text{ lb-ft.}$$

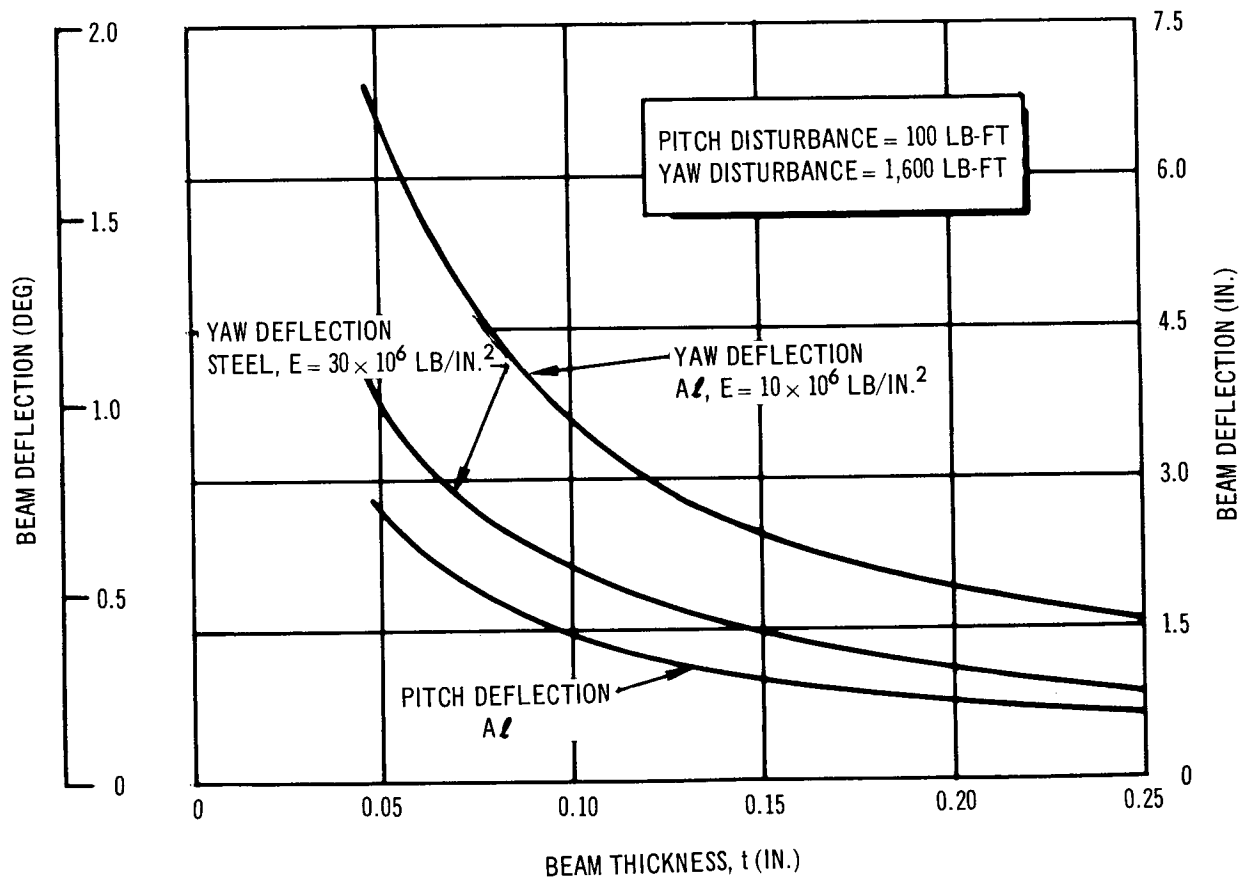
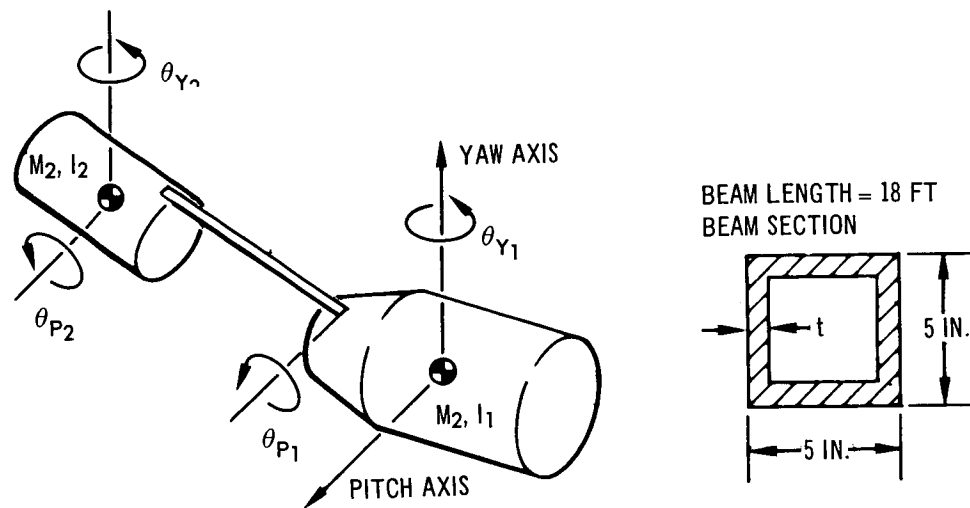


Figure A-7. Pitch and Yaw Beam Deflections

$$\begin{aligned}
K &= \frac{EI}{2L} \text{ (lb-ft/rad) - beam spring constant} \\
E &= 10 \times 10^6 \text{ lb/in.}^2 \text{ (modulus of elasticity for aluminum).} \\
I &= \text{in.}^4 \text{ (section inertia of beam).} \\
L &= 18 \text{ ft} \times 12 = 216 \text{ in.} \\
\beta &= \text{natural frequency.}
\end{aligned}$$

The beam deflection obtained from Equations A-2 and A-3 is

$$\theta_{Yb} = \theta_{Y1} - \theta_{Y2} = \frac{T_Y}{I_1 \beta_Y^2} = 1 - \cos \beta_Y t \quad (\text{A-4})$$

where

$$\beta_Y^2 = K \frac{I_1 + I_L}{I_1 I_L} \quad (\text{A-5})$$

The yaw deflection caused by the yaw thruster firing is plotted in Figure A-7. This plot shows the deflection in degrees and inches vs the beam thickness for both steel and aluminum beams.

In rotating the resupply craft into a stowed position, any beam deflection in yaw will result in misalignment of the locking hooks for holding the resupply craft to MORL. For the nominal aluminum beam with a thickness of 0.1 in., this misalignment is 3.7 in.

Again, with the aid of Figure A-7 the pitch motion is given by the following:

$$K\theta_{P1} = I_L \ddot{\theta}_{P2} + K\theta_{P2}$$

where K and I_L are the same as previously defined.

also

$$\theta = \frac{1}{2} \frac{T_P}{I_L} t^2 \text{ for } t \leq t_1 \quad (\text{A-6})$$

The pitch deflection in the beam is obtained from Equation A-6 as

$$\theta_{Pb} = \theta_{P1} - \theta_{P2} = \frac{T_P}{I_L \beta_P^2} (1 - \cos \beta_P t) \quad (\text{A-7})$$

where

$$\beta_P^2 = \frac{K}{I_L}$$

and

$$T_P = 100 \text{ lb-ft} \quad (\text{A-8})$$

The pitch deflection vs beam thickness is also shown in Figure A-7. It is noted to have a smaller amplitude than the yaw because of the smaller disturbance.

With the resupply craft almost in the stowed position, a pitch disturbance could cause an impact between the resupply craft and MORL because of the vibration of the beam. Figure A-8 shows the pitch impact load for various aluminum beam thicknesses. The kinetic energy for the impact load is obtained by differentiating Equation A-7 to obtain the velocity. Again for the nominal beam thickness of 0.1 in., and an assumed impact deflection of 0.1 in., the impact load is quite small (43 lb). Assuming MORL can withstand a maximum impact load of 500 lb, the assumed pitch impact deflection could be decreased to 0.01 in., which may be more realistic. Use of resilient material, as shown in Figures A-4 and A-5, would absorb the impact load and reduce the pitch load on MORL to an absolute minimum.

The dynamic equations for roll are obtained with the aid of Figure A-9. These are as follows:

$$T_R = J_1 \ddot{\theta}_{R1} + K_T (\theta_{R1} - \theta_{R2}) \quad (\text{A-9})$$

$$0 = J_2 \ddot{\theta}_{R2} - K_T (\theta_{R1} - \theta_{R2}) \quad (\text{A-10})$$

where

$$T_R = 1,600 \text{ lb-ft}$$

$$J_1 = 0.120 \times 10^6 \text{ slug-ft}^2$$

$$J_2 = 0.0445 \times 10^6 \text{ slug-ft}^2$$

$$K_T = \frac{\pi G (D_o^4 - D_i^4)}{32L} \text{ (lb in. / rad) (torsional beam spring constant)}$$

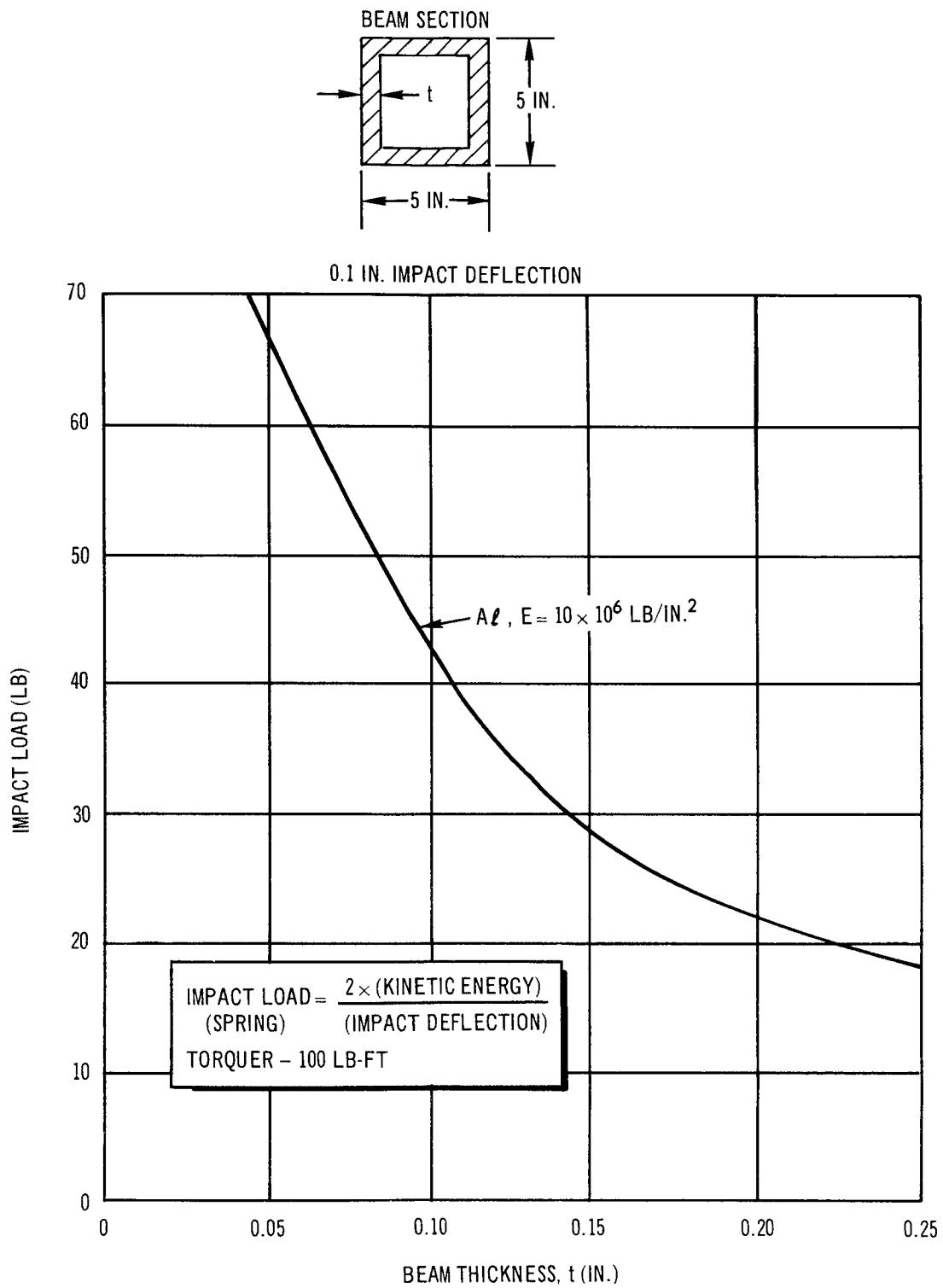


Figure A-8. Pitch Impact Load Caused by Torque

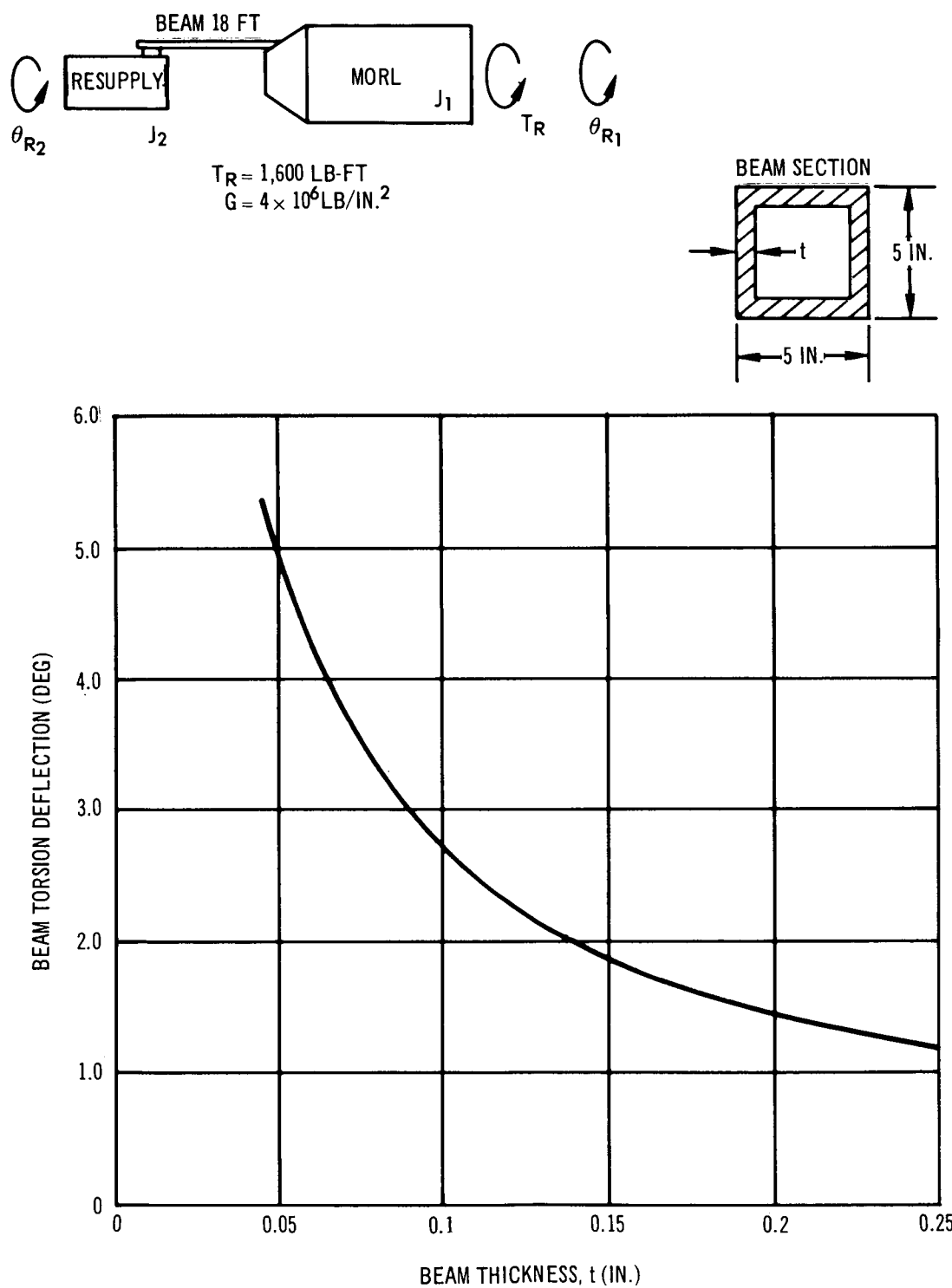


Figure A-9. Beam Torsion Deflection Caused by Roll Thrusters

$$L = 18 \text{ ft}$$

$$G = 4 \times 10^6 \text{ lb/in.}^2 \text{ (aluminum shear modulus)}$$

The beam torsional deflection is obtained from Equations A-9 and A-10 as the following:

$$\theta_{Rb} = \theta_{R1} - \theta_{R2} = \frac{T_R}{J_1 \beta_R^2} (1 - \cos B_R t) \quad (\text{A-11})$$

where

$$\beta_R^2 = K_T \frac{J_1 + J_2}{J_1 J_2} \quad (\text{A-12})$$

Figure A-9 shows the effect of a roll thruster disturbance on the torsional deflection of aluminum and steel beams of various beam thicknesses. The deflection caused by a roll disturbance is larger than the others.

A combination of roll and yaw motion can produce an impact load while storing the resupply craft. This impact load is produced by a yaw misalignment and a roll tilting of the stowing pad on MORL relative to the storing pad on the resupply craft. As shown in Figure A-5, the resilient material will strike the side edge of the center bumper post.

θ_{Rb} is the roll deflection of the beam and θ_{yb} is the yaw deflection of the beam.

Assuming a yaw and roll thruster firing, the impact velocity is obtained by differentiating Equations A-4 and A-11 and using the small angle approximation. The impact velocity is given as:

$$\begin{aligned} V_{Y-R} &= T_C \frac{I_2}{J_2 \beta_R} + \frac{I_1}{I_m \beta_Y} \sin \psi \cdot \theta_{Rb} \\ &= \frac{T_C^2}{J_2 \beta_R^2} \times \frac{I_2}{J_2 \beta_R} + \frac{I_1}{I_m \beta_Y} \sin \psi (1 - \cos \psi) \end{aligned} \quad (\text{A-13})$$

with

$$T_C = T_R = T_Y = 1,600 \text{ lb-ft}$$

Figure A-10 is a plot of the impact load, assuming 0.1-in. impact deflection for various aluminum beam thicknesses. The velocity in Equation A-13 is taken to be the maximum at the time of impact. Figure A-10 shows that the impact load is quite small (12 lb) for the 0.1-in. beam wall thickness.

Since the impact loads for the 0.1-in. impact deflection are shown to be small, one other possible parameter as a function of beam thickness will be considered. This parameter is the time to reduce the initial disturbance to 1 in. of pitch, yaw, or roll deflection for a structural damping coefficient of 0.7%. The time parameter is plotted in Figure A-11 vs beam thickness for the roll and yaw disturbances. Figure A-11 illustrates that it takes over 6 min. to damp the roll deflection to 1 in. for the 0.1-in. thick beam.

Figure A-12 is the same as Figure A-11, except that it is for the pitch axis deflection. As the beam is increased to about 0.2 in. thickness, the maximum beam deflection is less than 1 in. for the assumed pitch disturbance.

Since the torque requirement for stowing is a function of time, the size and weight of the torquer may be reduced by increasing the time spent in performing the angular movement. Changing the time from 130 sec to approximately 200 sec for the initial 90° of movement increases the total time for a transfer operation from approximately 5 min. to 7 min.

The size of the torquer is as follows:

$$\begin{aligned}
 T &= I_1 \ddot{\theta} + \Delta f \\
 \ddot{\theta} &= \frac{2\theta}{t^2} = \frac{2 \times 1.5708}{200^2} = 0.79 \times 10^{-4} \text{ rad/sec}^2 \\
 T &= 0.4 \times 10^6 \times 0.79 \times 10^{-4} + \Delta f = 31.6 \text{ lb-ft} + \Delta f \quad (\text{A-14})
 \end{aligned}$$

The use of a 50-lb-ft torquer provides up to 18 lb-ft for the Δf function.

A. 4. 2 Conclusions

1. The maximum loads in orbit are induced by RCS thruster firing in the roll and yaw axes. In the absence of thruster firing, crew motion produces the next largest disturbance (about 10% of the thruster disturbance). The disturbance load applied in the pitch

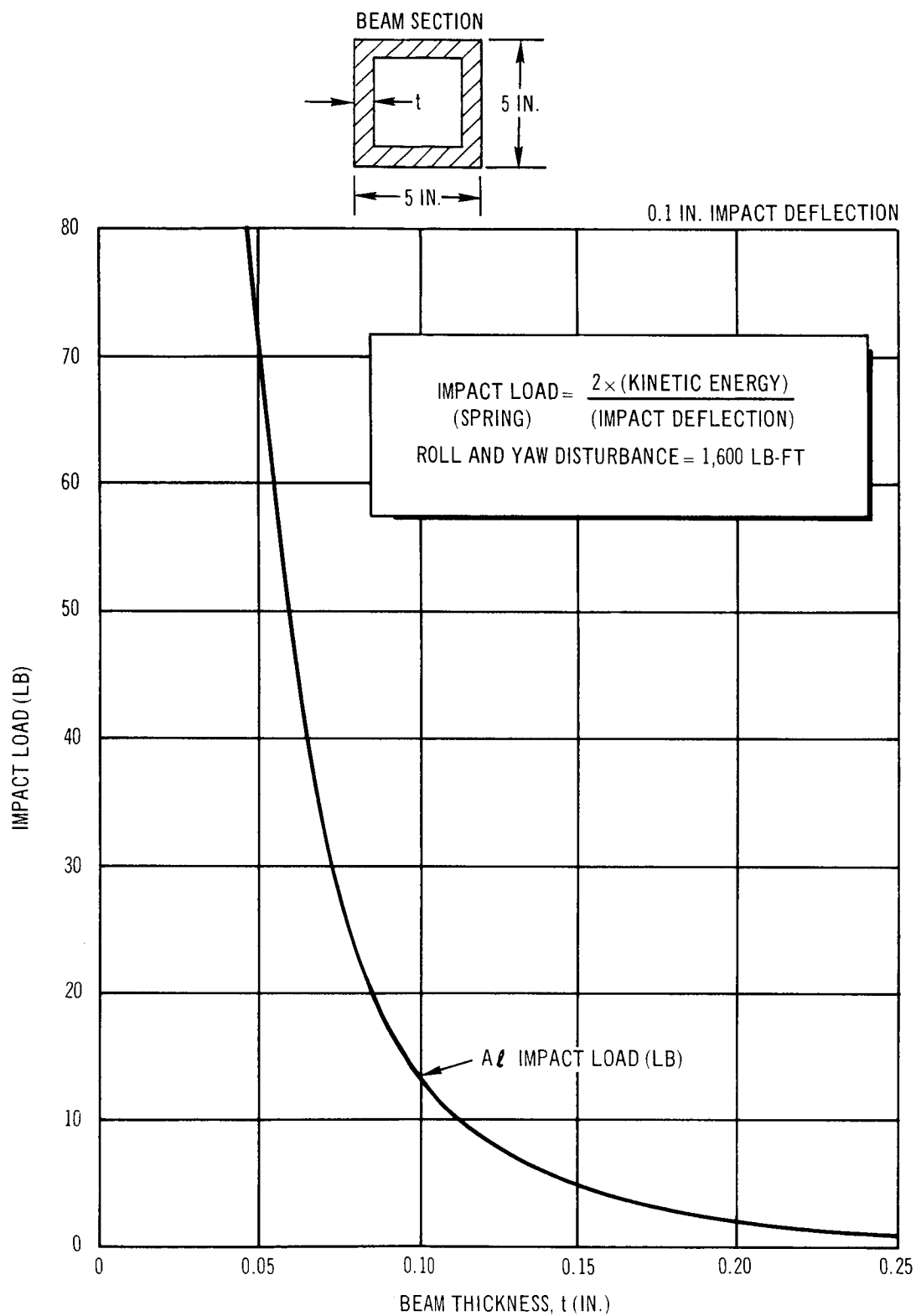


Figure A-10 Impact Load Caused by Roll and Yaw Disturbance

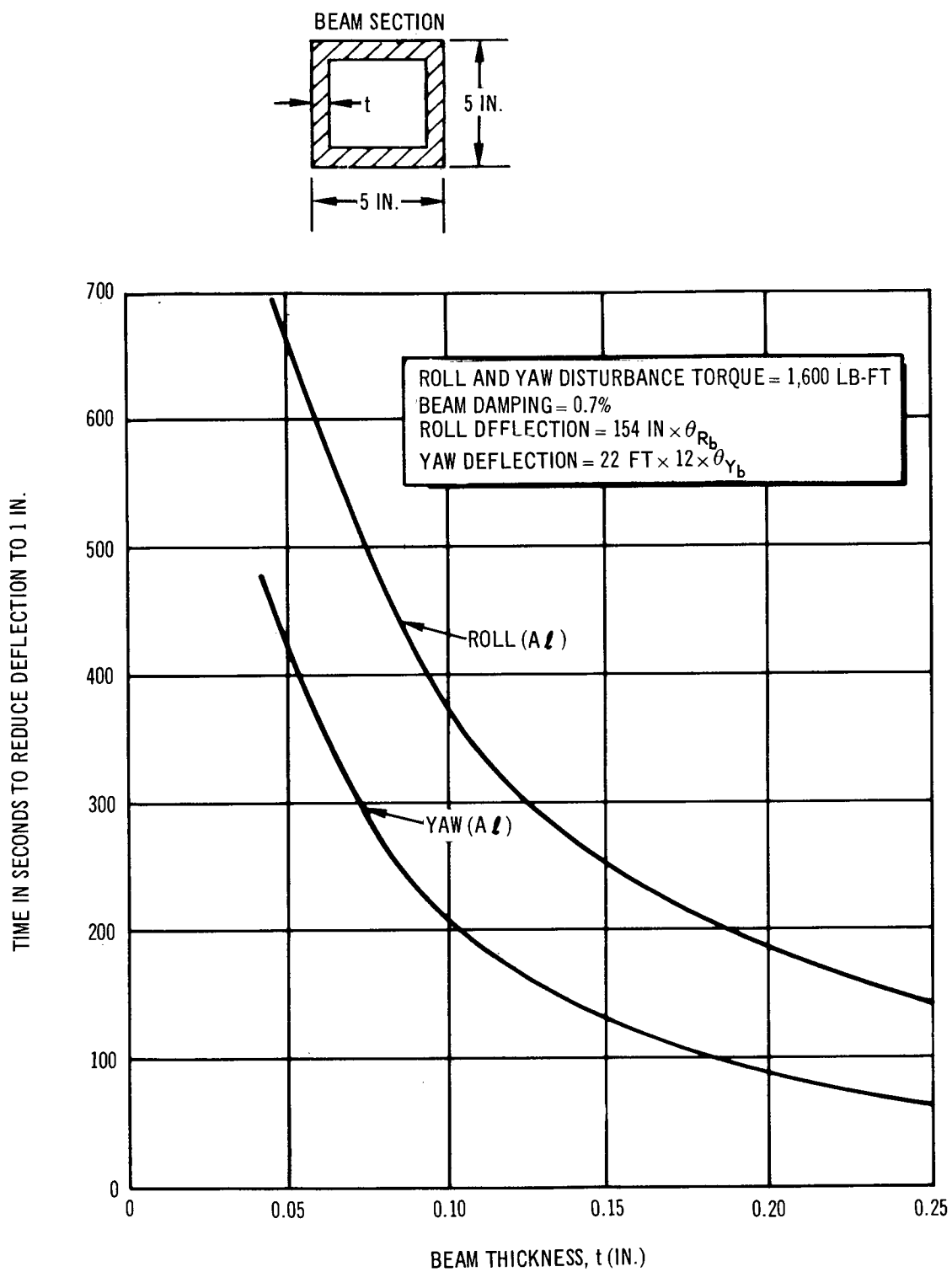


Figure A-11. Beam Damping for Roll and Yaw Thruster Disturbance

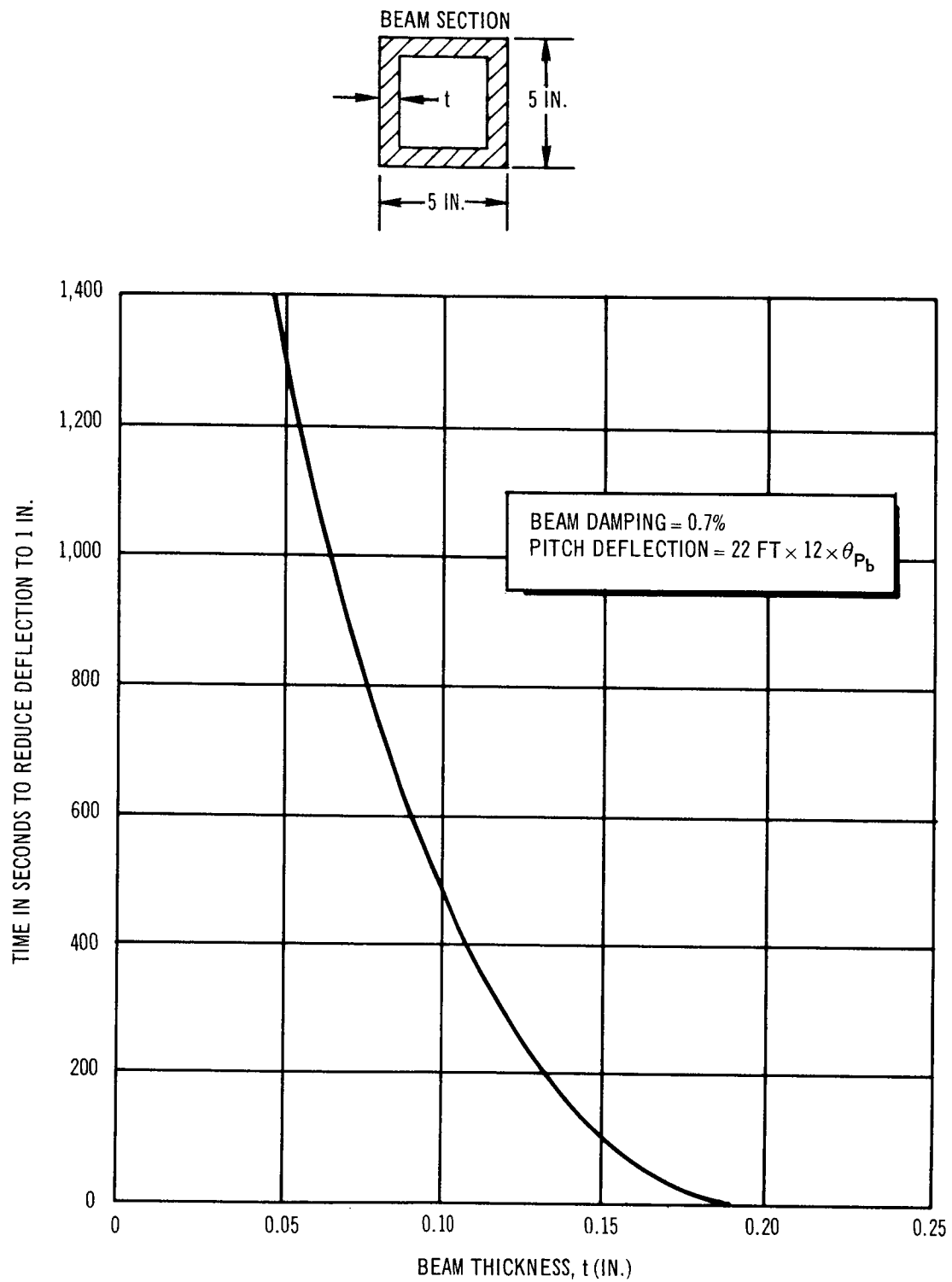


Figure A-12. Beam Damping for Pitch Disturbance of 100 Lb-Ft

axis is limited to the capacity of the reversible dc torquer, which is recommended to be 50 lb-ft.

2. It is recommended that the design loads be based on maintaining vehicle orientation with the RCS (that is, use the thruster-disturbance design criteria). Using an aluminum beam of 0.15-in. wall thickness, the maximum deflections are:
 - A. Pitch--1.0 in. with a natural frequency, $\beta_p = 0.24$ rad/sec.
 - B. Roll--1.8° with $\beta_R = 1.0$ rad/sec.
 - C. Yaw--2.5 in. with $\beta_y = 1.4$ rad/sec.
3. The impact loads for an impact deflection of 0.01 in. with the given deflections and natural frequencies are:
 - A. Pitch impact load--290 lb.
 - B. Roll and Yaw impact load--43 lb.
4. The capture radius for the latching mechanism is designed for 3.35 in., which is a large margin over the yaw deflection of 2.5 in.
5. To obtain a system time constant for damping of the beam vibration, the beam damping characteristic will be determined by ground testing. The assumed beam damping of 0.7% for the analysis may be too high or too low.
6. It is recommended that the torquer for stowing have a 50-lb-ft capacity. For a constant acceleration of the resupply craft through one-half of the stowing angle, 180°, and then a constant deceleration through the remaining half of the stowing angle, a total time for the stowing operation would be 7 min. The maximum rate of the resupply craft would be 1.2° per second.

Appendix B

SOLAR CELL PANEL SHADOWING

B.1 INTRODUCTION

A study was conducted to investigate the effects and the extent of shadowing on the MORL solar cell panels for the Phase IIa baseline, 6-kW solar cell system. The study was conducted because the shadowing of solar cells can reduce the solar panel output more than proportionally to the amount of panel shaded. The investigation included shadowing effects in both the roll solar and belly-down orientations. Each of these orientations were investigated for a 200-nmi, 50° launch inclination orbit, a 200-nmi polar orbit, and a high-altitude synchronous orbit. The extent of solar panel shadowing for each orbital position considered in this study was determined from photographs of a scale model of the MORL vehicle, with the solar panels ruled into squares. The investigation of shadowing effects showed that, as the launch inclination and the inclination to the ecliptic increased, so did the amount of shadowing on the panels; however, the required panel area to maintain laboratory operations decreased because of the increased periods of illumination and the shorter periods of darkness at the higher inclinations. This is illustrated in Figures B-1 and B-2 which show the time-power variations during a complete year for a 50° launch inclination and a polar orbit, respectively. It should be noted that the straight line at 6 kW is the average power required for normal operation; the upper curve is the average panel output because of variations in dark and light orbit times at higher inclinations. The lower curve is the average power loss from shadowing, and the dashed curve is the average power available when the orbital dark and light periods and shadowing are considered. A high-altitude synchronous orbit has the same extent of panel shadowing as the low-altitude orbits, but for larger periods of time. Figure B-1 shows that, in the belly-down orientation, the average power available falls below the average power required twice during each year. With a roll solar orientation, 18.5% of the solar panels

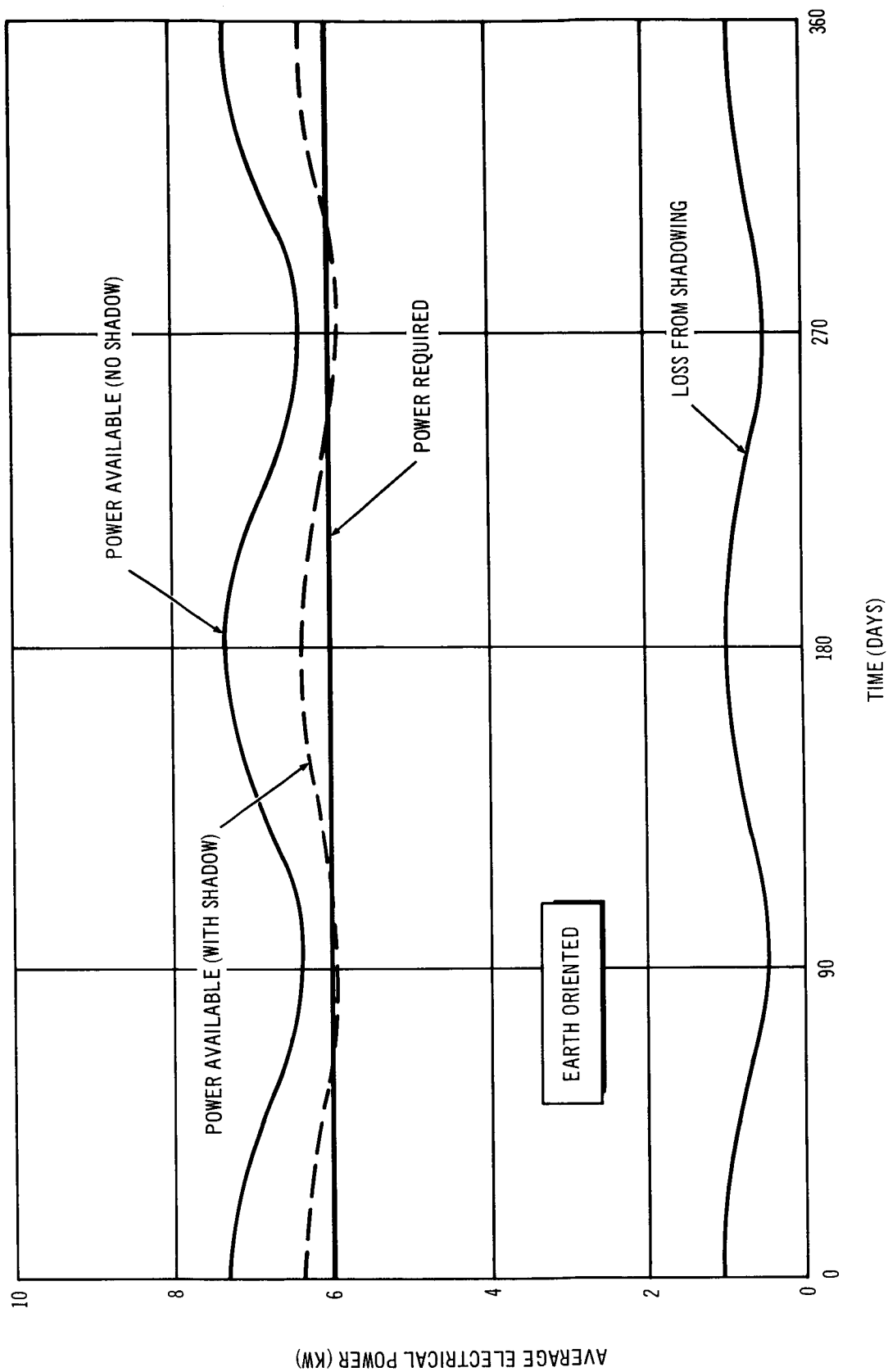


Figure B-1. Time-Power Variations (50° Launch Inclination)

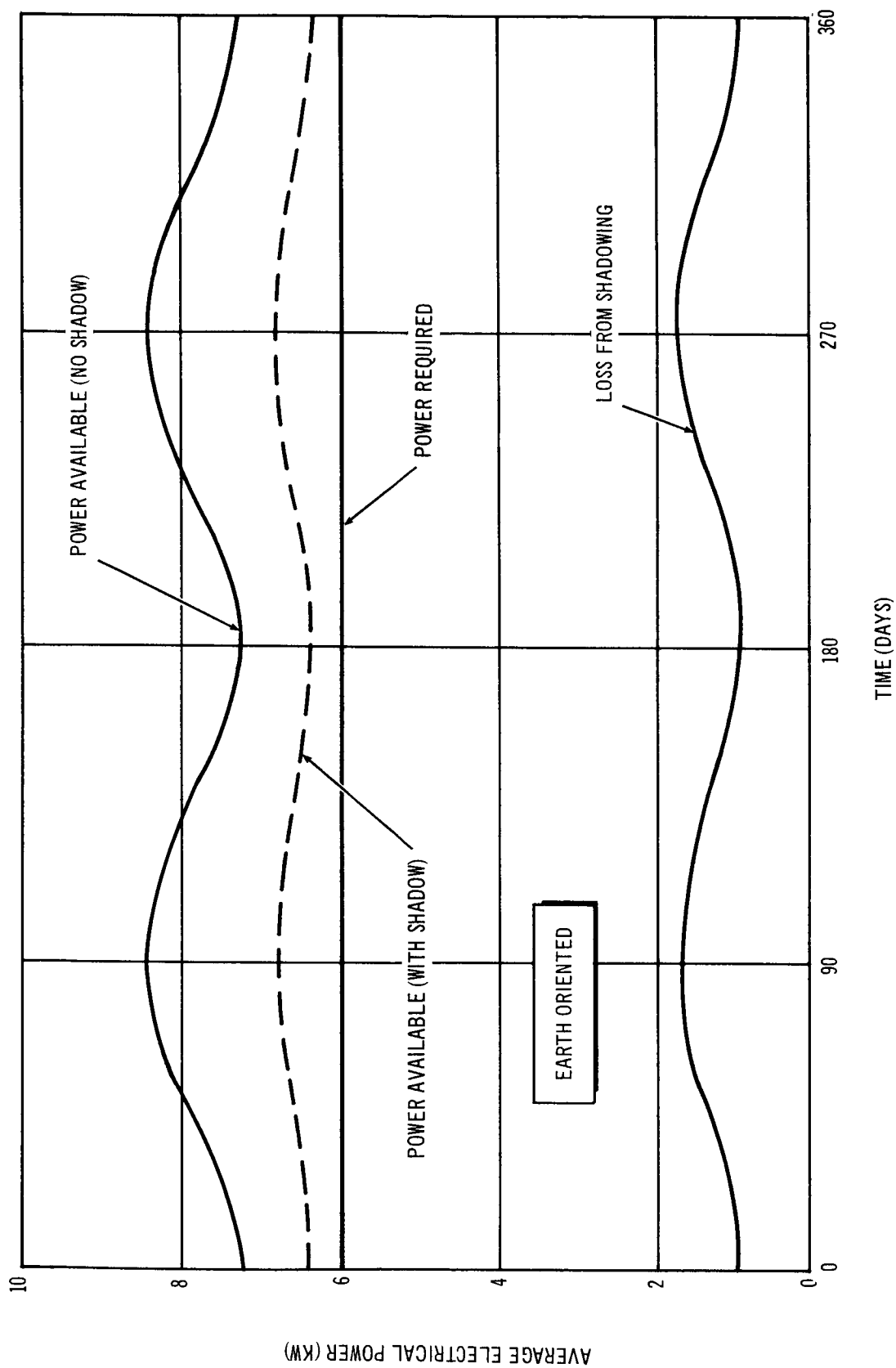


Figure B-2. Time-Power Variations (Polar Orbit)

are continuously shaded. The shadowing in a roll solar mode is independent of inclination or orbital position, and is caused by external laboratory appendages. Modification of the solar panels or of the vehicle orientation mode is therefore necessary in both the belly-down and roll solar orientations to assure that sufficient electrical power is available to the loads at all times.

The amount of shadowing in the belly-down orientation can be greatly reduced by using single rectangular solar cell extension panels. The single rectangular extension panels are achieved by moving the rectangular extension panels nearest the laboratory on each of the four main panels, and joining them with the rectangular extension panels located farthest away from the laboratory. Figure B-3 shows the time-power variation for a 50° launch inclination when using single extension panels. It can be seen that the average power available with a modified panel is always greater than the average power required.

In a roll solar orientation, the shadowing is reduced from 18.5 to 5.5% with the use of single rectangular extension panels, but the shadowing can be eliminated by rotating the laboratory 180° . Such a rotation will permit the sun to see the back rather than the front of the laboratory and will eliminate the shadowing caused by the exterior appendages. If the laboratory is rotated, the single extension panels are not required for the roll solar orientation.

The shadowing of the solar cell panels is not a serious problem. The rotating of the laboratory 180° in the roll solar orientation and the use of single rectangular solar cell extension panels will ensure continuous normal operation of the laboratory without extensive and heavy modifications to the system.

No special orientation of the MORL vehicle is required. A roll solar orientation was considered because of the solar cell panel but is no longer necessary, as a result of the shadowing study.

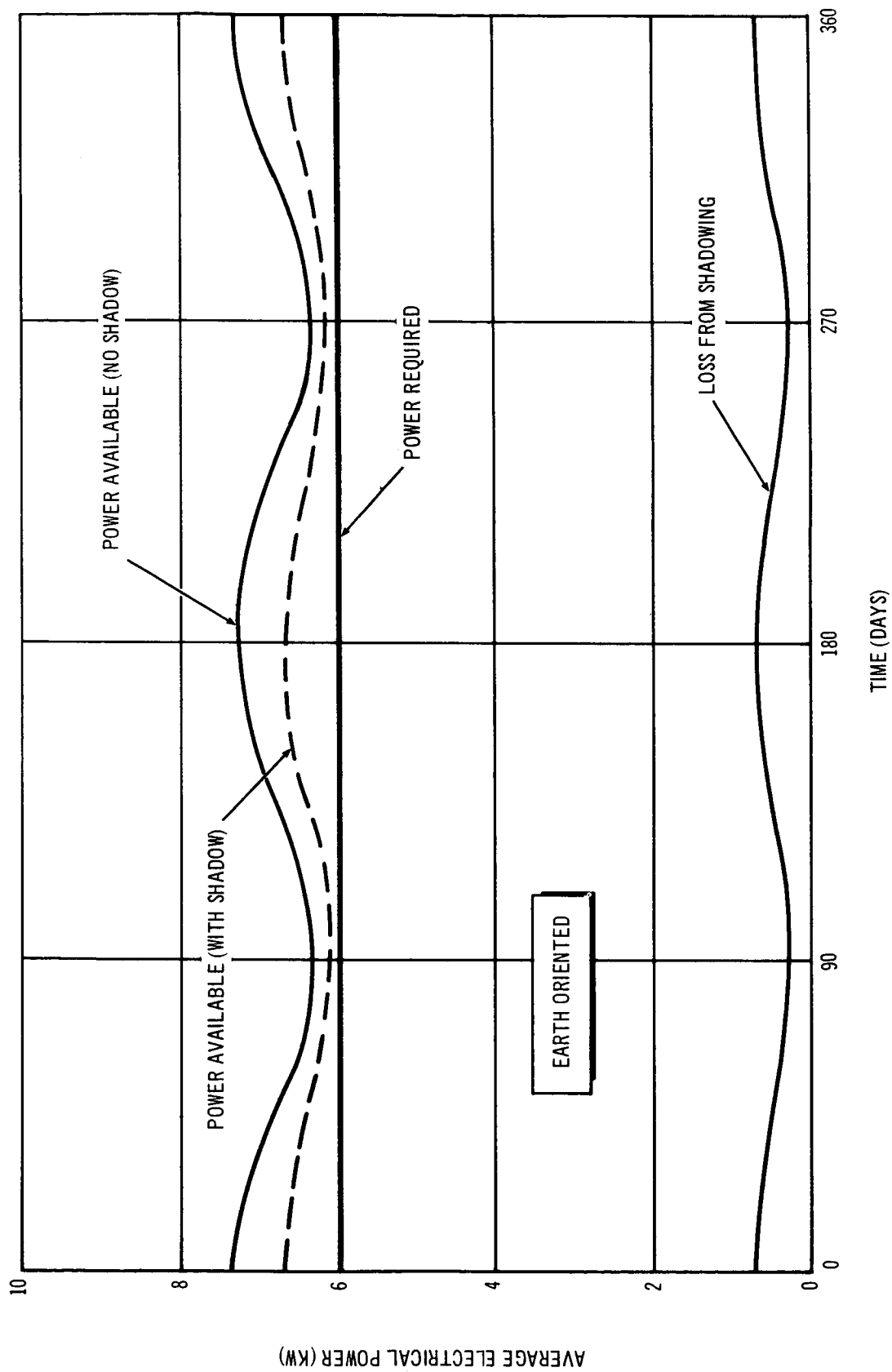


Figure B-3. Time-Power Variation (50° Launch Inclination) Single Rectangular Extension Panel

B.2 SOLAR CELL SHADOWING

Partial or total shadowing of one or more cells in a series-parallel arrangement of solar cells during the illuminated portion of an orbit could be a potential problem if not recognized in the design of the system. Shadowing of the solar cell panels occurs in all of the Phase IIa MORL baseline orientation modes. Therefore, an investigation to determine the effects of shadowing on the output of the electrical power system was conducted.

The shadowing effects can be extremely serious, since partial shadowing reduces the solar cell panel power output more than proportional to the shaded area. This is illustrated in Figure B-4, which shows the effect on total output when shading a portion of one cell in a 50-cell series string. The shadowing of one cell in a series string reduces the power output of the string to near zero if one or more of the cells are shaded. The effect of shadowing on cells connected in parallel is to reduce the current output proportional to the area of the cell that is shaded.

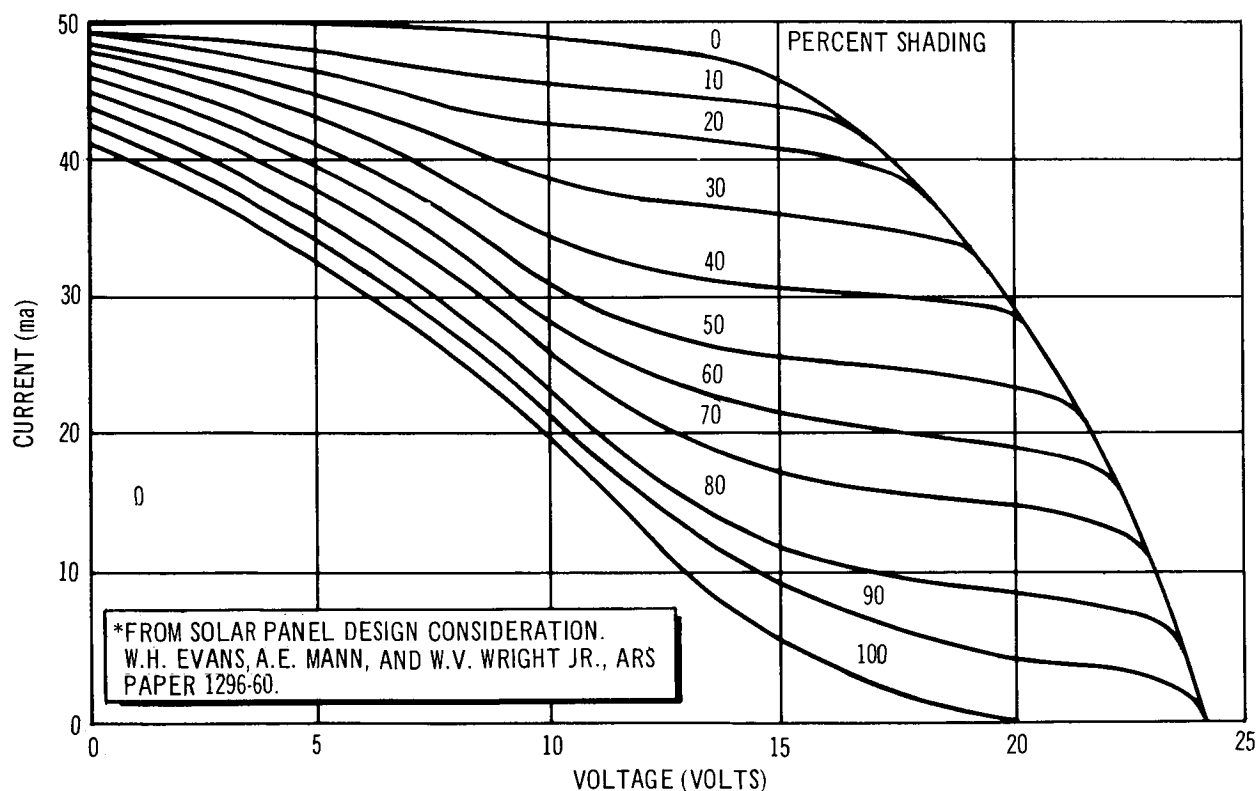


Figure B-4. Effect of Shading Portion of 1 Cell in a 50 Cell Series String*

The MORL solar cell panels consist of multicell modules which are formed by first connecting the solar cells into multicell parallel modules. The multicell parallel modules usually contain from 7 to 10 cells each. The multicell parallel modules are connected into multimodule strings which are then connected in a series-parallel arrangement to provide the panels with the proper voltage and current output. The multimodule series strings consists of about 70 multicell parallel modules to provide the necessary voltage output. Connection of cells and multimodules in parallel will provide the necessary current output. If any portion of a multimodule string is shadowed, its output voltage drops and that multimodule string does not contribute to the total panel output. Therefore, the shadowing of a small portion of several multicell modules could cause a large decrease in solar cell panel output.

B.2.1 Shadowing Effects

The effects of solar cell panel shadowing were investigated for all long-duration modes of laboratory operation of the Phase IIa baseline, 6-kW solar cell power system. The investigation included the roll solar and belly-down orientation modes for both 50° launch and polar orbits at 200 nmi. The effects of shadowing in a high-altitude synchronous orbit were briefly investigated but the effects do not differ from those of the other orbits considered.

A 1/100 scale model of the MORL was constructed for use in the investigation of the shadowing effects. The solar panels of the model were marked into squares so that the extent of shadowing could be determined with a reasonable amount of accuracy by counting the squares not shadowed. A partially shadowed square does not contribute to total panel output and was therefore not counted. The orientation of the laboratory and the panels was determined for several positions in each orbit and for several orbits during each seasonal period. December and June were used as one seasonal period with the other seasonal period represented by March and September, since these periods were found to exhibit the maximum and minimum shadowing conditions which repeated every 6 months. The positions considered in each orbit, solar noon, sunrise, and sunset, are defined below:

1. Solar noon--When the laboratory is directly between the Earth and the sun. (Closest point to the sun.)

2. Sunrise--90° before solar noon.
3. Sunset--90° after solar noon.

Photographs were taken for the roll solar orientation and for the belly-down orientation with a 50° launch inclination. The use of seven external appendages were used as a representative situation. The photographs did not include all orbital situations considered but gave sufficient information so that additional photographs were not necessary in determining the shadow effects and the extent of shadowing in all orbits considered.

The camera was used to represent the sun and therefore was placed a sufficient distance from the model so as to simulate the sun's position and obtain a correct view of the laboratory and solar panels as seen by the sun. A camera close to the model would give a distorted indication of the actual shadow because the light rays converge to the focal point of the camera lens; placement of the camera at a greater distance permits nearly parallel rays of light.

Four antennas extend from the MORL and beyond the solar cell panels. These antennas, required by the communications subsystem, are located 90° apart, and normally extend from near the front of the vehicle. In a roll solar orientation mode, the antennas can be placed so that they do not shadow the solar cell panels. In a belly-down orientation mode, the antennas will shadow the solar cell panels. Although the shadow is thin, it can extend across the entire panel and reduce the output of a large number of multi-module strings so that they do not contribute to the solar panel output. Thus a small shadow can cause a large degradation in the solar cell panel output.

The antennas could be moved to the rear of the vehicle to eliminate the shadowing but this placement would result in long coaxial cable antenna leads and rotating rf joints because of panel rotation requirements.

To give a better picture of what is happening with respect to shadowing of the solar cell panels, the effects of the variation in light and dark time are discussed in the following text, followed by consideration of shadowing effects

for each orientation considered. Possible modifications, changes, conclusions, and recommendations are also presented.

B.2.2 Dark and Light Time Variations

The solar cell/battery baseline system was designed for an orbital period of 92 min., with 56 min. illuminated and 36 min. dark. This amount of dark and light occurs at an orbit in the ecliptic (orbit plane parallel to sun's rays). As the angle of inclination of the ecliptic increases, the illuminated time in each orbit increases and the dark time decreases. For a 200-nmi orbit, 92 min. of illuminated time or a totally illuminated orbit is available at inclinations greater than about 73° to the ecliptic. The variations in dark and light time for a 200-nmi circular orbit at various inclinations to the ecliptic are shown in Figure B-5. Because of the decreased dark time at higher inclinations, less energy from the batteries is required and, therefore, less energy is required from the solar panels to recharge the batteries. Hence, more

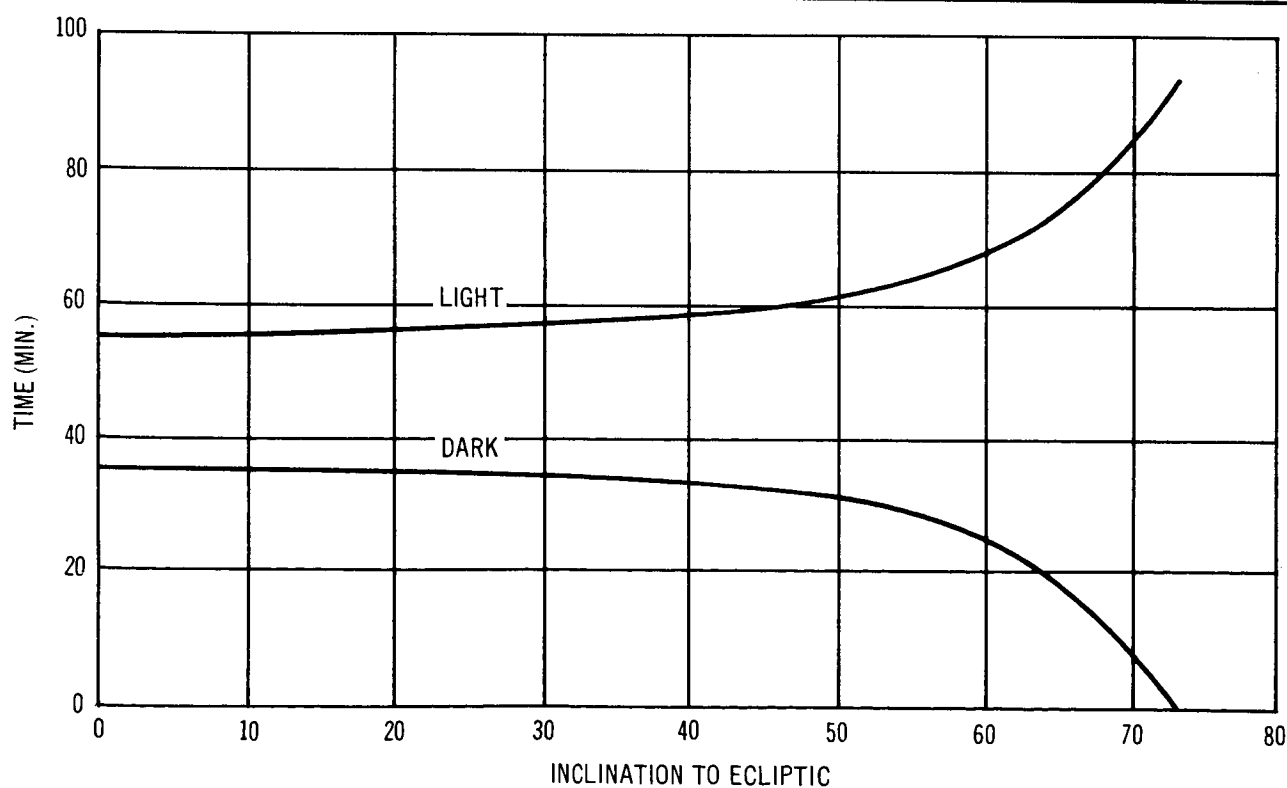


Figure B-5. Light and Dark Time Variations (200-nmi Circular Orbit)

of the solar panel power is available to supply the loads. In many cases, sufficient power is available for continuous operation of all subsystems even though shadowing does occur.

B. 2. 3 Roll Solar Orientation

Shadowing of the solar cell panels for a roll solar orientation is continuous and is independent of seasonal variations and orbital inclination or position. Shadowing in this orientation is dependent upon the number of appendages on the MORL. Figure B-6 is a photograph of the MORL scale model in a roll solar orientation and with seven external appendages. The portion of the solar cell panel that is continuously shadowed amounts to 18.5% of the total panel area. This is not an acceptable condition and requires increased panel area or other modification to the panels and/or vehicle.

The solar panel shadowing in the roll solar orientation mode can be reduced or eliminated in the following ways:

1. Extend the panels a greater distance from the laboratory.
2. Use a rectangular extension panel extended from the side of the main panel away from the vehicle rather than two rectangular extension panels extended from either side of the main solar cell panel.
3. Rotate the laboratory 180° so that the sun is looking at the back end rather than the front end of the laboratory.

Method 1 eliminates the shadowing but increases the weight of the extension erection mechanism up to several hundred pounds; further, the extended panels cause increased drag and additional torques on the laboratory, resulting in an increase in the orbit keeping-propellant requirements. Method 2 reduces the continuous shadowing from 18.5 to 5.5% but has drag and torque effects similar to the first method. The most promising approach to elimination of panel shadowing is Method 3. Since the shadowing in the roll solar orientation is caused entirely by the docked external appendages to the laboratory, 180° rotation of the laboratory will put all of the appendages behind the panels and no shadowing will occur. This method is the least complicated and results in only a small increase in propellant requirements because of aerodynamic changes.

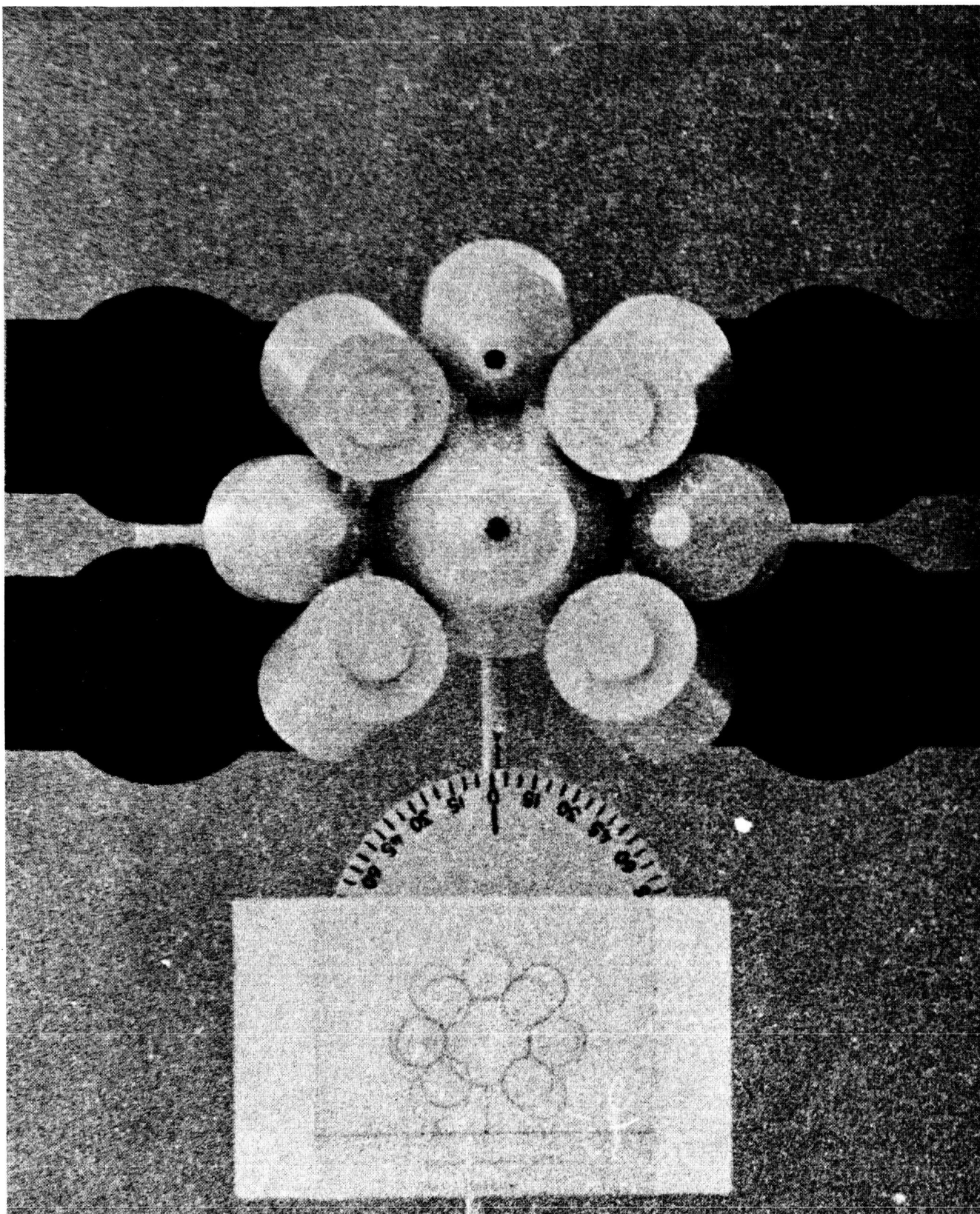


Figure B-6. Roll Solar Orientation Mode

B.2.4 Belly-Down Orientation

The shadow effects on solar cell panels were investigated for a belly-down orientation. The investigation included a 200-nmi 50° launch inclination, a 200-nmi polar orbit, and a high-altitude synchronous orbit. The synchronous orbit was investigated only briefly and although it has a much larger orbital period than a 200-nmi orbit, the shadowing is the same as that which occurs in the low Earth orbits. The shadowing that occurs in a belly-down orientation can be caused by the laboratory, other solar panels, docked vehicles, and other exterior appendages.

The extent of shadowing in the belly-down orientation was evaluated at various seasons, for the three positions in each orbit, and for 50° and 90° launch inclinations. Figures B-7, B-8, and B-9 show a typical 50° launch orbit at sunrise, solar noon, and sunset, respectively. Any one seasonal period will have variations in the amount of shadow that occurs and although month-to-month variations also occur, the shadow cycles repeat themselves every 6 months. The maximum and minimum shadows occur during either December and June or during March and September. The maximum and minimum shadows were determined and plotted as shown in Figures B-10, and B-11 through B-13. The orbit illumination time is shown by the extent of the lines before sunrise and after sunset. Figures B-10 and B-11 show the possible shadowing range at various orbit positions during December and June for 50° and 90° launch inclinations, respectively. Figures B-12 and B-13 show the possible shadowing range at various orbit positions for March and September. These illustrations are also applicable for a high-altitude synchronous orbit; each illustration shows the total and effecting panel shadowing represented by the different cross hatching and shading. The shaded area represents the effective panel shadowing or the shadowing range that occurs when dark and light time variations are considered. The unshaded area is the total shadowed area when a normal orbit period is considered, and has been shown for comparison purposes only. Only the shaded area is used for further considerations.

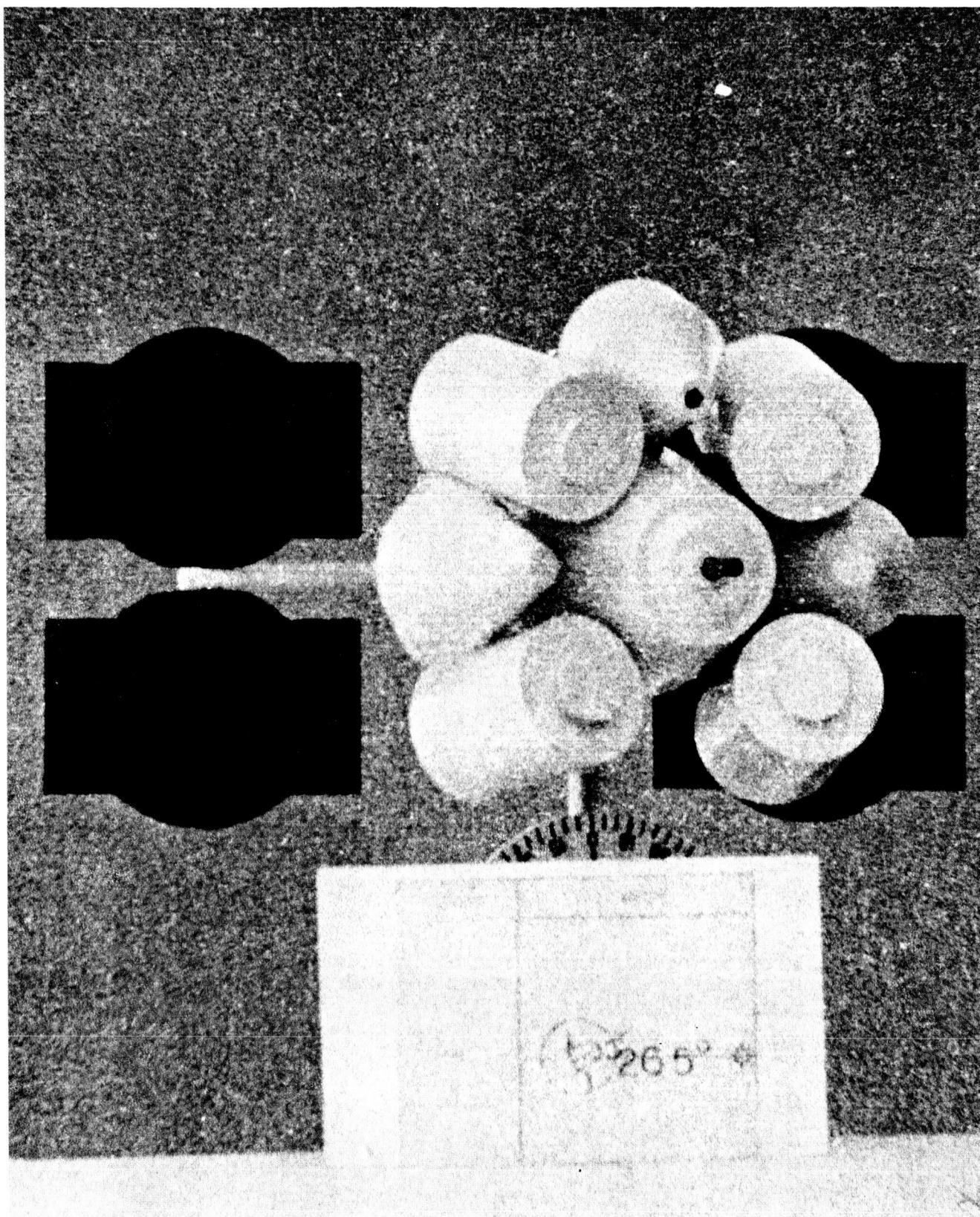


Figure B-7. Belly-Down Orientation – Sunrise December and June

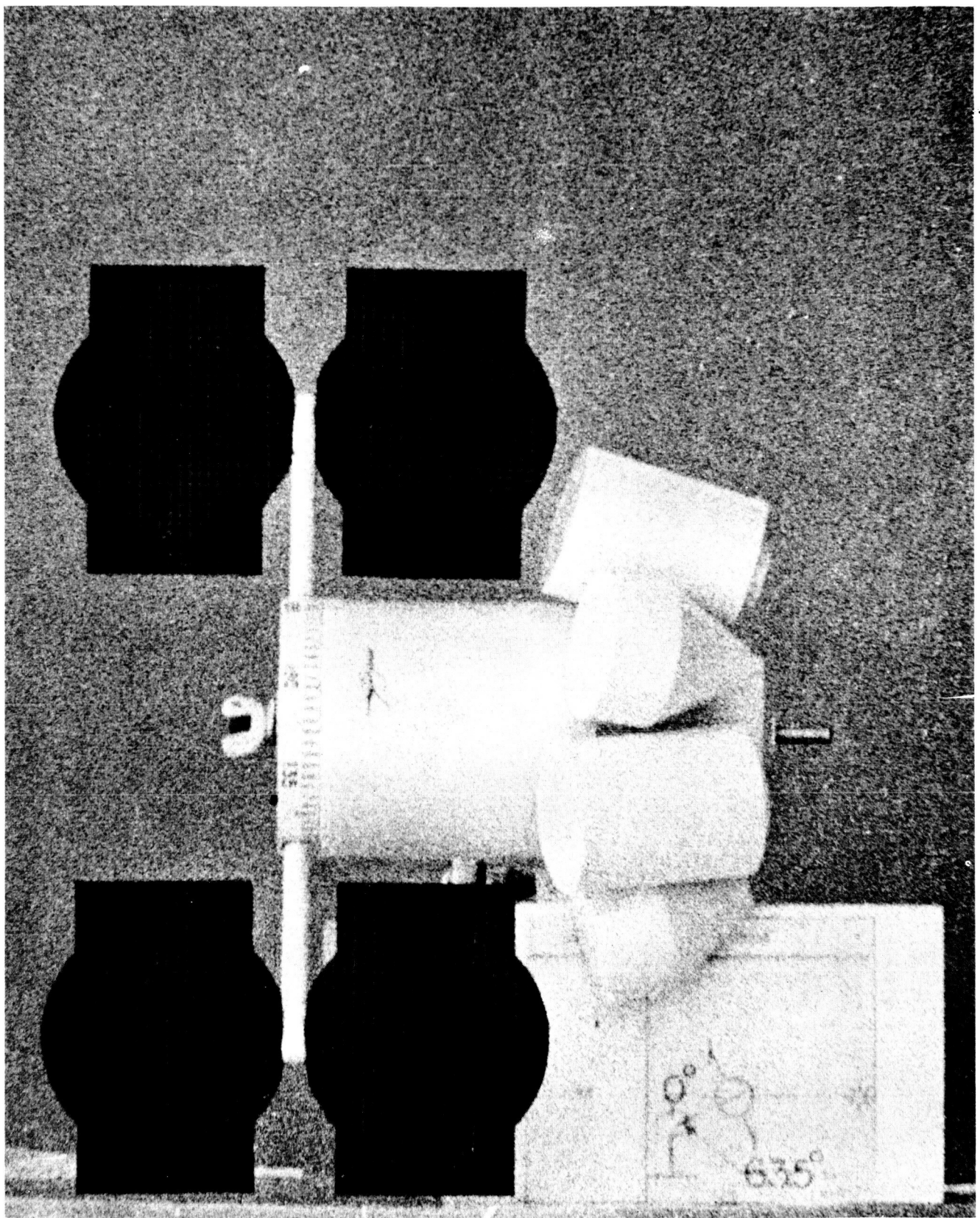


Figure B-8. Belly-Down Orientation – Solar Noon December and June

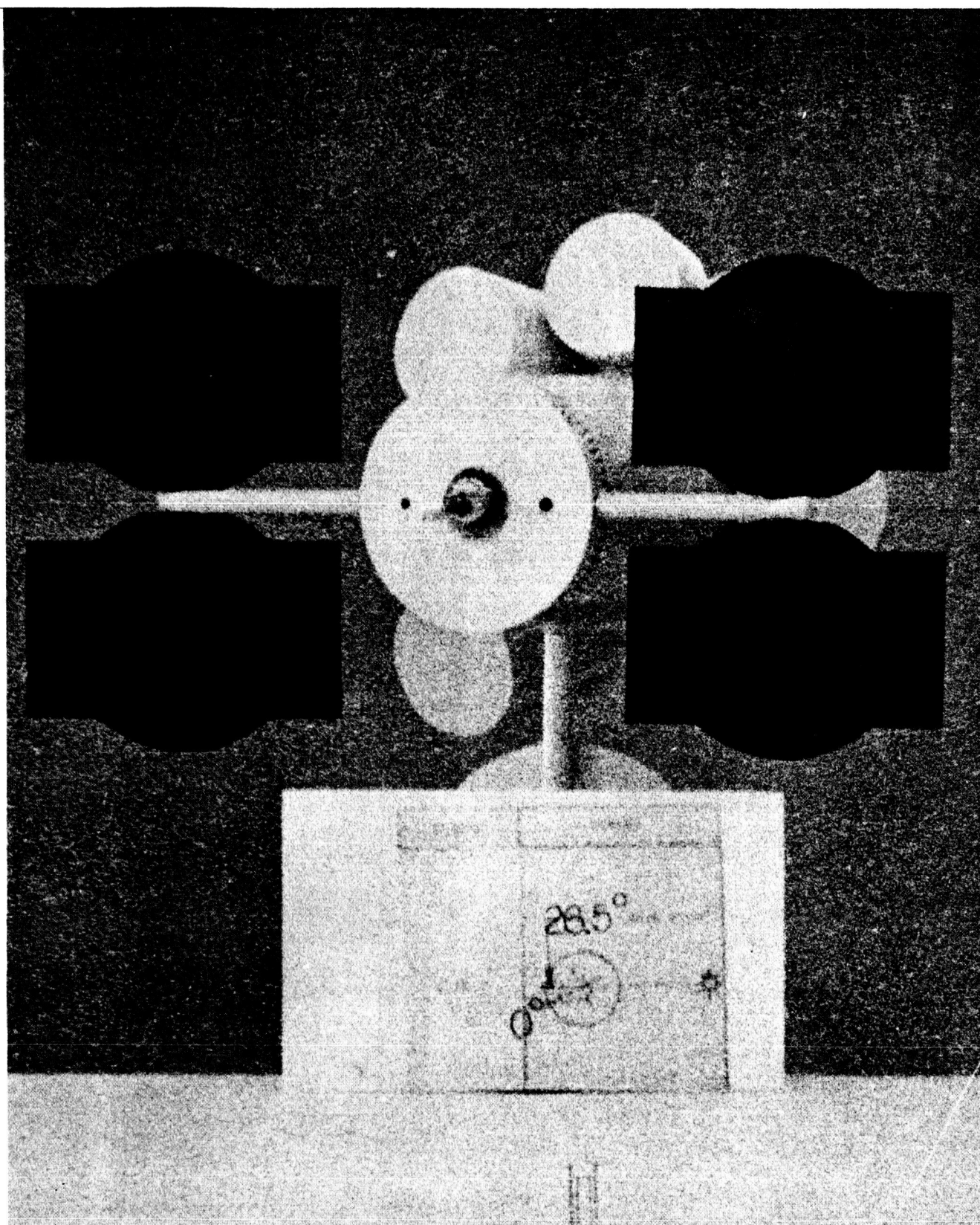


Figure B-9. Belly-Down Orientation – Sunset December and June

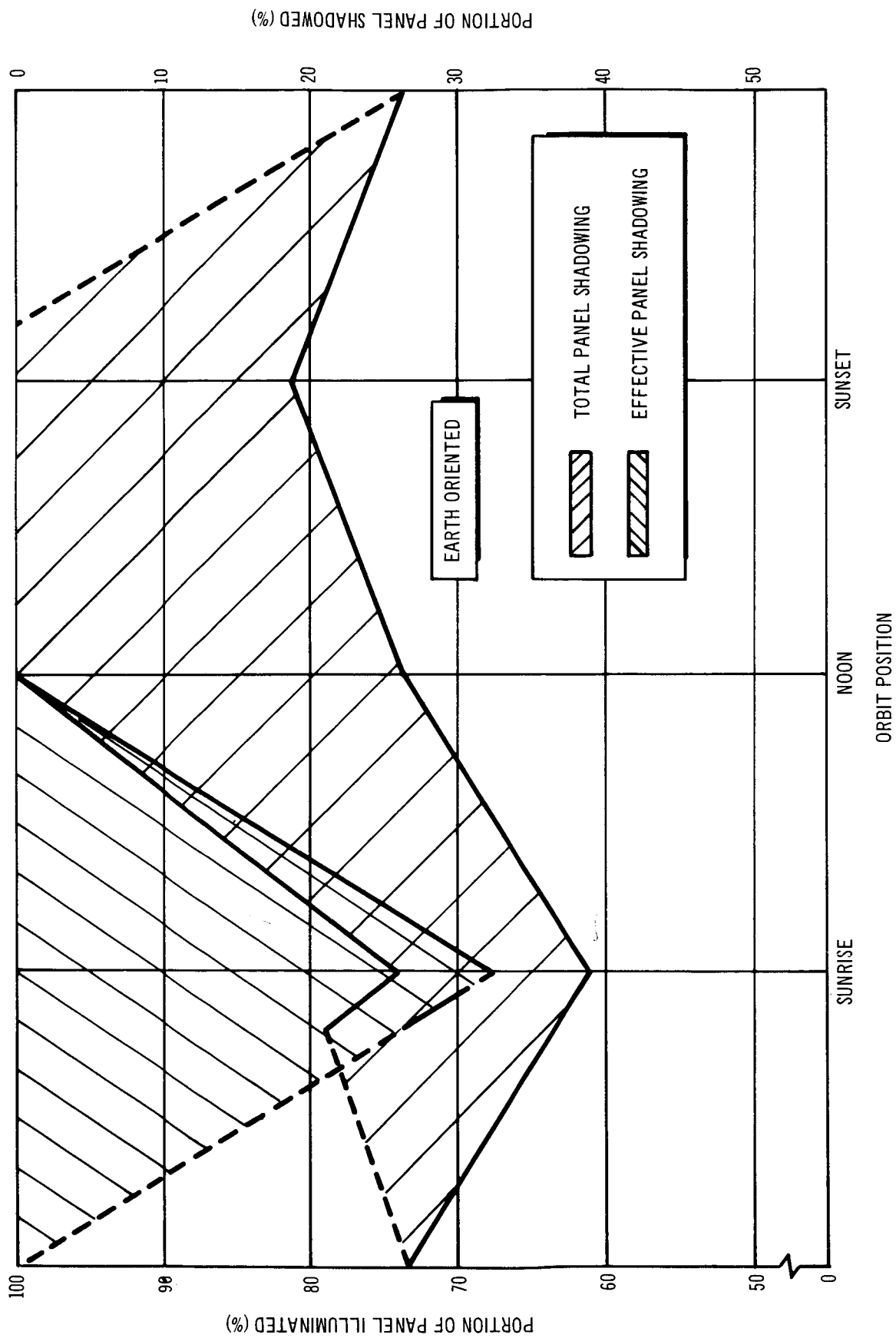


Figure B-10 Solar Panel Shadow History (50° Launch Inclination), December and June

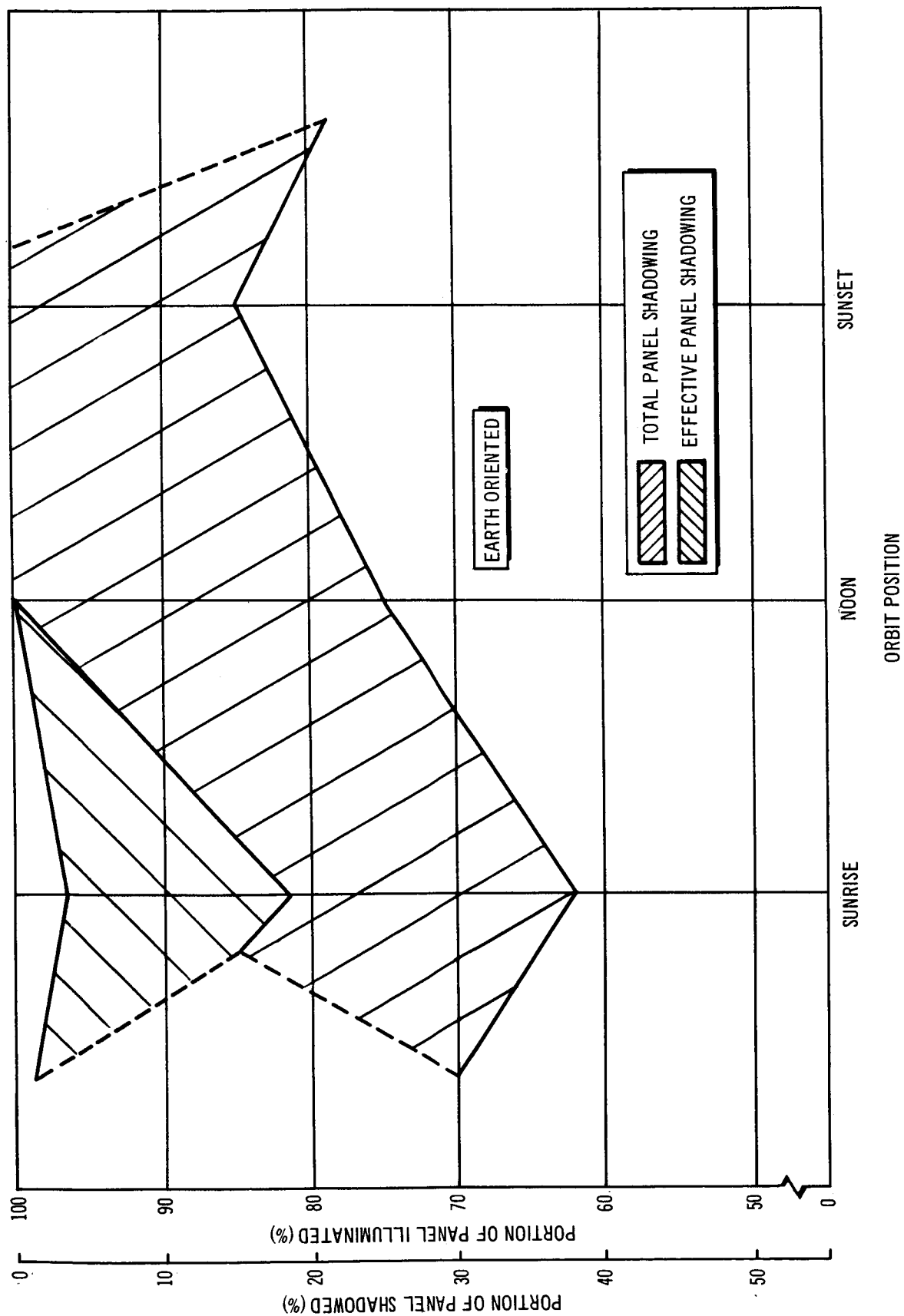


Figure B-11. Solar Panel Shadow History (Polar Orbit), December and June

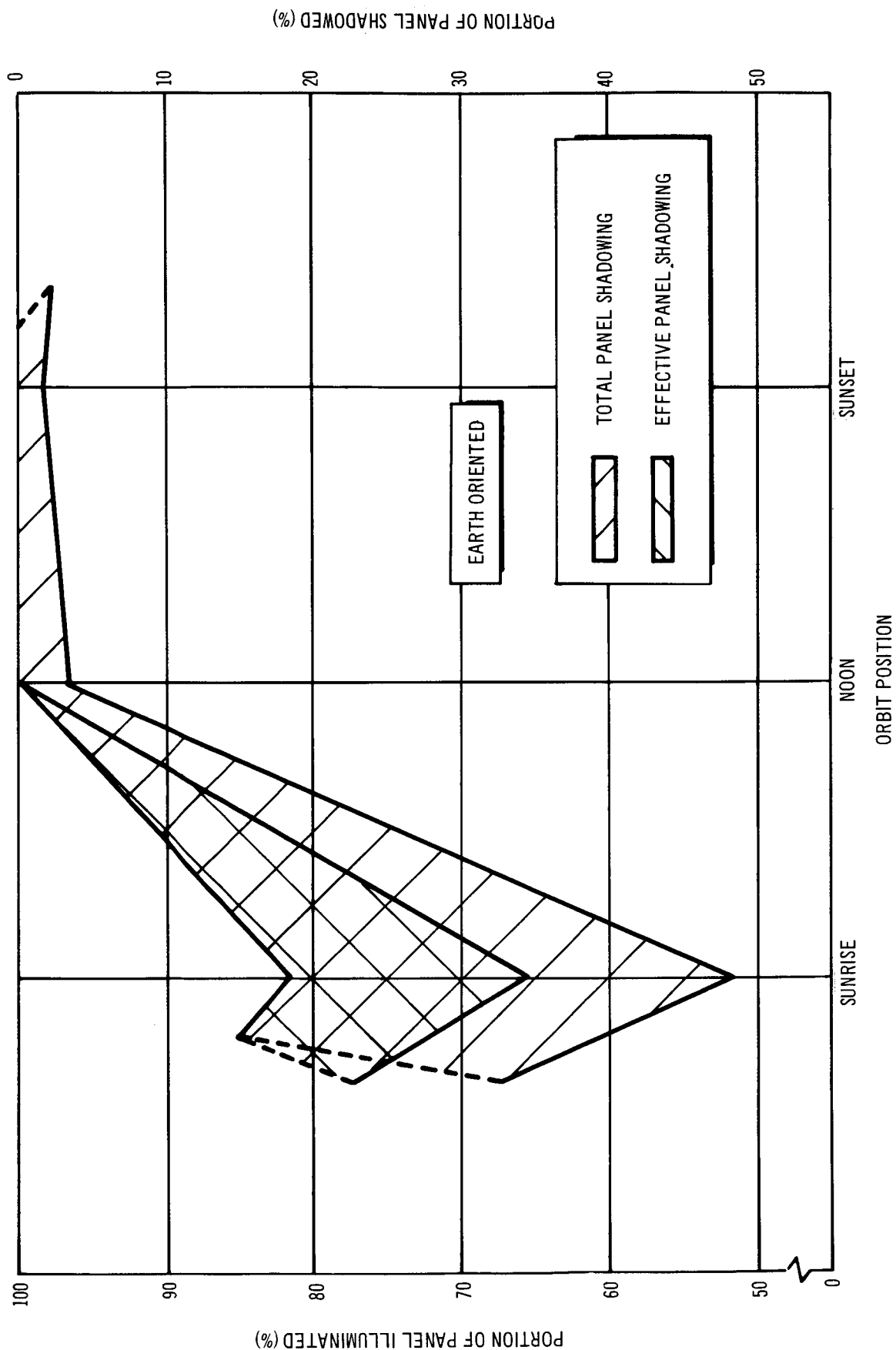


Figure B-12. Solar Panel Shadow History (50° Launch Inclination) March and September

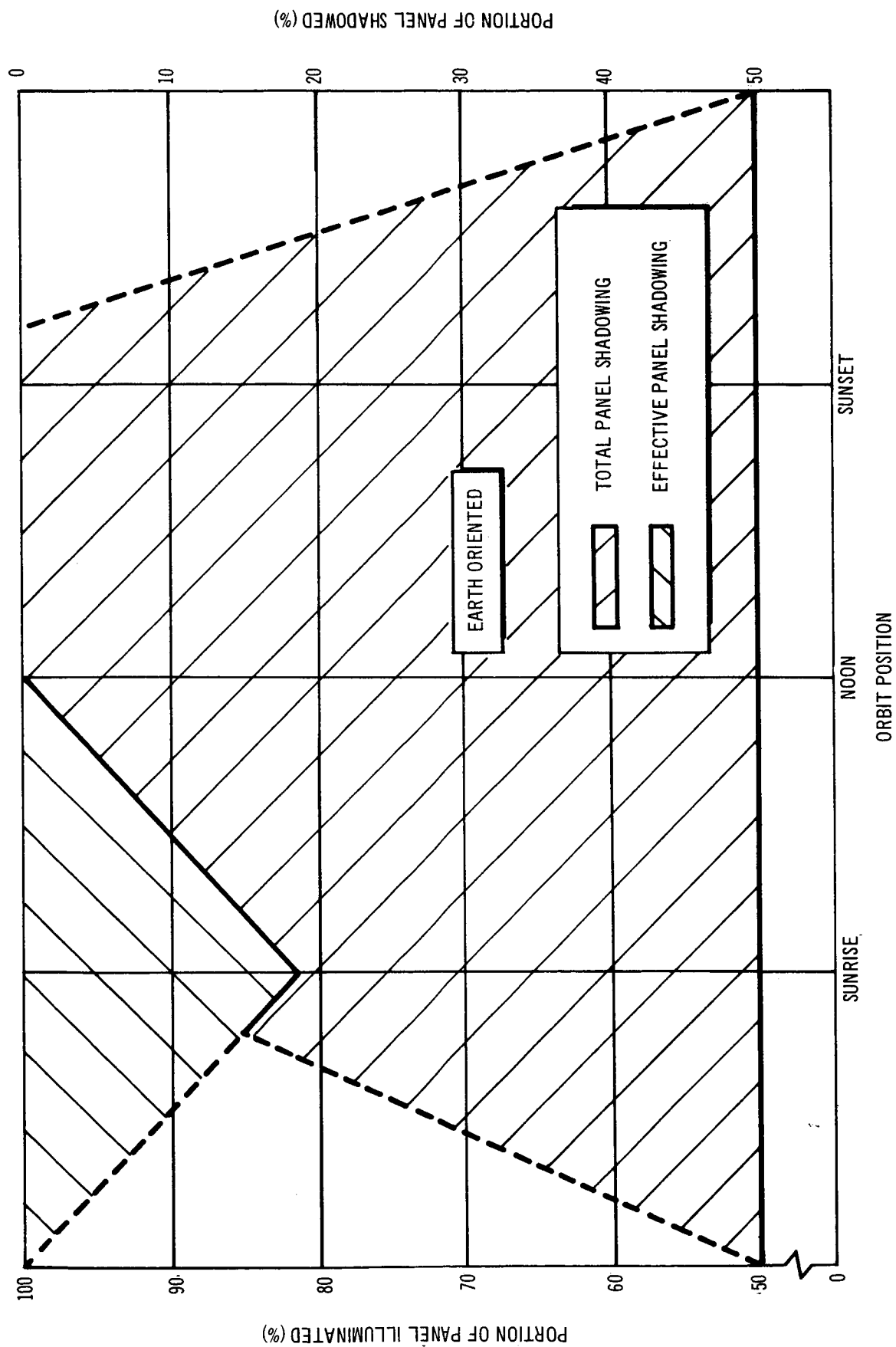


Figure B-13. Solar Panel Shadow History(Polar Orbit), March and September

The worst shadowing occurs in all cases at sunrise, while the least shadow occurs at sunset. The sun is looking at the front of the laboratory during sunrise, and the appendages, the laboratory, and other solar panels cast their shadow on the panels. At sunset, the sun is looking at the rear of the laboratory and the appendages, laboratory, and other solar panels cause significant shadow.

The extent of the shadowing in a belly-down orientation can be reduced from that shown in Figures B-10 through B-13 by using single rectangular extensions on the solar cell panels.

B.2.5 Single Rectangular Extension Panel

Single, rectangular-shaped panels are preferred for use over the rectangular panels on either side of the main solar cell panels. Rather than two panels, 69 in. by 172.6 in., there will be a single panel on the side away from the MORL vehicle. This method offers several advantages and some disadvantages.

The advantages of a single, rectangular-shaped extension panel are (1) less shadowing of solar cells, (2) a simpler erection mechanism than would be required to extend the panel a similar distance, and (3) less impingement of reaction control engines on the solar panels. This panel concept moves the solar cell panels almost 6 ft further from the vehicle without changing the erection and extension mechanisms. Moving the panels further away from the laboratory reduces the shadowing of the panels caused by other panels, the vehicle, and exterior appendages.

Figures B-14 and B-15 show the shadow ranges at various orbit positions for a belly-down orientation and a 50° launch orbit when the single extension panels are used. These illustrations are for shadowing in December and June, and March and September, respectively, and can be compared with Figures B-10 and B-12. Less impingement of the reaction control engines on the panels is assured by this concept but the extent of impingement has not been evaluated.

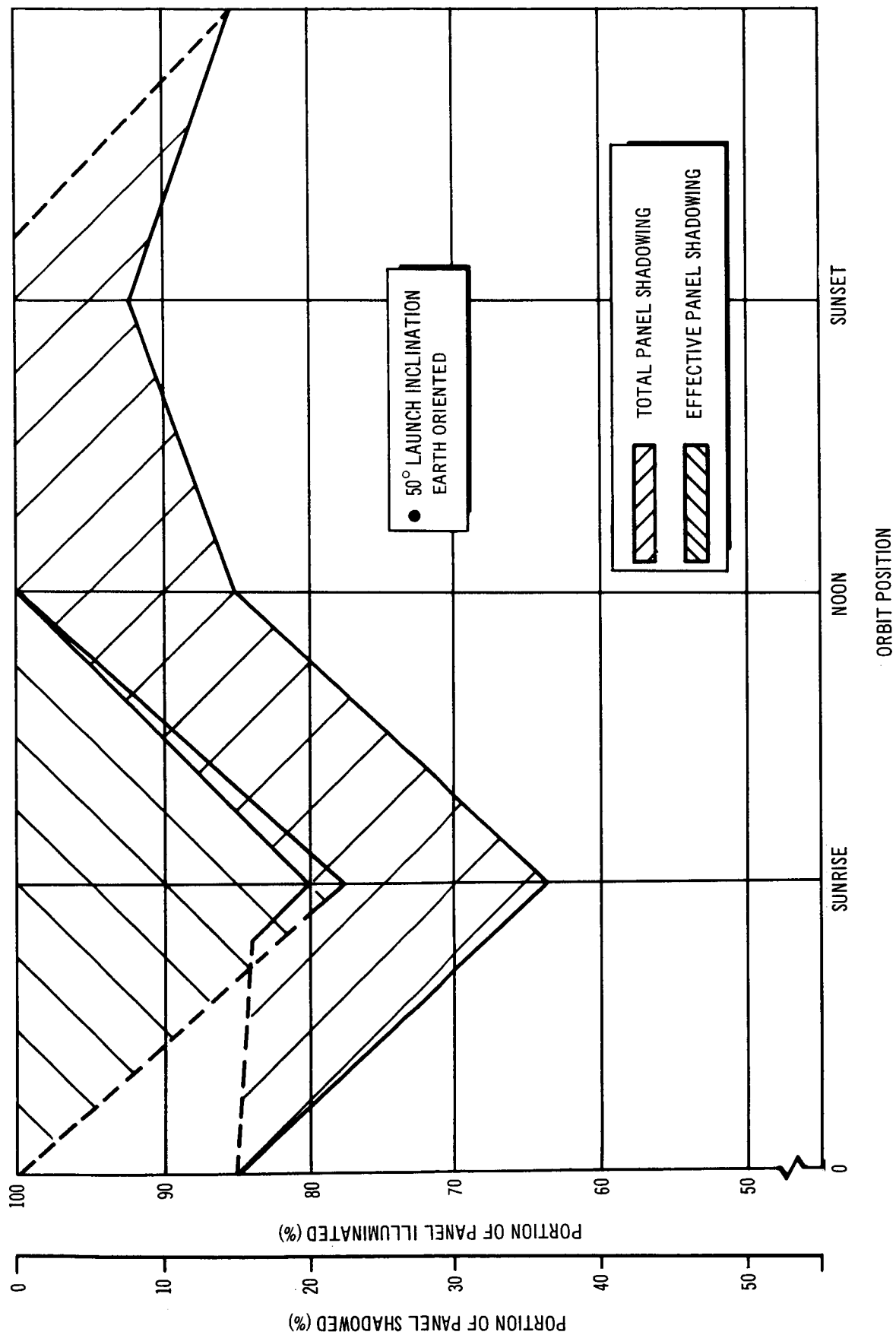


Figure B-14. Solar Panel Shadow History (Single Rectangular Extension Panel) December and June

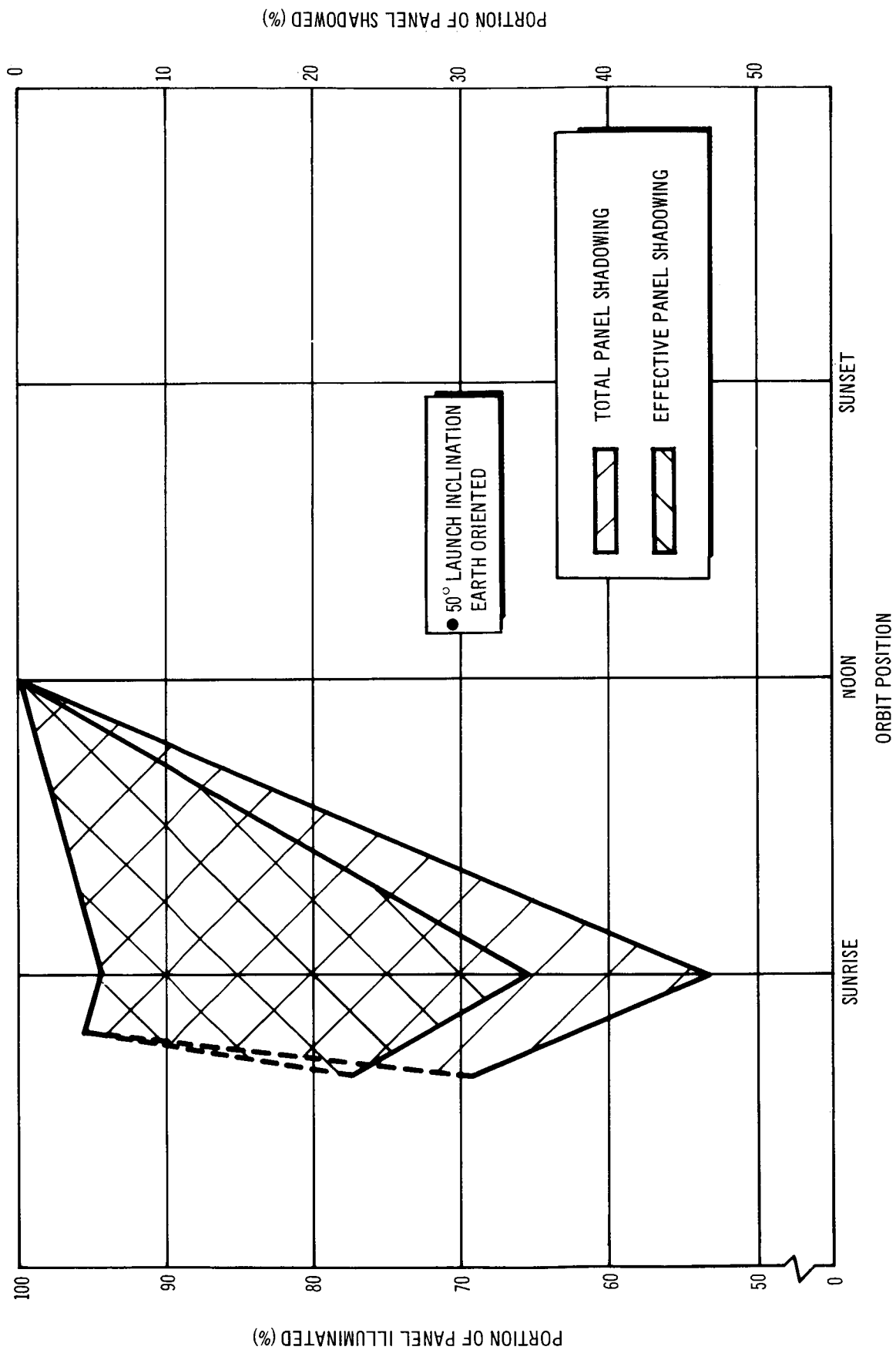


Figure B-15. Solar Panel Shadow History (Single Rectangular Extension Panel) March and September

The disadvantage of single rectangular extension panels is that the panel movements would have to be programmed or limited in some manner so that interference would not occur between the panels and the stowed appendages or the vehicle. The single extension panels will also cause a larger aerodynamic drag than the normal panel drag.

The improvement in available power because of decreased shadowing is shown by a comparison of Figures B-1 and B-3. These illustrations show that the average available panel output is increased by about 5% or 300 W. An important consideration is that (Figure B-1) the average power available (with shadowing) goes below the average power required. However, with the use of the single rectangular extension (Figure B-3), sufficient average power is available throughout the year.

In a polar orbit, the average power available is always sufficient to supply all the electrical power required for normal operation, as shown in Figure B-2. The use of single rectangular extension panels will increase the power available; however, because sufficient power is already available, an analysis to determine the increase in available power was not conducted. For launch inclination between 50° and polar orbit, the available power (with shadow) will be between the values shown in Figures B-1 and B-2.

B.3 CONCLUSIONS AND RECOMMENDATIONS

A first look at the extent of shadowing on the solar cell panels indicated a serious problem, as was shown in the unshaded areas of Figures B-6 through B-9. Further investigation showed that the effective shadow was actually much less than expected. When evaluating the MORL vehicle and other satellite or spacecraft using oriented solar arrays, where shadowing occurs, the variations in illuminated and dark time must be considered in determining the effective panel shadowing.

In any particular orbit, the worst shadow occurs at sunrise, but, averaged over a complete orbit, sufficient electrical power is available to maintain normal operation. Solar cell shadowing is therefore not a serious problem, since small modifications will reduce the effect of shadowing of the panels to acceptable levels.

It is recommended that single rectangular extension panels be used on MORL and that the laboratory be rotated 180° in the roll solar orientation if this orientation is used (roll solar orientation is no longer required for the solar panels). These changes will assure only small shadowing occurrences and an average available power sufficient to maintain normal laboratory operation.

The shadowing caused by the communications subsystem antenna can be eliminated by placing the antenna at the rear of vehicle, resulting in long coaxial cable leads and rotating rf joints. Further investigation of this interface is also recommended.

Appendix C
FLOW CHARTS

In this appendix, flow charts (Figure C-1) present the technological requirements of a solar cell/battery system that could be implemented in support of the MORL development. Development items are defined from their general function and functional requirement through their performance requirements, area of investigation, studies/analyses, and tests. Also included are subsystem orbital test requirements which could be demonstrated by an Apollo Applications Plan mission and items that are potential improvements over the baseline system.

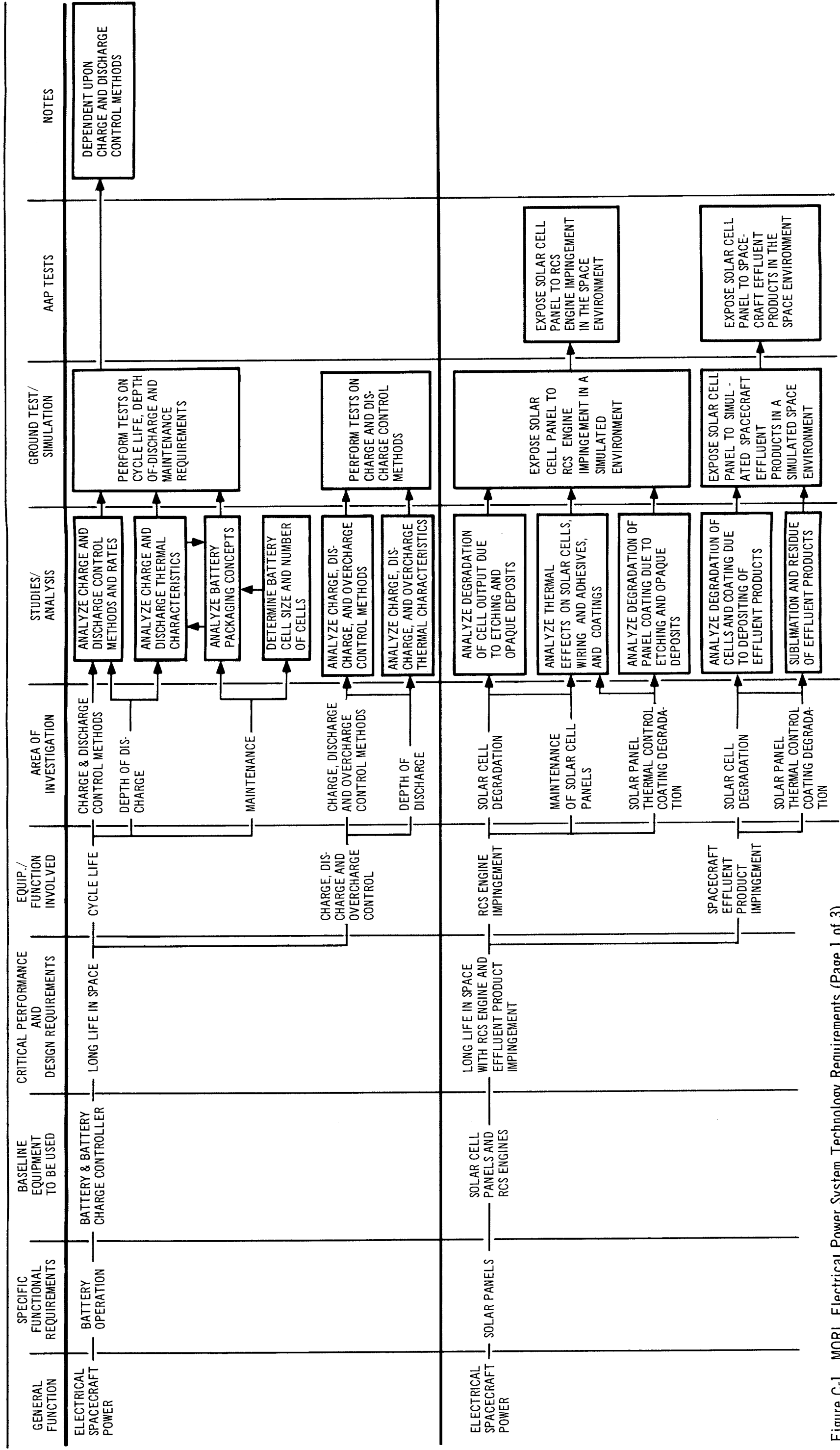


Figure C-1. MORL Electrical Power System Technology Requirements (Page 1 of 3)

294-2

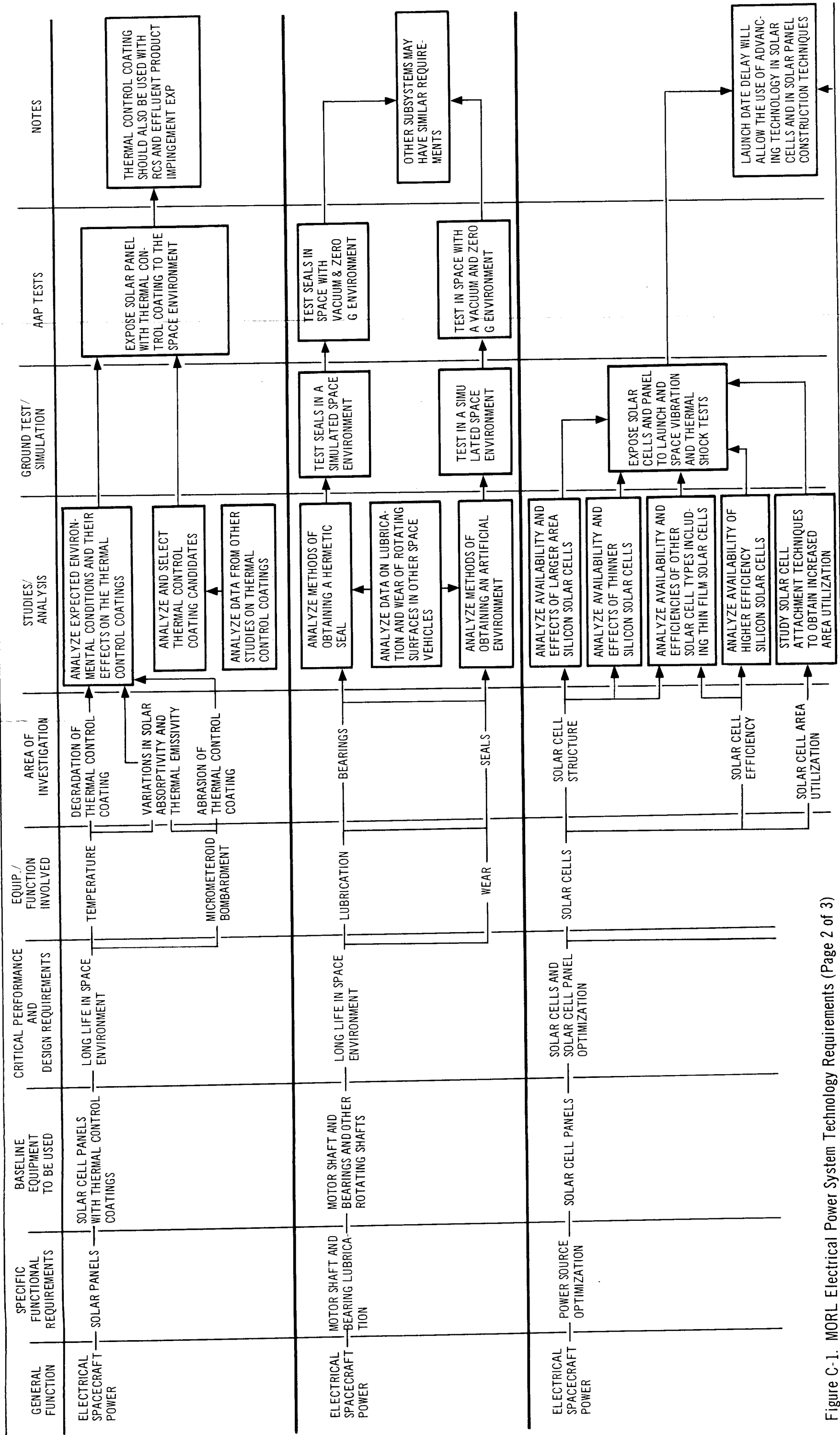


Figure C-1. MORL Electrical Power System Technology Requirements (Page 2 of 3)

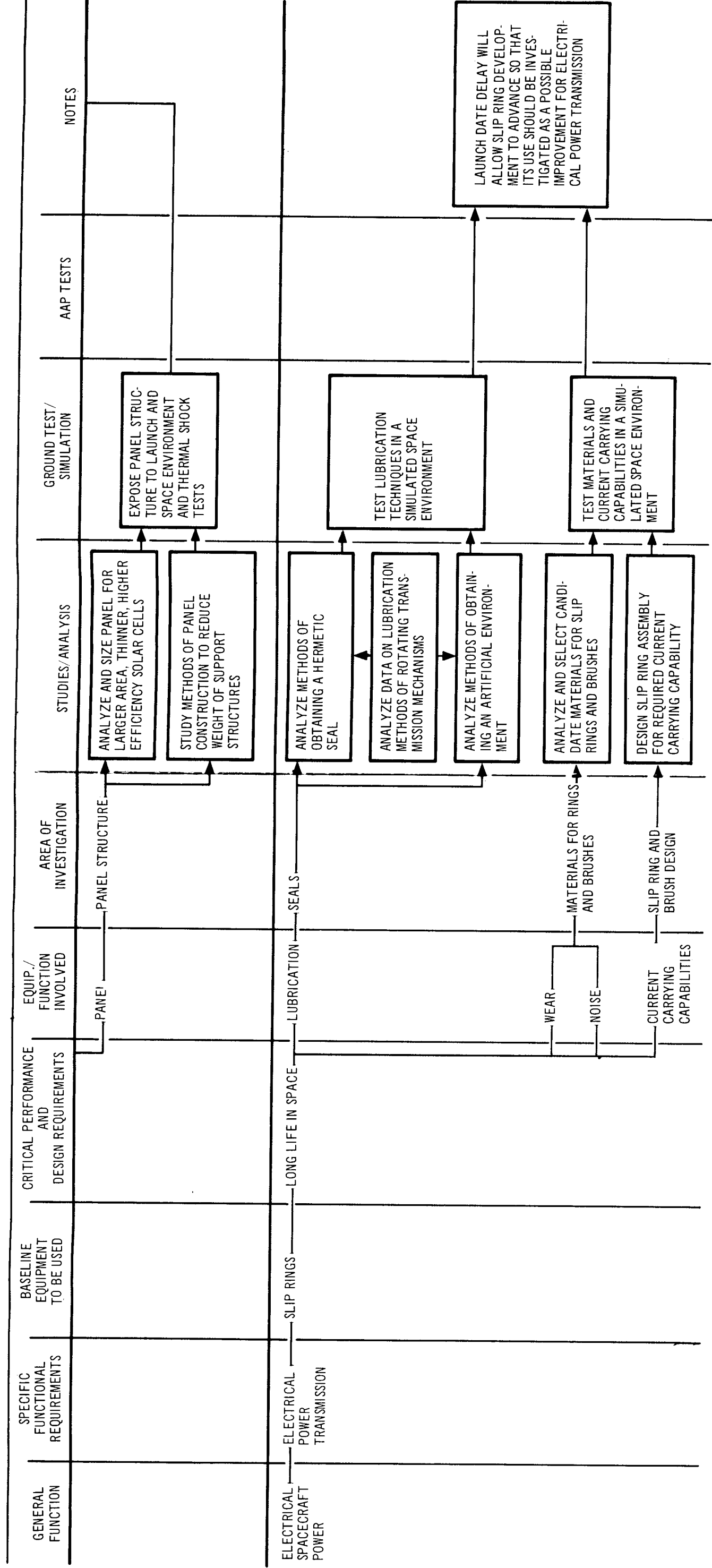


Figure C-1. MORL Electrical Power System Technology Requirements (Page 3 of 3)

296-2

Appendix D

ELECTRICAL LOAD ANALYSIS

The electrical loads were analyzed to determine the power and voltage requirements for each item of equipment. A detailed breakdown of all the individual items and their requirements are shown in Tables D-1 through D-7.

Each type of electrical power (that is, 115/200 V square wave, 115/200 V sine wave, and 56 ± 28 Vdc) from the data given in Tables D-1 through D-7 is totaled and summarized for each subsystem in Table D-8. The connected and average power include conversion to the type of power indicated, and are therefore reflected values at the alternator buses of the Isotope Brayton Cycle system.

Table D-1
GUIDANCE AND CONTROL

Item No.	Item Name	No. Installed	No. Operating Normally	Motor	Type of Power	Hr per Day	Unit Input (W)	Unit Source Power (W)	Total Connected (W)	Total Average (W)
101	Attitude gyro and accelerative assembly	2	2	No	115/200 V sine wave	24	4.0	4.6	9.2	9.2
102	Single Gimbal Triad	(2)*	(2)*	No	56 \pm 28 Vdc	24	28.8	34.9	69.8	69.8
		1	1	No	115/200 V sine wave	8	17.0	19.4	19.4	6.5
103	Star Tracker	(1)*	(1)*	No	56 \pm 28 Vdc	8	70.0	84.9	84.9	28.3
104	Horizon Scanner	2	2	No	56 \pm 28 Vdc	3	3.9	4.7	9.4	1.2
		2	1	No	56 \pm 28 Vdc	20	3.0	3.6	3.6	3.0
105	Sensor Electronics Assembly	1	1	No	115/200 V sine wave	24	1.1	1.3	1.3	1.3
		(1)*	(1)*	No	56 \pm 28 Vdc	24	40.0	48.5	48.5	48.5
106	IRIG Control Electronics	1	1	No	115/200 V sine wave	24	8.0	9.1	9.1	9.1
107	Reaction Control Amplifiers	(1)*	(1)*	No	56 \pm 28 Vdc	24	33.4	40.5	40.5	40.5
		1	1	No	115/200 V sine wave	1.5	3.0	3.4	3.4	0.2
108	Logic and Processing Electronics	(1)*	(1)*	No	56 \pm 28 Vdc	1.5	74.0	89.8	89.8	5.6
		1	1	No	115/200 V sine wave	24	22.8	26.0	26.0	26.0
109	CMG Control Electronics	(1)*	(1)*	No	56 \pm 28 Vdc	24	12.1	14.7	14.7	14.7
		1	1	No	56 \pm 28 Vdc	24	12.0	14.6	14.6	14.6
110	Regulated Power Supply	2	1	No	115/200 V sine wave	24	20.0	22.8	22.8	22.8
		(2)*	(1)*	No	56 \pm 28 Vdc	24	10.0	12.0	12.0	12.0
111	Attitude Reference Computer	1	1	No	115/200 V sine wave	8	1.0	1.1	1.1	0.4
		(1)*	(1)*	No	56 \pm 28 Vdc	8	27.0	32.7	32.7	10.9
112	Double Gimbal CMG	2	2	No	115/200 V square wave	24	15.0	16.7	33.5	33.5
		(2)*	(2)*	No	56 \pm 28 Vdc	24	5.5	6.7	13.3	13.3
113	Single Gimbal CMG	2	2	No	115/200 V square wave	24	14.5	16.2	32.4	32.4
		(2)*	(2)*	No	56 \pm 28 Vdc	24	2.75	3.3	6.6	6.6
114	Sensors - Rotating Mode	1	1	No	115/200 V sine wave	24	17.0	19.4	Rotating mode only	Rotating mode only
		(1)*	(1)*	No	56 \pm 28 Vdc	24	46.0	55.8	Rotating mode only	Rotating mode only
115	Electronics - Rotating Mode	1	1	No	56 \pm 28 Vdc	24	32.0	38.8	Rotating mode only	Rotating mode only

*Paranthesis denote items requiring dc as well as ac power.

Table D-2
COMMUNICATIONS AND DATA ACQUISITION

Item No.	Item Name	No. Installed	No. Operating Normally	Motor	Type of Power	Hr per Day	Unit Input (W)	Unit Source Power (W)	Total Connected (W)	Total Average (W)
201	Telemetry Converter/Multiplexer	1	1	No	56 \pm 28 Vdc	24	81.0	98.2	98.2	98.2
202	Telemetry Transmitter	2	2	No.	56 \pm 28 Vdc	2.4	70.0	84.9	169.8	17.0
203	Subcarrier Oscillators (Telemetry)	5	5	No	56 \pm 28 Vdc	2.4	0.4	0.5	2.4	0.2
204	Subcarrier Oscillators (Centrifuge)	14	14	No	56 \pm 28 Vdc	1.2	0.4	0.5	6.8	0.3
205	Receiver	1	1	No	56 \pm 28 Vdc	2.4	15.0	18.2	18.2	1.8
206	Subcarrier Discriminators	7	7	No	56 \pm 28 Vdc	2.4	2.3	2.8	19.4	1.9
207	Low Rate Tape Recorder	1	1	No	56 \pm 28 Vdc	24	25.0	30.3	30.3	30.3
208	Medium Speed Tape Recorder	1	1	No	56 \pm 28 Vdc	4.8	25.0	30.3	30.3	6.1
209	Analog Tape Recorder	1	1	No	56 \pm 28 Vdc	4.8	20.0	24.2	24.2	4.8
210	VHF Voice Communication	2	2	No	56 \pm 28 Vdc	13.5	40.0	48.5	97.0	54.6
211	Intercom	1	1	No	56 \pm 28 Vdc	24	15.0	18.2	18.2	18.2
212	Central Computer	1	1	No	56 \pm 28 Vdc	24	147.7	179.1	179.1	179.1
213	Data Adapter	1	1	No	56 \pm 28 Vdc	12	334.0	405.1	405.1	202.6
214	TV Camera	3	3	No	56 \pm 28 Vdc	2.4	9.9	12.0	36.0	3.6
215	TV Monitor	3	3	No	56 \pm 28 Vdc	2.4	50.0	60.6	181.8	18.2
216	TV Transmitter	1	1	No	56 \pm 28 Vdc	2.4	200.0	242.5	242.5	24.2
217	TV Controls	1	1	No	56 \pm 28 Vdc	2.4	19.5	23.6	23.6	2.4
218	C-Band Radar Transponder	1	1	No	56 \pm 28 Vdc	2.4	33.0	40.0	40.0	4.0
219	Acquisition Aid Beacon	1	1	No	56 \pm 28 Vdc	24	14.0	17.0	17.0	17.0
220	Digital Command System	1	1	No	56 \pm 28 Vdc	2.4	17.0	20.6	20.6	2.1
221	Facsimile System	1	1	No	115/200 V sine wave	1.2	115.0	131.3	131.3	6.6
222	Hard Copy System	1	1	No	115/200 V square wave	4.8	100.0	111.6	111.6	22.3
223	Rendezvous Radar Transponder	1	1	No	56 \pm 28 Vdc	1.	12.0	14.6	14.6	0.6
224	Film Projector/Scanner	1	1	No	56 \pm 28 Vdc	2.4	50.0	60.6	60.6	6.1
225	Antenna System	1	1	No	56 \pm 28 Vdc	2.4	3.0	3.6	3.6	0.4

Table D-3 (page 1 of 2)
ENVIRONMENTAL CONTROL AND LIFE SUPPORT

Item No.	Item Name	No. Installed	No. Operating Normally	Motor	Type of Power	Hr per Day	Unit Input (W)	Unit Source Power (W)	Total Connected (W)	Total Average (W)
301	Valve, On-Off (105)	6	1	No	56 ±28 Vdc	0.027	15.0	18.2	18.2	0.0
302	Canister, Silica Gel (201)	4	0	No	115/200 V square wave	Emergency only	400.0	446.7	Emergency only	
303	Canister, Zeolite (202)	4	0	No	115/200 square wave	Emergency only	400.0	446.7	Emergency only	
304	Valve, Diverter Dual (203)	2	2	No	115/200 V square wave	1.5	20.0	22.3	44.7	2.8
305	Separator, Water (204)	4	2	Yes	115/200 V square wave	24.0	6.0	6.7	13.4	13.4
306	Sensor, Relative Humidity (205)	2	2	No	56 ±28 Vdc	24.0	1.0	1.2	2.4	2.4
307	Valve, Diverter Dual (206)	2	2	No	56 ±28 Vdc	0.027	20.0	24.2	48.4	0.1
308	Timer (207)	2	2	No	115/200 V square wave	24.0	6.0	6.7	13.4	13.4
309	Valve, Diverter Dual (208)	2	2	No	115/200 V square wave	0.4	15.0	16.7	33.5	0.6
310	Valve, Diverter Dual (209)	4	2	No	56 ±28 Vdc	0.027	20.0	24.2	48.4	0.1
311	Valve, Diverter Dual (210)	2	2	No	115/200 V square wave	1.5	20.0	22.3	44.7	2.8
312	Pump, Vacuum (211)	2	2	Yes	115/200 V square wave	0.6	50.0	55.8	111.7	2.8
		2	2	Yes	115/200 V square wave	2.0	50.0	55.8	111.7	9.3
313	Valve, Shut-off, Vacuum (213)	2	2	No	115/200 V square wave	1.5	20.0	22.3	44.7	2.8
314	Fan, Suit (215)	6	2	No	115/200 V square wave	24.0	93.0	103.9	207.7	207.7
315	Burner, Catalytic (217)	3	3	No	115/200 V square wave	24.0	20.0	22.3	44.7	44.7
316	Sensor, Flow (218)	2	2	No	56 ±28 Vdc	16.0	1.0	1.2	2.4	1.6
317	Valve, Urine Flow (219)	2	2	No	56 ±28 Vdc	0.027	30.0	36.4	72.8	0.1
318	Fan, Contam Loop (226)	5	3	Yes	115/200 V square wave	24.0	108.5	121.2	363.5	363.5
319	Valve, Vent CO ₂ (610)	2	1	No	56 ±28 Vdc	Emergency only	20.0	24.2	Emergency only	
320	Pump, Vacuum (613)	1	0	Yes	115/220 V square wave	Hangar pump down only	986.0	1101.1	Hangar pump down only	
321	Probe, Conductivity (323)	1	1		56 ±28 Vdc	24.0	1.0	1.2	1.2	1.2
322	Freezer (327)	1	1		115/200 V square wave	24.0	37.0	41.3	41.3	41.3
323	Pump (402)	2	1	Yes	115/200 V square wave	24.0	25.0	27.9	27.9	27.9

Table D-3 (page 2 of 2)

Item No.	Item Name	No. installed	No. Operating Normally	Motor	Type of Power	Hr per Day	Unit Input Power (W)	Unit Source Power (W)	Total Connected (W)	Total Average (W)
324	Pump (403)	2	1	Yes	115/200 V square wave	24.0	32.0	35.7	35.7	35.7
325	Pump (419)	2	1	Yes	115/200 V square wave	24.0	45.0	50.2	50.2	50.2
326	Fan, Lab (502)	2	1	Yes	115/200 V square wave	24.0	233.0	260.2	260.2	260.2
327	Spectrometer (510)	1	1	No	56 \pm 28 Vdc	0.5	48.0	58.2	58.2	1.2
328	Lamp, Ultraviolet (511)	2	2	No	115/200 V square wave	24.0	20.0	22.3	44.7	44.7
329	Lamp, Ultraviolet (512)	1	1	No	115/200 V square wave	24.0	100.0	111.6	111.6	111.6
330	Fan, Hangar (515)	1	1	Yes	115/200 V square wave	24.0	100.0	111.6	111.6	111.6
331	Pump (812)	1	0	Yes	115/200 V square wave	Negligible	67.0	74.8	74.8	0.0
332	Cell, Electrolysis (901)	5	3	No	56 \pm 28 Vdc	24.0	495.0	600.4	1801.1	1801.1
333	Valve, Refill (121)	4	0	No	56 \pm 28 Vdc	Emergency only	20.0	24.2	Emergency only	Emergency only
334	Fan, Waste Management (704)	2	2	Yes	115/200 V square wave	1.0	18.0	20.1	20.1	0.9

Table D-4
DISPLAY, CONTROL, AND INSTRUMENTATION

Item No.	Item Name	No. Installed	No. Operating Normally	Motor	Type of Power	Hr per Day	Unit Input Power (W)	Unit Source Power (W)	Total Connected (W)	Total Average (W)
401	Instrumentation and Sensors	400	400	No	56 \pm 28 Vdc	24	0.5	0.6	242.4	242.4
402	Signal Conditioner	1	1	No	56 \pm 28 Vdc	24	20.0	24.2	24.2	24.2
403	Calibration Unit	1	1	No	56 \pm 28 Vdc	12	40.0	48.5	48.5	24.2
404	Electrical Power Display and Control	1	1	No	56 \pm 28 Vdc	24	10.0	12.0	12.0	12.0
405	Propulsion Display and Control	1	1	No	56 \pm 28 Vdc	0.5	17.1	20.7	20.7	0.4
406	EC/LS Display Panel	1	1	No	56 \pm 28 Vdc	24	30.0	36.4	36.4	36.4
407	Orbit Keeping Control Panel	1	1	No	56 \pm 28 Vdc	1.5 Hours every 4 days	3.0	3.6	3.6	0.1
408	Inertial Reference Control Panel	1	1	No	56 \pm 28 Vdc	8	20.0	24.2	24.2	8.1
409	SCS Mode Select Panel	1	1	No	56 \pm 28 Vdc	24	2.0	2.4	2.4	2.4
410	Dual Star Tracker Panel	1	1	No	56 \pm 28 Vdc	3	0.4	0.5	0.5	0.1
411	Horizon Scanner Control Panel	1	1	No	56 \pm 28 Vdc	20	0.4	0.5	0.5	0.4
412	FDAI (SCS)	1	1	No	56 \pm 28 Vdc	24	4.0	4.8	4.8	4.8
413	Miscellaneous Switching and Display (SCS)	1	1	No	56 \pm 28 Vdc	24	10.0	12.0	12.0	12.0
414	Test and Checkout	1	1	No	56 \pm 28 Vdc	24	5.7	6.9	6.9	6.9
415	Data Management	1	1	No	56 \pm 28 Vdc	24	5.1	6.2	6.2	6.2
416	Crew Support and Vehicle Status	1	1	No	56 \pm 28 Vdc	0.9	62.9	76.3	76.3	2.9
417	Engineering and Science Test Console	1	1	No	56 \pm 28 Vdc	1.2	5.0	6.1	6.1	0.6
418	Behavioral Measurement Test Bay	1	1	No	56 \pm 28 Vdc	1.2	130.0	157.7	157.7	7.9
419	Biomedical Experiment Test Console	1	1	No	56 \pm 28 Vdc	1.2	234.0	283.8	283.8	14.2

Table D-5
LOGISTICS VEHICLE, MAINTENANCE AND MISCELLANEOUS

Item No.	Item Name	No. * Installed	No. * Operating Normally	Motor	Type of Power	Hr per Day	Unit Input (W)	Unit Source Power (W)	Total Connected (W)	Total Average (W)
501	N ₂ O ₄ Prop Tank Heaters	2	2	No	115/200 V square wave	24.0	30	33.5	67.0	67.0
502	Navigation and Guidance and SCS Gyro Heaters	2	2	No	115/200 V square wave	24.0	230	256.8	513.7	513.7
503	ECS System Heating	2	2	No	115/200 V square wave	24.0	110	122.8	245.6	245.6
504	Navigation and Guidance Accelerometer Suspension	2	2	No	115/200 V sine wave	24.0	20	22.8	45.6	45.6
505	Continuous Monitor	2	2	No	115/200 V sine wave	24.0	20	22.8	45.6	45.6
506	Periodic Checkout	2	1	No	115/200 V sine wave	0.1	1990	2273.0	2273.0	9.5
507	Heating Prior to Separation	2	1	No	115/200 V square wave	0.3	40	44.7	44.7	0.6
601	Signal Generator	1	1	No	115/200 V sine wave	1.2	150	171.3	171.3	8.6
602	VTVM	1	1	No	115/200 V sine wave	4.8	80	91.3	91.3	18.3
603	Counter	1	1	No	115/200 V sine wave	2.4	38	43.3	43.3	4.3
604	Oscilloscope	1	1	No	115/200 V sine wave	4.8	50	57.1	57.1	11.4
605	Voltage Standard	1	1	No	115/200 V sine wave	2.4	20	22.8	22.8	2.3
701	Food Warmer	1	1	No	115/200 V square wave	2.0	120	134.0	134.0	11.2
702	Commode and Urinal	2	2	No	115/200 V square wave	1.0	40	44.7	89.4	3.7
703	Hygiene Equipment	1	1	No	115/200 V square wave	1.0	25	27.9	27.9	1.2
704	Recreational Equipment	1	1	No	115/200 V square wave	0.5	50	55.8	55.8	1.3

*Normally 2 Apollo Logistics Vehicles - 3 Vehicles for short periods of time unless nine-man crew is used.

Table D-6
LIGHTING

Item No.	Item Name	No. Installed	No. Operating Normally	Motor	Type of Power	Hr per Day	Unit Input (W)	Unit Source Power (W)	Total Connected (W)	Total Average (W)
801	Flight Compartment	4	4	No	115/200 V square wave	24.0	5.2	5.8	23.2	23.2
802	Supply Area	2	2	No	115/200 V square wave	24.0	5.2	5.8	11.6	11.6
803	Equipment Inspection	1	1	No	115/200 V square wave	24.0	30.0	33.5	33.5	33.5
804	Sanitation Area	3	3	No	115/200 V square wave	4.2	5.2	5.8	17.4	3.0
805	Galley	1	1	No	115/200 V square wave	8.0	5.2	5.8	5.8	1.9
806	Eating and Reading Area	2	2	No	115/200 V square wave	8.0	5.2	5.8	11.6	3.9
807	Crew Compartment	4	4	No	115/200 V square wave	24.0	2.6	2.9	11.6	11.6
808	Outside of Crew Compartment	2	2	No	115/200 V square wave	24.0	5.2	5.8	11.6	11.6
809	Bunks	6	6	No	115/200 V square wave	1.0	15.0	16.7	100.5	4.2
810	Storage Area	2	2	No	115/200 V square wave	0.5	15.0	16.7	33.5	0.7
811	Main Airlock	4	4	No	115/200 V square wave	1.0	15.0	16.7	67.0	2.8
812	Auxiliary Airlock	1	1	No	115/200 V square wave	1.0	15.0	16.7	16.7	0.7
813	Centrifuge	2	2	No	115/200 V square wave	2.0	15.0	16.7	33.5	2.8
814	Exterior Docking	2	2	No	115/200 V square wave	0.2	150.0	167.5	335.0	2.8
815	Operations Area	20	20	No	115/200 V square wave	24.0	5.2	5.8	116.1	116.1
816	Hangar Deck	6	6	No	115/200 V square wave	24.0	5.2	5.8	34.8	34.8

Table D-7
PROPULSION AND CENTRIFUGE

Item No.	Item Name	No. Installed	No. Operating Normally	Motor	Type of Power	Hr per Day	Unit Input (W)	Unit Source Power (W)	Total Connected (W)	Total Average (W)
901	Attitude Control Engine Valves	24		No	56 #28 Vdc	0.007	56.0	67.9	1630.1	0.5
902	Orbit Keeping Engine Valves	8		No	56 #28 Vdc	0.01	56.0	67.9	543.4	0.2
903	Spin/Despin Engine Valves	16		No	56 #28 Vdc	0.006	56.0	67.9	1086.7	0.3
1001	Centrifuge (Starting)	1	1	Yes	115/200 V square wave	0.7	470.0	524.8	524.8	15.3
	(Normal Operation)	1	1	Yes	115/200 V square wave	1.3	60.0	66.9	66.9	3.6

Table D-8

LOAD ANALYSIS SUMMARY
NORMAL OPERATION

System	Square Wave ac*			Square Wave ac*			56 (± 28) V dc*		
	Connected	Average		Connected	Average		Connected	Average	
Guidance and control	99	77	89	89	68		421	236	
Communications and data acquisition	100	100	115	115	115		1435	572	
Environmental control and life support	1593	1225					1658	1510	
Display, control and instrumentation							760	311	
Logistics vehicle and maintenance	780	740	2368	2368	87				
Lighting and miscellaneous	1063	268							
Propulsion							2688	1	
Totals	3635	2410	2572	2572	270		6962	2630	
*In watts									

Appendix E
ISOTOPE COST

Each vehicle requires two identical fuel blocks (one ship set) for a total of 42,400 thermal watts of isotope per MORL vehicle at launch. The average rate of decay used to calculate decay losses is 0.63% per year over the 5-year operational period. The basic Pu-238 cost is estimated at \$600 per thermal watt if the isotope is not returned.

Reliability calculations indicate an expected launch requirement of 1.12 laboratories per MORL placed in orbit. The probability that the isotope is recovered has been calculated to 0.925; thus, the probability that the isotope is not recovered is 0.075. The probabilistic cost of isotope, assuming post mission recovery, is defined by:

$$C_L = P_M \times P_L \times C_I \times P_I$$

where:

C_L = Probable cost of this isotope lost as the result of launch and/or recovery accidents.

P_M = Expected MORL usage.

P_L = Probability of not recovering isotope.

C_I = Basic cost of isotope (\$/watt).

P_I = Isotope power per block (thermal watts).

$$\begin{aligned} C_L &= 1.12 (0.075) \$600 (42,400) \\ &= \$2.48 \times 10^6 \end{aligned}$$

Thus, approximately \$2.5 million must be allocated for potential loss of fuel per MORL launch.

The rental cost of the isotope is determined from the charges for usage, decay, and reprocessing and can be calculated from the following equation:

$$C_R = P_I \times C_I \times B \times Y (I + D) + P_I \times C_I \times B \times R$$

where:

C_R = Rental cost of isotope.

B = Number of ship sets of fuel blocks.

Y = Fuel block rental period (years).

I = Interest rate for usage (%/year).

D = Decay rate (%/year).

R = Reprocessing charge (% of C_I).

The interest rate on the isotope is assumed to be 4.75% per year if the isotope is returned, and the reprocessing rate is 1.5% of the total cost. The isotope decays at about 0.635% per year during the first 5 years, and the decay cost is the cost of the isotope that actually decays. The interest rate of 4.75% per year is the same rate the AEC charges for the use of Pu-239. This interest problem has been discussed with the AEC, and it was concluded that this is the best presently available rate.

Figure E-1 shows the expected procurement and usage dates of the isotope fuel blocks. The isotope for the third flight is reserved, but not procured unless it is required. The third flight ship set is required in the event of failure and loss of flight ship sets No. 1 and 2. From Figure E-1, the ship sets of fuel block-years ($B \times Y$) for the two flight units is 9.3 ship sets of fuel block-years. Sensitivity of the costs derived below to the assumptions of Figure E-1 is significant. The rental cost of the isotope is calculated to be as follows:

$$\begin{aligned} C_R &= 42,400 (600) 9.3 (0.0475 + 0.00635) + 42,400 (600) 3 (0.015) \\ &= 254 \times 10^5 (9.3)(0.05385) + (254 \times 10^5) (0.045) \\ &= 254 \times 10^5 (0.5008 + 0.045) \\ &= \$13.86 \times 10^6 \end{aligned}$$

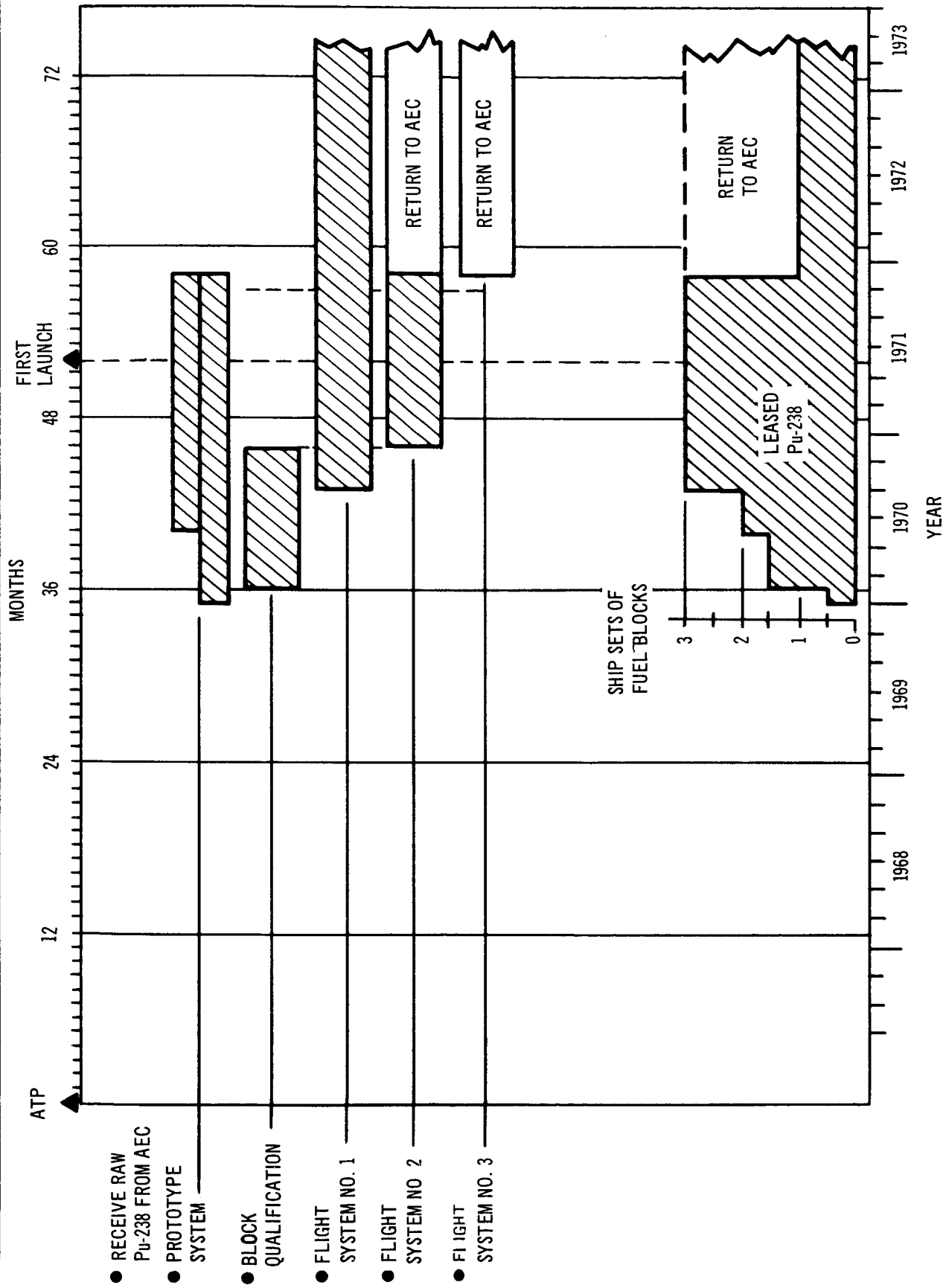


Figure E-1. Pu-238 Requirements

The cost of the isotope is then the sum of the cost caused by probable loss (C_L) and the cost of renting (C_R) or $\$16.34 \times 10^6$. A more detailed breakdown of the cost is shown below:

Probable loss	$\$ 2.48 \times 10^6$
Interest	11.22×10^6
Decay	1.50×10^6
Reprocessing	1.14×10^6
Total cost (recovery)	$\$16.34 \times 10^6$

It should be noted that the \$600 per watt price used above is based on the assumption that the AEC goes into production of Pu-238 as a prime product (as contrasted to production as a by-product of weapons materials). Also, at the present time, it is not clear how the MORL program would be charged for the isotope; that is, by either a purchase price or a lease arrangement. In addition, the uncertainties surrounding the manufacturing cost of the isotope are of a magnitude that is not consistent with the estimates for development and production of the remaining system elements.

APPENDIX F
REFERENCES

PRECEDING PAGE BLANK NOT FILMED.

REFERENCES

1. Report on the Optimization of the Manned Orbital Research Laboratory (MORL) System Concept-Subsystem Performance Specification, Part I. Douglas Report SM-48150.
2. Preliminary Design of a Pu-238 Isotope Brayton Cycle Power System for MORL, Volume I, Technical Summary. Douglas Report SM-48832. September 1965. (CRD)
3. Report on the Optimization of the Manned Orbital Research Laboratory (MORL) System Concept, Volume XI, Laboratory Configuration and Interiors. Douglas Report SM-46082.
4. Task III Report, MORL Concept Responsiveness Analysis. Book I, Douglas Report SM-48813. November 1965.
5. Raymond J. Roark. Formulas for Stress and Strain, Third Edition. McGraw-Hill Book Co., Inc. 1954.
6. Laboratory Mechanical Systems--Artificial Gravity System, Volume XIII. Douglas Report SM-46084. September 1964.
7. System Analysis--Flight Crew, Volume IV. Douglas Report SM-46075. September 1964.
8. David J. Peery. Aircraft Structures, First Edition. McGraw-Hill Book Co., Inc. 1959.
9. M. H. Schneider. Structural Optimization of Waffle Cylinders Under Axial Compression and External Pressure. Douglas Report SM-42441. October 1962.
10. George F. Gerard and Herbert Becker. Handbook of Structural Stability, Part III--Buckling of Curved Plates and Shells. NACA TN3783.
11. Preliminary Design of a Pu-238 Isotope Brayton Cycle Power System for MORL, Volume I, Technical Summary. Douglas Report SM-48832. September 1965. (CRD)
12. Preliminary Design of a Pu-238 Isotope Brayton Cycle Power System for MORL, Volume II, Model Specifications. Douglas Report SM-48833. September 1965. (CRD)

13. Preliminary Design of a Pu-238 Isotope Brayton Cycle Power System for MORL, Volume III, Preliminary Program Plans. Douglas Report SM-48834. September 1965. (CRD)
14. Preliminary Design of a Pu-238 Isotope Brayton Cycle Power System for MORL, Volume IV, Technical Appendix Book 1, Nuclear System. Douglas Report SM-48835. September 1965. (CRD)
15. Preliminary Design of a Pu-238 Isotope Brayton Cycle Power System for MORL, Volume IV, Technical Appendix Book 2, Brayton Cycle Power Conversion System. Douglas Report SM-48836. September 1965. (U)
16. Preliminary Design of a Pu-238 Isotope Brayton Cycle Power System for MORL, Volume IV, Technical Appendix Book 3, Vehicle Integration. Douglas Report SM-48837. September 1965. (U)
17. Report on the Optimization of the Manned Orbital Research Laboratory (MORL) System Concept, Volume XVII, Laboratory Electrical/Electronic Systems - Electrical Power. Douglas Report SM-46088.
18. Improved Solar Cells Planned for IMP-D. Aviation Week and Space Technology. July 26, 1965, Pages 53-60.
19. Fifth Photovoltaic Specialist Conference. NASA, Goddard Space Flight Center, Greenbelt, Maryland. October 18-20, 1965.
20. M. Wolf and E. L. Ralph. Effect of Thickness on Short Circuit Current, Fourth Annual Photovoltaic Specialists Conference, Cleveland, Ohio. June 1964.
21. Integral Glass Coatings for Solar Cells. Hoffman Electronics Corporation for NASA Goddard SFC, Greenbelt, Maryland. Contract No. NAS5-3857.
22. MORL System Concept, Volume XX, Logistics System. Douglas Report SM-46091. September 1964. (C)
23. MORL Interim Report on the Development of the MORL System Utilization Potential. Douglas Report SM-48157. February 1965.